Technische Universität München

Max-Planck-Institut für Physik
(Werner-Heisenberg-Institut)

On the Phenomenology of Charged Higgs Bosons in the Complex MSSM

Thị Nhung Đào

Abstract

In this thesis, we study various decay and production processes of charged Higgs bosons at the Large Hadron Collider (LHC) in the context of a general complex Minimal Supersymmetric Standard Model (MSSM) with minimal flavor violation. We investigate the effect of the complex phases of the soft supersymmetry breaking parameters and of the Higgsino mixing parameter, μ, on the decay widths and production rates. The CP violating asymmetries induced by those phases are also considered.

The calculations are done at the one-loop level. This is nontrivial since there are a large number of Feynman diagrams and various types of singularities (UV divergences, soft and collinear singularities, threshold singularities). We discuss in detail our calculation method and how to handle those divergences. In particular, the topic of one-loop remormalization and neutral-Higgs mixing effects in the complex MSSM for processes involving Higgs bosons are addressed.

The higher order corrections to the decay of charged Higgs bosons into a W-boson and the lightest neutral Higgs boson are calculated and shown to be significantly large. The CP asymmetry arising from all complex phases is considered, especially from the top-quark trilinear coupling, A_t, and μ, which induce a large contribution to the CP asymmetry.

We perform a complete calculation of the next-to-leading order (NLO) electroweak (EW) corrections to the charged Higgs production in association with a W-boson via the $b\bar{b}$ annihilation channel and a consistent combination with other contributions including the standard and supersymmetric-QCD corrections and the gg fusion, with resummation of the leading radiative corrections to the bottom-Higgs couplings and the neutral Higgs-boson propagators. We observe a strong dependence of the production rates on the phases of A_t and of the gluino-mass parameter M_3 and a large CP asymmetry arising mainly from the gg fusion.

The NLO EW corrections to the charged Higgs production in association with a top quark and a tagged bottom quark via gg fusion are calculated and shown to be still sizable even after subtracting the large $\tan\beta$ enhancement. The strong dependence of the NLO EW corrections on the phase of A_t is observed.

Our studies show the importance of the higher order corrections to the decays and the productions of the charged Higgs bosons in the complex MSSM. For the searches of charged Higgs bosons at the LHC, those corrections should be taken into account when doing analysis.

Acknowledgments

First of all, I would like to thank my PhD supervisor, Prof. Dr. Wolfgang Hollik, for accepting me as his student, giving me an interesting topic, continuous support and encouragement during my PhD study.

I would like to thank Dr. Lê Đức Ninh, my collaborator, for many helpful discussions, for patiently answering my countless questions and for using his private loop-integral code. Many thanks are also given to him for proof-reading this thesis and giving me many good suggestions.

My computational codes could not have run without a good computer system performed by Dr. Thomas Hahn and Dr. Peter Breitenlohner. Many thanks are given to them.

I would like to thank Dr. Frank Steffen for running the PhD life and organizing many fruitful block courses from which I have benefited. I would like also to thank the secretaries of the theory group, Rosita Jurgeleit and Monika Goldammer.

Sincere thanks are also given to many people in the phenomenology group including my office mates: Jan Germer, Edoardo Mirabella, Ananda Landwehr, Davide Pagani, Sophia Borowka for creating enjoyable working environment and helpful discussions. Especially many thanks are given to Jan Germer for proof-reading several chapters of this thesis, pointing out many mistakes and giving many good suggestions. I would like also to thank Michael Rauch for his help in translating the abtract to German and helpful suggestions.

Last but not at least, I thank my husband, Lê Đức Ninh, my daughter, Lê Chi Lan and my parents for their unconditional love and support.

Table of Contents

Chapter 1

Introduction

The Standard Model (SM) has successfully described three fundamental interactions (strong, weak and electromagnetic interactions) by using local gauge symmetry [1, 2, 3, 4, 5, 6, 7]. It is successful in the sense that most of its predictions have been shown to be consistent with experimental data. In the SM, the Higgs mechanism is used to break the electroweak (EW) gauge symmetry and thus generates masses for weak gauge bosons [8, 9, 10, 11, 12]. After EW symmetry breaking, there exists a neutral spin-0 particle, the Higgs boson. It is the only ingredient of the SM which has not been observed so far.

In spite of its success there exist many open questions indicating that the SM is only a limiting case of a more fundamental theory. Among many extensions of the SM, the Minimal Supersymmetric Standard Model (MSSM) is a promising one [13, 14, 15]. It extends the Poincaré group to include fermionic operators which can transform bosonic states to fermionic states and vice versa. As a consequence, each SM particles has a superpartner. However, supersymmetry (SUSY) cannot be an exact symmetry because if it were the superparticle mass should be equal to the mass of its corresponding SM partner and hence the superparticles should have been detected. No observation of superparticles indicates that if they exist they must be heavier than the SM partners and hence SUSY must be somehow broken. Independently of the SUSY breaking mechanism, soft SUSY breaking terms can be introduced to the low energy Langrangian [16]. The soft SUSY breaking parameters and the Higgsino mixing parameter, μ, in general are complex. If those parameters are assumed to be real, it is known as the real MSSM (rMSSM). Otherwise, one speaks of the complex MSSM (cMSSM).

With the new symmetry, the MSSM can provide good solutions to many problems of the SM. One of them is the well-known hierarchy problem: owing to the contribution of new particles, all quadratic divergences are cancelled and thus the EW scale is stablized [17, 18]. The MSSM allows for the unification of the three gauge couplings and gives an explanation for the EW symmetry breaking. The lightest superparticle can be a candidate for dark matter. Another problem relates to the matter-antimatter asymmetry which requires the existence of CP violation.

With only one complex phase of the Cabibbo-Kobayashi-Maskawa (CKM) matrix [19], the SM cannot explain the observed asymmetry. The cMSSM, however, can provide the required CP violation of the matter-antimatter asymmetry, but still satisfy other CP violating observables [20].

The MSSM Higgs sector has a richer structure than that of the SM. Unlike the SM where one Higgs doublet and its complex conjugate can be used to give masses to all fermions, the MSSM requires the existence of at least two Higgs doublets with opposite hypercharges. After EW symmetry breaking, there are three neutral (h, H and A) and a pair of charged Higgs ($H^{\pm}$) bosons. The discovery of charged Higgs bosons will be an unambiguous signal of physics beyond the SM. The Large Hadron Collider (LHC) has been successfully operating at 7 TeV center-of-mass energy and will be at 14 TeV for a future upgrade. Search for charged Higgs bosons is one of the purposes of the LHC [21, 22].

This thesis studies charged Higgs boson production and decay processes in the context of the cMSSM with minimal flavor violation. We consider the impact of the complex phases of the soft SUSY breaking parameters and of the Higgsino mixing parameter on the production rates and decay widths. We study also CP violating asymmetry arising from those phases. That observable quantifying the difference between a process and its CP conjugate process can be easily measured in experiment. Our studies are done for the LHC at both 7 TeV and 14 TeV.

We calculate the production rates and decay widths at one-loop level. There are at least two reasons to go beyond the tree level. First, the theoretical uncertainties are reduced. Second, the higher order corrections involve the entire particle spectrum and thus can be used to get more information of the theory. From the technical point of view, next-to-leading order (NLO) calculation is challenging since there are a large number of Feynman diagrams and various types of singularities (UV divergences, soft and collinear singularities, threshold singularities). We discuss in detail our calculation method and how to handle those divergences.

We first study the charged Higgs boson decay into a W-boson and the lightest neutral Higgs, h_1, which is one of important decay modes. Through loop contributions, the complex phases of the soft SUSY breaking parameters and of the Higgsino mixing parameter enter the Higgs sector, which is CP conserving at lowest order (see for example [23] and references therein). As a consequence, the three neutral Higgs bosons in general mix and form the neutral mass eigenstates $h_{1,2,3}$ with both CP-even and CP-odd properties, giving rise to a CP violating asymmetry in the decays $H^{\pm} \to W^{\pm} h_1$. A first calculation of the asymmetry arising from the phases of the trilinear $\tilde{\tau}$ coupling, A_{τ} and of gaugino mass, M_1, was done in [24]. In this thesis, we extend the calculation of [24] including contributions from all complex phases in the cMSSM, in particular from A_t, A_b and μ, which enter through Feynman diagrams with stop and sbottom involving large Yukawa couplings, further enhanced by the color factor. We show the results from the complete set of one-loop diagrams, including besides the Higgs self energies all the loop contributions to the $H^{\pm} \to W^{\pm} h_1$ vertex.

$pp \to W^{\mp}H^{\pm}$ is an interesting mechanism for charged Higgs boson production at the LHC. It does not only give a considerable production rate but also allows to study CP violating effects. There have been many discussions devoted to the $pp \to W^{\mp}H^{\pm}$ processes in the MSSM over the last two decades. These studies assume all the soft SUSY breaking parameters to be real and hence CP violation is absent [25, 26, 27, 28, 29, 30, 31, 32, 33, 34]. In this thesis, we extend the calculation for $pp \to W^{\pm}H^{\mp}$ to the MSSM with complex parameters. For the first time, the full NLO EW corrections to the $b\bar{b}$ annihilation channel are calculated and consistently combined with the other contributions including the standard and supersymmetric-QCD corrections and the gg fusion. We discuss CP-violating effects arising from the complex phases of A_t and M_3. The important issues related to the neutral Higgs mixing and large radiative corrections to the bottom–Higgs couplings are also systematically addressed.

Another mechanism for charged Higgs boson production is the one in association with a top quark and a bottom quark where the bottom quark is considered to be tagged. This is a potential channel for the searches of charged Higgs bosons at the LHC. The NLO SM-QCD and SUSY-QCD corrections to $pp \to H^-t\bar{b}$ were calculated in [35, 36]. Ref. [36] shows that the NLO QCD corrections are negative and their absolute values are smaller than 20% for a charged Higgs boson mass from 200 to 500 GeV with $p_{T,b} > 20$ GeV, $p_{T,b}$ is the transverse momentum of the bottom quark. The EW corrections may have large impact on the cross section and distributions and have not been studied yet. In this thesis, we study the EW corrections to the $gg \to H^-t\bar{b}$ process, which gives dominant contribution to $pp \to H^-t\bar{b}$, in the cMSSM.

The outline of this thesis is as follows. In Chapter 2, we give an overview of the SM, particle content, the Lagrangian density, and the Higgs mechanism. We discuss also several interesting features of a simple extension of the SM, the Two-Higgs-Doublet Models (THDMs), with an emphasis on the presence of the charged Higgs bosons. Some open questions of the SM are addressed.

In Chapter 3, we motivate the MSSM as a promising extension of the SM. We briefly describe the construction of a supersymmetric theory and apply it for the SM. The particle spectrum of the MSSM is also described in detail. We emphasize the Higgs sector with a richer structure than that of the SM but more predictive than the THDMs. We keep all the phases of the soft parameters which have considerable impacts on our calculations. A short review of the published results of the searches for the charged Higgs bosons is presented at the end of the chapter.

In Chapter 4, we discuss various singularities of the scalar integrals, UV divergences, soft and collinear singularities (they are considered as the special cases of Landau singularities). We describe in detail their conditions and treatments. For the UV divergences, we need regularization to calculate the divergent integrals and renormalization to remove the divergences. We address regularization schemes of dimensional regularization and of dimensional reduction, which is used in our calculation. We discuss the renormalization of the MSSM, in particular the Higgs and

gauge sector and the quark sector. For the soft and collinear singularities, we use the mass regularization scheme to separate the singular part and the finite part. To cancel the soft and collinear singularities the contributions from the radiation of a massless particle are added to the virtual contributions. We describe the phase space slicing and the dipole subtraction methods for phase space integration.

In Chapter 5, we first discuss how higher order corrections are included in the determination of the neutral Higgs boson masses. We then describe one-loop calculations involving the Higgs bosons in the external lines. Two improvements used in our calculation, the neutral Higgs boson propagator resummation and the effective bottom–Higgs couplings, are addressed in detail.

In Chapter 6, we consider all possible decay modes of the charged Higgs bosons. We then concentrate on the one-loop contributions to the charged Higgs decay modes $H^{\pm} \to W^{\pm}h_1$ and the CP asymmetry. The CP asymmetry arising from the phases of the trilinear couplings A_t, A_b, A_{τ}, of the gaugino mass M_1 and of the Higgsino mixing parameter μ are considered. We discuss also the normal threshold singularities (two-point Landau singularities enhanced by derivative) encountered in our calculations and how to treat them properly.

In Chapter 7, the NLO cross sections and CP asymmetry of the charged Higgs production in association with a W boson at the LHC are investigated. There are two partonic processes: $b\bar{b}$ annihilation and gg fusion. We present the calculation of the SM-QCD, SUSY-QCD and EW corrections to the former. gg fusion is a loop-induced process with the contributions arising from quark and squark loops, mainly of the third generation. We discuss also the check of QCD gauge invariance and the three-point Landau singularities. We use the two improvements mentioned in Chapter 5 and show that they have large impact on the cross sections and the CP asymmetry.

In Chapter 8, we study the exclusive cross section for the charged Higgs production in association with top and bottom quarks. At leading order, we compute all contributions of the order $\mathcal{O}(\alpha_s^2\alpha)$. They arise from the partonic processes, gg fusion, $q\bar{q}$ annihilations $q = u, d, c, s, b$. Other contributions of order $\mathcal{O}(\alpha_s\alpha^2)$ arising from $g\gamma$ induce is also included. The gg contribution is dominant. We present the calculation of the NLO EW corrections to $gg \to H^-t\bar{b}$ and show that the corrections are still sizable even after subtracting the large $\tan\beta$ enhancement effects.

The conclusions are presented in Chapter 9.

This thesis includes several appendices. The notations and conventions are presented in Appendix A. In Appendix B, we list the dipole subtraction functions used in our calculations. The counterterms and renormalization constants are collected in Appendix C. We present an explicit calculation of Δm_b in Appendix D. Appendix E contains the two-body decay widths of all possible decay modes of the charged Higgs bosons. In Appendix F, we describe our input parameters.

Chapter 2

The Standard Model

2.1 Introduction

The Standard Model is a fundamental theory which describes the electromagnetic, weak and strong interactions. Many of its predictions have been tested and are in good agreement with experimental results [37, 38]. These successes make it play a center role in particle physics. It is a Yang-Mills theory based on the direct product of the external Poincarè symmetry group and the internal gauge symmetry group SU(3)$_C\otimes$ SU(2)$_L\otimes$U(1)$_Y$ group. The gauge group SU(3)$_C$ is used to describe strong interaction in terms of Quantum Chromodynamics (QCD) [4, 5, 6, 7]. The electromagnetic and weak interactions are unified in the EW theory based on the symmetry group SU(2)$_L\otimes$U(1)$_Y$ [1, 2, 3].

The particle spectrum of the SM consists of 6 leptons $(\nu_e, e, \nu_\mu, \mu, \nu_\tau, \tau)$, 6 quarks (u, d, c, s, t, b) divided into 3 generations, 8 gluons (g^a) mediating strong interaction and 4 gauge bosons $(W^\pm, Z, \gamma)$ mediating electroweak interaction. The left-handed fermions are in doublets representations of SU(2)$_L$ while the right-handed (R) ones are singlets, except that there is no right-handed neutrino. The gauge bosons are in the adjoint representations of the corresponding gauge group. Gauge invariance requires all particles to be massless, however experiments show that particles mediating weak interaction $Z, W^\pm$ must be massive. This means the gauge symmetry must be broken somehow. In the SM one introduces the Higgs mechanism [8, 9, 10, 11, 12] to generate masses for the gauge bosons. Fermion masses arise from Yukawa interactions. The Higgs mechanism is based on the idea of spontaneous symmetry breaking, *i.e.* Lagrangian is gauge invariant but the vacuum is not [39, 40]. More details will be given in the next section. With a Higgs doublet of SU(2), the SM gauge group will be broken to SU(3)$_C\otimes$U(1)$_Q$, U(1)$_Q$ is symmetry group for Quantum Electrodynamics (QED). SU(3)$_C\otimes$U(1)$_Q$ is an exact symmetry of the theory since there is no evidence showing gluons and photon to be massive. Concerning other discrete symmetries, the model violates parity (P), charge conjugate (C) and also their combination CP. However, it automatically conserves the

baryon and lepton numbers.

The free parameters of the SM are three gauge couplings (g_s, g, g'), one vacuum expectation value (vev) of the Higgs field, the Higgs mass, nine fermion masses (neutrinos are assumed to be massless), three angles and one phase of the CKM matrix. In total, there are eighteen free parameters. All particles have been discovered in experiments except for the Higgs boson. The three gauge couplings have been measured quite accurately [37]. The relation between W-mass and Z-mass, the couplings among the three electroweak gauge bosons measured in experiments are in agreement with those predicted by the SM. Only the Higgs boson has not been observed so far.

2.2 The SM Lagrangian and the Higgs mechanism

The classical Lagrangian of the SM is composed of gauge, fermion, Higgs and Yukawa parts,

$$\mathcal{L} = \mathcal{L}_G + \mathcal{L}_F + \mathcal{L}_H + \mathcal{L}_Y. \tag{2.1}$$

Explicitly, the gauge part of the Lagrangian is given by

$$\mathcal{L}_G = -\frac{1}{4} G^a_{\mu\nu} G^{a\mu\nu} - \frac{1}{4} F^i_{\mu\nu} F^{i\mu\nu} - \frac{1}{4} B_{\mu\nu} B^{\mu\nu}, \tag{2.2}$$

where $a = 1, ..., 8$; $i = 1, 2, 3$ and

$$G^a_{\mu\nu} = \partial_\mu g^a_\nu - \partial_\mu g^a_\nu + g_s f^{abc} g^b_\mu g^c_\nu,$$
$$F^i_{\mu\nu} = \partial_\mu W^i_\mu - \partial_\mu W^i_\nu + g \epsilon^{ijk} W^j_\mu W^k_\nu,$$
$$B_{\mu\nu} = \partial_\mu B_\mu - \partial_\mu B_\nu, \tag{2.3}$$
$$\tag{2.4}$$

g^a are the SU(3) gauge fields, W^i are the SU(2) gauge fields, B is the U(1) gauge field, f^{abc} are the structure constants of SU(3) and ϵ^{ijk} are the structure constant of SU(2). The structure constants are real and totally antisymmetric in all indices. The fermionic part of the Lagrangian reads

$$\mathcal{L}_F = i\bar{l}_{iL}\gamma^\mu D_\mu l_{iL} + i\bar{e}_{iR}\gamma^\mu D_\mu e_{iR}$$
$$+ i\bar{Q}_{iL}\gamma^\mu D_\mu Q_{iL} + i\bar{u}_{iR}\gamma^\mu D_\mu u_{iR} + i\bar{d}_{iR}\gamma^\mu D_\mu d_{iR}, \tag{2.5}$$

where i is the generation index ($i = 1, 2, 3$),

$$l_{iL} = \left\{ \begin{pmatrix} \nu_e \\ e \end{pmatrix}_L, \begin{pmatrix} \nu_\mu \\ \mu \end{pmatrix}_L, \begin{pmatrix} \nu_\tau \\ \tau \end{pmatrix}_L \right\}, \qquad e_{iR} = \{e_R, \mu_R, \tau_R\}, \tag{2.6}$$

$$Q_{iL} = \left\{ \begin{pmatrix} u \\ d \end{pmatrix}_L, \begin{pmatrix} c \\ s \end{pmatrix}_L, \begin{pmatrix} t \\ b \end{pmatrix}_L \right\}, \qquad u_{iR} = \{u_R, c_R, t_R\}, \quad d_{iR} = \{d_R, s_R, b_R\}. \tag{2.7}$$

and the covariant derivatives

$$
D_\mu = \begin{cases}
\partial_\mu - ig T^i W^i_\mu - ig' Y B_\mu, & \text{for } l_{iL} \\
\partial_\mu - ig' Y B_\mu, & \text{for } l_{iR} \\
\partial_\mu - ig_s T^a_s G^a_\mu - ig T^i W^i_\mu - ig' Y B_\mu, & \text{for } Q_{iL} \\
\partial_\mu - ig_s T^a_s G^a_\mu - ig' Y B_\mu, & \text{for } u_{iR}, d_{iR},
\end{cases}
$$

contain group generators: $T^a_s = \lambda_a/2$, $T^i = \sigma_i/2$, λ_a are the Gell-Mann matrices, σ_i are the Paulli matrices and Y is the hypercharge ($Q = I_3 + Y/2$).

A SU(2) Higgs doublet, $\Phi = (\phi^+, \phi^0)^T$, with hypercharge ($Y = 1$) is introduced to the SM in order to give masses for the gauge bosons. The Higgs Lagrangian reads

$$
\mathcal{L}_H = (D_\mu \Phi)^\dagger (D^\mu \Phi) - V(\Phi), \quad V(\Phi) = -\mu^2 \Phi^\dagger \Phi + \lambda (\Phi^\dagger \Phi)^2, \tag{2.8}
$$

with μ^2 and λ constants.

Fermion masses are obtained from Yukawa interactions,

$$
\mathcal{L}_Y = -\lambda^e_{ij} \bar{L}^i \tilde{\Phi} e^j_R - \lambda^d_{ij} \bar{Q}^i \tilde{\Phi} d^j_R - \lambda^u_{ij} \bar{Q}^i \Phi u^j_R + \text{ h.c}, \tag{2.9}
$$

where $\lambda^{e,d,u}_{ij}$ ($i,j = 1,2,3$) are Yukawa couplings, and $\tilde{\Phi} = i\sigma_2 \Phi^*$.

Now we discuss the Higgs mechanism. The conditions for the scalar potential given in Eq. (2.8) to develop a non-zero expectation value ($\langle \Phi \rangle \neq 0$) to break the electroweak symmetry SU(2)$_L \times$U(1)$_Q$ down to the electromagnetic symmetry U(1)$_Q$ are following:

- the potential has to be bounded from below, therefore $\lambda > 0$,

- the potential has an unstable maximum at zero, hence $\mu^2 > 0$,

- the potential has stable minima which are degenerate.

Combining all above requirements, one can show that the vev of the Higgs doublet is

$$
\langle \Phi \rangle = \begin{pmatrix} |\langle \phi^+ \rangle| \\ |\langle \phi^0 \rangle| \end{pmatrix} = \begin{pmatrix} 0 \\ \frac{v}{\sqrt{2}} \end{pmatrix}, \quad v = \sqrt{\frac{\mu^2}{\lambda}}. \tag{2.10}
$$

The upper component carrying electric charge $Q = +1$ cannot have a non-zero expectation value since one requires unbroken U(1)$_Q$ symmetry. $|\langle \phi^0 \rangle| = v/\sqrt{2}$ coressponds to a circle on a complex plane, since ϕ^0 is complex scalar field. Choosing a specific point on that circle and expanding Higgs field around that point give

$$
\Phi(x) = \begin{pmatrix} \phi^+(x) \\ \phi^0(x) \end{pmatrix} = \begin{pmatrix} G^+(x) \\ (v + H(x) - iG^0(x))/\sqrt{2} \end{pmatrix}. \tag{2.11}
$$

Substituting the above expression into the scalar potential, one finds the neutral Higgs boson H to have a mass $m_H = \sqrt{2\lambda v^2}$. $G^\pm$ and G^0 are massless. They are

well known as Nambu-Goldstone bosons. They are unphysical states and can be absorbed by the gauge fields to generate masses for physical gauge bosons $W^\pm$ and Z,

$$
\begin{cases}
W_\mu^\pm = \frac{W_\mu^1 \mp i W_\mu^2}{\sqrt{2}}, \\
Z_\mu = c_W W_\mu^3 - s_W B_\mu, \\
A_\mu = s_W W_\mu^3 + c_W B_\mu,
\end{cases}
\tag{2.12}
$$

where $c_W = \cos\theta_W$, $s_W = \sin\theta_W$, θ_W is called the weak mixing angle and

$$
c_W = \frac{g}{\sqrt{g^2 + g'^2}}, \quad s_W = \frac{g'}{\sqrt{g^2 + g'^2}}.
\tag{2.13}
$$

The masses of W- and Z-bosons are given by

$$
M_W = \frac{gv}{2}, \quad M_Z = \frac{gv}{2c_W}.
\tag{2.14}
$$

The photon A_μ remains massless, since $U(1)_Q$ is not broken. The mass terms for the fermionic fields are obtained by substituting (2.11) into (2.9),

$$
\mathcal{L}_{\text{mass}}^f = -\frac{\lambda_{ij}^e v}{\sqrt{2}} \bar{e}_L^i e_R^j - \frac{\lambda_{ij}^d v}{\sqrt{2}} \bar{d}_L^i d_R^j - \frac{\lambda_{ij}^u v}{\sqrt{2}} \bar{u}_L^i u_R^j + \text{ h.c},
\tag{2.15}
$$

where the fermionic fields are the flavor states. In order to find mass eigenstates one needs to diagonalise the $\lambda^{e,u,d}$ matrices by unitary matrices, $V_{L,R}^{e,u,d}$ as follows,

$$
\lambda_f^{\text{diag}} = V_L^f \lambda^f V_R^{f\dagger}, \quad f_{L,R}^i \to V_{L,R,ij}^f f_{L,R}^j, \quad f = e, u, d.
\tag{2.16}
$$

Then the masses of the fermions are given by

$$
m_f = \frac{\lambda_f v}{\sqrt{2}}, \quad f = e, \mu, \tau, u, c, t, d, s, b.
\tag{2.17}
$$

Neutrinos are kept massless since they are purely left-handed in the minimal model and do not couple to the Higgs field. Those unitary transformations lead to the appearance of a unitary matrix in the charged current interaction, in particular

$$
\mathcal{L}_{Wud} = ig V_{\text{CKM}}^{*ij} \bar{d}_L^i \gamma^\mu u_L^j W_\mu^- + \text{ h.c}, \quad V_{\text{CKM}} = V_L^u V_L^{d\dagger}.
\tag{2.18}
$$

V_{CKM} is the well-known CKM matrix [19]. A general 3×3 unitary matrix can be parameterized by nine independent parameters. For the CKM matrix, one can remove five of them by rephasing six quark fields. The four remaining parameters are three mixing angles and one phase which are the only source of flavor and CP violations in the SM. For the lepton sector, there is no such similar matrix since neutrinos are massless one can chose their rotation matrice equal to the one of the charged leptons, then that matrix is a unit matrix.

However, the evidence of the neutrino oscillations requires massive neutrinos (at least two of three neutrinos have masses), then there is an appearance of a flavor

mixing matrix V^{PMNS} [41]. Different from the CKM matrix, the PMNS matrix can have two additional complex phases due to the possibility of neutrinos being Majorana fermions. It is an interesting topic for many extensions of the SM. In this thesis we always consider neutrinos to be massless. Neutrino masses are irrelevant for our considered processes.

Another observation is that the unitarity of the CKM matrix assures the absence of the flavor changing neutral currents (FCNC) at tree level. This property is known as the GIM mechanism [42].

2.3 The Two-Higgs-Doublet models

One introduces the Higgs mechanism to break the EW symmetry spontaneously, thus to generate particle masses. The Higgs sector of the SM is minimal since only one Higgs doublet is used. However, there is no experimental and theoretical constraint on the number of the Higgs bosons. It is possible to extend the Higgs sector of the SM. A simple extension is the one with an addition of an extra Higgs doublet. These models are called the Two-Higgs-Doublet models. The addition of the new Higgs doublet leads to several interesting features as follows.

1. The spectrum of the Higgs sector consists of three neutral Higgs bosons (two CP-even states h, H and one CP-odd state A) and two charged Higgs bosons $H^{\pm}$.

2. The models can introduce a new source of CP violation [43]. Besides CP symmetry is broken explicitly by the complex phase of the CKM matrix in the SM, the THDMs can introduce a new phase which is the relative phase between the two expectation values (v_1 and v_2) of the two Higgs doublets leading to the spontaneous CP symmetry breaking.

3. The free parameters of the Higgs sector are four masses ($m_h, m_H, m_A, m_{H^{\pm}}$) and two mixing angles ($\tan \beta = v_2/v_1$ and the mixing angle α between the two CP-even Higgs bosons).

4. FCNCs can appear at tree level due to the fact that both the Higgs doubles can couple to all fermions. The experimental restrictions on the FCNCs lead to three types of models.

   - The THDM type I, only one Higgs doublet couples to all fermions [44]. This model is similar to the SM. The differences are a smaller vev and larger Yukawa couplings.

   - The THDM type II, one Higgs doublet couples to up-type fermions while the other couples to down-type fermions [45]. The MSSM belongs to this type.

- The THDM type III, this is the most general THDM without FCNC at tree level [46]. Both the two Higgs doublets couple to the up- and down-type fermions but their Yukawa couplings matrices must be diagonalized simultaneously with the quark mass matrix.

In a general THDM, there is the appearance of charged Higgs bosons. The finding of these charged Higgs bosons would confirm a richer spectrum of the Higgs sector compared to the one of the SM.

2.4 Why go beyond the SM?

Despite of great agreements between the SM predictions and the experimental data. The SM is not satisfactory. The reasons can be classified into two groups. The first group is related to the following conceptual problems.

- The SM does not describe gravity which becomes important at small distance (equivalently high energy like the Planck scale, 10^{-19} GeV). An attempt to incorporate gravitational force together with other forces is string theory.

- The SM is not the ultimate theory. It is believed to be an effective theory valid to a certain energy scale. Then this leads to the hierarchy problem. It is due to the appearance of quadratic divergences in the theory. More details are given in Section 3.1.

- The SM describes three interactions but their gauge couplings do not unify: $\alpha_s = g_s^2/4\pi$ and $\alpha = g^2/4\pi$ meet at 10^{16} GeV while α and $\alpha' = g'^2/4\pi$ meet at about 10^{13} GeV. In *Grand Unified Theories* (GUT), by using one simple Lie group as the symmetry group, the three interactions emerge into a single interaction. Examples of GUT groups are SU(5) and SO(10); for a review see [47].

- The SM does not explain why the number of generations is three. An possible extension of the SM such as the 331 models based on the symmetry group $SU(3)_C \otimes SU(3)_L \otimes U(1)_N$ [48] can give an explanation. In such models, the absence of chiral anomaly requires the number of generations to be three.

The second group is related to the following experimental indications of new physics beyond the SM.

- Experiments on neutrino oscillations have established that neutrinos have a mass (for a review see [49]). The SM assumes neutrinos to be massless. The neutrino mass-squared differences and mixing angles are measured by the oscillation experiments. Limits on the absolute mass scale which are obtained from non-oscillation experiments show that neutrino masses are very small ($m_\nu < 2$ eV) [37].

- An impressive amount of data from the observations of the rotation curves of galaxies, studies of microwave background radiation and supernova distant measurements indicates the existence of dark matter. The observations do not provide any information about what the dark matter is made of, but give some properties of dark matter. It must be stable (its lifetime must be higher than the age of the Universe), slow (cold dark matter), electrically and color neutral and massive; for a review see [50]. The SM cannot provide any candidate for dark matter. Even if the neutrinos are massive, they cannot be viable dark matter candidates since their masses are not sufficient to provide the observed dark matter densities.

- The observable universe has more matter than antimatter. This is well known as the matter-antimatter asymmetry. In order to explain such asymmetry, the three Sakharov conditions must be fulfilled [51]. One of the three conditions is the existence of CP violation. With only one CKM phase, the SM does not contain enough CP violation to explain the observed asymmetry, for a review see [20]. This makes many extensions of the SM which provide new sources of CP violation very attractive.

- The anomalous magnetic moment of muon is measured accurately in experiment and precisely predicted in the SM [52]. The experimental measurements have shown a deviation of about 3σ above the SM prediction (for a review see [53]). This has led to many speculations on the presence of new physics. SUSY extensions can provide a good explanation for this discrepancy, thanks to the additional contributions from the supersymmetric particle loops.

Among many extensions of the SM, we focus on the supersymmetric version of the SM, especially the MSSM which is a promising candidate. It can provide solutions to many of the above questions. We discuss it in the next chapter.

Chapter 3

Supersymmetry

3.1   Introduction

Supersymmetry (SUSY) is a symmetry between bosons and fermions. In other words, this symmetry allows bosonic particles, which have integer spin and obey Bose-Einstein statistics, and fermionic particles, which have half-integer spin and obey Fermi-Dirac statistics, to be in the same multiplet. It was born in the early 1970s, but there is, to date, no direct experimental evidence of its relevance to nature. However, its beautiful idea and mathematical formulation have been applied widely, then resulted in many theories such as the MSSM, supergravity and superstring, etc. Especially the MSSM has inspired an enormous amount of theoretical and experimental studies. Indeed, supersymmetry plays a central role in the development of physics beyond the SM.

Here some important historical events related to the birth of supersymmetry are reviewed. Supersymmetry started with a desire to find a symmetry that relates particles with different spins. In the 1960s, some attempts to find such a symmetry have been made but failed. One example is SU(6) symmetry in the non-relativistic quark model. Those failures led to the so-called no-go theorem [54] proved by Coleman and Mandula in 1967. They shown that the most general Lie algebra of symmetry operators consists of the generators P_μ and $M_{\mu\nu}$ of the Poincaré group and internal symmetry generators, *e.g.* SU(3) color, SU(2) isospin, U(1) hypercharge generators, etc. The latter must commute with the former. It means that the internal symmetries cannot relate particles with different masses and spins. One of the assumptions in Coleman and mandula's proof turned out to be unnecessary: they had made all transformation parameters to be ordinary numbers and their corresponding operators to obey the commutation relations. In fact this theorem does not apply for the Grassmann numbers and fermionic symmetry generators which obey anticommutation relations. This was first proposed by Golfand and Likhtman in 1971 [55]. They extended the Poincaré algebra to include fermionic generators. Followed up by Volkov and Akulov, they discovered supersymmetry in four dimensions in a non-

linear realization in 1973 [56]. Independently, Wess and Zumino [57, 58] presented a renormalizable field model of a spin-1/2 particle in interaction with two spin-0 particles where particles are related by a symmetry transformation. In 1976, Freedman, van Nieuwenhuizen and Ferrara [59] and independently Deser and Zumino [60] used the idea of local supersymmetry to construct the supergravity.

The first classification of all supersymmetry algebras was done by Haag, Lopuszanski and Sohnius [61] in 1974. They built the supersymmetry algebra based on the generators of the Poincaré group and additional fermionic generators $Q_{\alpha i}$ and their Hermitian adjoint $\bar{Q}^i_{\dot{\alpha}}$; $\alpha, \dot{\alpha}$ are spinor indices taking two values $1, 2$ while the indices i, j label different Q_α and run from 1 to some integer N, see Section 3.2 for more details. These fermionic operators change a bosonic state into a fermionic state and vise versa. In particular, they raise or lower the projection value of spin along the z axis by one half. In general, there are at most $2N$ independent raising operators and $2N$ lowering operators. For $N = 1$, there is only one Q. This is known as the simple supersymmetry. If $N > 1$, we speak of an extended supersymmetry. However, N cannot be arbitrary. $N \leq 8$ if one requires no particles with spin > 2 in the supermultiplets. Now one wishes to incorporate those supersymmetry into a realistic theory, particularly the SM which is based on the $SU(3) \otimes SU(2) \otimes U(1)$ gauge group. Since quarks and leptons belong to chiral representations (complex representations), it is impossible to apply the extended supersymmetry. Because in the extended supersymmetry, fermions and vector bosons are in the same multiplet and the latter belongs to a real representation, not a complex one. The only case can be used is $N = 1$. This makes our supermultiplets much simpler. There is only one superpartner corresponding to a particle in a supermultiplet. The superpartners of quarks and leptons are now scalar bosons.

Although no experimental evidence shows to date the existence of supersymmetry in nature, many physicists find it interesting and think that it may relate to the real world. Here we review two major arguments in favor of supersummetry. The first argument is based on Haag, Lopuszanski and Sohnius theorem [61] from which we learn that the largest symmetry an interaction theory may have is the direct product of a supersymmetry and an internal gauge group. One has been very successful in describing three fundamental interactions by using two of its three ingredients, the Poincaré group and the internal gauge group. It would be better if one could incorporate all three ingredients into a theory.

The second argument relates to the hierarchy problem [17, 18]: why $M_Z \ll M_P$? Here M_Z is a typical electroweak scale and M_P is the Planck scale where gravity becomes as strong as the other interactions. This hierarchy problem leads to the instability of the electroweak scale as seen in the following. Consider a theory which contains fermions and bosons like the SM. When one computes the radiative corrections to the Higgs boson mass, one encounters quadratic divergences. At one-

loop level, the correction is given by (see for example [62]),

$$\delta m_H^2 = \frac{1}{8\pi^2} \left(N_B \lambda_B - N_F \lambda_F^2 \right) \Lambda^2$$
$$+ \frac{1}{4\pi^2} \left(N_B \lambda_B m_B^2 \log \frac{\Lambda}{m_B} - N_F \lambda_F^2 m_F^2 \log \frac{\Lambda}{m_F} \right) + \cdots \qquad (3.1)$$

where the cutoff Λ represents the scale up to which the SM remains valid, the dots stand for finite terms, N_B, N_F are the number of bosons and fermions corresponding to their masses m_B, m_F and their couplings λ_B, λ_F, respectively. In the SM there is neither a relation between N_B and N_F nor λ_B and λ_F. If we chose the cutoff to be the GUT scale, $M_{\text{GUT}} \sim 10^{16}$ GeV, or the Planck mass $M_P \sim 10^{19}$ GeV, this radiative correction will be much larger than the physical Higgs mass which is bounded ($m_H \lesssim 1$ TeV) due to unitarity and perturbative reasons. The same problem happens to the radiative corrections to W and Z boson masses. One can say this is not a problem for a renormalizable theory: one can redefine bare parameter, which is not physical value, to absorb all divergences. Then the quantum corrections remain small. However, this seems unnatural in comparison with the case of fermions or photon: for fermions one-loop corrections are proportional to its mass m_F and only logarithmically divergent, owing to a chiral symmetry that keep the corrections naturally small, for photon radiative corrections to its mass vanish at all order due to gauge symmetry. For bosons, there is no such symmetry that renders small boson mass natural.

In supersymmetry, there are equal numbers of fermions and bosons, $N_B = N_F$. The couplings are also equal, $\lambda_B = \lambda_F^2$. These lead to cancellation of the quadratic divergences, leaving

$$\delta m_H^2 = \frac{N_F \lambda_F^2}{4\pi^2} \left(m_B^2 - m_F^2 \right) \log \frac{\Lambda}{m_B} + \cdots . \qquad (3.2)$$

The correction remains small even for $\Lambda \sim M_P$ provided that $|m_B^2 - m_F^2| \lesssim 1\text{TeV}^2$. In fact the correction will vanish if the boson and the fermion masses are the same. That happens when supersymmetry is not broken. Supersymmetry is not the only way to solve this naturalness problem. There are other solutions. For example in technicolour model the Higgs boson is not a fundamental particle but a composite state, for a review see [63] and references therein. Lagrangian for the Higgs sector becomes an effective theory and valid up to a scale which the composite state reveals. This scale should not be as large as the Planck mass and not too far from electroweak scale, then $\delta m_H^2 \sim m_H^2$. However, the argument based on symmetry to prevent large quantum corrections is, in general, more favored by theorists.

Apart from the aforementioned arguments there are additional motivations existing in some specific realizations of supersymmetry. The MSSM is the most famous example.

- The MSSM allows for the unification of three gauge couplings at GUT scale (for a review see [64]).

- The lightest Higgs particle is predicted to have mass less than 140 GeV while it is a free parameter in the SM [65, 66].

- It provides a possible explanation for the origin of the electroweak symmetry breaking [64].

- The lightest superparticle can be a candidate for dark matter.

- It contains new sources of CP violation.

- The predicted anomalous magnetic moment of muon is consistent with the measured value [67].

Now we are going to construct the Lagrangian of a supersymmetric theory. It is compact and elegant to use the superfield language. In the following sections we discuss all the necessary ingredients used for our purpose.

3.2 Supersymmetry algebra

In Haag, Lopuszanski and Sohnius theorem [61], the most general supersymmetry algebra or Poincaré superalgebra is given by

$$[P_\mu, P_\nu] = 0, \tag{3.3}$$

$$[P_\mu, M_{\rho\sigma}] = i(\eta_{\mu\rho}P_\sigma - \eta_{\mu\sigma}P_\rho), \tag{3.4}$$

$$[M_{\mu\nu}, M_{\rho\sigma}] = i(\eta_{\nu\rho}M_{\mu\sigma} + \eta_{\mu\sigma}M_{\nu\rho} - \eta_{\mu\rho}M_{\nu\sigma} - \eta_{\nu\sigma}M_{\mu\rho}), \tag{3.5}$$

$$[Q_{\alpha i}, M_{\mu\nu}] = \frac{1}{2}(\sigma_{\mu\nu})_\alpha{}^\beta Q_{i\beta}, \tag{3.6}$$

$$[\bar{Q}^i_{\dot{\alpha}}, M_{\mu\nu}] = -\frac{1}{2}\bar{Q}^i_{\dot{\beta}}(\bar{\sigma}_{\mu\nu})^{\dot{\beta}}{}_{\dot{\alpha}}, \tag{3.7}$$

$$[Q_{\alpha i}, P_\mu] = [\bar{Q}^i_{\dot{\alpha}}, P_\mu] = 0, \tag{3.8}$$

$$\{Q_{\alpha i}, \bar{Q}^j_{\dot{\beta}}\} = 2\delta^j_i(\sigma^\mu)_{\alpha\dot{\beta}}P_\mu, \tag{3.9}$$

$$\{Q_{\alpha i}, Q_{\beta j}\} = 2\varepsilon_{\alpha\beta}Z_{ij}, \tag{3.10}$$

$$\{\bar{Q}^i_{\dot{\alpha}}, \bar{Q}^j_{\dot{\beta}}\} = 2\varepsilon_{\dot{\alpha}\dot{\beta}}Z^{ij}, \quad \text{with } Z^{ij} = Z^\dagger_{ij}, \ Z_{ij} = -Z_{ji}, \tag{3.11}$$

where $\alpha, \beta(\dot{\alpha}, \dot{\beta})$ are undotted (dotted) spinor indices, $i, j = 1, N$ with N being an integer, Z_{ij} are some linear combination of internal symmetry generators. Z_{ij} commute with anything, therefore they are called central charges. The largest possible internal symmetry which can act non-trivially on Q is $U(N)$. It, however, is unnecessary to be a symmetry of action. When $N = 1$, there is only one Q. Due to the antisymmetric characteristic, Z vanishes. The non-trivial acting internal symmetry now is the $U(1)$ which has become known as R-symmetry. The supersymmetry

algebra has its simplest form,

$$\begin{aligned}
\{Q_\alpha, Q_\beta\} = \{\bar{Q}_{\dot{\alpha}}, \bar{Q}_{\dot{\beta}}\} &= 0, \\
\{Q_\alpha, \bar{Q}_{\dot{\beta}}\} &= 2(\sigma^\mu)_{\alpha\dot{\beta}} P_\mu, \\
[Q_\alpha, P_\mu] &= [\bar{Q}_{\dot{\alpha}}, P_\mu] = 0.
\end{aligned} \tag{3.12}$$

3.3 Superspace and superfields

Superspace is the Minkowski space plus four additional coordinates which are anti-commuting Grassmann numbers (see Appendix A.3). Hence, superspace has eight dimensions. A point in the superspace is given by the supercoordinates $(x^\mu, \theta_\alpha, \bar{\theta}_{\dot{\alpha}})$, $\mu = 1, 2, 3, 4$, $\alpha = 1, 2$ and $\dot{\alpha} = \dot{1}, \dot{2}$. Here we use the Weyl formalism. θ and $\bar{\theta}$ are Weyl spinors (see Appendix A.2 for more details). A superfield is an operator-valued function defined on the superspace. A general superfield can be expanded in terms of the Grassmann variables θ and $\bar{\theta}$ as

$$\begin{aligned}
\Phi(x, \theta, \bar{\theta}) =~& \phi(x) + \theta\psi(x) + \bar{\theta}\bar{\chi}(x) + \theta\theta F(x) + \bar{\theta}\bar{\theta} F'(x) + (\theta\sigma^\mu\bar{\theta}) V_\mu(x) \\
& + (\theta\theta)\bar{\theta}\bar{\lambda}(x) + (\bar{\theta}\bar{\theta})\theta\lambda'(x) + (\theta\theta)(\bar{\theta}\bar{\theta}) D(x).
\end{aligned} \tag{3.13}$$

Owing to the anticommuting properties of Grassmann variables, the higher power terms of θ and $\bar{\theta}$ vanish. All x-dependent functions on the right-hand side of Eq. (3.13) are called component fields. Since the superfield is a Lorentz scalar or pseudoscalar, the Lorentz properties of the component fields are given by

$$\begin{aligned}
\phi(x), F(x), F'(x), D(x) &: \text{complex scalar or pseudoscalar fields,} \\
\psi(x), \lambda'(x) &: \text{left-handed Weyl spinor fields,} \\
\bar{\chi}(x), \bar{\lambda}(x) &: \text{right-handed Weyl spinor fields,} \\
V_\mu(x) &: \text{complex vector field.}
\end{aligned}$$
$$\tag{3.14}$$

A general superfield contains 16 bosonic and 16 fermionic real degrees of freedom. Now we need to know how the superfield transforms under a supersymmetry transformation. First, we use the operator

$$L(x, \theta, \bar{\theta}) = e^{i(x^\mu P_\mu + \theta_\alpha Q^\alpha + \bar{\theta}^{\dot{\alpha}} \bar{Q}_{\dot{\alpha}})}, \tag{3.15}$$

to define

$$\Phi(x, \theta, \bar{\theta}) = L(x, \theta, \bar{\theta}) \Phi(0, 0, 0). \tag{3.16}$$

With the help of the *Baker-Campbell-Hausdorff formula* ($e^A e^B = e^{A+B+\frac{1}{2}[A,B]}$) and supersymmetry algebra (3.12), one can show that under a finite supersymmetry transformation denoted by T_ξ, a superfield transforms as

$$\begin{aligned}
T_\xi \Phi(x^\mu, \theta, \bar{\theta}) &= L(0, \xi, \bar{\xi}) \Phi(x^\mu, \theta, \bar{\theta}) \\
&= \Phi(x^\mu + i\xi\sigma^\mu\bar{\theta} - i\theta\sigma^\mu\bar{\xi}, \theta + \xi, \bar{\theta} + \bar{\xi}).
\end{aligned} \tag{3.17}$$

We now can find out a differential operator representation of Q and $\bar{Q}$ by using an infinitesimal supersymmetry transformation T_ρ to act on the superfield, thus

$$L(0, \rho, \bar{\rho})\Phi(x^\mu, \theta, \bar{\theta}) - \Phi(x^\mu, \theta, \bar{\theta}) = \Phi(x^\mu + i\rho\sigma^\mu\bar{\theta} - i\theta\sigma^\mu\bar{\rho}, \theta + \rho, \bar{\theta} + \bar{\rho}) - \Phi(x^\mu, \theta, \bar{\theta}).$$
(3.18)

Expanding the two sides of Eq. (3.18) in terms of infinitesigmal parameters $\rho, \bar{\rho}$ we get the left-hand side (LHS)

$$\text{LHS} = (i\rho_\alpha Q^\alpha + i\bar{\rho}^{\dot{\alpha}}\bar{Q}_{\dot{\alpha}})\Phi(x^\mu, \theta, \bar{\theta}),$$
(3.19)

and the right-hand side (RHS)

$$\text{RHS} = \Big[(i\rho\sigma^\mu\bar{\theta} - i\theta\sigma^\mu\bar{\rho})\partial_\mu + \rho_\alpha\frac{\partial}{\partial\theta_\alpha} + \bar{\rho}^{\dot{\alpha}}\frac{\partial}{\partial\bar{\theta}^{\dot{\alpha}}}\Big]\Phi(x^\mu, \theta, \bar{\theta}).$$
(3.20)

Identifying terms on two sides, one gets

$$Q^\alpha = -i\frac{\partial}{\partial\theta_\alpha} + (\sigma^\mu\bar{\theta})^\alpha\partial_\mu, \quad \bar{Q}_{\dot{\alpha}} = -i\frac{\partial}{\partial\bar{\theta}^{\dot{\alpha}}} - (\theta\sigma^\mu)_{\dot{\alpha}}\partial_\mu.$$
(3.21)

The supersymmetry covariant derivatives, which are useful for the construction of the supersymmetric Lagrangian, are invariant under the supersymmetry transformation in the sense that

$$\{D_\alpha, Q_\alpha\} = \{D_\alpha, \bar{Q}_\alpha\} = \{\bar{D}_\alpha, Q_\alpha\} = \{\bar{D}_\alpha, \bar{Q}_\alpha\} = 0,$$
(3.22)

then one finds

$$D_\alpha = \frac{\partial}{\partial\theta^\alpha} + i(\sigma^\mu\bar{\theta})_\alpha\partial_\mu, \quad \bar{D}_{\dot{\alpha}} = -\frac{\partial}{\partial\bar{\theta}^{\dot{\alpha}}} - i(\theta\sigma^\mu)_{\dot{\alpha}}\partial_\mu.$$
(3.23)

With the help of the covariant derivatives, one defines the following irreducible representations of the superfields,

$$\bar{D}_{\dot{\alpha}}\Phi(x, \theta, \bar{\theta}) = 0 \qquad \Rightarrow \text{(left-handed) chiral superfield,} \tag{3.24}$$

$$D_\alpha\Phi^\dagger(x, \theta, \bar{\theta}) = 0 \qquad \Rightarrow \text{(right-handed) anti-chiral superfield,} \tag{3.25}$$

$$\Phi(x, \theta, \bar{\theta}) = \Phi^\dagger(x, \theta, \bar{\theta}) \quad \Rightarrow \text{vector superfield.} \tag{3.26}$$

We now want to find the expression of the chiral superfield in terms of component fields by solving the condition (3.24). It can be easily done by changing variables $x^\mu \to y^\mu = x^\mu + i\theta\sigma^\mu\bar{\theta}$. One can show that $\bar{D}_{\dot{\alpha}}\Phi_1(y, \theta) = 0$. Therefore, the chiral superfield $\Phi_1(x, \theta, \bar{\theta}) = \Phi_1(y, \theta)$ which has the power series expansion in θ:

$$\Phi_1(y, \theta) = \phi(y) + \sqrt{2}\theta\psi(y) + \theta\theta F(y). \tag{3.27}$$

In terms of the original variables $(x, \theta, \bar{\theta})$,

$$\begin{aligned}
\Phi_1(x, \theta, \bar{\theta}) &= e^{i\theta\sigma^\mu\bar{\theta}\partial_\mu}\Big(\phi(x) + \sqrt{2}\theta\psi(x) + \theta\theta F(x)\Big) \\
&= \phi(x) + \sqrt{2}\theta\psi(x) + i\theta\sigma^\mu\bar{\theta}\partial_\mu\phi(x) + \frac{i}{\sqrt{2}}(\theta\theta)(\bar{\theta}\bar{\sigma}^\mu\partial_\mu\psi(x)) \\
&\quad + \theta\theta F(x) - \frac{1}{4}(\theta\theta)(\bar{\theta}\bar{\theta})\Box\phi(x).
\end{aligned} \tag{3.28}$$

Similarity for the anti-chiral superfield, one can solve the constraint (3.25) by changing variables $x^\mu \to z^\mu = x^\mu - i\theta\sigma^\mu\bar\theta$. Then the solution is

$$\Phi_2(x, \theta, \bar\theta) = \Phi_2(z, \bar\theta) = e^{-i\theta\sigma^\mu\bar\theta\partial_\mu}\left(\phi(x) + \sqrt{2}\bar\theta\bar\psi(x) + \bar\theta\bar\theta F(x)\right). \qquad (3.29)$$

One can easily show that the Hermitian conjugate of the chiral superfield is a anti-chiral superfield. Under an infinitesimal supersymmetry transformation, the component fields of a chiral superfield transform as

$$\begin{aligned}
\delta_S\phi(x) &= \sqrt{2}\theta\psi(x), & (3.30)\\
\delta_S\psi(x) &= i\sqrt{2}\sigma^\mu\bar\theta\partial_\mu\phi(x) + \sqrt{2}\theta F(x), & (3.31)\\
\delta_S F(x) &= \partial_\mu\left(-i\sqrt{2}\psi(x)\sigma^\mu\bar\theta\right). & (3.32)
\end{aligned}$$

For the vector superfield denoted as V, the condition (3.26) requires it to be real. Hence its complete expansion is

$$\begin{aligned}
V &= C(x) + \theta\chi(x) + \bar\theta\bar\chi(x) + \frac{1}{2}\theta\theta\left(M(x) + iN(x)\right)\\
&\quad + \frac{1}{2}\bar\theta\bar\theta\left(M(x) - iN(x)\right) + (\theta\sigma^\mu\bar\theta)V_\mu(x) + (\theta\theta)\bar\theta\left(\bar\lambda(x) + \frac{i}{2}\bar\sigma^\mu\partial_\mu\chi(x)\right)\\
&\quad + (\bar\theta\bar\theta)\theta\left(\lambda(x) + \frac{i}{2}\sigma^\mu\partial_\mu\bar\chi(x)\right) + \frac{1}{2}(\theta\theta)(\bar\theta\bar\theta)\left(D(x) - \frac{1}{2}\partial_\mu\partial^\mu C(x)\right). (3.33)
\end{aligned}$$

The supersymmetric generalization of a gauge transformation for a general non-Abelian case is defined as

$$\begin{aligned}
\Phi &\to e^{-i2g\mathbf{\Lambda}}\Phi, & (3.34)\\
\Phi^\dagger &\to \Phi^\dagger e^{i2g\mathbf{\Lambda}^\dagger}, & (3.35)\\
e^{2g\mathbf{V}} &\to e^{-i2g\mathbf{\Lambda}^\dagger}e^{2g\mathbf{V}}e^{i2g\mathbf{\Lambda}}, & (3.36)
\end{aligned}$$

where g is coupling constant and $\mathbf{\Lambda} = \Lambda^a T^a$ and $\mathbf{V} = V^a T^a$ with Λ^a being chiral superfields, V^a being vector superfield and T^a being the generators of the gauge group.

Eq. (3.33) shows that the vertor superfield contains many component fields. Some of them can be eliminated by exploiting gauge invarance. In practice, it is convenient to work in the Wess-Zumino gauge [58] where C, χ, M and N fields are set to be zero, then

$$V = (\theta\sigma^\mu\bar\theta)V_\mu(x) + (\bar\theta\bar\theta)\theta\lambda(x) + (\theta\theta)\bar\theta\bar\lambda(x) + \frac{1}{2}(\theta\theta)(\bar\theta\bar\theta)D(x). \qquad (3.37)$$

For an Abelian gauge theory, the behaviors of the component fields under an infinitesimal supersymmetry transformation are

$$\begin{aligned}
\delta_S\lambda &= -iD\theta - \frac{1}{2}\sigma^\mu\bar\sigma^\nu\theta(\partial_\mu V_\nu - \partial_\nu V_\mu), & (3.38)\\
\delta_S V^\mu &= i(\theta\sigma^\mu\bar\lambda - \lambda\sigma^\mu\bar\theta), & (3.39)\\
\delta_S D &= \partial_\mu\left(-\theta\sigma^\mu\bar\lambda + \lambda\sigma^\mu\bar\theta\right). & (3.40)
\end{aligned}$$

We now discuss the F and D component fields. They are auxiliary fields, F is a complex scalar field while D is a real scalar field. The appearance of these auxiliary fields is to ensure the equality of the bosonic and fermionic degrees of freedom in a supermultiplet for off-shell as well as on-shell consideration. In a four-dimensional theory those F and D fields have mass dimension two. They do not contribute to the propagating degrees of freedom because the kinetic terms are absent. They will be eliminated by applying the on-shell equation of motion. It is important to note that they transform into total space-time derivatives under the supersymmetry transformation, see Eq. (3.32) and Eq. (3.40). Therefore, the space-time integrals of those terms are supersymmetry invariances. This characteristic is used to build the supersymmetric Lagrangian.

Finally, we list here some useful characteristics of the superfields which are needed in the construction of a supersymmetric Lagrangian.

- The product and sum of two chiral superfields are again chiral superfields.

- The product and sum of two vector superfields are also vector superfields.

- The sum of a chiral superfield and an anti-chiral superfield is a vector superfield.

- The product of a chiral superfield and an anti-chiral superfield is a vector superfield.

3.4   Supersymmetric Lagrangian

As we have seen in the previous section, the space-time integrals of the F-term of the chiral superfields and the D-term of the vector superfields are invariant under the supersymmetry transformation. One can build a general supersymmetric Lagrangian as the sum of these terms. The F- and D-terms are found by integrating out the Grassmann variables of a superfield, particularly

$$\mathcal{L}_{\text{SUSY}} = \mathcal{L}_F + \mathcal{L}_D = \int d^2\theta \mathcal{L}_f + \int d^2\theta d^2\bar{\theta} \mathcal{L}_d, \qquad (3.41)$$

where $\mathcal{L}_f$ is a chiral superfield and $\mathcal{L}_d$ is a vector superfield.

Now we consider the first term. We can use the property of the superfields, namely the product and sum of two chiral superfields is a chiral superfield. The general chiral superfield $\mathcal{L}_f$ can be built from other chiral superfields as

$$\mathcal{L}_f \equiv \mathcal{W} = \sum_i a_i \Phi_i + \frac{1}{2} \sum_{ij} m_{ij} \Phi_i \Phi_j + \frac{1}{3!} \sum_{ijk} \lambda_{ijk} \Phi_i \Phi_j \Phi_k, \qquad (3.42)$$

where m_{ij} and λ_{ijk} are totally symmetric matrices and $i, j = 1, ..., N$ with N being the number of chiral superfields. This part is so-called superpotential $\mathcal{W}$. Since we

work in a renormalizable theory, there is no terms with product of more than three superfields. Then $\mathcal{L}_F$ can be expressed in terms of component fields,

$$
\begin{aligned}
\mathcal{L}_F &= \sum_i a_i F_i + \sum_{ij} m_{ij} \left(\phi_i F_j - \frac{1}{2} \psi_i \psi_j \right) + \sum_{ijk} \frac{\lambda_{ijk}}{2} \left(\phi_i \phi_j F_k - \phi_i \psi_j \psi_k \right) \\
&= \sum_i \frac{\partial \mathcal{W}}{\partial \phi_i} F_i - \frac{1}{2} \sum_{ij} \frac{\partial^2 \mathcal{W}}{\partial \phi_i \partial \phi_j} \psi_i \psi_j,
\end{aligned}
\tag{3.43}
$$

which contains the mass terms and the interaction terms of scalar and fermionic fields. The chiral superfield can be constructed from the vector superfields by defining a supersymmetric field strength tensor,

$$
W_\alpha = \frac{1}{4} \bar{D} \bar{D} e^{-2g\mathbf{V}} D_\alpha e^{2g\mathbf{V}}.
\tag{3.44}
$$

It is of course a chiral superfield since $\bar{D}W = 0$. The F-term which must be gauge invariant quantity is given by

$$
\mathcal{L}_F = \int d^2\theta \frac{1}{16g^2} \text{Tr}(W_\alpha W^\alpha) = -\frac{1}{4} F_{\mu\nu}^a F^{a\mu\nu} + i\bar{\lambda}^a \bar{\sigma}^\mu (D_\mu \lambda)^a + \frac{1}{2} D^a D^a,
\tag{3.45}
$$

where the usual field strength tensors are

$$
F_{\mu\nu}^a = \partial_\mu V_\nu^a - \partial_\nu V_\mu^a + g f^{abc} V_\mu^b V_\nu^c,
\tag{3.46}
$$

with coupling constant g, the structure constants f^{abc} and the gauge covariant derivative

$$
D_\mu = \partial_\mu + ig T^a V_\mu^a.
\tag{3.47}
$$

We now construct $\mathcal{L}_D$ which generates the kinetic terms for the scalars and fermions. We use the property of chiral superfield: the product of a chiral superfield and an anti-chiral superfield is a vector superfield. The Lagrangian has to be gauge invariant, hence for a non-Abelian gauge $\mathcal{L}_D$ is given by

$$
\begin{aligned}
\mathcal{L}_D &= \sum_i \int d^2\theta d^2\bar{\theta} \Phi_i^\dagger e^{2g\mathbf{V}} \Phi_i \\
&= \sum_i \left[(D_\mu \phi_i)^\dagger D^\mu \phi_i + i\bar{\psi}_i \bar{\sigma}^\mu D_\mu \psi_i - \sqrt{2} g \left(\bar{\psi}_i \bar{\lambda}^a T^a \phi_i + \phi_i^\dagger \lambda^a T^a \psi_i \right) \right. \\
&\quad \left. + g\phi_i^\dagger D^a T^a \phi_i + F_i^* F_i \right].
\end{aligned}
\tag{3.48}
$$

To summarize, the general supersymmetric Lagrangian reads,

$$
\mathcal{L} = \int d^2\theta \left(\frac{1}{16g^2} \text{Tr}(W_\alpha W^\alpha) + \mathcal{W} \right) + \sum_i \int d^2\theta d^2\bar{\theta} \Phi_i^\dagger e^{2g\mathbf{V}} \Phi_i + \text{ h.c.}
\tag{3.49}
$$

The auxiliary fields F and D do not have kinetic terms. Their equation of motions are simply

$$
F_i = -\frac{\partial \mathcal{W}^*}{\partial \phi_i}, \quad D_a = -g \sum_i \phi_i^\dagger T_a \phi_i.
\tag{3.50}
$$

Substitute the above expressions in the Lagrangian, one finds the scalar potential

$$W(\phi) = \sum_i F_i F_i^* + \frac{1}{2} \sum_a D^a D^a = \sum_i \frac{\partial \mathcal{W}}{\partial \phi_i} \frac{\partial \mathcal{W}^*}{\partial \phi_i^*} + \frac{1}{2} \sum_{a,i} (g \phi_i^\dagger T_a \phi_i)^2. \qquad (3.51)$$

We will use the above procedure to construct the supersymmetric Lagrangian of the MSSM.

3.5 The Minimal Supersymmetric Standard Model

3.5.1 Particle content

The SM [1, 2, 3] based on the gauge group $\mathrm{SU}(3)_C \times \mathrm{SU}(2)_L \times \mathrm{U}(1)_Y$ contains the matter fields (fermions and Higgs boson) and the gauge fields (gluons, W and Z bosons, photon). Since they are in different representations of the gauge group, the fermions and the Higgs boson belong to complex representations while the gauge bosons belong to real representations, they cannot be superpartners of each other. In order to construct the MSSM one has to introduce new particles. Each known particle has a superpartner: the superpartners of fermions are called sfermions (squarks and sleptons) and the ones of gauge bosons are called gauginos (gluinos, winos, bino). The field content of the MSSM are shown in Table 3.1.

The MSSM and the SM Higgs sectors are different. While the SM consists of only one Higgs doublet and its complex conjugate to give masses to all the matter fermions, in the MSSM two Higgs doublets H_1 and H_2 with opposite hypercharges are needed. This has the following reasons. First, the holomorphic property of the MSSM superpotential does not allow for the appearance of both a superfield and its complex conjugate. Thus the trick to use one Higgs doublet and its complex conjugate as in the SM fails. Secondly, the superpartners of the Higgs bosons (Higgsino) contribute to gauge anomaly. Thus two Higgs doublets with opposite hypercharges are needed to make the theory anomaly free.

The particles listed in the Table 3.1 are not necessarily the physical states of the theory. After SUSY breaking and electroweak breaking, particles carrying the same quantum numbers can mix to form the mass eigenstates. For example, the charged Higgsinos and the charged winos generate charginos, the neutral Higgsinos and the neutral wino and bino generate neutralinos, the left-handed sfermions and the right handed sfermions mix also to form sfermion-1 and sfermion-2, etc. The gluinos are an exception, they are color-octet fermions and hence do not mix with other particles. More details of those mixings and the mass eigenstates will be given in the Subsection 3.5.3.

Super-fields	Bosons	Fermions	$(SU(3)_C, SU(2)_L, U(1)_Y)$	Name
$\hat{V}_s$	g	$\tilde{g}$	(8, 1, 0)	gluons, gluinos
$\hat{V}$	$W^\pm, W^0$	$\widetilde{W}^\pm, \widetilde{W}^0$	(1, 3, 0)	W-bosons, Winos
$\hat{V}'$	B	$\widetilde{B}$	(1, 1, 0)	B-boson, Bino
$\hat{Q}$	$\tilde{Q} = \begin{pmatrix} \tilde{u}_L \\ \tilde{d}_L \end{pmatrix}$	$Q = \begin{pmatrix} u_L \\ d_L \end{pmatrix}$	(3, 2, 1/3)	squarks, quarks
$\hat{U}$	$\tilde{U} = \tilde{u}_R^*$	$U = u_R^\dagger$	$(3^*, 1, -4/3)$	
$\hat{D}$	$\tilde{D} = \tilde{d}_R^*$	$D = d_R^\dagger$	$(3^*, 1, 2/3)$	
$\hat{L}$	$\tilde{L} = \begin{pmatrix} \tilde{\nu}_L \\ \tilde{e}_L \end{pmatrix}$	$L = \begin{pmatrix} \nu_L \\ e_L \end{pmatrix}$	(1, 2, -1)	sleptons, leptons
$\hat{E}$	$\tilde{E} = \tilde{e}_R^*$	$E = e_R^\dagger$	(1, 1, 2)	
$\hat{H}_1$	$H_1 = \begin{pmatrix} H_{11}^0 \\ H_{12}^- \end{pmatrix}$	$\widetilde{H}_1 = \begin{pmatrix} \widetilde{H}_{11}^0 \\ \widetilde{H}_{12}^- \end{pmatrix}$	(1, 2,-1)	Higgs, Higgsinos
$\hat{H}_2$	$H_2 = \begin{pmatrix} H_{21}^+ \\ H_{22}^0 \end{pmatrix}$	$\widetilde{H}_2 = \begin{pmatrix} \widetilde{H}_{21}^+ \\ \widetilde{H}_{22}^0) \end{pmatrix}$	(1, 2, 1)	

Table 3.1: The MSSM particle content. The superfields are denoted with a hat. The superpartners of the SM particles carry a tilde. The generation and color indices have been suppressed. The numbers in parentheses denote the dimension of the representations of the corresponding gauge groups. The stars present the complex conjugate representations.

3.5.2 Lagrangian of the MSSM

If supersymmetry were an exact symmetry then the SM particles and their corresponding superpartners would have the same masses and the SM superparticles would be detected. Up to now, no experiment has discovered any of them. If the superparticles exist, they must be heavier than their corresponding SM partners. This means supesymmetry must be broken at an energy scale Λ. In general, the Lagrangian of the MSSM at low energy ($E < \Lambda$) can be written as

$$\mathcal{L}_{\text{MSSM}} = \mathcal{L}_{\text{SUSY}} + \mathcal{L}_{\text{soft}}. \tag{3.52}$$

The first term is invariant under supersymmetry transformations while the second term breaks softly supersymmetry. However both of them are SM gauge invariant. Further restrictions can be imposed on these terms such as renormalizability, baryon and lepton number conservations, R-parity, flavour conservation, ect.

To construct the supersymmetric part of the Lagrangian, we use the superfield formalism established in Section 3.4. With the help of Grassmann variables, the

expansions of the supperfields in Table 3.1 in terms of component fields read

$$\hat{V}_s = \theta\sigma^\mu\bar{\theta}g_\mu + (\bar{\theta}\bar{\theta})\theta\tilde{g} + \frac{1}{2}(\theta\theta)(\bar{\theta}\bar{\theta})D_{V_s}, \tag{3.53}$$

$$\hat{V} = \theta\sigma^\mu\bar{\theta}W_\mu + (\bar{\theta}\bar{\theta})\theta\tilde{W} + \frac{1}{2}(\theta\theta)(\bar{\theta}\bar{\theta})D_V, \tag{3.54}$$

$$\hat{V}' = \theta\sigma^\mu\bar{\theta}B_\mu + (\bar{\theta}\bar{\theta})\theta\tilde{B} + \frac{1}{2}\theta\theta(\bar{\theta}\bar{\theta})D_{V'}, \tag{3.55}$$

$$\hat{Q} = e^{i\theta\sigma^\mu\bar{\theta}\partial_\mu}\left(\tilde{Q} + \sqrt{2}\theta Q + \theta\theta F_Q\right), \tag{3.56}$$

$$\hat{U} = e^{i\theta\sigma^\mu\bar{\theta}\partial_\mu}\left(\tilde{U} + \sqrt{2}\theta U + \theta\theta F_U\right), \tag{3.57}$$

$$\hat{D} = e^{i\theta\sigma^\mu\bar{\theta}\partial_\mu}\left(\tilde{D} + \sqrt{2}\theta D + \theta\theta F_D\right), \tag{3.58}$$

$$\hat{L} = e^{i\theta\sigma^\mu\bar{\theta}\partial_\mu}\left(\tilde{L} + \sqrt{2}\theta L + \theta\theta F_L\right), \tag{3.59}$$

$$\hat{E} = e^{i\theta\sigma^\mu\bar{\theta}\partial_\mu}\left(\tilde{E} + \sqrt{2}\theta E + \theta\theta F_E\right), \tag{3.60}$$

$$\hat{H}_i = e^{i\theta\sigma^\mu\bar{\theta}\partial_\mu}\left(\tilde{H}_i + \sqrt{2}\theta H_i + \theta\theta F_{H_i}\right), \quad i = 1, 2, \tag{3.61}$$

where the color indices and the generation indices have been suppressed. For the vector superfields, the supersymmetric field strength tensors are given by

$$
\begin{aligned}
W_{\hat{V}_s\alpha} &= \frac{1}{4}\bar{D}\bar{D}e^{-2g_s\hat{\mathbf{V}}_s}D_\alpha e^{2g_s\hat{\mathbf{V}}_s}, \\
W_{\hat{V}\alpha} &= \frac{1}{4}\bar{D}\bar{D}e^{-2g\hat{\mathbf{V}}}D_\alpha e^{2g\hat{\mathbf{V}}}, \\
W_{\hat{V}'\alpha} &= \frac{1}{4}\bar{D}\bar{D}e^{-2g'\hat{\mathbf{V}}'}D_\alpha e^{2g'\hat{\mathbf{V}}'},
\end{aligned}
\tag{3.62}
$$

where

$$\hat{\mathbf{V}}_s = T_s^a\hat{V}_s^a, \quad \hat{\mathbf{V}} = T^a\hat{V}^a, \quad \hat{\mathbf{V}}' = \frac{Y}{2}\hat{V}', \tag{3.63}$$

with T_s^a, T^a and $Y/2$ being generators of $SU(3)_C$, $SU(2)_L$ and $U(1)_Y$, respectively.

Now we construct the superpotential. The requirement of the renormalizability leads to a structure of the MSSM superpotential similar to Eq. (3.42). In addition, the gauge invariant restrictions eliminate the linear terms (there is no chargeless gauge singlet in SM). Then the superpotential reads

$$\mathcal{W}_{\text{MSSM}} = \epsilon^{ij}\left(\lambda_e^{IJ}\hat{H}_1^i\hat{L}^{jI}\hat{R}^J - \lambda_u^{IJ}\hat{H}_2^i\hat{Q}^{jI}\hat{U}^J + \lambda_d^{IJ}\hat{H}_1^i\hat{Q}^{jI}\hat{D}^J - \mu\hat{H}_1^i\hat{H}_2^j\right), \tag{3.64}$$

where λ_e, λ_u and λ_d are 3×3 Yukawa coupling matrices, i, j are weak isospin indices and I, $J = 1, 2, 3$ are generation indices. μ is called the Higgsino mixing parameter and is in general a complex number. It should be observed that this superpotential satisfies the requirement of the baryon (B) and lepton (L) number conservation. However, B and L number conservations cannot be treated as fundamental symmetries since they are known to be violated by non-perturbative electroweak effects

[68]. Hence a new symmetry, the so-called R-parity or equivalently matter parity is introduced. If we require R-parity to be a symmetry of the MSSM, then the terms which violate B and L number conservations are not allowed. More about this symmetry will be given at the end of this section.

One can now write down the general expression of the supersymmetric part of the MSSM Lagrangian in terms of both chiral superfields and vector superfields,

$$
\begin{aligned}
\mathcal{L}_{\text{SUSY}} = \int d^2\theta \Big(& \frac{1}{16g_s^2}\text{Tr}(W_{\hat{V}_s\alpha}W_{\hat{V}_s}^\alpha) + \frac{1}{16g^2}\text{Tr}(W_{\hat{V}\alpha}W_{\hat{V}}^\alpha) \\
& + \frac{1}{16g'^2}\text{Tr}(W_{\hat{V}'\alpha}W_{\hat{V}'}^\alpha) + \mathcal{W}_{\text{MSSM}} \Big) \\
+ \int d^2\theta d^2\bar{\theta} \Big(& \hat{L}^\dagger e^{2g\hat{\mathbf{V}}+2g'\hat{\mathbf{V}}'}\hat{L} + \hat{E}^\dagger e^{2g'\hat{\mathbf{V}}'}\hat{E} + \hat{Q}^\dagger e^{2g_s\hat{\mathbf{V}}_s+2g\hat{\mathbf{V}}+2g'\hat{\mathbf{V}}'}\hat{Q} \\
+ \hat{U}^\dagger e^{2g_s\hat{\mathbf{V}}_s+2g'\hat{\mathbf{V}}'}\hat{U} + & \hat{D}^\dagger e^{2g_s\hat{\mathbf{V}}_s+2g'\hat{\mathbf{V}}'}\hat{D} + \hat{H}_i^\dagger e^{2g\hat{\mathbf{V}}+2g'\hat{\mathbf{V}}'}\hat{H}_i \Big) + \text{ h.c.}
\end{aligned}
$$

$$(3.65)$$

It should be observed that the above Lagrangian contains no mass terms. The mass terms for the superparticles will be generated after supersummetry is broken and the masses for the SM particles are generated after EW symmetry breaking. So far, $\mathcal{L}_{\text{SUSY}}$ introduces only one more prarameter μ in comparason to the SM parameters.

As we have mentioned supersymmetry is not an exact symmetry. It must be broken. The origin of supersymmetry breaking is not clear. Many models proposed spontaneous SUSY breaking mechanism, for a review see [64] and references therein. Independence of the nature of SUSY breaking mechanism, the Lagrangian at low energy contains terms which break SUSY explicitly. Those terms should be soft since they have couplings of positive mass dimension. This restriction is to prevent the appearance of quadratic divergence in quantum corrections to scalar mass, which may kill the advantage of SUSY where all quadratic divergences are cancelled stabilizing the EW scale. In the MSSM, the soft breaking terms found by Girardello and Grisaru [16] are used. Then possible terms which violate supersymmetry but are gauge and R-parity invariant reads

$$
\begin{aligned}
\mathcal{L}_{\text{soft}} = & -\frac{1}{2}\Big(M_3\tilde{g}^a\tilde{g}^a + M_2\tilde{W}^i\tilde{W}^i + M_1\tilde{B}\tilde{B} + \text{ h.c}\Big) \\
& -\tilde{Q}^\dagger\mathbf{M}_{\tilde{Q}}^2\tilde{Q} - \tilde{L}^\dagger\mathbf{M}_{\tilde{L}}^2\tilde{L} - \tilde{\bar{u}}\mathbf{M}_{\tilde{U}}^2\tilde{\bar{u}}^\dagger - \tilde{\bar{d}}\mathbf{M}_{\tilde{D}}^2\tilde{\bar{d}}^\dagger - \tilde{\bar{e}}\mathbf{M}_{\tilde{E}}^2\tilde{\bar{e}}^\dagger \\
& -m_{H_1}^2 H_1^\dagger H_1 - m_{H_2}^2 H_2^\dagger H_2 - (bH_1H_2 + \text{ h.c}) \\
& -\Big(\tilde{\bar{u}}\mathbf{A}_u\tilde{Q}H_1 - \tilde{\bar{d}}\mathbf{A}_d\tilde{Q}H_2 - \tilde{\bar{e}}\mathbf{A}_e\tilde{L}H_2 + \text{ h.c}\Big),
\end{aligned}
$$

$$(3.66)$$

where $\mathbf{M}_{\tilde{F}}^2$ ($F = Q, U, D, L, E$) and $\mathbf{A}_f$ ($f = u, d, e$) are 3×3 matrices in flavor space, M_i (i=1,2,3) are gaugino masses. Adding these soft SUSY breaking terms, one has introduced 105 additional free parameters to the MSSM (26 masses, 37 mixing angles and 42 CP-violating phases). It should be observed that the soft parameters can be complex and thus provide new sources of flavor and CP violations.

To quantize the theory, gauge fixing terms are used. Since the gauge sector of the MSSM is the same as of the SM, the 't Hooft linear gauge fixing Lagrangian can be chosen as

$$\mathcal{L}_{\text{fix}} = -\frac{1}{2\xi_G}(F_G^a)^2 - \frac{1}{2\xi_A}F_A^2 - \frac{1}{2\xi_Z}F_Z^2 - \frac{1}{2\xi_W}F_W^+ F_W^-, \qquad (3.67)$$

where

$$
\begin{aligned}
F_G^a &= \partial_\mu G^{a\mu}, \\
F_A &= \partial_\mu A^\mu, \\
F_Z &= \partial_\mu Z^\mu - M_Z \xi_Z G^0, \\
F_W^+ &= \partial_\mu W^{+\mu} + i M_W \xi_W G^+,
\end{aligned}
\qquad (3.68)
$$

with $\xi_G, \xi_A, \xi_Z, \xi_W$ being the gauge fixing parameters. Since our theory is gauge invariant, any physical quantity is independent of gauge fixing parameters. Then in a practical calculation, one can chose specific values for them. For the simplicity of the gauge boson propagators, one commonly uses the 't Hooft Feynman gauge $\xi_G = \xi_A = \xi_Z = \xi_W = 1$. In such gauge, the unphysical Nambu-Goldstone bosons, $G^\pm$ and G^0 have masses equal to the masses of corresponding gauge bosons. In addition the mixing terms between the Nambu-Goldstone bosons and the longitudinal gauge bosons are eliminated. In one-loop calculations, we use the 't Hooft Feynman gauge since we do not want the appearance of high rank tensor one-loop integrals. However in tree-level calculation we prefer to use the unitary gauge, in which gauge fixing parameters are infinite, because of less number of Feynman diagrams.

It is clear that the gauge fixing terms are not gauge invariant. They could give unphysical contributions to physical processes, in particular at loop-level. One has to eliminate these contributions to restore gauge invariance. This is done by introducing the Faddeev-Popov ghost terms [69],

$$\mathcal{L}_{\text{ghost}} = \bar{c}^\alpha \frac{\delta F_\alpha}{\delta \theta^\beta} c^\beta, \quad \alpha, \beta \in \{G, A, Z, W^\pm\}, \qquad (3.69)$$

where $c^\alpha, \bar{c}^\alpha$ is ghost and anti-ghost field corresponding to the gauge boson α; θ^α are infinitesimal gauge transformation parameters and F_α are given in Eq. (3.68). The ghost fields are scalar fields but have fermionic properties. They belong to the adjoint representation of the gauge group. From Eq. (3.67) and Eq. (3.69), one sees that the ghost and Nambu-Goldstone boson squared masses are proportional to the squared masses of the corresponding gauge boson:

$$M_{c_G}^2 = M_{c_A}^2 = 0, \qquad (3.70)$$

$$M_{c_Z}^2 = M_{G^0}^2 = \xi_Z M_Z^2, \qquad (3.71)$$

$$M_{c_W^\pm}^2 = M_{G^\pm}^2 = \xi_Z M_W^2. \qquad (3.72)$$

Both the ghosts and the Nambu-Goldstone bosons are unphysical fields and hence do not appear as external lines of Feynman diagrams.

To summarize, the quantized Lagrangian of the MSSM reads

$$\mathcal{L}_{\text{MSSM}} = \mathcal{L}_{\text{SUSY}} + \mathcal{L}_{\text{soft}} + \mathcal{L}_{\text{fix}} + \mathcal{L}_{\text{ghost}}. \tag{3.73}$$

R-parity

R-parity is a discrete multiplicative symmetry. R-parity of a particle can be defined as

$$P_R = (-1)^{2s+3(B-L)}, \tag{3.74}$$

where s is the spin, B is baryon number and L is lepton number. An assignment of quantum numbers for the superfields is following: B is $1/3$ for $\hat{Q}$, $-1/3$ for $\hat{U}$, $\hat{D}$ and zero for the remaining superfields; L is 1 for $\hat{L}$, -1 for $\hat{R}$ and zero for other superfields. With this definition, the SM fields have $P_R = +1$ while their supersymmetric partners have $P_R = -1$. If R-parity is an exact symmetry then sparticles cannot mix with particles and only vertices with an even number of sparticles are allowed. This leads to the following phenomenological consequences.

- The lightest supersymmetry particle (LSP) with $P_R = -1$ must be stable. It can be an attractive candidate for dark matter.

- Sparticles can only decay into a state which contains an odd number of LSP plus the SM particles.

- At the colliders, sparticles can only be produced in pairs.

There is a well-known phenomenological motivation in favor of R-parity conservation which will be shortly discussed below. Without R-parity conservation, then following terms are allowed in the superpotential (see for example [70])

$$\mathcal{W}_{\not{R}} = \epsilon^{ij} \left(\lambda_{IJK} \hat{L}_I^i \hat{L}_J^j \hat{R}_K + \lambda'_{IJK} \hat{L}_I^i \hat{Q}_J^j \hat{D}_K + m^I \hat{L}_I^i \hat{H}_1^j \right) + \epsilon_{ijk} \lambda''_{IJK} \hat{U}_I^i \hat{D}_J^j \hat{D}_K^k, \tag{3.75}$$

where λ, λ' and λ'' are Yukawa couplings, m^I are mass parameters, $I, J, K = 1, 2, 3$ and $i, j = 1, 2$. It should be observed that the first three terms violate lepton number by one unit while the fourth term violates baryon number by one unit. Those terms leads to the B- and L-violating processes. Especially if both λ' and λ'' are present, then proton will decay for example into $e^+\pi^0$ or e^+K^0. The mean time of proton has lower limit about 2.1×10^{29} years [71]. This severe constraint makes the value of any product of couplings λ' and λ'' extremely small, for squark masses below 1 TeV $|\lambda' \cdot \lambda''| < 10^{-9}$ in the absence of squark flavor mixing and $|\lambda' \cdot \lambda''| < 10^{-11}$ in the present of squark flavor mixing [72]. So one sees that R-parity conservation is not the only way to keep the proton stable. However, the model with R-parity conservation has lesser number of free parameters and thus is simpler. In this thesis, we therefore perform our calculations in the MSSM with R-parity conservation.

Parameters of the MSSM

The general MSSM at low energy where no specific assumptions are made about the underlying SUSY breaking mechanism consists of 105 parameters (26 masses, 37 mixing angles and 42 complex phases) of the soft SUSY breaking terms and 18 parameters of the SUSY conserving terms. Performing analysis in the general MSSM then comparing with experimental data are very difficult due to the large number of soft parameters which can have arbitrary values. Most of analysis in both experiment and theory have been done with some assumptions to restrict the number free parameter. In our calculation we use also the common restriction on the FCNCs. Unlike the SM where the GIM mechanism ensure the absence of the FCNCs at tree-level, the MSSM can contains the FCNCs in interactions with the Z-boson, the neutral Higgs bosons and the gauginos already at tree-level. These new interactions can give large contributions to FCNC processes such as $K^0 - \bar{K}^0$ mass difference. The experimental data of FCNC processes have put severe bounds on the favor mixing parameters. For simplicity, we assume that FCNCs are absent at tree-level, *i.e.* the mass matrices and trilinear couplings are diagonal in the generation space. This assumption is reasonable since our calculations mainly concern the third generation of fermions. The effects of the CKM matrix are negligible for processes discussed here, we therefore set it to be diagonal. To study CP violating effects, we therefore still keep the possible phases of the remaining parameters which are the gaugino masses M_i ($i = 1, 2, 3$), the Higgsino mass parameter μ and the trilinear couplings A_f:

$$
\begin{aligned}
M_i &= |M_i| e^{i\phi_i}, \\
\mu &= |\mu| e^{i\phi_\mu}, \\
\mathbf{A_f} &= |\mathbf{A_f}| e^{i\phi_f}, \quad f = u, c, t, d, s, b, e, \mu, \tau.
\end{aligned}
\tag{3.76}
$$

In summary, the MSSM parameters consist of

- gauge couplings: g_s, g, g';

- fermion masses: m_f ($f = u, c, t, d, s, b, e, \mu, \tau$);

- gaugino masses: M_i ($i = 1, 2, 3$);

- sfermion masses: $M_{\tilde{Q}}^2, M_{\tilde{U}}^2, M_{\tilde{D}}^2, M_{\tilde{L}}^2, M_{\tilde{E}}^2$ for each generation;

- Higgsino mixing parameter: μ;

- trilinear couplings A_f for each fermion species;

- Higgs sector parameters: $M_{H^\pm}$, $\tan\beta = v_2/v_1$ with v_1 and v_2 being the vacuum expectation values of the two Higgs doublets.

3.5.3 The MSSM mass spectrum

If the supesymmetry and gauge symmetry are not broken, then the MSSM particles are massless. The explicit soft supersymmetry breaking and spontaneous electroweak symmetry breaking generates mass terms for the particles. In many cases, particles which have the same spin, electric charge, color charge and R-parity do mix with each other. Unitary transformations are needed to find mass eigenstates. In this section, we discuss the masses of the MSSM particles.

Higgs bosons and gauge bosons

The scalar Higgs potential is given by

$$
\begin{aligned}
V_H &= (|\mu|^2 + m_{H_1}^2)H_{1i}^*H_{1i} + (|\mu|^2 + m_{H_2}^2)H_{2i}^*H_{2i} + \epsilon_{ij}[bH_{1i}H_{2j} + b^*H_{1i}^*H_{2j}^*] \\
&+ \frac{1}{8}(g^2 + g'^2)(H_{1i}^*H_{1i} - H_{2i}^*H_{2i})^2 + \frac{1}{2}g^2|H_{1i}^*H_{2i}|^2,
\end{aligned}
\tag{3.77}
$$

where $i, j = 1, 2$. The terms proportional to $|\mu|^2$ are from the F-terms. The terms proportional to gauge couplings are from the D-terms and the remaining terms are from the soft SUSY breaking terms. Unlike the SM where the quartic coupling is a free parameter, it however relates to the gauge couplings g, g' in the MSSM. This interesting feature leads to the restrictions on mass of the lightest Higgs bosons. The parameter b in the potential can be complex, however we can rephase the two Higgs doublets to make b real. As of now b is considered as real parameter. For short notation, we denote $\tilde{m}_{H_1}^2 = |\mu|^2 + m_{H_1}^2$ and $\tilde{m}_{H_2}^2 = |\mu|^2 + m_{H_2}^2$. Like the SM, the Higgs mechanism is used to break the EW symmetry and hence generate masses for gauge bosons. The two Higgs doublets having non-vanishing vacuum expectation values can be decomposed as follows,

$$
\begin{aligned}
H_1 &= \begin{pmatrix} H_{11}^0 \\ H_{12}^- \end{pmatrix} = \begin{pmatrix} (v_1 + \phi_1^0 - i\chi_1^0)/\sqrt{2} \\ -\phi_1^- \end{pmatrix}, \\
H_2 &= \begin{pmatrix} H_{21}^+ \\ H_{22}^0 \end{pmatrix} = e^{i\xi} \begin{pmatrix} \phi_2^+ \\ (v_2 + \phi_2^0 + i\chi_2^0)/\sqrt{2} \end{pmatrix},
\end{aligned}
\tag{3.78}
$$

where ξ is a possible relative phase between the two Higgs doublets. The vacuum expectation values v_1 and v_2 can be chosen to be real and positive.

Using the decomposition of the Higgs fields, one can find the W boson and Z boson masses

$$
\begin{aligned}
M_W^2 &= \frac{1}{4}g^2(v_1^2 + v_2^2), \\
M_Z^2 &= \frac{1}{4}(g^2 + g'^2)(v_1^2 + v_2^2),
\end{aligned}
\tag{3.79}
$$

and the photon remains massless. These relations are identical to those of the SM with $v^2 = v_1^2 + v_2^2$. As usual, one defines the weak mixing angle θ_W and $\tan\beta$ as

follows,

$$t_W \equiv \tan\theta_W = \frac{g}{g'}, \quad \tan\beta = \frac{v_2}{v_1}. \tag{3.80}$$

We now want to find the Higgs mass spectrum. Substituting Eq. (3.78) into Eq. (3.77), one gets

$$V_H = \cdots + T_{\phi_1^0}\phi_1^0 + T_{\phi_2^0}\phi_2^0 + T_{\chi_1^0}\chi_1^0 + T_{\chi_2^0}\chi_2^0 \tag{3.81}$$

$$+\frac{1}{2}\left(\phi_1^0, \phi_2^0, \chi_1^0, \chi_2^0\right)\mathbf{M_n}\begin{pmatrix}\phi_1^0\\\phi_2^0\\\chi_1^0\\\chi_2^0\end{pmatrix} + \left(\phi_1^-, \phi_2^-\right)\mathbf{M_c}\begin{pmatrix}\phi_1^+\\\phi_2^+\end{pmatrix} + \cdots.$$

Here we consider only the linear and quadratic terms, the dots refer to the constant and higher power terms. $T_{\phi/\chi}$ are the tadpole coefficients and are given by

$$T_{\phi_1^0} = \tilde{m}_{H_1}^2 v_1 + b v_2\cos\xi + \frac{1}{8}(g^2 + g'^2)(v_1^2 - v_2^2)v_1, \tag{3.82}$$

$$T_{\phi_2^0} = \tilde{m}_{H_2}^2 v_2 + b v_1\cos\xi + \frac{1}{8}(g^2 + g'^2)(v_2^2 - v_1^2)v_2, \tag{3.83}$$

$$T_{\chi_1^0} = b v_2\sin\xi, \tag{3.84}$$

$$T_{\chi_2^0} = -b v_1\sin\xi. \tag{3.85}$$

The stable minimum point of the potential requires the tadpole coefficients to be zero. Consequently, $\xi = 0$. This means that the Higgs sector is CP conserving at tree-level, and the Higgs mass eigenstates have defined CP numbers. Now one can express the symmetric 4×4 mass matrix $\mathbf{M_n}$ and 2×2 mass matrix $\mathbf{M_c}$ as

$$\mathbf{M_n} = \begin{pmatrix}\mathbf{M}_{\phi\phi} & \mathbf{M}_{\phi\chi}\\\mathbf{M}_{\phi\chi} & \mathbf{M}_{\chi\chi}\end{pmatrix}, \tag{3.86}$$

with

$$\mathbf{M}_{\phi\phi} = \begin{pmatrix}\frac{T_{\phi_1^0}}{v\cos\beta} - b\tan\beta\cos\xi + M_Z^2\cos^2\beta & b\cos\xi - M_Z^2\sin\beta\cos\beta\\b\cos\xi - M_Z^2\sin\beta\cos\beta & \frac{T_{\phi_2^0}}{v\sin\beta} - b\cot\beta\cos\xi + M_Z^2\sin^2\beta\end{pmatrix}, \tag{3.87}$$

$$\mathbf{M}_{\phi\chi} = \begin{pmatrix}0 & -\frac{T_{\chi_1^0}}{v\sin\beta}\\\frac{T_{\chi_1^0}}{v\sin\beta} & 0\end{pmatrix}, \tag{3.88}$$

$$\mathbf{M}_{\chi\chi} = \begin{pmatrix}\frac{T_{\phi_1^0}}{v\cos\beta} - b\tan\beta\cos\xi & b\cos\xi\\b\cos\xi & \frac{T_{\phi_2^0}}{v\sin\beta} - b\cot\beta\cos\xi\end{pmatrix}, \tag{3.89}$$

and

$$\mathbf{M_c} = \begin{pmatrix}\frac{T_{\phi_1^0}}{v\cos\beta} - b\tan\beta\cos\xi + M_W^2\sin^2\beta & e^{i\xi}b - M_W^2\sin\beta\cos\beta\\e^{-i\xi}b - M_W^2\sin\beta\cos\beta & \frac{T_{\phi_2^0}}{v\sin\beta} - b\cot\beta\cos\xi + M_W^2\cos^2\beta\end{pmatrix}. \tag{3.90}$$

Here we keep the tadpoles for the later purpose of renormalization. To find the Higgs mass eigenstates, one has to diagonalize those mass matrices by orthogonal transformations

$$\begin{pmatrix} h \\ H \\ A \\ G \end{pmatrix} = \mathbf{U_n} \begin{pmatrix} \phi_1^0 \\ \phi_2^0 \\ \chi_1^0 \\ \chi_2^0 \end{pmatrix}, \quad \begin{pmatrix} H^\pm \\ G^\pm \end{pmatrix} = \mathbf{U_c} \begin{pmatrix} \phi_1^\pm \\ \phi_2^\pm \end{pmatrix} \tag{3.91}$$

which satisfy

$$\mathbf{M_n}^{\text{diag}} = \mathbf{U_n M_n U_n^T}, \quad \mathbf{M_c}^{\text{diag}} = \mathbf{U_c M_c U_c^T}. \tag{3.92}$$

The transformation matrices can be parameterized as in the following way,

$$\mathbf{U_n} = \begin{pmatrix} -\sin\alpha & \cos\alpha & 0 & 0 \\ \cos\alpha & \sin\alpha & 0 & 0 \\ 0 & 0 & -\sin\beta_n & \cos\beta_n \\ 0 & 0 & \cos\beta_n & \sin\beta_n \end{pmatrix}, \quad \mathbf{U_c} = \begin{pmatrix} -\sin\beta_c & \cos\beta_c \\ \cos\beta_c & \sin\beta_c \end{pmatrix}. \tag{3.93}$$

It is not difficult to show that at tree level $\beta_n = \beta_c = \beta$, $\xi = 0$ and

$$m_A^2 = -\frac{2b}{\sin 2\beta} \cos\xi \cos^2(\beta - \beta_n) = -\frac{2b}{\sin 2\beta}, \tag{3.94}$$

$$m_{h/H}^2 = \frac{1}{2} \left[m_A^2 + M_Z^2 \mp \sqrt{(m_A^2 - M_Z^2)^2 + 4m_A^2 M_Z^2 \sin^2(2\beta)} \right], \tag{3.95}$$

$$M_{H^\pm}^2 = m_A^2 + M_W^2, \tag{3.96}$$

$$m_G^2 = m_{G^\pm}^2 = 0, \tag{3.97}$$

and the mixing angle α is determined through

$$\tan\alpha = -\frac{(m_A^2 + M_Z^2)\sin\beta\cos\beta}{M_Z^2 \cos^2\beta + m_A^2 \sin^2\beta - m_h^2}, \quad -\frac{\pi}{2} < \alpha < 0, \tag{3.98}$$

where α is conventionally chosen to be negative. In the decoupling limit $m_A \to \infty$ then $(\beta - \alpha) \to \pi/2$. From Eq. (3.97), one should observe that m_A, m_H and $M_{H^\pm}$ can be arbitrarily large, however m_h is bounded above: $m_h < M_Z |\cos 2\beta|$. This is a consequence of a fixed Higgs quartic coupling as we have already mentioned. The lightest neutral Higgs h is commonly considered as the SM like Higgs boson since in the limit $m_A \gg M_Z$ its couplings with fermions and gauge bosons are identical to those of the SM.

In summary, the Higgs sector has the following spectrum:

$$\begin{aligned} &\text{2 CP even neutral Higgs bosons}: h, H \\ &\text{1 CP odd neutral Higgs boson}: A \\ &\text{2 charged Higgs bosons}: H^-, H^+ \\ &\text{3 Nambu-Goldstone bosons}: G^0, G^-, G^+. \end{aligned} \tag{3.99}$$

Neutralinos and charginos

The two neutral gauginos $(\tilde{W}^0, \tilde{B})$ and the two neutral Higginos $(\tilde{H}_1^0, \tilde{H}_2^0)$ do mix to form four mass eigenstates called neutralinos. The mass mixing matrix written in the basis $(\tilde{W}^0, \tilde{B}, \tilde{H}_1^0, \tilde{H}_2^0)$ is given by

$$\mathbf{M}_{\tilde{\chi}^0} = \begin{pmatrix} M_1 & 0 & -M_Z s_W \cos\beta & M_Z s_W \sin\beta \\ 0 & M_2 & M_Z c_W \cos\beta & M_Z c_W \sin\beta \\ -M_Z s_W \cos\beta & M_Z c_W \cos\beta & 0 & -\mu \\ M_Z s_W \sin\beta & M_Z c_W \sin\beta & -\mu & 0 \end{pmatrix}. \tag{3.100}$$

The neutralino masses can be achieved by diagonalizing this matrix with a unitary transformation $\mathbf{N}$

$$\begin{pmatrix} \tilde{\chi}_1^0 \\ \tilde{\chi}_2^0 \\ \tilde{\chi}_3^0 \\ \tilde{\chi}_4^0 \end{pmatrix} = \mathbf{N} \begin{pmatrix} \tilde{B}^0 \\ \tilde{W}^0 \\ \tilde{H}_1^0 \\ \tilde{H}_2^0 \end{pmatrix}, \qquad \begin{pmatrix} m_{\tilde{\chi}_1^0} & 0 & 0 & 0 \\ 0 & m_{\tilde{\chi}_2^0} & 0 & 0 \\ 0 & 0 & m_{\tilde{\chi}_3^0} & 0 \\ 0 & 0 & 0 & m_{\tilde{\chi}_4^0} \end{pmatrix} = \mathbf{N}^* \mathbf{M}_{\tilde{\chi}^0} \mathbf{N}^\dagger, \tag{3.101}$$

where the masses in accordance with the convention $m_{\tilde{\chi}_1^0} < m_{\tilde{\chi}_2^0} < m_{\tilde{\chi}_3^0} < m_{\tilde{\chi}_4^0}$ are all positive and real. Neutralinos are Majorana fermions. The lightest one $\tilde{\chi}_1^0$ is the lightest supersymmetric particle in a wide range of the mSUGRA parameter space which can be a good dark matter candidate.

For the charged gauginos $\tilde{W}^\pm$ and the charged Higgsinos $\tilde{H}_1^-, \tilde{H}_2^+$, their mixing matrix reads

$$\mathbf{M}_{\tilde{\chi}^\pm} = \begin{pmatrix} M_2 & \sqrt{2}\sin\beta M_W \\ \sqrt{2}\cos\beta M_W & \mu \end{pmatrix}. \tag{3.102}$$

Unlike the neutralino case, this mass matrix is not symmetric. To diagonalize it, one needs two unitary transformations $\mathbf{U}$ and $\mathbf{V}$

$$\begin{pmatrix} \tilde{\chi}_1^+ \\ \tilde{\chi}_2^+ \end{pmatrix} = \mathbf{V} \begin{pmatrix} \tilde{W}^+ \\ \tilde{H}_2^+ \end{pmatrix}, \qquad \begin{pmatrix} \tilde{\chi}_1^- \\ \tilde{\chi}_2^- \end{pmatrix} = \mathbf{U} \begin{pmatrix} \tilde{W}^- \\ \tilde{H}_1^- \end{pmatrix}, \tag{3.103}$$

with

$$\begin{pmatrix} m_{\tilde{\chi}_1^\pm} & 0 \\ 0 & m_{\tilde{\chi}_1^\pm} \end{pmatrix} = \mathbf{U}^* \mathbf{M}_{\tilde{\chi}^\pm} \mathbf{V}^\dagger, \tag{3.104}$$

where the non-negative entries $m_{\tilde{\chi}_1^\pm}, m_{\tilde{\chi}_2^\pm}$ are

$$m_{\tilde{\chi}_{1,2}^\pm} = \frac{1}{2}\left[|M_2|^2 + |\mu|^2 + 2M_W^2 \right.$$
$$\left. \mp \sqrt{(|M_2|^2 + |\mu|^2 + 2M_W^2)^2 - 4|\mu M_2 - M_W^2 \sin 2\beta|^2} \right]. \tag{3.105}$$

Last but not at least, the gaugino masses M_1, M_2 and the Higgsino mixing parameter μ, which in general are complex, enter those mass mixing matrices. After diagonalization the mass matrices are real and positive, the effect of the complex phases presents in the transformation matrices. As a result the couplings of neutralinos and charginos may have complex phases.

Quarks and leptons

Similar to the SM fermions, the fermion masses come from the Yukawa interaction terms where the Yukawa couplings are exactly the same as those in the superpotential. The mass matrices which mix fermions with different flavors arise after two Higgs fields getting vacuum expectation values. A difference with the SM where one Higgs doublet couples with both up- and down-type fermions, in the MSSM H_1 couples with down-type fermions while H_2 couples with up-type fermions.

For the lepton sector, we treat neutrinos as massless with only left-handed components. The charged-lepton mass eigenstates can be set equal to their flavor states with masses

$$m_l = \frac{\lambda_l v_1}{\sqrt{2}} = \frac{\sqrt{2}\lambda_l M_W s_W \cos\beta}{e}, \tag{3.106}$$

where $l = e, \mu, \tau$.

For the quark sector, four unitary matrix $V_{L,R}^{u,d}$ are used to rotate flavor states to mass eigenstates, yielding

$$m_q = \frac{\lambda_q v_2}{\sqrt{2}} = \frac{\sqrt{2}\lambda_q M_W s_W \sin\beta}{e}, \quad m_{q'} = \frac{\lambda_{q'} v_1}{\sqrt{2}} = \frac{\sqrt{2}\lambda_{q'} M_W s_W \cos\beta}{e}, \tag{3.107}$$

where $q = u, c, t$ and $q' = d, s, b$.

Squarks and sleptons

The left- and right-handed sfermions with the same flavor mix after the EW symmetry breaking. Their mass terms in the Lagrangian are given by

$$\mathcal{L}_{\text{sfermion masses}} = - \left(\tilde{f}_L^*, \tilde{f}_R^* \right) \mathbf{M}_{\tilde{f}} \begin{pmatrix} \tilde{f}_L \\ \tilde{f}_R \end{pmatrix} - \tilde{\nu}^* m_{\tilde{\nu}}^2 \tilde{\nu}, \tag{3.108}$$

where $f \in \{e, u, d\}$ and the generation index has been suppressed,

$$m_{\tilde{\nu}}^2 = M_{\tilde{L}}^2 + \frac{1}{2} M_Z^2 \cos 2\beta, \tag{3.109}$$

and

$$\mathbf{M}_{\tilde{f}} = \begin{pmatrix} m_f^2 + M_{\tilde{f}L}^2 + M_Z^2 \cos 2\beta(I_3^f - Q_f s_W^2) & m_f X_f^* \\ m_f X_f & m_f^2 + M_{\tilde{f}R}^2 + M_Z^2 \cos 2\beta Q_f s_W^2 \end{pmatrix}, \tag{3.110}$$

with

$$X_f = A_f - \mu^* \{\cot\beta, \tan\beta\}. \tag{3.111}$$

Here $\{\cot\beta, \tan\beta\}$ apply for up- and down-type sfermions, respectively. $M_{\tilde{f}L}^2$ are $M_{\tilde{Q}}$ for squarks and $M_{\tilde{L}}$ for sleptons. $M_{\tilde{f}R}^2$ are $M_{\tilde{U}}$ for up-type squarks and $M_{\tilde{D}}$ for

down-type squarks and $M_{\tilde{E}}$ for sleptons. Note that if one allows flavor mixing then the mass matrices will be 3×3 for sneutrinos and 6×6 for the charged sleptons, up-type squarks and down-type squarks.

The masses $M_{\tilde{f}L}^2$ and $M_{\tilde{f}R}^2$ coming from the soft SUSY breaking terms are real and positive while A_f, μ are complex. Their phases are independent parameters. In fact, only the phases of X_f ($\phi_{X_f} = \arg(X_f)$) are important for this sector. The unitary transformations can be used to diagonalize these mass matrices,

$$\begin{pmatrix} \tilde{f}_1 \\ \tilde{f}_2 \end{pmatrix} = \mathbf{U}_{\tilde{f}} \begin{pmatrix} \tilde{f}_L \\ \tilde{f}_R \end{pmatrix}, \quad \begin{pmatrix} m_{\tilde{f}_1}^2 & 0 \\ 0 & m_{\tilde{f}_2}^2 \end{pmatrix} = \mathbf{U}_{\tilde{f}} \mathbf{M}_{\tilde{f}} \mathbf{U}_{\tilde{f}}^\dagger, \quad \mathbf{U}_{\tilde{f}} = \begin{pmatrix} c_{\tilde{f}} & s_{\tilde{f}} \\ -s_{\tilde{f}}^* & c_{\tilde{f}} \end{pmatrix}, \quad (3.112)$$

where

$$c_{\tilde{f}} = \frac{\sqrt{m_f^2 + M_{\tilde{f}L}^2 + M_Z^2 \cos 2\beta(I_3^f - Q_f s_W^2) - m_{\tilde{f}_2}}}{\sqrt{m_{\tilde{f}_1}^2 - m_{\tilde{f}_2}^2}}, \quad (3.113)$$

$$s_{\tilde{f}} = \frac{m_f X_f^*}{\sqrt{m_f^2 + M_{\tilde{f}L}^2 + M_Z^2 \cos 2\beta(I_3^f - Q_f s_W^2) - m_{\tilde{f}_2}} \sqrt{m_{\tilde{f}_1}^2 - m_{\tilde{f}_2}^2}}, \quad (3.114)$$

and

$$\begin{aligned} m_{\tilde{f}_{1,2}}^2 &= m_f^2 + \frac{1}{2}\Bigg[M_{\tilde{f}L}^2 + M_{\tilde{f}R}^2 + I_3^f M_Z^2 \cos 2\beta \\ &\mp \sqrt{[M_{\tilde{f}L}^2 - M_{\tilde{f}R}^2 + M_Z^2 \cos 2\beta(I_3^f - 2Q_f s_W^2)]^2 + 4m_f^2 |X_f|^2} \Bigg]. \end{aligned} (3.115)$$

We can parameterize $c_{\tilde{f}} = \cos \theta_{\tilde{f}}$ and $s_{\tilde{f}} = e^{-i\phi_{X_f}} \sin \theta_{\tilde{f}}$; $\theta_{\tilde{f}}$ are rotation angles. The short relation

$$\sin 2\theta_{\tilde{f}} = \frac{2|X_f|m_f}{m_{\tilde{f}_1}^2 - m_{\tilde{f}_2}^2}. \quad (3.116)$$

is very convenient for later calculations.

The off-diagonal elements of the sfermion mixing matrices are proportional to the corresponding fermion masses. The first and second generation fermion masses are small and hence the mixing angles and the CP-violating effects due to the complex phases of X_f are small.

Gluinos

The gluinos are superpartners of gluons. They belong to the adjoint representation of SU(3) group. There are eight of them. They are Majorana fermions and carry color charge. Therefore, they do not mix with any other particles in the MSSM. At tree level, the gluino mass is determined by the soft SUSY breaking parameter M_3, $m_{\tilde{g}} = |M_3|$. M_3 can have arbitrary complex phase. This phase enters the gluino-quark-squark interactions and hence induces CP-violating effects in physical processes.
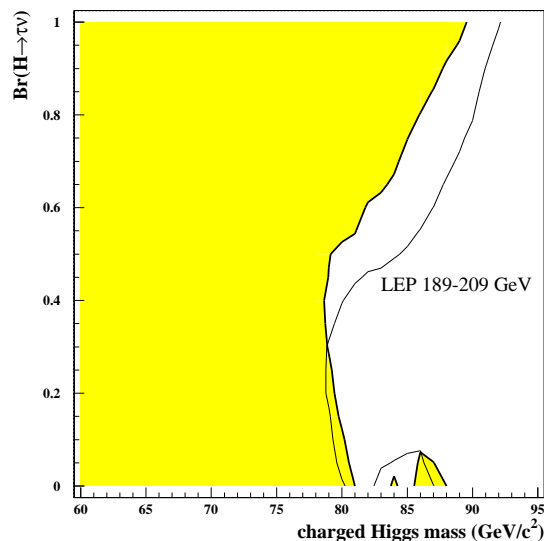
Figure 3.1: The LEP 95% C.L bounds on the mass of charged Higgs as a function of the branching ratio of decay mode $H^- \to \tau \nu_\tau$. The analysis was done based on the collected dada of the four experiments at energies from 189 to 209 GeV. The thin solid line indicates the expected exclusion limits while the thick solid one indecates the observed limits. The shaded region is excluded at 95% confidence level.

3.6 Experimental searches for charged Higgs bosons

The charged Higgs bosons have been searched in experiments. No signal has been found. Some constraints are obtained. In this section we review the published results of the searches for charged Higgs bosons in a general THDM.

3.6.1 Direct searches

Direct searches are based on the charged Higgs boson production processes at colliders. The produced charged Higgs bosons decay into SM particles or an even number of sparticles if allowed by kinematics. The mass of the charged Higgs boson determines the dominant decay modes. A consistent combination of the production cross sections with the decay widths provides signals of particular final state configurations. In principle all the final configurations should be studied. However, some may be more favored than the others. In the searches at LEP, Tevatron and LHC, the dominant production processes and dominant decay modes are considered.

Charged Higgs boson searches at LEP

The Large Electron-Positron Collider (LEP) with four detectors (ALEPH, DELPHI, L3 and OPAL) operating from 1989 to 2000 had been searching for charged Higgs bosons produced through the channel $e^-e^+ \to H^-H^+$. The center-of-mass energy ranging from 189 GeV to 209 GeV allow them to search for charged Higgs bosons in the low mass region where they decay mainly into $\tau\nu_\tau$ or cs. The analyses were done in the framework of the THDMs where the charged Higgs mass is a free parameter, thus can be arbitrarily small. The MSSM belongs also to the THDMs, but the charged Higgs mass has a constraint due to the tree-level relation $M_{H^\pm}^2 = M_A^2 + M_W^2$. If one takes into account the quantum corrections then the mass of the charged Higgs bosons can be less than M_W in some special regions of parameter space. No charged Higgs event was found then they required $M_{H^\pm} > 78.9$ GeV at 95% confidence level [73] regardless of the value of $\mathrm{Br}(H^- \to \tau\nu_\tau)$. For the dependence on $\mathrm{Br}(H^- \to \tau\nu_\tau)$, one can see in Fig. 3.1.

For the MSSM, the constraint on the mass of the CP-odd Higgs boson A is an useful information to set a constraint on the mass of the charged Higgs bosons. At LEP, A can be produced in association with h and H. A combined LEP analysis derived a low mass bound, $m_A > 93.4$ GeV for the CP conserving scenario [74]. This leads to a limit $M_{H^\pm} > 120$ GeV. For the CP violating scenario the limits are much weaker.

Charged Higgs boson searches at Tevatron

The Tevatron was colliding protons and anti-protons at energies of 1.8 TeV for Run I and of 1.96 TeV for Run II. The two experiments CDF and D0 have been searching for charged Higgs bosons. Their analyses were done for two Higgs mass region: light mass region is defined as $M_{H^\pm} < m_t$ and the remaining heavy mass region. For the light mass region, they used the collected data for $t\bar{t}$ production and then a (anti)top quark decay into a charged Higgs boson and a bottom quark [75, 76, 77, 78]. The charged Higgs bosons then decay into following final states: cs, $\tau\nu_\tau$, t^*b and Wh. No further exclusion bound on $M_{H^\pm}$ was found. The CDF experiment reported an excluded region in the $(M_{H^\pm}, \tan\beta)$ plane for the specified MSSM parameters as can be seen in Fig. 3.2 [77]. The same analysis at D0 has set an upper limit on $\mathrm{Br}(t \to H^+b)$ for the charged Higgs mass from 80 to 155 GeV. They exclude $\mathrm{Br}(t \to H^+b) > 0.2$ at 95% C.L. [79].

For the charged Higgs mass range from 180 to 300 GeV, the D0 experiment reported a search using the channel $q\bar{q}' \to H^+ \to t\bar{b} \to W^+b\bar{b} \to l^+\nu b\bar{b}$ where l represents an electron or a muon [80]. The analysis has been done in the context of the THDM. An excluded region in the $(M_{H^\pm}, \tan\beta)$ plane was found in the THDM type I, see in Fig. 3.3. For the THDM type II and type III, their analysis sensitivity is not sufficient to exclude regions. No similar analysis has been presented for the MSSM charged Higgs bosons.
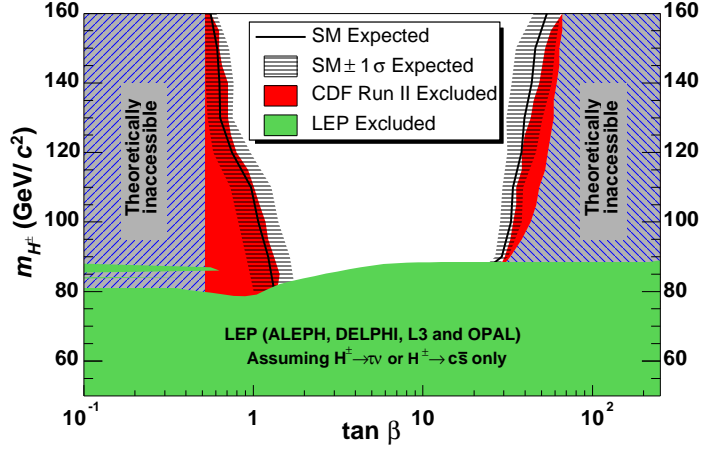
Figure 3.2: The CDF 95% C.L excluded region in the $(M_{H^\pm}, \tan\beta)$ plane. The MSSM parameters are set to $M_{SUSY} = 1000$ GeV, $\mu = -500$ GeV, $A_t = A_b = 2000$ GeV, $A_\tau = 500$GeV, $M_2 = M_3 = M_{\tilde{Q}} = M_{\tilde{U}} = M_{\tilde{D}} = M_{\tilde{E}} = M_{\tilde{L}} = M_{SUSY}$, and $M_1 = 0.498\ M_2$. The SM-expected exclusion limits are indicated by black solid lines and the $\pm 1\sigma$ confidence band around it is obtained by generating pseudo-experiments.

Charged Higgs boson searches at the LHC

The Large Hadron Collider (LHC) colliding opposite beams of either protons has been successfully operating at the center-of-mass energy of 7 TeV. The two experiments ATLAS and CMS are designed to hunt the SM Higgs boson and new physics. To date they have recorded an amount of data of about 4 fb^{-1}. A few analyses for the charged Higgs bosons have been presented and focused on the light mass region [81, 82, 83]. Similar to the Tevatron the charged Higgs bosons are mainly produced from $pp \to t\bar{t} \to H^+ b W^- \bar{b}$ mechanism and $pp \to t\bar{t} \to H^+ b H^- \bar{b}$ to a lower extent. Compared to the Tevatron results, ATLAS has obtained a stronger limit on the branching fraction, $\mathrm{Br}(t \to bH^+) < 0.1$. It is based on the data set of the integrated luminosity of 1.03 fb^{-1} and valid for $80\,\mathrm{GeV} < M_{H^\pm} < 160\,\mathrm{GeV}$ [83]. At CMS, the limit is a bit stronger, $\mathrm{Br}(t \to bH^+) < 0.05$ [82] in the same mass range. There is, to date, no available analysis for the heavy mass region.

3.6.2 Indirect searches

Most of the indirect searches for charged Higgs bosons have been done in the rare decays of B mesons where an intermediated charged Higgs boson can give significant contributions due to the large bottom charged Higgs couplings. There are three important decay modes: leptonic decay $B \to \tau + \nu_\tau$, semileptonic decay $B \to D + \tau + \nu_\tau$ and $B \to X_s + \gamma$. The charged Higgs bosons together with the W bosons contribute already at tree level. Comparing experimental data with theoretical predictions has led to severe excluded region on the $(\tan\beta, M_{H^\pm})$ plane as seen in
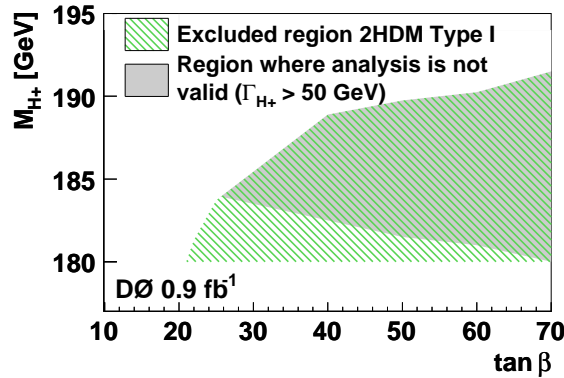
Figure 3.3: The D0 95% C.L excluded region in the $(M_{H^\pm}, \tan\beta)$ plane for THDM type I. The region for which $\Gamma_{H^+} > 50$ GeV indicates the approximate area where the charged Higgs width is significantly larger than the detector resolution and hence the analysis is not valid. The analysis was based on 0.9 fb^{-1} data collected at a center-of-mass energy of 1.96 TeV.

Fig. 3.4 [84]. These analyses have been done in the context of the THDM type II. The limits are not applied for the MSSM. Unlike the THDM, the SUSY loop contributions can be rather large depending on the soft SUSY parameters.
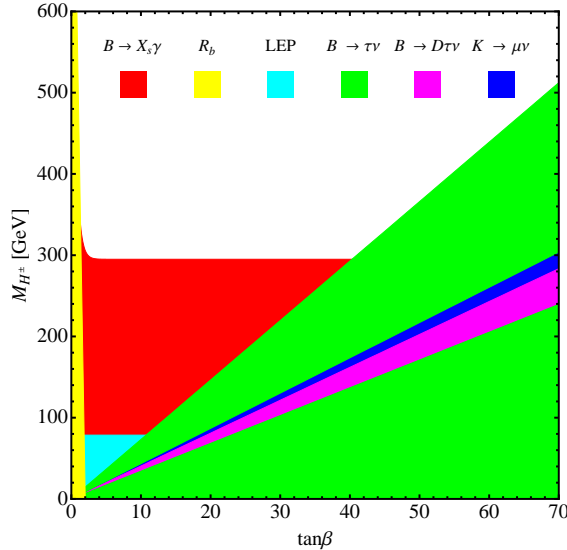

Figure 3.4: Combined direct and indirect bounds on $M_{H^\pm}$ in the THDM type II as a function of $\tan\beta$. The colored areas are excluded by the constraints at 95% C.L.

Chapter 4

Treatment of divergences in one-loop calculations

In this chapter, we discuss the divergences which we encounter in our computations of the one-loop EW and QCD corrections.

4.1 Singularities of one-loop integrals

A generic Feynman diagram in Fig. 4.1 involves an integral over the loop momentum q in D-dimensional space time,

$$\mathcal{T}^N_{\mu_1\cdots\mu_P} = \int_{-\infty}^{\infty} \frac{d^D q}{(2\pi)^D} \frac{q_{\mu_1}\cdots q_{\mu_P}}{\prod_{i=1}^{N}[(q+k_i)^2 - m_i^2 + i\varepsilon]}, \tag{4.1}$$

where N is the number of loop propagators, P is the tensor rank ($P < N$ for a renormalisable theory), p_i are external momenta,

$$k_1 = p_1, \ k_2 = p_1 + p_2, \ \cdots, \ k_N = 0, \tag{4.2}$$
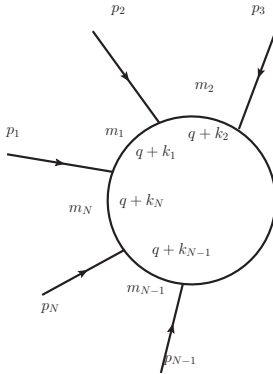

Figure 4.1: A generic one-loop diagram

and ε is an infinitesimally possitive parameter.

The one-loop integral in Eq. (4.1) is divergent in the limit $q \to \infty$, provided that $4 + P \geq 2N$. This is called ultraviolet (UV) divergence and can be computed by using a regularization method. The divergences are removed in renormalization process, more details will be discussed in Section 4.2.

It is well known that any tensor one-loop integral can be decomposed into a set of four scalar integrals (one-, two-, three-, four-point scalar integrals) by making use of the Passarino-Veltman reduction method [85]. As of now we focus only on the scalar integral $\mathcal{T}_0^N$. It can be rewitten in the Feynman parameter representation as

$$\mathcal{T}_0^N = \int_0^\infty \prod_{i=1}^N dx_i \delta(1 - \sum_{i=1}^N x_i) \int_{-\infty}^\infty \frac{d^D q}{(2\pi)^D} \frac{1}{\{\sum_{i=1}^N x_i[(q + k_i)^2 - m_i^2 + i\varepsilon]\}^N}. \tag{4.3}$$

There are two types of singularities of complex integrals which cannot be avoided by deforming the contour of the integral: end-point singularities happen when the integrand is singular at one of the end-points of the contour, pinch singularities happen when two or more singular points of the integrand approach the contour from opposite sides and coincide. The scalar loop integrals in general may contain these two types of singularities and they are called Landau singularities.

The necessary conditions for the singularities of this integral in the physical region are [86, 87, 88, 89, 90, 91]:

$$\begin{cases} x_i[(q + k_i)^2 - m_i^2] = 0, \ \forall i \in \{1, ..., N\}, \\ \sum_{i=1}^N x_i(q + k_i)^\mu = 0, \\ x_i \text{ real and } x_i \geq 0, \\ q + k_i = (q + k_i)^*. \end{cases} \tag{4.4}$$

If there exists a solution with some parameters x_i not equal to zero then the first equation means that the corresponding internal particles are on mass shell and the second one means that momentum of those particles are linear dependent. The two last equations define the physical region. Now we focus on the solution with non-zero x_i, $i = 1, ..., M$ ($M \leq N$). Multiplying the second condition with $(q + k_j)_\mu$, $j = 1, ..., M$, then we get a set of equations

$$\begin{cases} Q_{11}x_1 + Q_{12}x_2 + \cdots + Q_{1M}x_M &= 0, \\ Q_{21}x_1 + Q_{22}x_2 + \cdots + Q_{2M}x_M &= 0, \\ \vdots \\ Q_{M1}x_1 + Q_{M2}x_2 + \cdots + Q_{MM}x_M &= 0, \end{cases} \tag{4.5}$$

where Q_{ij} elements are

$$Q_{ij} = 2(q + k_i)(q + k_j) = m_i^2 + m_j^2 - (k_i - k_j)^2, \quad i, j = 1, ..., M. \tag{4.6}$$

Here the first condition has been used. Q matrix is called Landau matrix. The above equations have non trivial solutions for x_i if and only if $\det(Q) = 0$. The necessary conditions for the appearance of the singularities in the physical region is therefore rewritten as

$$
\begin{cases}
\det(Q) = 0, \\
(q + k_i)^2 = m_i^2, \forall i \in \{1, \ldots, M\}, \\
x_i > 0, \forall i \in \{1, \ldots, M\}, \\
q = q^*.
\end{cases}
\tag{4.7}
$$

For $M = N$, we have leading Landau singularity (LLS). For $M < N$, it is sub-leading Landau singularity (sub-LLS). In practice, it is important to know the nature of these singularity and whether they are integrable. The singular part can be calculated in the following way. First, performing integration over loop momentum q, we get

$$
\mathcal{T}_0^N = T(N) \int_0^\infty \prod_{i=1}^N dx_i \delta(1 - \sum_{i=1}^N x_i) \frac{1}{\Delta^{N-D/2}},
\tag{4.8}
$$

where

$$
T(N) = \frac{(-1)^N \Gamma(N - D/2)}{(4\pi)^{D/2}}, \quad \Delta = \frac{1}{2} \sum_{i,j=1}^N x_i x_j Q_{ij} - i\varepsilon,
\tag{4.9}
$$

the factor $T(N)$ is responsible for UV-divergence. Now we denote $\bar{x} = \{\bar{x}_1, \bar{x}_2, ..., \bar{x}_N\}$ which satisfies Landau equations

$$
\begin{cases}
\Delta(\bar{x}) & = 0, \\
\bar{x}_i & = 0, \forall i \in \{M, \ldots, N\}, \\
\frac{\partial \Delta}{\partial x_i}\big|_{x_i = \bar{x}_i} & = 0, \forall i \in \{1, \ldots, M\}.
\end{cases}
\tag{4.10}
$$

Expanding Δ about $\bar{x}$ one gets

$$
\Delta = \Delta(\bar{x}) + \sum_{i=1}^N (x_i - \bar{x}_i) \frac{\partial \Delta}{\partial x_i}\big|_{x_i = \bar{x}_i} + \frac{1}{2} \sum_{i=1}^N (x_i - \bar{x}_i) \frac{\partial^2 \Delta}{\partial x_i \partial x_j}(x_j - \bar{x}_j) - i\varepsilon.
\tag{4.11}
$$

Then performing integration over x_i, the singular part in the limit $x_i \to 0^+$, $i = M, \ldots, N$ is given by (more details see for example [91])

$$
(\mathcal{T}_0^N)_{\text{sing}} \propto [\Delta(\bar{x}) - i\varepsilon]^{(D-M-1)/2}.
\tag{4.12}
$$

Here we assume that the singularities are not further enhanced. The Landau singularity appears when $\Delta(\bar{x}) \to 0$. In four dimensions we have

- for $M = 4$, $(\mathcal{T}_0^N)_{\text{sing}} \propto \frac{1}{\sqrt{\Delta(\bar{x})}}$, this is a four-point Landau singularity;

- for $D = 4, M = 3$, $(\mathcal{T}_0^N)_{\text{sing}} \propto \ln \Delta(\bar{x})$, this is a three-point Landau singularity;

- for $D = 4, M = 2$, $(\mathcal{T}_0^N)_{\text{sing}} \propto \sqrt{\Delta(\bar{x})}$, this is two-point Landau singularity (normal threshold);

- for $D = 4, M = 1$; $(\mathcal{T}_0^N)_{\text{sing}} \propto \Delta(\bar{x})$, this is regular.

We observe that only the three- and four-point Landau singularities are divergent. In our one-loop calculation for the process $gg \to W^\mp H^\pm$ we encounter three-point singularities. Fortunately, these singularities are integrable. Hence they do not cause problems for hadronic cross section, but the partonic cross section is divergent at the singular point. We will discuss this interesting issue in Subsection 7.3.3.

On the other hand, there exist cases in which the effects of landau singularities can be enhanced and make the loop integrals divergent. Indeed the soft and collinear singularities are enhanced Landau singularities. They will be discussed in detail in Section 4.3.

4.2 UV divergences

4.2.1 Regularization

To deal with the UV-divergent integrals it is convenient to use a regularization method to separate the results into a finite part and a divergent part. There are several different regularization schemes. They all introduce new parameters such as a cut-off Λ in Pauli-Villars method [92], an ϵ-dimensional parameter in dimensional regularization [93]. The divergent part then can be expressed in terms of those parameters and will be removed by renormalization process in which counterterms are introduced to precisely cancel UV divergences. In practical calculation, it is more convenient to use a regularization scheme which respects a given symmetry of the theory, *e.g.* gauge symmetry, supersymmetry. Of course, this does not mean one cannot use other schemes which violate the symmetry. However in such cases the symmetry restoring counterterms need to be added. It is well known the dimensional regularization preserves gauge invariance and its variant dimensional reduction [94] preserves supersymmetry. For our purpose, we will discuss those two schemes in more detail. There is a another approach known as differential regularization [95] which provides finite Green functions without any intermediate regulator or counterterms, however it introduces many arbitrary constants which have to be fixed at the end of the calculations by requiring the fulfillment of the relevant symmetry identities. A constrained version has been shown to be equivalent to dimensional reduction at one-loop level [96].

Dimensional regularization

Dimensional regularization (DREG) is an elegant and convenient way which calculate ill-defined loop integrals by moving from 4 to d dimensional space where $d = 4 - 2\epsilon$. Then one can compute the loop-integrals without worrying about divergences. The results then can be expanded in terms of ϵ. The results in 4 dimensions are obtained by taking the limit $\epsilon \to 0$. The UV-divergent terms appear as ϵ-poles. This process is gauge invariant since the Ward identities holds for any value of d [93]. Dimensional regularisation introduces also an arbitrary mass parameter, renormalization scale μ_R, to take care of the dimension of the couplings in d dimensional space. How to deal with this scale relates to definition of renormalization schemes. The only disadvantage in the application of this scheme is the difficulty with the definition of γ^5 matrix in d-dimensional space, since it is an intrinsically 4-dimensional object. 't Hooft and Veltman [93] used the definition $\gamma^5 = i\gamma^0\gamma^1\gamma^2\gamma^3$ in d dimensions. It however leads to the violation of the axial-vector Ward identities. An alternative definition where $\{\gamma^5, \gamma^\mu\} = 0$ for all d is preferred for theories being free of axial anomalies like the SM. Therefore, this prescription is commonly used for the SM. Unfortunately, this scheme does not preserve supersymmetry manifestly. Because the number of the components of the supersymetric generators Q_α depends on d. This leads to the number of bosonic fields may not equal to the number of fermionic fields for any d dimensions. Therefore DREG needs to be modified if one wishes to apply it for the supersymmetric theory.

Dimensional reduction

Dimensional reduction (DRED) was first proposed by Siegel [94] to modify DREG by fixing the number of the components of Q_α for any d to preserve supersymmetry. In practical calculations it is done as follows. Momenta, space-time coordinate vertors, metric tensor are in d dimensions while vector fields and γ matrices are still in 4 dimensions. To distinguish the 4-dimensional vectors and its d-dimensional ones he separated a vector into a d vector and a $d - 4$ vector. It is done for γ^μ matrices and polarization vectors ϵ^μ. Then he pointed out an inconsistency related to the analytic continuation [97]. The combination of ϵ tensor and γ matrices leads to the relation, $0 = d(d - 1)(d - 2)(d - 3)(d - 4)$, which is true for $d = 0, 1, 2, 3, 4$ and is not applicable for non-integer d. A mathematically consistent way of using DRED was formulated in [98] by realizing the 4-dimensional space as a *quasi-4-dinemsional space*. Such space have the essential 4-dimensional properties but is in fact infinite dimensional. Concerning the γ^5 problem, the two definitions as in DREG can be used in an axial anomaly free theory. DRED was proven to preserve supersymmetry at one-loop level. A general proof for higher oder has not been available.

4.2.2   Renormalization

After using a consistent regularisation to compute the UV-divergent loop integrals, one needs to remove all the divergent parts to obtain finite S-matrix elements. Renormalization is a procedure which absorbs all those divergences into the couplings and the masses the classical Lagrangian. We can do that because they are unphysical quantities (bare quantities). Based on renormalizablity, one can classify three groups of theories:

- super-renormalizable theories contain only couplings with positive mass dimension,

- reromalizable theories contain only couplings with non-negative mass dimension,

- non-renormalizable theories contain couplings with negative mass dimension.

The SM and MSSM belong to the second group.

There are different renormalization approaches. We will use the counterterm method for convenience. In this method, one first has to chose a set of independent parameters, then replacing the bare couplings g_0 and masses m_0^2 by the renormalized ones g and m^2, respectively,

$$g_0 = Z_g g = (1 + \delta Z_g)g, \quad m_0 = m + \delta m, \tag{4.13}$$

where the renormalization constants δZ_g and δm^2 are UV-divergent. Renormalization of masses and couplings are enough to make all S-matrix elements finite. However, it is not enough to make all Green functions finite. For this purpose one has to renormalize fields by replacing the bare fields by the renormalized ones

$$\Phi_0 = \sqrt{Z_\Phi}\Phi = (1 + \frac{1}{2}\delta Z_\Phi)\Phi. \tag{4.14}$$

Using those relations, the classical Lagrangian can be split into a renormalized part and a counterterm part

$$\mathcal{L}(g_0, m_0, \Phi_0) = \mathcal{L}(g, m, \Phi) + \delta\mathcal{L}(g, m, \delta Z_g, \delta m, \delta Z_\Phi). \tag{4.15}$$

Now one has to use a set of rules to define the renormalization constants. That set of rules determine a renormalization scheme. Then in the computation of the virtual correction one has to compute all loop diagrams and the counterterm diagrams. All the UV-divergences from loop diagrams will be canceled precisely with the ones from the counterterm diagrams. The results are finite and only depend on the renormalized parameters and possibly on μ_R.

In the following we discuss three popular renormalization schemes used in this thesis. It is noted that the renormalization constants in every renormalization schemes have the same divergent part but differ in the finite part.

On-shell scheme

In the on-shell scheme [99, 100, 101], the renormalization constants are chosen in a way that the renormalized parameters are equal to the physical parameters order by order in perturbation theory. A physical mass is the real part of the pole of the propagator. They can often be measured with high accuracy such as the masses of the W and Z bosons and of the charged leptons. If there exists a mixing of particles, the on-shell scheme requires their mass matrix to be diagonal. For a coupling one needs to associate it with a specific vertex. Then on-shell coupling means that all corrections to the vertex vanish when external fields are on-shell, *i.e.* $p_i^2 = m_i^2$. The only electromagnetic coupling e of the vertex $ee\gamma$ is measured in the low energy limit. That is why this scheme is favored in QED and in the electroweak theory. The on-shell renormalization of a field requires the residue of its propagator to be one. Therefore, in actual loop calculation, one simply removes all the wave function corrections since they vanish in the on-shell scheme. However using the on-shell scheme is questionable in many cases such as the quark masses, the unknown Higgs masses and the strong coupling, since they are not well defined. Other renormalization scheme may be helpful.

$\overline{\text{MS}}$ scheme

In dimensional regularization, the UV-divergent parts are proportional to $\Delta = 2/\epsilon - \gamma_E + \ln 4\pi$ at one-loop level, γ_E is Euler-Mascheroni constant. A simplest way to remove all UV divergences is to define renormalization constants in such a way that they precisely cancel only the terms proportional to $1/\epsilon$. This scheme is called Minimal Subtraction scheme (MS) [102]. One can do more than that by absorbing not only ϵ-poles but also the constant $-\gamma_E + \ln 4\pi$. This is done in Modified Minimal Subtraction scheme ($\overline{\text{MS}}$) [103, 104] where the counterterms are now proportional to Δ.

$\overline{\text{DR}}$ scheme

It is identical to $\overline{\text{MS}}$ scheme but it is used in the dimensional reduction. At one-loop level the renormalization constants in two schemes are identical. In higher order, they may be different.

It should be noted that, the S-matrix elements do not depend on the renormalization scheme, if contributions from all orders are included. However we cannot do that. In practice we have to truncate the calculation at some fixed order. Consequently, the S-matrix elements now depend on which renormalization scheme is used. The difference between them is of the higher order effects. In many cases choosing a good renormalization scheme leads to a more reliable prediction. In our calculation we will use a combination of two schemes, the on-shell and the $\overline{\text{DR}}$ schemes.

4.2.3 Renormalization of the MSSM

For the evaluation of one-loop diagrams, we will use `FeynArts` [105] and `FormCalc` [96] packages. In `FeynArts` there is a MSSM model file which contains all couplings in MSSM at tree-level. For our calculations we have to implement all necessary counterterms. In this section, we discuss renormalization of those parts of the MSSM which we need.

The Higgs and gauge sectors

We focus only on one-loop corrections in the complex MSSM. We will follow closely the conventions of [101, 23]. Now we have to chose a set of independent parameters for the sectors. It must satisfy the completeness property so that all remaining parameters can be expressed in terms of the independent parameters. The two sectors depend on eight real parameters $\{v_1, v_2, g, g', \tilde{m}_1^2, \tilde{m}_2^2, b, \xi\}$. For the sake of convenience we shift to another set of eight parameters $\{M_W, M_Z, e, M_{H^\pm}, \tan\beta, T_h, T_H, T_A\}$, where T_h, T_H and T_A are tadpoles corresponding to the tree-level Higgs mass eigenstates h, H and A, respectively. Instead of $M_{H^\pm}$ one can choose m_A since they are related by $M_{H^\pm}{}^2 = m_A^2 + M_W^2$. However we are working in the complex MSSM where A mixes with h and H beyond tree level. It is therefore better to choose $M_{H^\pm}$.

Now we define the relations between the bare parameters and the renormalized parameter as follows

$$
\begin{aligned}
e_0 &= e(1 + \delta Z_e), & T_{h0} &= T_h + \delta T_h, \\
M_{W0}^2 &= M_W^2 + \delta M_W^2, & T_{H0} &= T_H + \delta T_H, \\
M_{Z0}^2 &= M_Z^2 + \delta M_Z^2, & T_{A0} &= T_A + \delta T_A, \\
\mathbf{M_{n0}} &= \mathbf{M_n} + \delta\mathbf{M_n}, & \tan\beta_0 &= \tan\beta(1 + \delta\tan\beta), \\
\mathbf{M_{c0}} &= \mathbf{M_n} + \delta\mathbf{M_n}, & &
\end{aligned}
\tag{4.16}
$$

where the bare parameters are denoted by an index 0, $\mathbf{M_n}$ is a neutral Higgs mass matrix written in the basis (h, H, A, G), $\mathbf{M_c}$ is a charged Higgs mass matrix written in the basis $(H^\pm, G^\pm)$ and the counterterm mass matrices are

$$
\delta\mathbf{M_n} = \begin{pmatrix} \delta m_h^2 & \delta m_{hH}^2 & \delta m_{hA}^2 & \delta m_{hG}^2 \\ \delta m_{hH}^2 & \delta m_H^2 & \delta m_{HA}^2 & \delta m_{HG}^2 \\ \delta m_{hA}^2 & \delta m_{HA}^2 & \delta m_A^2 & \delta m_{AG}^2 \\ \delta m_{hG}^2 & \delta m_{HG}^2 & \delta m_{AG}^2 & \delta m_G^2 \end{pmatrix}, \quad \delta\mathbf{M_c} = \begin{pmatrix} \delta M_{H^\pm}^2 & \delta m_{H^-G^+}^2 \\ \delta m_{G^-H^+}^2 & \delta m_{G^\pm}^2 \end{pmatrix}. \tag{4.17}
$$

The explicit expression for mass counterterms $\delta m_{h/H/A/H^\pm/G^\pm}$ can be found in [23].

In order to have finite Green functions we need to renormalize the fields. For the gauge fields, we have

$$
W_0^\pm = (1 + \frac{1}{2}\delta Z_W)W^\pm, \tag{4.18}
$$

$$
\begin{pmatrix} \gamma \\ Z \end{pmatrix}_0 = \begin{pmatrix} 1 + \frac{1}{2}\delta Z_{\gamma\gamma} & \frac{1}{2}\delta Z_{\gamma Z} \\ \frac{1}{2}\delta Z_{Z\gamma} & 1 + \frac{1}{2}\delta Z_{ZZ} \end{pmatrix} \begin{pmatrix} \gamma \\ Z \end{pmatrix}. \tag{4.19}
$$

For the neutral Higgs fields, we define

$$
\begin{pmatrix} h \\ H \\ A \\ G \end{pmatrix}_0 = \begin{pmatrix} 1+\frac{1}{2}\delta Z_{hh} & \frac{1}{2}\delta Z_{hH} & \frac{1}{2}\delta Z_{hA} & \frac{1}{2}\delta Z_{hG} \\ \frac{1}{2}\delta Z_{hH} & 1+\frac{1}{2}\delta Z_{HH} & \frac{1}{2}\delta Z_{HA} & \frac{1}{2}\delta Z_{HG} \\ \frac{1}{2}\delta Z_{hA} & \frac{1}{2}\delta Z_{HA} & 1+\frac{1}{2}\delta Z_{AA} & \frac{1}{2}\delta Z_{AG} \\ \frac{1}{2}\delta Z_{hG} & \frac{1}{2}\delta Z_{HG} & \frac{1}{2}\delta Z_{AG} & 1+\frac{1}{2}\delta Z_{GG} \end{pmatrix} \begin{pmatrix} h \\ H \\ A \\ G \end{pmatrix}, \quad (4.20)
$$

and the charged Higgs fields

$$
\begin{pmatrix} H^+ \\ G^+ \end{pmatrix}_0 = \begin{pmatrix} 1+\frac{1}{2}\delta Z_{H^-H^+} & \frac{1}{2}\delta Z_{H^-G^+} \\ \frac{1}{2}\delta Z_{G^-H^+} & 1+\frac{1}{2}\delta Z_{G^-G^+} \end{pmatrix} \begin{pmatrix} H^+ \\ G^+ \end{pmatrix},
$$

$$
\begin{pmatrix} H^- \\ G^- \end{pmatrix}_0 = \begin{pmatrix} 1+\frac{1}{2}\delta Z_{H^-H^+} & \frac{1}{2}\delta Z_{G^-H^+} \\ \frac{1}{2}\delta Z_{H^-G^+} & 1+\frac{1}{2}\delta Z_{G^-G^+} \end{pmatrix} \begin{pmatrix} H^- \\ G^- \end{pmatrix}. \quad (4.21)
$$

For the purpose of later uses we list the tree-level relations of various renormalization constants in the following.

- For the weak mixing angle

$$
c_W \equiv \cos\theta_W = \frac{M_W}{M_Z}, \qquad s_W^2 \equiv \sin^2\theta_W = 1 - \frac{M_W^2}{M_Z^2},
$$

$$
s_{W0} = s_W + \delta s_W, \qquad \delta s_W = \frac{c_W^2}{2s_W}\left(\frac{\delta M_Z^2}{M_Z^2} - \frac{\delta M_W^2}{M_W^2}\right). \quad (4.22)
$$

- For the two Higgs doublets, one can introduce two renormalization constants before the rotation (this was done in the papers [106, 107, 108])

$$
(H_1)_0 = \left(1+\frac{1}{2}\delta Z_{H_1}\right) H_1, \quad (H_2)_0 = \left(1+\frac{1}{2}\delta Z_{H_2}\right) H_2, \quad (4.23)
$$

then

$$
\begin{aligned}
\delta Z_{hh} &= \sin^2\alpha\,\delta Z_{H_1} + \cos^2\alpha\,\delta Z_{H_2}, \\
\delta Z_{AA} &= \sin^2\beta\,\delta Z_{H_1} + \cos^2\beta\,\delta Z_{H_2}, \\
\delta Z_{hH} &= \sin\alpha\cos\alpha(\delta Z_{H_2} - \delta Z_{H_1}), \\
\delta Z_{AG} &= \sin\beta\cos\beta(\delta Z_{H_2} - \delta Z_{H_1}), \\
\delta Z_{HH} &= \cos^2\alpha\,\delta Z_{H_1} + \sin^2\alpha\,\delta Z_{H_2}, \\
\delta Z_{GG} &= \cos^2\beta\,\delta Z_{H_1} + \sin^2\beta\,\delta Z_{H_2}, \\
\delta Z_{H^-H^+} &= \sin^2\beta\,\delta Z_{H_1} + \cos^2\beta\,\delta Z_{H_2}, \\
\delta Z_{G^-G^+} &= \cos^2\beta\,\delta Z_{H_1} + \sin^2\beta\,\delta Z_{H_2}, \\
\delta Z_{H^-G^+} &= \delta Z_{G^-H^+} = \sin\beta\cos\beta(\delta Z_{H_2} - \delta Z_{H_1}), \\
\delta Z_{hA} &= \delta Z_{HA} = \delta Z_{hG} = \delta Z_{HG} = 0,
\end{aligned} \quad (4.24)
$$

where the last equation is the consequence of CP-conserving Higgs sector at the tree level.

- For two vacuum expectation values

$$(v_1)_0 = (1 + \frac{1}{2}\delta Z_{H_1})(v_1 + \delta v_1), \quad (v_2)_0 = (1 + \frac{1}{2}\delta Z_{H_2})(v_2 + \delta v_2), \quad (4.25)$$

then

$$\delta \tan \beta = \frac{1}{2}(\delta Z_{H_2} - \delta Z_{H_1}) + \frac{\delta v_2}{v_2} - \frac{\delta v_1}{v_1}. \tag{4.26}$$

Renormalized self energies

The above renormalization constants will be fixed by applying a set of renormalization conditions on the renormalized tadpoles, self energies and three vertex functions. We list here explicit expressions of the self energies needed. The gauge boson self energies can be decomposed into the transverse and longitudinal parts as

$$\Sigma_{VV}^{\mu\nu}(k) = \left(g^{\mu\nu} - \frac{k^\mu k^\nu}{k^2}\right)\Sigma_{VV}^T(k^2) + \frac{k^\mu k^\nu}{k^2}\Sigma_{VV}^L(k^2), \tag{4.27}$$

and the Higgs to gauge boson mixing self energies

$$\Sigma_{SV}^\mu(k) = k^\mu \Sigma_{SV}(k^2). \tag{4.28}$$

We use h_i $(i = 1, 2, 3)$ to denote the neutral Higgs bosons (h, H, A) and V for W, Z. The renormalized self energies denoted by a hat are given by

$$\hat{\Sigma}^T_{VV}(k^2) = \Sigma^T_{VV}(k^2) + (k^2 - M^2_V)\delta Z_V - \delta M^2_V,$$

$$\hat{\Sigma}^L_{VV}(k^2) = \Sigma_{VV}(k^2) - M^2_V \delta Z_V - \delta M^2_V,$$

$$\hat{\Sigma}^T_{\gamma Z}(k^2) = \Sigma^T_{\gamma Z}(k^2) + k^2 \left(\frac{\delta Z_{\gamma Z}}{2} + \frac{\delta Z_{Z\gamma}}{2} \right) - M^2_Z \frac{\delta Z_{Z\gamma}}{2},$$

$$\hat{\Sigma}^L_{\gamma Z}(k^2) = \Sigma^L_{\gamma Z}(k^2) - M^2_Z \frac{\delta Z_{Z\gamma}}{2},$$

$$\hat{\Sigma}^T_{\gamma\gamma}(k^2) = \Sigma^T_{\gamma\gamma}(k^2) + k^2 \delta Z_{\gamma\gamma},$$

$$\hat{\Sigma}_{h_i h_j}(k^2) = \Sigma_{h_i h_j}(k^2) + \left(k^2 - \frac{m^2_{h_1} + m^2_{h_j}}{2} \right) \delta Z_{h_i h_j} - \delta m^2_{h_i h_j},$$

$$\hat{\Sigma}_{h_i G}(k^2) = \Sigma_{h_i G}(k^2) - \delta m^2_{h_i G},$$

$$\hat{\Sigma}_{GG}(k^2) = \Sigma_{GG}(k^2) + k^2 \delta Z_{GG} - \delta m^2_{GG}, \tag{4.29}$$

$$\hat{\Sigma}_{H^-H^+}(k^2) = \Sigma_{H^-H^+}(k^2) + \delta Z_{H^-H^+}(k^2 - M^2_{H^\pm}) - \delta M^2_{H^\pm},$$

$$\hat{\Sigma}_{H^-G^+}(k^2) = \Sigma_{H^-G^+}(k^2) + \delta Z_{H^-G^+}(k^2 - \frac{1}{2}M^2_{H^\pm}) - \delta m^2_{H^-G^+},$$

$$\hat{\Sigma}_{G^-H^+}(k^2) = \hat{\Sigma}^*_{H^-G^+}(k^2),$$

$$\hat{\Sigma}_{G^-G^+}(k^2) = \Sigma_{G^-G^+}(k^2) + k^2 \delta Z_{G^-G^+} - \delta m^2_{G^\pm},$$

$$\hat{\Sigma}_{AZ}(k^2) = \Sigma_{AZ}(k^2) + \frac{M_Z}{2}(\delta Z_{AG} + \sin 2\beta \delta \tan \beta),$$

$$\hat{\Sigma}_{GZ}(k^2) = \Sigma_{GZ}(k^2) + \frac{M_Z}{2} \left(\delta Z_{GG} + \delta Z_{ZZ} + \frac{\delta M^2_Z}{M^2_Z} \right),$$

$$\hat{\Sigma}_{H^-W^+}(k^2) = \Sigma_{H^-W^+}(k^2) + \frac{M_W}{2}(\delta Z_{G^-H^+} + \sin 2\beta \delta \tan \beta),$$

$$\hat{\Sigma}_{G^-W^+}(k^2) = \Sigma_{G^-W^+}(k^2) + \frac{M_W}{2}(\delta Z_{G^-G^+} + \delta Z_W + \frac{\delta M^2_W}{M^2_W}).$$

Renormalization conditions

The renormalization conditions are used to fix all the aforementioned renormalization constants.

- The vanishing tadpole conditions

$$T^{\text{1-loop}}_h + \delta T_h = 0, \ T^{\text{1-loop}}_H + \delta T_H = 0, \ T^{\text{1-loop}}_A + \delta T_A = 0, \tag{4.30}$$

  to ensure v_1, v_2 are the minimum of the one-loop Higgs potential. So, in actual calculations all tadpoles are removed.

- The gauge boson masses and fields are renormalized in on-shell scheme as in the SM. The mass renormalization constants $\delta M^2_W, \delta M^2_Z$ and the field renormalization constants $\delta Z_W, \delta Z_Z, \delta Z_{\gamma Z}, \delta Z_{Z\gamma}, \delta Z_{\gamma\gamma}$ are defined from the following

on-shell conditions

$$\widetilde{\mathrm{Re}}\,\hat{\Sigma}^T_{W^-W^+}(M_W^2) = 0, \qquad\qquad \mathrm{Re}\,\hat{\Sigma}^T_{ZZ}(M_Z^2) = 0,$$

$$\mathrm{Re}\,\hat{\Sigma}^T_{\gamma Z}(M_Z^2) = 0, \qquad\qquad \mathrm{Re}\,\hat{\Sigma}^T_{Z\gamma}(0) = 0,$$

$$\mathrm{Re}\,\hat{\Sigma}^T_{\gamma\gamma}(0) = 0,$$

$$\widetilde{\mathrm{Re}}\,\frac{\partial\hat{\Sigma}^T_{W^-W^+}(k^2)}{\partial k^2}\bigg|_{k^2=M_W^2} = 0, \qquad \mathrm{Re}\,\frac{\partial\hat{\Sigma}^T_{ZZ}(k^2)}{\partial k^2}\bigg|_{k^2=M_Z^2} = 0,$$

$$\mathrm{Re}\,\frac{\partial\hat{\Sigma}^T_{\gamma\gamma}(k^2)}{\partial k^2}\bigg|_{k^2=0} = 0, \tag{4.31}$$

where $\widetilde{\mathrm{Re}}$ takes only the real part of loop integrals.

- The electromagnetic coupling e is renormalized in the on-shell scheme, *i.e.* the amputated renormalized $ee\gamma$ vertex function receives no correction,

$$\hat{\Gamma}^\mu_{ee\gamma}(k,p,p')\big|_{k^2=0,p^2=p'^2=m_e^2} = ie\gamma^\mu. \tag{4.32}$$

This leads to [101]

$$\delta Z_e = -\frac{1}{2}\delta Z_{\gamma\gamma} + \frac{s_W}{2c_W}\delta Z_{Z\gamma} = \frac{1}{2}\frac{\partial\Sigma^T_{\gamma\gamma}(k^2)}{\partial k^2}\bigg|_{k^2=0} + \frac{s_W}{c_W}\frac{\Sigma^T_{\gamma Z}(0)}{M_Z^2}. \tag{4.33}$$

- The charged Higgs mass are renormalized in on-shell scheme

$$\widetilde{\mathrm{Re}}\,\hat{\Sigma}_{H^-H^+}(M_{H^\pm}^2) = 0. \tag{4.34}$$

- The last point is the renormalization of $\tan\beta$. This is problematic because of the fact that $\tan\beta$ is not a directly measurable quantity. Unlike the electron charge e and particle masses there is no obvious way to relate $\tan\beta$ to an observable. There exists in literature a number of renormalization schemes for $\tan\beta$; see [109] for a review. The following are two oft used schemes.

  - Dabelstein, Chankowski, Pokorski and Rosiek scheme (DCPR) [107, 106]:

$$\frac{\delta v_1}{v1} = \frac{\delta v_2}{v_2}, \quad \hat{\Sigma}_{AZ}(M_A^2) = 0. \tag{4.35}$$

  From Eq. (4.26), Eq. (4.31) and Eq. (4.35), one gets

$$\delta\tan\beta = \frac{1}{\sin 2\beta M_Z}\Sigma_{AZ}(M_A^2). \tag{4.36}$$

  One can alternatively use the vanishing condition for $\hat{\Sigma}_{H^-W^+}(M_{H^\pm}^2)$[110] instead of $\hat{\Sigma}_{AZ}(M_A^2)$ and gets

$$\delta\tan\beta = \frac{1}{\sin 2\beta M_W}\Sigma_{H^-W^+}(M_{H^\pm}^2). \tag{4.37}$$

– The $\overline{\text{DR}}$ scheme [111] imposes conditions

$$
\begin{aligned}
\frac{\delta v_1}{v1} &= \frac{\delta v_2}{v_2}, \\
\delta Z_{H_1} &= -\left[\text{Re}\,\frac{d\hat{\Sigma}_{HH}}{dk^2}\Big|_{\alpha=0}\right]^{\text{div}}, \\
\delta Z_{H_2} &= -\left[\text{Re}\,\frac{d\hat{\Sigma}_{hh}}{dk^2}\Big|_{\alpha=0}\right]^{\text{div}}, \\
\delta\tan\beta &= \frac{1}{2}(\delta Z_{H_2} - \delta Z_{H_1}),
\end{aligned}
\tag{4.38}
$$

where $^{\text{div}}$ takes only the UV-divergent part which proportional to $\Delta = 2/\epsilon - \gamma_E + \ln 4\pi$ in dimensional reduction.

Unfortunately, as shown by Freitas and Stökinger [109], there is no satisfactory scheme which is simultaneously gauge-independent, process-independent and numerically stable. However, $\overline{\text{DR}}$ appears to be a good scheme since it is manifestly process-independent and it is numerically stable [111, 112]. It is not gauge-independent in general gauge but it is gauge-independent at one-loop level in R_ξ gauges [109]. Moreover, this scheme is technically convenient in implementation. So it is often used in one-loop calculations. In our calculations we will use this scheme. It should be mentioned that there exists process-dependent schemes such as the ones based on the decay modes $A \to \tau^-\tau^+$ or $H^- \to \tau^-\nu$. They are manifestly gauge independent. In those schemes $\tan\beta$ can be computed from physical observables (decay widths of those decay modes). They are not often used in practical because of technical difficulties in implementation (*e.g.* three-point functions with infrared singularities appear). Recently, the on-shell($A \to \tau^-\tau^+$) scheme has been implemented in SLOOPS [113] for the real MSSM.

Renormalization of the fermion sector

The renormalization of the fermion fields in the presence of CP violation is a bit more involved than the CP-conserving case. We therefore give here explicit formulae for mass and wave function renormalization constants of the quark fields. The quark self-energy can be decomposed as

$$
\Sigma_q(p) = \not{p}P_L\Sigma_{q,L}(p^2) + \not{p}P_R\Sigma_{q,R}(p^2) + P_L\Sigma_{q,l}(p^2) + P_R\Sigma_{q,r}(p^2). \tag{4.39}
$$

We note that $\Sigma_{q,l}(p^2) = \Sigma_{q,r}(p^2) = \Sigma_{q,S}(p^2)$ in the case of CP invariance. The renormalized self-energy is written as

$$\hat{\Sigma}_q(p) = \Sigma_q(p) + \tilde{\Sigma}_q(p), \tag{4.40}$$

$$\tilde{\Sigma}_q(p) = \frac{1}{2}(\delta Z_{q,L} + \delta Z_{q,L}^*)\not{p}P_L + \frac{1}{2}(\delta Z_{q,R} + \delta Z_{q,R}^*)\not{p}P_L$$

$$+ \frac{m_q}{2}(2\frac{\delta m_q}{m_q} + \delta Z_{q,L} + \delta Z_{q,R}^*)P_L + \frac{m_q}{2}(2\frac{\delta m_q}{m_q} + \delta Z_{q,L}^* + \delta Z_{q,R})P_R. \tag{4.41}$$

In general, $\delta Z_{q,L}$ and $\delta Z_{q,R}$ are complex[1]. δm_q can always be made real by rephasing the field ψ_L (or ψ_R). At this step any phases can be absorbed into the two factors $\delta Z_{q,L}$ and $\delta Z_{q,R}$ which will have to be determined. It is obvious that the squared amplitude is invariant under a global rephasing

$$\psi = \psi_L + \psi_R \longrightarrow e^{i\phi_\psi}(\psi_L + \psi_R). \tag{4.42}$$

From this freedom we can, for example, make $\delta Z_{q,R}$ real while $\delta Z_{q,L}$ remains complex. We therefore need 4 conditions to determine the 3 renormalization constants. The OS conditions are

$$\widetilde{\text{Re}}\,\hat{\Gamma}_q(p)u(m_q) = 0, \quad \left[\frac{1}{\not{p} - m_q}\widetilde{\text{Re}}\,\hat{\Gamma}_q(p)\right]u(m_q) = iu(m_q), \tag{4.43}$$

$$\widetilde{\text{Re}}\,\bar{u}(m_q)\hat{\Gamma}_q(p) = 0, \quad \bar{u}(m_q)\left[\widetilde{\text{Re}}\,\hat{\Gamma}_q(p)\frac{1}{\not{p} - m_q}\right] = i\bar{u}(m_q), \tag{4.44}$$

where $\hat{\Gamma}_q(p) = i[\not{p} - m_q + \hat{\Sigma}_q(p)]$ and $p^2 = m_q^2$. $\widetilde{\text{Re}}$ sets the imaginary part of the loop integrals to zero since they are not involved in the renormalization. The hermiticity of the Lagrangian imposes [99]

$$\hat{\Gamma}_q(p) = -\gamma_0^\dagger \hat{\Gamma}_q^\dagger(p)\gamma_0. \tag{4.45}$$

It is obvious that Eq. (4.44) can be derived from Eq. (4.43) and Eq. (4.45). From these conditions we get the following results

$$\delta m_q = \frac{1}{2}\widetilde{\text{Re}}\left\{m_q\left[\Sigma_{q,L}(m_q^2) + \Sigma_{q,R}(m_q^2)\right] + \Sigma_{q,l}(m_q^2) + \Sigma_{q,r}(m_q^2)\right\},$$

$$\delta Z_{q,L} = -\widetilde{\text{Re}}\left\{\Sigma_{q,L}(m_q^2) - \frac{1}{2m_q}\left(\Sigma_{q,l}(m_q^2) - \Sigma_{q,r}(m_q^2)\right)\right.$$

$$+ m_q\frac{d}{dp^2}\left[m_q\left(\Sigma_{q,L}(p^2) + \Sigma_{q,R}(p^2)\right) + \Sigma_{q,l}(p^2) + \Sigma_{q,r}(p^2)\right]_{p^2=m_q^2}\right\},$$

$$\delta Z_{q,R} = -\widetilde{\text{Re}}\left\{\Sigma_{q,R}(m_q^2) - \frac{1}{2m_q}\left(\Sigma_{q,r}(m_q^2) - \Sigma_{q,l}(m_q^2)\right)\right.$$

$$+ m_q\frac{d}{dp^2}\left[m_q\left(\Sigma_{q,L}(p^2) + \Sigma_{q,R}(p^2)\right) + \Sigma_{q,l}(p^2) + \Sigma_{q,r}(p^2)\right]_{p^2=m_q^2}\right\}, \tag{4.46}$$

where we have used the freedom Eq. (4.42) to take $\text{Im}(\delta Z_{q,R}) = -\text{Im}(\delta Z_{q,L})$. These results agree with the ones in [114].

---

[1]If we impose CP invariance then $\delta Z_{q,L}$ and $\delta Z_{q,R}$ can be taken real.

4.3 Soft and collinear singularities

Now we turn to two special solutions of the Landau equations, which lead to divergences in loop integrals. They are known as mass singularities. We have seen that a general one-loop scalar integral $\mathcal{T}_0^N$ is a function of internal masses and external momenta. In some cases $\mathcal{T}_0^N$ can contain singularities at the origin of the mass variables independently of the orientation of the external momenta. It has been shown by Kinoshita [115] there are two physical configurations that both lead to logarithmic mass divergences. The soft singularity occurs when two external on-shell particles exchange a massless particle (photon or gluons). The collinear singularity arises when an external massless particle splits into two massless particles inside a loop. Both of them can be separated and computed by using mass regularization or dimensional regularization. In mass regularization photon or gluons are given a regularized mass λ, then the divergent parts appear as $\ln(\lambda)$. In dimensional regularization the divergences appear as $1/\epsilon^n$ pole ($\epsilon = (4 - D)/2$), $n = 1, 2$. Both singularities are in fact related to the singularities of real radiation of massless particles. In particular, the mass divergent parts in virtual contributions exactly cancel with the singularities in the real radiation contributions order by order when summed over all degenerate states. This is known as Kinoshita-Lee-Nauenberg (KLN) theorem [115, 116]. In the following we will discuss in detail the treatment of those singularities. We will use the mass regularization scheme. Therefore we consistently work in four space-time dimensions. One should be careful when using mass regularization for QCD correction calculations since giving a small mass to gluons may break gauge invariance, in particularly, when the QCD loops involve three-gluon couplings. In our QCD one-loop calculation involving only quark-antiquark-gluon couplings it is safe to use mass regularization.

4.3.1 Conditions

Assuming there is at least one massless particle at nth position in the scalar one-loop integral (4.3) then the Landau matrix contains the element $Q_{nn} = 2m_n^2$. The Landau equations can have a solution (we follow the convention in Section 4.1)

$$
\begin{cases}
(q + k_n)^2 & = m_n^2 \to 0, \\
\bar{x}_n & = 1, \\
\bar{x}_i & = 0, \forall i \in \{1, \ldots, n - 1, n + 1, \ldots, N\}, \\
\Delta(\bar{x}) & = m_n^2 \to 0,
\end{cases}
\tag{4.47}
$$

$\bar{x}_n = 1$ due to the constraint $\sum_{i=1}^{N} x_i - 1 = 0$. Here we only concentrate in mass singularities therefore we will ignore other possible solutions. Now the expansion

(4.11) becomes

$$
\begin{aligned}
\Delta \;=\; & m_n^2 + \sum_{i\neq n} x_i \frac{\partial\Delta}{\partial x_i} + \frac{1}{2}\sum_{i,j(\neq n)=1}^{N} x_i x_j \frac{\partial^2\Delta}{\partial x_i \partial x_j} - \frac{1}{2}\sum_{i,j(\neq n)=1}^{N} x_i x_j \frac{\partial^2\Delta}{\partial x_n \partial x_j} \\
& -\frac{1}{2}\sum_{i,j(\neq n)=1}^{N} x_i x_j \frac{\partial^2\Delta}{\partial x_n \partial x_i} + \frac{1}{2}\sum_{i,j(\neq n)=1}^{N} x_i x_j \frac{\partial^2\Delta}{\partial x_n \partial x_n}.
\end{aligned}
\tag{4.48}
$$

Substituting

$$
\Delta = \sum_{i=1}^{N} x_i m_i^2 - \sum_{i<j}^{N} x_i x_j (k_i - k_j)^2,
\tag{4.49}
$$

into Eq. (4.48) we get

$$
\Delta = m_n^2 + \sum_{i\in B} x_i \beta_i + \sum_{i\in C} x_i \beta_i + \frac{1}{2}\sum_{i,j(\neq n)=1}^{N} x_i x_j G_{ij},
\tag{4.50}
$$

where

$$
\beta_i = m_i^2 - (k_i - k_n)^2, \forall i \in B, C,
\tag{4.51}
$$

and

$$
G_{ij} = 2 k_i k_j.
\tag{4.52}
$$

B is the largest set of i such that $\beta_i = 0$ and C is for non-vanishing β_i. n_B is the number of elements of set B. The scalar integral in Eq. (4.3) becomes

$$
\mathcal{T}_0^N = T(N) \int_0^\infty \prod_{i=1}^{N} dx_i \frac{\delta(1 - \sum_{i=1}^{N} x_i)}{(m_n^2 + \sum_{i\in B} x_i \beta_i + \sum_{i\in C} x_i \beta_i + \frac{1}{2}\sum_{i,j(\neq n)=1}^{N} x_i x_j G_{ij})^{N-2}}.
\tag{4.53}
$$

Now we consider some special cases:

- $n_B = 0, 1$ the singular parts of one-loop integral which are taken in the limit $x_n \to 1$ will vanish if $m_n^2 \to 0$.

- $n_B = 2$ then the singular parts is logarithmic as we can see easily in the 3-point function (we assume $m_3 \to 0$)

$$
\mathcal{T}_0^3 = T(3) \int dx_1 dx_2 \frac{1}{m_3^2 + \frac{1}{2}\sum_{i,j=1}^{2} x_i x_j G_{ij}},
\tag{4.54}
$$

which can be integrated around $x_1 = x_2 = 0$ to get

$$
(\mathcal{T}_0^3)_{\text{sing}} \propto \ln m_3^2.
\tag{4.55}
$$

The two elements of B must be direct neighbors of nth particle, *i.e.* ,

$$
m_{n-1}^2 = (k_{n-1} - k_n)^2 = p_{n-1}^2, \quad m_{n+1}^2 = (k_{n+1} - k_n)^2 = p_n^2.
\tag{4.56}
$$

If an element of set B is not a direct neighbor of nth particle, for example $i = n + 2$, then the condition $m_{n+2}^2 = (k_{n+2} - k_n)^2 = (p_n + p_{n+1})^2$ cannot happen for every orientation of momenta p_n and p_{n+1}. The same reason does not allow for $n_B > 2$. The momentum transfer of nth propagator $q + k_n$ goes to zero. Therefore this is called soft singularity. Any loop diagrams which contain photon or gluons satisfy the above conditions hence are soft divergent.

We have seen that soft singularity is one-point Landau singularity enhanced by conditions in Eq. (4.56). The number of propagators involved are three. Therefore $N < 3$ there is no soft singularity. For $N > 3$, soft singularities of N-point integrals can always expressed in terms of 3-point integrals, more details are given in [117].

The scalar N-point function in Eq. (4.53) can have mass divergence if the following conditions are fulfilled

$$m_n^2 \to 0, m_{n+1}^2 \to 0, \quad (k_{n+1} - k_n)^2 \to 0. \tag{4.57}$$

In fact, it gives the following solution of the Landau equations,

$$\begin{cases} (q + k_n)^2 & = m_n^2 \to 0, \\ (q + k_{n+1})^2 & = m_{n+1}^2 \to 0, \\ \bar{x}_n + \bar{x}_{n+1} & = 1, \\ \bar{x}_i & = 0, \forall i \in \{1, \ldots, n-1, n+2, \ldots, N\}, \\ \Delta(\bar{x}) & = m_n^2 + m_{n+1}^2 \to 0. \end{cases} \tag{4.58}$$

In this case the nth and $(n+1)$th propagator are on mass shell and their transfer momenta tend to collinear to each other. Therefore this is called collinear singularity. It involves two propagators hence for $N < 2$ there is no collinear singularity. The nature of this singularity is also logarithmic. We encounter the collinear singularities in loop diagrams which contain interactions of light quarks with photon or gluons and of charged fermions with photon and triplet gluon couplings. In addition to the collinear conditions, if β_{n-1} or β_{n+2} also vanish then the collinear and soft singularities overlap. The divergent part will be proportional to $\ln m_n^2 \ln m_{n+1}^2$.

4.3.2 Real radiations of massless particles

The mass singularities in real radiation processes arise from the phase space integral

$$I = \int \frac{d^3q}{q_0} \frac{1}{(2p_i q)(2p_j q)}, \tag{4.59}$$

where p_i, p_j are the momenta of the particles that emit the massless particle, q is momentum of the massless particle. The product of two momenta can be expressed as

$$2p_i q = 2q_0 p_{i0} \left(1 - \sqrt{1 - \frac{m_i^2}{p_{i0}^2}} \cos \theta_c \right), \tag{4.60}$$

where θ_c is the angle between $\vec{p}_i$ and $\vec{q}$. Since the momentum of massless particle can go to zero, the above integral has end point singularity in the limit $q_0 \to 0$. This singularity is called the soft singularity as in the case of virtual loop. If the emitting particle is aslo massless, *i.e.* $m_i^2 \to 0$ then the integrand has a pole at $\theta_c = 0$. The integral has also end point singularity. Since two particles are collinear to each other, this is called the collinear singularity.

In one-loop calculations these bremsstrahlung processes are combined with the virtual contribution although they appear to have different final states. The reasons are very simple: i) experimentally they are not distinguishable in the soft and collinear limits, ii) they have the same power of coupling constants, hence of the same order in the perturbative theory. In practice, the two parts are computed separately but they are divergent. The numerical results can have large integration errors and thus make prediction unreliable. Fortunately, the divergent part can be factorized and computed analytically in virtual corrections. We expect to do the same in the real radiation processes. Then the divergences will be eliminated before doing the numerical integrations. It turns out to be more difficult than in the virtual parts. There are essentially two types of methods to carry out real radiation contributions: the phase space slicing (PSS) method [118, 119, 120, 121] and subtraction method [122, 123].

The PSS method is based on the idea to separate the integration region into soft and collinear region and the hard non collinear region with the help of two cutoff parameters. In the soft and collinear region, matrix elements can be approximated and hence the integration can be computed analytically. In the hard non collinear region the integrand are finite and thus are integrated numerically. In principle, the final results are independent of the two cut-offs. However there are subtleties in practice. If the cut-offs are large then the integration error of the finite part is small but the approximation of matrix elements in the soft and collinear region is not good enough. The serults can be wrong in this case. If the cut-offs are small then the integration error is large. Therefore one has to choose the right cutoffs to get a reliable result. This method is intuitive and simple in implementation but not very efficient in performance.

The subtraction method is based on the idea to add and subtract counterterms. The counterterms are the approximation of the real radiation matrix elements. They are exactly equal to the real radiation matrix element in the soft and collinear limits. There exists two general formulations of the subtraction method: residue approach [124] and dipole subtraction [125]. The dipole subtraction uses the subtraction method together with factorization formulae of the approximated matrix element in the soft and collinear regions as in the PSS method. Compared to the PSS method, the subtraction dipole method need more analytical work, and thus is more difficult to implement. But in exchange, its numerical error is smaller than that of the PSS method as it was pointed out in [126].

In our calculations we implement both the PSS method and the dipole subtraction. In the following we discuss them in more details to understand and implement

them properly.

A. Phace space slicing method

Let us describe this method for one-loop contributions to a generic process with n particles in the initial state ($n = 1$ for decay processes while $n = 2$ for collider processes) and m particles in the final state. The real contribution to this process can be written as

$$\sigma_{n \to m+1} = \int d\Phi_{m+1} |\mathcal{M}_1|^2, \tag{4.61}$$

where the phase space measure is given by

$$d\Phi_{m+1} = \prod_{i=1}^{m} \frac{dk_i^3}{2k_{i0}(2\pi)^3} \frac{dq^3}{2q_0(2\pi)^3} (2\pi)^4 \delta^4 \left(\sum_{a=1}^{n} p_a - \sum_{i=1}^{m} k_i - q \right), \tag{4.62}$$

p_a, k_i and q are momenta of initial states, final states and of the emitted massless particle, respectively (we use a, b indices for initial states while i, j indices for final states). $\mathcal{M}_1$ is the tree-level amplitude of the $n \to m+1$ process. The integral phase space can be decomposed into soft and hard region. If collinear singularities exist then the hard region can be decomposed into hard-collinear and hard-non-collinear region. Therefore, the real contribution is written as

$$\sigma_{n \to m+1} = \sigma_{n \to m+1}^{\mathrm{S}} + \sigma_{n \to m+1}^{\mathrm{H}}, \tag{4.63}$$

$$\sigma_{n \to m+1}^{\mathrm{H}} = \sigma_{n \to m+1}^{\mathrm{HC}} + \sigma_{n \to m+1}^{\overline{\mathrm{HC}}}. \tag{4.64}$$

The soft region is determined by $0 \leq q_0 \leq \Delta E$ ($\Delta E = \delta_s \sqrt{s}/2$), $\sqrt{s}$ is the center-of-mass energy of the process and δ_s is the soft cutoff parameter. Thus $2q_0/\sqrt{s} > \delta_s$ defines the hard region. The hard-colinear region satisfies additional collinear condition: the angle between an emitted particle and an emitting particle θ_c becomes smaller than δ_c, δ_c is collinear cutoff. The complement region is hard-non-collinear.

Here we present the approximation formulae used in our calculations in the soft and collinear region for photon radiations.

Soft region

The squared matrix element $|\mathcal{M}_1|^2$ is approximately proportional to $|\mathcal{M}_0|^2$ of the tree-level process without radiation of photon, (see *e.g.* Ref. [101]). We can write

$$\sigma_{n \to m+1} = \int d\Phi_m |\mathcal{M}_0|^2 \sum_{i,j} -\frac{\alpha}{4\pi^2} (\pm Q_i)(\pm Q_j) I_{ij}, \tag{4.65}$$

where Q_i is the relative electric charge of ith external particle, $+$ sign is for in-comming parrticle, $-$ sign is for out-going particles and

$$I_{ij} = \int_{q_0 \leq \Delta E} \frac{dq^3}{2q_0} \frac{2p_i p_j}{(p_i q)(p_j q)}. \tag{4.66}$$

This integral has been calculated analytically by 't Hooft and Veltman [127] using a mass regulator (λ) for photon,

$$I_{ij} = 4\pi \frac{\alpha p_i p_j}{(\alpha p_i)^2 - p_j^2} \left\{ \frac{1}{2} \ln \frac{(\alpha p_i)^2}{p_j^2} \ln \frac{4\Delta E^2}{\lambda^2} + \right. \tag{4.67}$$
$$\left. + \left[\frac{1}{4} \ln^2 \frac{u_0 - |\vec{u}|}{u_0 + |\vec{u}|} + \text{Li}_2\left(1 - \frac{u_0 + |\vec{u}|}{v}\right) + \text{Li}_2\left(1 - \frac{u_0 - |\vec{u}|}{v}\right) \right]_{u=p_j}^{u=\alpha p_i} \right\},$$

with

$$v = \frac{(\alpha p_i)^2 - p_j^2}{2(\alpha p_{i0} - p_{j0})}, \tag{4.68}$$

and α is a solution of

$$\alpha^2 p_i^2 - 2\alpha p_i p_j + p_j^2 = 0, \tag{4.69}$$

satisfying $\frac{\alpha p_{i0} - p_{j0}}{p_{j0}} > 0$. The spence function is defined as

$$\text{Li}_2(x) = -\int_0^1 \frac{\ln(1 - xy)}{y} dy. \tag{4.70}$$

Some special limits are useful. For $p_i = p_j$, one can get the result by taking the limit of the expression in Eq. (4.68) as α approaches 1 and using the following formulae

$$\lim_{\alpha \to 1} \frac{\alpha \ln \alpha}{\alpha^2 - 1} = \frac{1}{2},$$
$$\lim_{\alpha \to 1} \frac{\text{Li}_2(1 - \alpha x) - \text{Li}_2(1 - x)}{\alpha^2 - 1} = \frac{x \ln x}{2(1 - x)}, \tag{4.71}$$

then

$$I_{ii} = 2\pi \left(\ln \frac{4\Delta E^2}{\lambda^2} + \frac{p_{i0}}{|\vec{p}|} \ln \frac{p_{i0} - |\vec{p}_i|}{p_{i0} + |\vec{p}_i|} \right). \tag{4.72}$$

If the ith particle is massless then the above formula is simplified as

$$I_{ii} = 2\pi \left(\ln \frac{\Delta E^2}{\lambda^2} + \ln \frac{m_i^2}{|p_i|^2} \right), \tag{4.73}$$

which is the sum of soft and collinear singularities. m_i is a mass regulator. For $\vec{p}_i = -\vec{p}_j = \vec{p}$, we have

$$I_{ij} = 2\pi \frac{p_i p_j}{(p_{i0} + p_{j0})|\vec{p}|} \left[\frac{1}{2} \ln \frac{p_{i0} + |\vec{p}|}{p_{i0} - |\vec{p}|} \ln \frac{4\Delta E^2}{\lambda^2} - \text{Li}_2\left(\frac{2|\vec{p}|}{p_{i0} + |\vec{p}|}\right) \right.$$
$$\left. - \frac{1}{4} \ln^2 \frac{p_{i0} + |\vec{p}|}{p_{i0} - |\vec{p}|} + (i \leftrightarrow j) \right]. \tag{4.74}$$

If $p_{i0} = p_{j0} = p_0$ and $m_i \to 0$ then

$$I_{ij} = 2\pi \left[\ln \frac{4|\vec{p}|^2}{m_i^2} \ln \frac{4\Delta E^2}{\lambda^2} - \frac{1}{2} \ln^2 \frac{4|\vec{p}|^2}{m_i^2} - \frac{\pi^2}{3} \right]. \tag{4.75}$$

In this case, the soft and collinear singularities overlap and appear as the product of the two logarithms.

In practice, the integrated soft contributions can be combined with the virtual parts since they have the same phase-space integral.

Hard-collinear region

The collinear singularities appear in the initial state contributions and final state contributions (the interference is collinear finite). Therefore one can treat them separately. In the collinear region, the phase space integral can be factorized into a m-particle part and a collinear part. For the squared matrix element, one can use leading pole or collinear approximation where it can be factorized into a leading order squared matrix element and a splitting kernel. Then the cross section is simple enough to be integrated over the collinear phase space. The results are presented as [128]

- for initial state

$$\sigma_{n\to m+1}^{\mathrm{HC},initial}(s) = \sum_a \int_0^{1-\delta_s} dz \frac{\alpha}{2\pi} Q_a^2 \left(P_{ff}(z) \ln \frac{s_{ba}'\delta_c}{2zm_a^2} - \frac{2z}{1-z} \right) \sigma_{n\to m}^{\mathrm{born}}(s_{ab}'),$$

(4.76)

- for final state

$$\sigma_{n\to m+1}^{\mathrm{HC},final}(s) = \sum_i \int_0^{1-\delta_s} dz \frac{\alpha}{2\pi} Q_i^2 \left(P_{ff}(z) \ln \frac{s_{ji}'\delta_c z^2}{2m_i^2} - \frac{2z}{1-z} \right) \sigma_{n\to m}^{\mathrm{born}}(s_{ij}'),$$

(4.77)

where $P_{ff}(z)$ is the splitting function

$$P_{ff}(z) = \frac{1+z^2}{1-z},$$

(4.78)

and $s_{xy}' = (p_x + zp_y)^2$, p_x stands for the sum of the momenta of the remaining particles in the initial or final states. It should be emphasized that the final state collinear singularities cancel with the one in the virtual contributions. However the initial state collinear singularities do not since they are not summed over all degenerated states. Therefore one has to deal with them in a proper way depending on which collider machine we are working with. For e^-e^+ collider, one can factorize initial collinear singularities and define a density function to resum these singularities. For hardron collider, one can redefine parton distribution functions to absorb them. In our processes we have initial collinear singularities in the $b\bar{b} \to W^{\mp}H^{\pm}$ processes

and final collinear singularities in $gg \to H^- t\bar{b}$ process. Redefinition of bottom distribution is necessary. We will discuss more detail in the following Subsection C.

The above discussion can be also applied for gluon emission. However a lot of care must be taken since gluons carry color charge. In general there exist color correlations between soft (collinear) factor with the leading order squared matrix element. In our QCD contributions to $b\bar{b} \to W^\mp H^\pm$, there exists only $b\bar{b}g$ couplings and thus gluons behave like photon. All the above formulae can be used with the replacement $\alpha Q_a^2 \to \alpha_s 4/3$ and λ^2 is now an infinitesimal mass of gluons.

The emission of light fermions lead also to collinear singularities (there is no soft singularities related to massless fermions). The phase space now is divided into the collinear and hard parts with only one cutoff δ_c. We focus on the processes where light quarks are emitted from photon or gluons in the initial states. In particular we denote them as $a + \gamma(g) \to q + X$, a is an incomming parton, X is a set of final states. These processes are called photon- or gluon-induced processes. The collinear contribution for photon-induced processes is given by [129]

$$\sigma_{a\gamma \to qX} = 3\frac{Q_q^2 \alpha}{2\pi} \int_0^1 dz \left(P_{q\gamma}(z) \ln \frac{\delta_c^2 p_{q0}^2 (1-z)^2}{m_q^2} + 2z(1-z) \right) \sigma_{a\bar{q} \to X}(zs), \quad (4.79)$$

where the splitting function is

$$P_{q\gamma}(z) = z^2 + (1-z)^2, \quad (4.80)$$

and $s = (p_a + p_\gamma)^2$. For the gluon-induced process, the factor $3Q_q^2 \alpha$ is replaced by $1/2\alpha_s$. These singularities still remain after adding of virtual and real contributions and are removed by redefining distribution function of quark q.

B. Dipole subtraction method

In this section, we discuss the dipole subtraction method implemented in our calculations. We follow the procedure described in [126]. In subtraction method, the real contribution is computed by adding an integral

$$\sigma_{n \to m+1} = \int d\Phi_{m+1}(|\mathcal{M}_1|^2 - |\mathcal{M}_{\text{sub}}|^2) + \int d\Phi_{m+1}|\mathcal{M}_{\text{sub}}|^2, \quad (4.81)$$

where the subtraction function $|\mathcal{M}_{\text{sub}}|^2$ must approach $|\mathcal{M}_1|^2$ in the soft and collinear regions and must be simple enough to be integrated analytically over the singularity regions. It should be noted that the first integral can be done numerically over the full phase space with vanishing photon, gluon and fermion masses. For the second integral, the integration over the singular variables can be carried out analytically with the help of a regulator (the photon mass, gluon mass and light quark masses). In general it consists of two pieces: one piece contains all soft and collinear singularities which can be combined with the virtual contribution to cancel all the soft singularities and the other one is a convolution piece which contains only collinear

singularities. First, we discuss photon radiations. The subtraction function can be constructed from the auxiliary functions $g_{ff'}^{\mathrm{sub}}$ and the leading squared matrix element $|\mathcal{M}_0|^2$ without photon emission,

$$|\mathcal{M}_{\mathrm{sub}}(a+b \to X+q)|^2 = -\sum_{f \neq f'} Q_f Q_{f'} e^2 g_{ff'}^{\mathrm{sub}}(p_f, p_{f'}, q)|\mathcal{M}_0(\tilde{a}+\tilde{b} \to \tilde{X})|^2, \quad (4.82)$$

where f, f' are the charged particles which can be fermions or massive bosons, f is called the emitter whereas f' is called the spectator and q is momenta of photon. The tilde notations imply that the momenta of those particles can be different with the ones in the left hand side. For the evaluation of $|\mathcal{M}_0(\tilde{a}+\tilde{b} \to \tilde{X})|^2$ one has to define a mapping from Φ_{m+1} to Φ_m for each dipole term on the right hand side. The auxiliary functions must contain all soft and collinear singularities, see in Appendix B. Now we proceed to calculate the second term in Eq. (4.81). Performing the integration over the singular region, we get [126]

$$\int d\Phi_{m+1}|\mathcal{M}_{\mathrm{sub}}|^2 = -\frac{\alpha}{2\pi} \sum_{f \neq f'} Q_f Q_{f'} \Bigg\{ \int_0^1 dx \bigg[\int d\Phi_m(x) \frac{1}{x} \mathcal{G}_{ff'}(x)|\mathcal{M}_0(xp_f, p_{f'})|^2$$

$$- \int d\Phi_m(1)\mathcal{G}_{ff'}(x)|\mathcal{M}_0(p_f, p_{f'})|^2 \bigg]$$

$$+ \int d\Phi_m G_{ff'}|\mathcal{M}_0(p_f, p_{f'})|^2 \Bigg\}, \quad (4.83)$$

where the distributions $\mathcal{G}_{ff'}(x)$ contain collinear singularities and the endpoint functions $G_{ff'}$ contains both soft and and collinear singularities. Note that for final state emitter and final state spectator $\mathcal{G}_{ff'}(x)$ vanish. For the gluon radiation in our calculations for $b\bar{b} \to W^{\mp}H^{\pm}$ process, we have to replace $\alpha Q_f Q_{f'}$ by $4/3\alpha_s$.

For a light quark emitted from a photon in initial state, the dipole subtraction result consists of a finite part and a convolution part,

$$\sigma_{a\gamma \to qX} = \int d\Phi_{m+1}(|\mathcal{M}_1|^2 - |\mathcal{M}_{\mathrm{sub}}|^2) + \sigma_{a\gamma \to fX}^{\mathrm{sub}}, \quad (4.84)$$

where

$$|\mathcal{M}_{\mathrm{sub}}|^2 = Q_q^2 e^2 h_{\gamma a}(q, p_a, p_f)|\mathcal{M}_{a\bar{f} \to X}(p_a, x_{\gamma a} p_\gamma)|^2, \quad (4.85)$$

and

$$\sigma_{a\gamma \to fX}^{\mathrm{sub}} = 3\frac{Q_f^2 \alpha}{2\pi} \int_0^1 dx \mathcal{H}_{\gamma a}(m_f, x, p_a q)\sigma_{a\bar{f} \to X}(p_a, xq). \quad (4.86)$$

For the process $ag \to qX$ occured in our calculation, we have to replace $3Q_f^2\alpha$ by $1/2\alpha_s$. All the necessary subtraction functions $(g_{ff'}^{\mathrm{sub}}, \mathcal{G}_{ff'}, G_{ff'}, h_{\gamma a}, \mathcal{H}_{\gamma a})$ are presented in Appendix B.

C. Regularized parton distribution functions

As mentioned, the initial state collinear singularities still remain after adding the virtual and the real corrections. For hardon colliders we can absorb these collinear singularities into the parton distribution functions (PDF). For the processes that involve only the (anti-)quarks in the initial states in the lowest order, one only needs to replace the unrenormalized quark PDF by the renormalized one and a counterterm part

$$q(x) \rightarrow q(x, \mu_R^2) + \delta q(x, \mu_R^2), \tag{4.87}$$

where

$$
\begin{aligned}
\delta q(x, \mu_R^2) &= -\frac{\alpha Q_q^2}{2\pi} \int_x^1 \frac{dz}{z} q\left(\frac{x}{z}, \mu_F^2\right) \left\{ \ln\left(\frac{\mu_F^2}{m_b^2}\right) [P_{qq}(z)]_+ \right. \\
&\quad - [P_{qq}(z)(\ln(1-z)^2 + 1)]_+ + C_{qq}(z) \Big\} \\
&\quad - \frac{3\alpha Q_q^2}{2\pi} \int_x^1 \frac{dz}{z} \gamma\left(\frac{x}{z}, \mu_F^2\right) \left[\ln\left(\frac{\mu_F^2}{m_b^2}\right) P_{q\gamma} + C_{q\gamma}(z) \right]. \tag{4.88}
\end{aligned}
$$

The splitting functions are given by

$$P_{qq}(z) = \frac{1+z^2}{1-z}, \quad P_{qg}(z) = P_{q\gamma}(z) = z^2 + (1-z)^2, \tag{4.89}$$

and the $[\ldots]_+$ prescription is understood in the usual way,

$$\int_x^1 dz f(z) \left[\frac{g(z)}{1-z}\right]_+ = \int_x^1 dz \frac{[f(z) - f(1)]g(z)}{1-z} - f(1) \int_0^x dz \frac{g(z)}{1-z}. \tag{4.90}$$

Following the standard conventions of QCD, the factorization schemes are specified by

$$
\begin{aligned}
C_{qq}^{\overline{\rm MS}}(z) &= C_{qg}^{\overline{\rm MS}}(z) = 0, \\
C_{qq}^{\rm DIS}(z) &= \left[P_{qq}(z) \left(\ln(\frac{1-z}{z}) - \frac{3}{4} \right) + \frac{9+5z}{4} \right]_+, \\
C_{q\gamma}^{\rm DIS}(z) &= P_{q\gamma} \ln(\frac{1-z}{z}) - 8z^2 + 8z - 1. \tag{4.91}
\end{aligned}
$$

For photon-like gluon radiation processes, one can still apply the above formulae with a replacement of αQ_q^2 by $4/3\alpha_s$ and the photon PDF by the gluon PDF. In this thesis we use the MRST2004qed set of PDFs [130] which include $\mathcal{O}(\alpha_s)$ QCD and $\mathcal{O}(\alpha)$ photonic corrections. As explained in [129], the consistent use of these PDFs requires the $\overline{\rm MS}$ factorization scheme for the QCD, but the DIS scheme for the photonic corrections.

Chapter 5

Higher order corrections and resummations

In this chapter we first give a brief review of the higher corrections to the Higgs boson masses and mixing. We discuss also the using of the $\overline{\text{DR}}$ scheme in one-loop calculations involving Higgs bosons in the external lines. For the last two sections, we give an introduction of the resummation of the higher order corrections to the Higgs mixing propagators and to the bottom–Higgs couplings used in our calculations.

5.1 Higher order corrections to Higgs masses and mixings

As we have seen in Subsection 3.5.3, at tree level the MSSM Higgs sector are defined by two input parameters, $\tan\beta$ and $M_{H^\pm}$. All the remaining parameters (the neutral boson masses, mixing angles) are predicted. The masses of the lightest Higgs boson is bounded from above by $m_h < |M_Z \cos 2\beta|$ as a consequence of the fixed quartic Higgs couplings. It has been known that the loop effects can modify significantly the Higgs boson masses and mixings. In particular, the corrections including the one- and two-loop contributions can raise the upper bound of m_h to about 140 GeV [23, 65, 66].

We now discuss how to define the loop corrected masses for the neutral Higgs bosons in the Feynman diagram approach. For simplicity we first consider the case where a scalar Higgs boson does not mix with other particles (one can require the mixing to vanish in a renormalization scheme). The full propagator is defined by

$$
\begin{aligned}
\Delta_{hh} &= \frac{i}{p^2 - m_h^2} \left\{ 1 + \frac{-\hat{\Sigma}_{hh}(p^2)}{p^2 - m_h^2} + \left[\frac{-\hat{\Sigma}_{hh}(p^2)}{p^2 - m_h^2} \right]^2 + \cdots \right\} \\
&= \frac{i}{p^2 - m_h^2 + \hat{\Sigma}_{hh}(p^2)},
\end{aligned}
\tag{5.1}
$$

where $\hat{\Sigma}_{hh}(p^2)$ is the renormalized self-energy and m_h is the tree-level Higgs mass. The loop corrected Higgs mass M_h is defined as the pole of this full propagator, *i.e.*

$$\left[p^2 - m_h^2 + \hat{\Sigma}_{hh}(p^2)\right]_{p^2 = M_h^2 - iM_h\Gamma_h} = 0, \tag{5.2}$$

where Γ_h is the total decay width of the Higgs boson. If $\hat{\Sigma}_{hh}(p^2)$ is computed up to all orders of the perturbation theory then M_h is equal to the physical Higgs mass. Solving Eq. (5.2) analytically or numerically with full complex momentum dependence is in general very difficult. Therefore, instead of using Eq. (5.2) one can use an approximation equation provided that $\Gamma_h \ll M_h$,

$$M_h^2 - m_h^2 + \text{Re}\,\hat{\Sigma}_{hh}(M_h^2) + \frac{\text{Im}\,\hat{\Sigma}_{hh}(M_h^2)(\text{Im}\,\hat{\Sigma}_{hh})'(M_h^2)}{1 + (\text{Re}\,\hat{\Sigma}_{hh})'(M_h^2)} = 0, \tag{5.3}$$

where we have used a short-hand notation $F' = dF/dp^2$.

At higher order, mixing between h, H and A occurs (if all complex phases are vanishing h, H do not mix with A). Moreover, there is the mixing of the neutral Higgs bosons with G and Z, but they yield only sub-leading two-loop contributions to the Higgs boson masses, see [23]. We do not consider such mixing in the determination of the neutral Higgs masses, but they are taken into account in actual one-loop calculations involving the neutral Higgs bosons, see Section 5.2. The loop-corrected masses (pole masses) of the neutral Higgs boson are the poles of the propagator matrix,

$$\Delta_{hHA} = -\left[\hat{\Gamma}_{hHA}(p^2)\right]^{-1}, \tag{5.4}$$

with

$$\hat{\Gamma}_{hHA}(p^2) = i\left[p^2 - M(p^2)\right],$$

$$M(p^2) = \begin{pmatrix} m_h^2 - \hat{\Sigma}_{hh}(p^2) & -\hat{\Sigma}_{hH}(p^2) & -\hat{\Sigma}_{hA}(p^2) \\ -\hat{\Sigma}_{hH}(p^2) & m_H^2 - \hat{\Sigma}_{HH}(p^2) & -\hat{\Sigma}_{HA}(p^2) \\ -\hat{\Sigma}_{hA}(p^2) & -\hat{\Sigma}_{HA}(p^2) & m_A^2 - \hat{\Sigma}_{AA}(p^2) \end{pmatrix}. \tag{5.5}$$

The mixing mass matrix $M(p^2)$ contains the renormalized Higgs self-energies, $\hat{\Sigma}_{ij}$, $i, j = h, H, A$, defined in Eq. (4.31). In general, the three poles are complex and written as

$$\mathcal{M}_{h_a}^2 = M_{h_a}^2 - iM_{h_a}\Gamma_{h_a}, \quad a = 1, 2, 3, \tag{5.6}$$

where M_{h_a} are the loop-corrected masses with the convention

$$M_{h_1} < M_{h_2} < M_{h_3}, \tag{5.7}$$

and Γ_{h_a} are the corresponding total decay widths. The evaluation of the poles can be performed by diagonalising the mass matrix $M(p^2)$. For more details of the diagonalisation method with full mometa dependence we refer to [23].

There are two public Fortran codes which help to evaluate the loop corrected masses and mixings of the MSSM Higgs bosons in the general complex MSSM. The program FeynHiggs is based on Feynman diagrammatic approach [65, 131, 132, 66, 133], which we have described above. The other code, CPsuperH [134], is based on the renormalization group improved effective potential approach [135, 136, 137, 138]. In our calculation we use FeynHiggs where one has the possibility to include various important two-loop contributions to the renormalized self energies. We include the full-phase-dependent $\alpha_s\alpha_t$ corrections and the $(\alpha_s\alpha_b, \alpha_t\alpha_t, \alpha_t\alpha_b)$ corrections with interpolated complex phases dependence for the charged Higgs decay calculation (see Chapter 6).

For the charged Higgs bosons, they do mix with the charged Nambu-Goldstone bosons $G^{\pm}$ and the longitudinal part of the W-bosons. In the real MSSM, one can choose m_A as input parameter. The loop-corrected mass for the charged Higgs boson then can be determined through the pole of its propagator. In the complex MSSM, we chose $M_{H^{\pm}}$ as an input parameter and hence it is renormalized on-shell. Similar to the neutral Higgs case, the mixing between $H^{\pm}$ and $G^{\pm}, W^{\pm}$ contributes to the processes involving the charged Higgs bosons at one-loop order, see Section 5.2.

5.2 Amplitudes of processes with external Higgs bosons

In $\overline{\mathrm{DR}}$ scheme we are using for the Higgs field renormalization, the residue of the Higgs boson propagators are not equal to one. Finite wave-function renormalization therefore has to be taken into account, together with Higgs mixings. Moreover such inclusion is to ensure the on-shell property of the Higgs bosons [23, 139]. In our calculations, the neutral and charged Higgs bosons can appear in the external lines. We present the expressions of the amplitudes for such processes in the following.

For a neutral Higgs boson h_i $(i = 1, 2, 3)$ with loop-corrected mass M_{h_i} in the external state, the one-loop amplitude is given by

$$
\begin{aligned}
\mathcal{M}_{h_i}(M_{h_i}) \;=\; & \sqrt{Z_i}\left(\mathcal{M}_{h_i^0} + \sum_{j\neq i} Z_{ij}\mathcal{M}_{h_j^0}\right) \\
& + \frac{\hat{\Sigma}_{G^0 h_i}(p^2)}{p^2 - M_Z^2}\mathcal{M}_{G^0} + \frac{p_\mu\hat{\Sigma}_{Zh_i}(p^2)}{p^2 - M_Z^2}\mathcal{M}_Z^\mu,
\end{aligned}
\tag{5.8}
$$

where the wave function renormalization factors

$$
Z_i = \frac{1}{\left(\frac{i}{\Delta_{ii}(p^2)}\right)'(M_i^2)},
$$

$$
Z_{ij} = \left.\frac{\Delta_{ij}(p^2)}{\Delta_{ii}(p^2)}\right|_{p^2=M_i^2},
\tag{5.9}
$$

involve the elements Δ_{ij} of the the propagator matrix Δ_{hHA} in Eq. (5.4), h_i^0 (i=1,2,3) refer to h, H, A, respectively. p is the momentum of h_i, $p^2 = M_i^2$. $\mathcal{M}_{h_i^0}$ denote the amplitudes of the tree-level and one-loop Feynman diagrams with external Higgs bosons h_i^0. $\mathcal{M}_{h_j^0}$, $\mathcal{M}_{G^0}$ and $\mathcal{M}_Z$ are the tree-level amplitudes with h_j^0 ($j \neq i$), G^0 and Z, respectively. $\hat{\Sigma}_{G^0 h_i}$ and $\hat{\Sigma}_{Z h_i}$ are the renormalized self-energies defined in Eq. (4.31). For short notation we define the $\mathbf{Z}$ matrix as

$$\mathbf{Z} = \begin{pmatrix} \sqrt{Z_h} & \sqrt{Z_h} Z_{hH} & \sqrt{Z_h} Z_{hA} \\ \sqrt{Z_H} Z_{Hh} & \sqrt{Z_H} & \sqrt{Z_H} Z_{HA} \\ \sqrt{Z_A} Z_{Ah} & \sqrt{Z_A} Z_{AH} & \sqrt{Z_A} \end{pmatrix}. \tag{5.10}$$

Eq. (5.8) can be expressed in terms of elements of $\mathbf{Z}$ matrix,

$$\mathcal{M}_{h_i} = \sum_j \mathbf{Z}_{ij} \mathcal{M}_{h_j^0} + \frac{\hat{\Sigma}_{G^0 h_i}(p^2)}{p^2 - M_Z^2} \mathcal{M}_{G^0} + \frac{p_\mu \hat{\Sigma}_{Z h_i}(p^2)}{p^2 - M_Z^2} \mathcal{M}_Z^\mu. \tag{5.11}$$

For a charged Higgs boson, the loop amplitudes are given by

$$\begin{aligned} \mathcal{M}_{H^\pm} &= \sqrt{Z_{H^- H^+}} \mathcal{M}_{H^\pm} \\ &+ \frac{\hat{\Sigma}_{G^\pm H^\mp}(p^2)}{p^2 - M_W^2} \mathcal{M}_{G^\pm} + \frac{p_\mu \hat{\Sigma}_{W^\pm H^\mp}(p^2)}{p^2 - M_W^2} \mathcal{M}_{W^\pm}^\mu, \end{aligned} \tag{5.12}$$

where the wave function renormalization factor is given by

$$Z_{H^- H^+} = \left[1 + \text{Re} \frac{\partial}{\partial p^2} \hat{\Sigma}_{H^- H^+} \right]^{-1} \Big|_{p^2 = M_{H^\pm}^2}, \tag{5.13}$$

with the $\overline{\text{DR}}$-renormalized self-energy $\hat{\Sigma}_{H^- H^+}$ and p being the momentum of $H^\pm$, $p^2 = M_{H^\pm}^2$. The renormalized self-energies $\hat{\Sigma}_{G^\pm H^\mp}$ and $\hat{\Sigma}_{W^\pm H^\mp}$ are defined in Eq. (4.31). To simplify calculations the following Slavnov-Taylor identities (see for example [113, 114]) can be used.

$$\hat{\Sigma}_{hG}(p^2) + \frac{ip^2}{M_Z} \hat{\Sigma}_{hZ}(p^2) = 0, \tag{5.14}$$

$$\hat{\Sigma}_{HG}(p^2) + \frac{ip^2}{M_Z} \hat{\Sigma}_{HZ}(p^2) = 0, \tag{5.15}$$

$$\hat{\Sigma}_{AG}(p^2) + \frac{ip^2}{M_Z} \hat{\Sigma}_{AZ}(p^2) = (p^2 - m_A^2) f_0(p^2), \tag{5.16}$$

$$\hat{\Sigma}_{G^+ H^-}(p^2) - \frac{p^2}{M_W} \hat{\Sigma}_{W^+ H^-}(p^2) = (p^2 - M_{H^\pm}^2) f_\pm(p^2), \tag{5.17}$$

where

$$f_0(p^2) = \frac{\alpha \sin 2(\beta - \alpha) M_Z^2}{32\pi s_W^2 M_W^2} [B_0(p^2, m_h^2, M_Z^2) - B_0(p^2, m_H^2, M_Z^2)], \tag{5.18}$$

$$f_\pm(p^2) = \frac{\alpha \sin 2(\beta - \alpha)}{32\pi s_W^2} [B_0(p^2, m_h^2, M_W^2) - B_0(p^2, m_H^2, M_W^2)]. \tag{5.19}$$

5.3 Amplitudes of the processes with internal neutral Higgs bosons

In our calculation of $W^{\mp}H^{\pm}$ productions at the LHC, both subprocesses, $b\bar{b} \to W^{\mp}H^{\pm}$ and $gg \to W^{\mp}H^{\pm}$, include s-channel diagrams with internal neutral Higgs bosons. The loop effects to the neutral Higgs boson masses and mixing should be taken into account. We will verify in our numerical studies that the effects of this inclusion are significant for both cross section and CP asymmetry.

In a general amplitude with external neutral Higgs bosons that do not appear inside loops, the structure describing the Higgs-exchange part of an amplitude is given by

$$\mathcal{M}(p^2) = \sum_{ij} \Gamma_i \Delta_{ij}(p^2)\Gamma_j, \quad i,j = h/H/A, \tag{5.20}$$

where $\Gamma_{i,j}$ are the one-particle irreducible Higgs vertices. p^2 is the momentum of the Higgs propagator which is given in terms of 3×3 matrix Δ_{hHA} in Eq. (5.4). By using this matrix we effectively resum all the one-loop corrections to the Higgs propagators.

There are several approximations one can do to simplify the above expression as done in [23]. They introduced the concept of effective couplings.

- In the $p^2 = 0$ approximation, the mass matrix in Eq. (5.5) can be diagonalized by a rotation matrix

$$\begin{pmatrix} h_1 \\ h_2 \\ h_3 \end{pmatrix} = \mathbf{R_n} \begin{pmatrix} h \\ H \\ A \end{pmatrix}, \quad \mathbf{R_n}M(0)\mathbf{R_n^T} = \mathrm{diag}(M^2_{h_1,p^2=0}, M^2_{h_2,p^2=0}, M^2_{h_3,p^2=0}).$$
$$\tag{5.21}$$

  Since the mass matrix $M(0)$ is real and symmetric in this approximation, $\mathbf{R_n}$ is a real and orthogonal matrix. Therefore one can define the effective Higgs couplings as

$$\Gamma_i^{\mathrm{eff}} = \sum_j \mathbf{R_n}_{ij}\Gamma_j,. \tag{5.22}$$

  The amplitude now reads

$$\mathcal{M} = \sum_j \Gamma_j^{\mathrm{eff}} \frac{i}{p^2 - M^2_{h_j,p^2=0}} \Gamma_j^{\mathrm{eff}}. \tag{5.23}$$

- In the p^2 on-shell approximation, the self-energies are defined as

$$\hat{\Sigma}_{ii}(p^2) \to \mathrm{Re}\,\hat{\Sigma}_{ii}(m_i^2), \quad \hat{\Sigma}_{ii}(p^2) \to \mathrm{Re}\,\hat{\Sigma}_{ii}((m_i^2 + m_j^2)/2), \tag{5.24}$$

where only the real parts are taken. The mass matrix then can be diagonalized by a unitary transformation

$$
\begin{pmatrix} h_1 \\ h_2 \\ h_3 \end{pmatrix} = \mathbf{U_n} \begin{pmatrix} h \\ H \\ A \end{pmatrix},
$$

$$
\mathbf{U_n} M(p^2 \text{on-shell}) \mathbf{U_n^\dagger} = \mathrm{diag}(M^2_{h_1, p^2\text{on-shell}}, M^2_{h_2, p^2\text{on-shell}}, M^2_{h_3, p^2\text{on-shell}}).
$$

(5.25)

The effective couplings are then defined as in Eq. (5.22) with a replacement $\mathbf{R_n} \to \mathbf{U_n}$.

In our calculation we keep the full momentum dependence of self-energies and their imaginary parts. This imaginary part can give strong effects in the large momentum region.

5.4   Effective bottom–Higgs couplings

The Yukawa Lagrangian expressed in the quark flavor states reads

$$
\mathcal{L}_Y = \lambda_d^{ij} \epsilon_{IJ} \bar{d}_R^i q_{LI}^j H_{1J} - \lambda_u^{ij} \epsilon_{IJ} \bar{u}_R^i q_{LI}^j H_{2J} + \text{ h.c,}
$$

(5.26)

where $i, j = 1, 2, 3$, $I, J = 1, 2$ and the antisymmetric tensor $\epsilon_{12} = -\epsilon_{21} = +1$. One can perform a rotation on quark fields to transform it from the flavor eigenstates to the mass eigenstates with the help of the unitary matrices $(V_{L/R}^{u,d})$. For Higgs phenomena the interactions with the third generation are important and therefore we can neglect the flavor mixing. The Lagrangian now reads

$$
\mathcal{L}_Y = \lambda_b \epsilon_{IJ} \bar{b}_R q_{LI} H_{1J} - \lambda_t \epsilon_{IJ} \bar{t}_R q_{LI} H_{2J} + \text{ h.c,}
$$

(5.27)

where λ_b and λ_t are Yukawa couplings. Then one can express the Lagrangian in terms of the tree-level Higgs mass eigenstates $(h, H, A, G, H^\pm, G^\pm)$ by using the rotations defined in Eq. (3.91) and gets the tree-level bottom–Higgs couplings:

$$
\begin{aligned}
\lambda_{b\bar{b}h} &= i \frac{\lambda_b}{\sqrt{2}} \sin\alpha (P_L + P_R), \\
\lambda_{b\bar{b}H} &= -i \frac{\lambda_b}{\sqrt{2}} \cos\alpha (P_L + P_R), \\
\lambda_{b\bar{b}A} &= \frac{\lambda_b}{\sqrt{2}} \sin\beta (P_L - P_R), \\
\lambda_{b\bar{b}G} &= -\frac{\lambda_b}{\sqrt{2}} \cos\beta (P_L - P_R), \\
\lambda_{b\bar{t}H^+} &= i \left(\lambda_t \cos\beta P_L + \lambda_b \sin\beta P_R \right), \\
\lambda_{t\bar{b}H^-} &= i \left(\lambda_b \sin\beta P_L + \lambda_t \cos\beta P_R \right), \\
\lambda_{b\bar{t}G^+} &= i \left(\lambda_t \sin\beta P_L - \lambda_b \cos\beta P_R \right), \\
\lambda_{t\bar{b}G^-} &= i \left(-\lambda_b \cos\beta P_L + \lambda_t \sin\beta P_R \right),
\end{aligned}
$$

(5.28)

where $P_{L,R} = (1 \mp \gamma_5)/2$, the bottom and top couplings are related to their corresponding masses as $\lambda_b = \sqrt{2} m_b/(v\cos\beta)$ and $\lambda_t = \sqrt{2} m_t/(v\sin\beta)$, $v = \sqrt{v_1^2 + v_2^2} = 2 M_W s_W/e$.

It is well known that the bottom–Higgs couplings can get large SM-QCD, SUSY-QCD and SUSY-EW corrections. In order to obtain reliable predictions these large universal corrections should be absorbed into the the bottom–Higgs couplings. This can be done in two steps. First, the large SM-QCD corrections which is proportional to $\alpha_s \ln(m_b^2)$ are absorbed by using the running bottom-quark mass [140]. Second, the large SUSY-QCD and SUSY-EW corrections which are proportional to $\tan\beta$ can be resummed by using the effective bottom–Higgs couplings. In the following we discuss this procedure in detail.

5.4.1 The running bottom quark mass

For calculating one-loop SM-QCD corrections, if one renormalizes the bottom mass in on-shell scheme then the bottom mass is defined as the pole mass while in $\overline{\text{DR}}$ scheme it is understood as the running $\overline{\text{DR}}$ mass. At one-loop level, they are related by the following relation

$$m_b^{\overline{\text{DR}}}(\mu_R) = m_b \left[1 - \frac{\alpha_s}{\pi} \left(\frac{5}{3} - \ln\frac{m_b^2}{\mu_R^2}\right)\right].$$
(5.29)

We note, in passing, that the relation between the pole mass and the $\overline{\text{MS}}$ mass is different

$$m_b^{\overline{\text{MS}}}(\mu_R) = m_b \left[1 - \frac{\alpha_s}{\pi} \left(\frac{4}{3} - \ln\frac{m_b^2}{\mu_R^2}\right)\right].$$
(5.30)

We see that the $\overline{\text{DR}}$ mass depends explicitly on the renormalization scale μ_R which is often chosen to be the characteristic scale of a given process. This mass is sensitive only to short distance aspect of QCD. It is therefore advantageous to adopt the $\overline{\text{DR}}$ scheme for our processes in which the characteristic scale is large compared to the bottom mass. Moreover this scheme leads to the one-loop QCD corrections to be independent of $\alpha_s \ln(m_b^2)$. For processes in which the characteristic scale is of the order of the bottom mass, the $\overline{\text{DR}}$ mass is not an useful quantity. It is better to use the pole mass in those processes. However, one should keep in mind that the pole mass of a quark is not a physical quantity in a truly non-perturbative sense. Since the confinement of quarks in QCD implies that there is no pole in the quark propagator.

We take the QCD-$\overline{\text{MS}}$ mass $\overline{m}_b(\overline{m}_b)$, which is extracted from experimental data, as an input parameter. In order to compute the $\overline{\text{MS}}$ mass at a higher energy scale one can use the renormalization group equation (RGE) of the bottom mass and thus

$$m_b^{\overline{\text{MS}}}(\mu_R) = \begin{cases} U_6(\mu_R, m_t) U_5(m_t, \overline{m}_b) \overline{m}_b(\overline{m}_b) & \text{for} \quad \mu_R > m_t \\ U_5(\mu_R, \overline{m}_b) \overline{m}_b(\overline{m}_b) & \text{for} \quad \mu_R \leq m_t \end{cases}$$
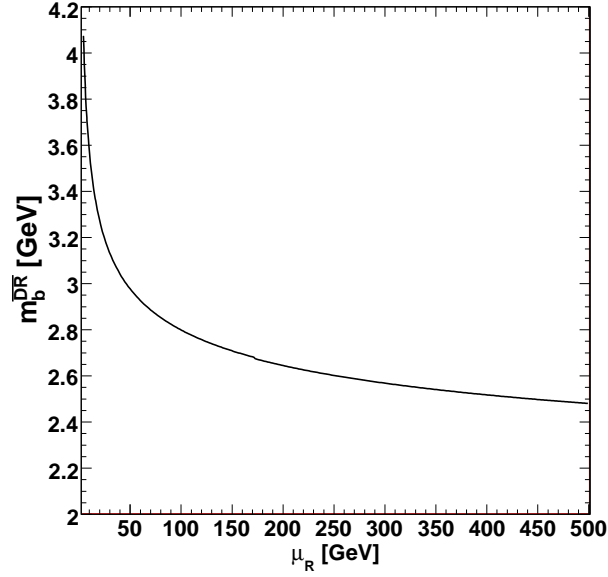(5.31)

Figure 5.1: The $\overline{\text{DR}}$ bottom mass as a function of the energy scale.

where the evolution factor U_n reads (see *e.g.* [141])

$$
\begin{aligned}
U_n(Q_2, Q_1) &= \left(\frac{\alpha_s(Q_2)}{\alpha_s(Q_1)} \right)^{d_n} \left[1 + \frac{\alpha_s(Q_1) - \alpha_s(Q_2)}{4\pi} J_n \right], \quad Q_2 > Q_1 \\
d_n &= \frac{12}{33 - 2n}, \quad J_n = -\frac{8982 - 504n + 40n^2}{3(33 - 2n)^2}.
\end{aligned}
\tag{5.32}
$$

with n being the number of active quark flavors ($n = 5$ for $\overline{m}_b(\overline{m}_b) < Q \leq m_t$ and $n = 6$ for $Q > m_t$). From the $\overline{\text{MS}}$ mass we can compute the $\overline{\text{DR}}$ mass by using the two-loop order relation [142]

$$
m_b^{\overline{\text{DR}}}(\mu_R) = m_b^{\overline{\text{MS}}}(\mu_R) \left[1 - \frac{\alpha_s(\mu_R)}{3\pi} - \frac{\alpha_s^2(\mu_R)}{144\pi^2}(73 - 3n) \right].
\tag{5.33}
$$

For the running α_s which appears in the above relations, we use the approximate analytic solution of renormalization group equation of α_s at three-loop level

$$
\alpha_s(\mu_R) = \frac{4\pi}{\beta_0 t} \left(1 - \frac{\beta_1}{\beta_0^2} \frac{\ln t}{t} + \frac{\beta_1^2(\ln^2 t - \ln t - 1) + \beta_0 \beta_1}{\beta_0^4 t^2} \right),
\tag{5.34}
$$

where $t = \ln(\mu_R^2/\Lambda_n^2)$; Λ_n is a constant of integration at which the perturbatively-defined strong couplings would diverge; and $\beta_0 = 11 - 2/3n$, $\beta_1 = 51 - 19/3n$, $\beta_2 = 2857 - 5033/9n + 325/27n$. We chose $\Lambda_5 = 228.9 \times 10^{-3}$ GeV to reproduce the world average $\alpha_s(M_Z) = 0.1197$ [143] and Λ_6 can be computed from the relation

$$
\Lambda_6 = \Lambda_5 \left(\frac{m_t}{\Lambda_5} \right)^{-2/21} \left(2 \ln \frac{m_t}{\Lambda_5} \right)^{-107/1127},
\tag{5.35}
$$
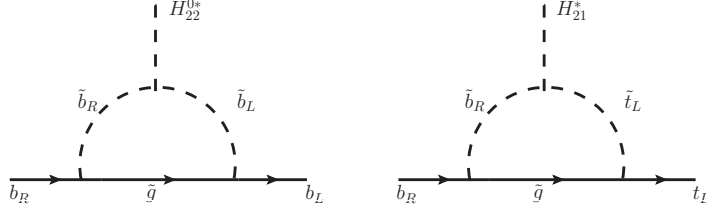
Figure 5.2: One-loop QCD contribution to $\delta\tilde{\lambda}_b^d$ (left pannel) and $\delta\tilde{\lambda}_b^u$ (right pannel). Similar diagrams with the replacement of H_{22}^{0*} by H_{11}^0 and H_{21}^* by H_{12} will contribute to $\delta\lambda_b^u$ and $\delta\lambda_b^d$, respectively.

which is derived from the requiring that $\alpha_s(\mu_R)$ is continuous at $\mu_R = m_t$ up to the first order term.

In Fig. 5.1 we show the running $m_b^{\overline{\text{DR}}}$ as a function of the energy scale. There is a negligible discontinuity at $\mu_R = m_t$ because the higher order terms are not included in Eq. (5.35).

In our calculation, we use the $\overline{\text{DR}}$ scheme for renormalization of bottom mass, therefore in the bottom–Higgs couplings listed in Eq. (5.29) m_b is replaced by $m_b^{\overline{\text{DR}}}$.

5.4.2 Δm_b resummation

The subject has been widely studied in the literature. In summary, there two approaches for the resummation of large $\tan\beta$ effect: the diagrammatic resummation [144, 145] and effective Lagrangian approach [141, 146, 147, 148]. The discussion in this section follows the latter. As seen in Eq. (5.26), at tree level the interaction of the down-type quarks to H_2 doublet are forbidden to ensure the analytic property of the superpotential. Once the higher order corrections are considered, these interactions are not vanishing and hence appear in the effective Lagrangian as follows

$$
\begin{aligned}
\mathcal{L}_Y &= (\lambda_b + \delta\lambda_b^{u/d})\epsilon_{IJ}\bar{b}_R q_{LI} H_{1J} + \delta\tilde{\lambda}_b^{u/d}\epsilon_{IJ}\bar{b}_R q_{LI}\tilde{H}_{2J} \\
&\quad -\lambda_t\epsilon_{IJ}\bar{t}_R q_{LI} H_{2J} + \text{ h.c} + \cdots,
\end{aligned}
\tag{5.36}
$$

where $\tilde{H}_2 = i\sigma_2 H_2^*$, index u is for $i = 1, J = 2$ and index d is for $I = 2, J = 1$. For example at one-loop level the SUSY-QCD contributions to $\delta\tilde{\lambda}_b^{u/d}$ comes from Feynman diagrams depicted in Fig. 5.2. In general, $\delta\tilde{\lambda}_b^u$ and $\delta\tilde{\lambda}_b^d$ are different by the $SU(2)_L$-breaking terms. For simplicity we set $\delta\lambda_b^u = \delta\lambda_b^d = \delta\lambda_b$ and $\delta\tilde{\lambda}_b^u = \delta\tilde{\lambda}_b^d = \delta\tilde{\lambda}_b$. This is done in the decoupling limits where M_{SUSY} is much larger than the EW scale. Therefore one can neglect the EW breaking effects. Now we can write the effective Lagrangian as

$$
\begin{aligned}
\mathcal{L}_Y &= \lambda_b(1 + \Delta_1)\epsilon_{IJ}\bar{b}_R q_{LI} H_{1J} + \lambda_b\Delta m_b\epsilon_{IJ}\bar{b}_R q_{LI}\tilde{H}_{2J} \\
&\quad -\lambda_t\epsilon_{IJ}\bar{t}_R q_{LI} H_{2J} + \text{ h.c} + \cdots,
\end{aligned}
\tag{5.37}
$$

where we have replaced $\delta\lambda_b = \lambda_b\Delta_1$ and $\delta\tilde{\lambda}_b = \lambda_b\Delta m_b$. Substituting the expressions of the two Higgs doublet Eq. (3.78) into Eq. (5.37) we get the relation of the bottom Yukawa coupling and the bottom mass

$$\lambda_b = \frac{\sqrt{2}m_b}{v\cos\beta(1 + \Delta_1 + \Delta m_b\tan\beta)}. \tag{5.38}$$

One should keep in mind that m_b is real and positive while Δ_1 and Δm_b are in general complex. The effective bottom–Higgs couplings are as follows:

$$\bar{\lambda}_{b\bar{b}h} = \frac{iem_b^{\overline{\mathrm{DR}}}}{2s_W M_W}\frac{\sin\alpha}{\cos\beta}\left(\Delta_b^1 P_L + \Delta_b^{1*} P_R\right),$$

$$\bar{\lambda}_{b\bar{b}H} = \frac{-iem_b^{\overline{\mathrm{DR}}}}{2s_W M_W}\frac{\cos\alpha}{\cos\beta}(\Delta_b^2 P_L + \Delta_b^{2*} P_R),$$

$$\bar{\lambda}_{b\bar{b}A} = \frac{em_b^{\overline{\mathrm{DR}}}}{2s_W M_W}\tan\beta(\Delta_b^3 P_L - \Delta_b^{3*} P_R),$$

$$\bar{\lambda}_{b\bar{t}H^+} = \frac{ie}{\sqrt{2}s_W M_W}\left(\frac{m_t}{\tan\beta}P_L + m_b^{\overline{\mathrm{DR}}}\tan\beta\Delta_b^{3*} P_R\right),$$

$$\bar{\lambda}_{t\bar{b}H^-} = \frac{ie}{\sqrt{2}s_W M_W}\left(m_b^{\overline{\mathrm{DR}}}\tan\beta\Delta_b^3 P_L + \frac{m_t}{\tan\beta}P_R\right), \tag{5.39}$$

where

$$\Delta_b^1 = \frac{1 - \Delta_b/(\tan\beta\tan\alpha)}{1 + \Delta_b},$$

$$\Delta_b^2 = \frac{1 + \Delta_b\tan\alpha/\tan\beta}{1 + \Delta_b},$$

$$\Delta_b^3 = \frac{1 - \Delta_b/(\tan\beta)^2}{1 + \Delta_b},$$

$$\Delta_b = \frac{\Delta m_b}{1 + \Delta_1}. \tag{5.40}$$

In these couplings m_b has been replaced by $m_b^{\overline{\mathrm{DR}}}$ to include the large QCD correction as mentioned in previous section. It should be noted that the couplings of the bottom quark and the Nambu-Goldstone bosons $(G^0, G^\pm)$ are the same as the tree-level couplings written in Eq. (5.29). This is a consequence of gauge invariance.

In order to compute Δm_b and Δ_1 one has to consider all one-loop contributions to vertex $H_{22}^0\bar{b}_R b_L$, but take only the terms proportional to $\tan\beta$. One commonly takes masses of the external lines to zero limit. In the Appendix D we present

explicit calculation for Δm_b in the complex MSSM. Here are the results we found

$$\Delta m_b = \Delta m_b^{SQCD} + \Delta m_b^{SEW},$$

$$\Delta m_b^{SQCD} = \frac{2\alpha_s(Q)}{3\pi} M_3^* \mu^* \tan\beta \, I(m_{\tilde{b}_1}^2, m_{\tilde{b}_2}^2, m_{\tilde{g}}^2), \quad Q = (m_{\tilde{b}_1} + m_{\tilde{b}_2} + m_{\tilde{g}})/3,$$

$$\Delta m_b^{SEW} = \Delta m_b^{\tilde{H}\tilde{t}} + \Delta m_b^{\tilde{W}} + \Delta m_b^{\tilde{B}},$$

$$\Delta m_b^{\tilde{H}\tilde{t}} = \frac{\alpha_t}{4\pi} A_t^* \mu^* \tan\beta \, I(m_{\tilde{t}_1}^2, m_{\tilde{t}_2}^2, |\mu|^2)$$

$$\Delta m_b^{\tilde{W}} = -\frac{\alpha}{8\pi s_W^2} M_2^* \mu^* \tan\beta \left[2|U_{11}^{\tilde{t}}|^2 I(m_{\tilde{t}_1}^2, |M_2|^2, |\mu|^2) + 2|U_{21}^{\tilde{t}}|^2 I(m_{\tilde{t}_2}^2, |M_2|^2, |\mu|^2) \right.$$

$$\left. + |U_{11}^{\tilde{b}}|^2 I(m_{\tilde{b}_1}^2, |M_2|^2, |\mu|^2) + |U_{21}^{\tilde{b}}|^2 I(m_{\tilde{b}_2}^2, |M_2|^2, |\mu|^2) \right]$$

$$\Delta m_b^{\tilde{B}} = -\frac{\alpha}{72\pi c_W^2} M_1^* \mu^* \tan\beta \left[3(|U_{11}^{\tilde{b}}|^2 + 2|U_{12}^{\tilde{b}}|^2) I(m_{\tilde{b}_1}^2, |M_1|^2, |\mu|^2) \right.$$

$$\left. + 3 \, (2|U_{22}^{\tilde{b}}|^2 + |U_{21}^{\tilde{b}}|^2) I(m_{\tilde{b}_2}^2, |M_1|^2, |\mu|^2) + 2I(m_{\tilde{b}_1}^2, m_{\tilde{b}_2}^2, |M_1|^2) \right], \qquad (5.41)$$

with the auxiliary function

$$I(a, b, c) = -\frac{1}{(a-b)(b-c)(c-a)} \left(ab \ln\frac{a}{b} + bc \ln\frac{b}{c} + ca \ln\frac{c}{a} \right), \qquad (5.42)$$

and

$$\Delta_1 = -\frac{2\alpha_s(Q)}{3\pi} M_3^* A_b I(m_{\tilde{b}_1}^2, m_{\tilde{b}_2}^2, m_{\tilde{g}}^2). \qquad (5.43)$$

By setting all the phases to zero we obtain the results for the real MSSM (rMSSM), which agree with those given in [149, 141].

We remark that Δ_b is complex and depends on ϕ_μ, ϕ_f, ϕ_i with $i = 1, 2, 3$. The effective couplings Eq. (5.39) are used in the calculations of the $pp \to W^\mp H^\pm$ and $pp \to H^- t\bar{b}$ processes. For the NLO EW corrections we use the tree-level couplings Eq. (5.29) with $m_b = m_b^{\overline{\mathrm{DR}}}(\mu_R)$.

In the explicit one-loop calculations, we have to subtract the Δ_b-related corrections which have already included into the tree-level contribution to avoid double counting. This can be done by adding the following counterterms

$$\delta m_b^h = m_b^{\overline{\mathrm{DR}}} \left(1 + \frac{1}{\tan\alpha \tan\beta} \right) (\Delta_b P_L + \Delta_b^* P_R),$$

$$\delta m_b^H = m_b^{\overline{\mathrm{DR}}} \left(1 - \frac{\tan\alpha}{\tan\beta} \right) (\Delta_b P_L + \Delta_b^* P_R),$$

$$\delta m_b^A = m_b^{\overline{\mathrm{DR}}} \left[1 + \frac{1}{(\tan\beta)^2} \right] (\Delta_b P_L - \Delta_b^* P_R),$$

$$\delta m_b^{H^+} = m_b^{\overline{\mathrm{DR}}} \left[1 + \frac{1}{(\tan\beta)^2} \right] \Delta_b^* P_R,$$

$$\delta m_b^{H^-} = m_b^{\overline{\mathrm{DR}}} \left[1 + \frac{1}{(\tan\beta)^2} \right] \Delta_b P_L, \qquad (5.44)$$

to δm_b in the corresponding bottom–Higgs-coupling counterterms, as listed in Appendix C. Moreover, Eq. (5.44) is used with $\Delta_b = \Delta m_b^{SQCD}$, Δm_b^{SEW} for the SUSY-QCD and EW corrections, respectively.

Chapter 6

$H^\pm \to W^\pm h_1$: decay widths and CP violating asymmetry

Understanding the decays of the charged Higgs bosons is an important step for their searches at any collider. This chapter will summarize all possible two-body decay modes and focus on one specific mode ($H^\pm \to W^\pm h_1$).

6.1 Introduction

The charged Higgs bosons in the MSSM can have following two-body decay modes.

- Decays into fermions are $H^- \to f f'$, where $f \in \{e, \mu, \tau, d, s, b\}$ and f' are their corresponding $SU(2)_L$ doublet partners, and $H^- \to \tilde{\chi}_i^0 \tilde{\chi}_j^-$, $i = 1, \ldots, 4$ and $j = 1, 2$. The dominant decay modes are the decay into fermions of the third generation due to the large Yukawa couplings.

- Decays into one vertor boson and one scalar boson are $H^\pm \to W^\pm h_i$, $i = 1, 2, 3$. In the decoupling limit, the decay into $W^\pm h_1$ is suppressed due to the tree-level coupling $\propto \cos(\beta - \alpha)$ going to zero while decays to other Higgs bosons h_2, h_3 are kinematically supressed because of mass degeneration $M_{H^\pm} \sim M_{h_2} \sim M_{h_3}$. However we will show in the this chapter the decay modes $H^\pm \to W^\pm h_1$ receive large one-loop corrections and have large CP violating effect.

- Decays into two scalar bosons are $H^- \to \tilde{f}_i \tilde{f}'_j$ where the sfermions $\tilde{f}_i, \tilde{f}'_j$ ($i, j = 1, 2$) are the corresponding superpartners of the fermions. Decaying into the third generation sfermions are dominant if the charged Higgs mass is large enough.

In the literature, there are extensive studies for those decay modes and the one-loop corrections to some of those modes have been calculated: one-loop SM-QCD corrections to $H^- \to qq'$ [150, 151] and to $H^- \to \tilde{b}\bar{\tilde{t}}$ [152] one-loop QCD
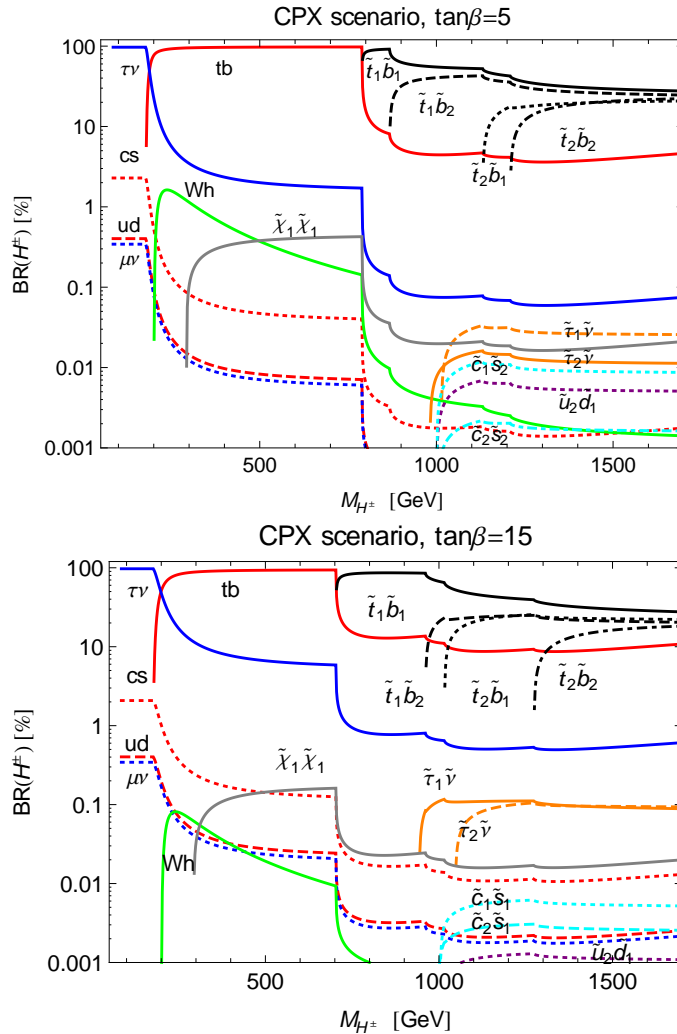
Figure 6.1: The branching ratios of the charged Higgs boson as functions of the charged Higgs mass. The upper panel is for $\tan\beta = 5$ while the lower panel is for $\tan\beta = 15$.

to $H^- \to \tilde{q}\tilde{q}'$ [153]. There are several public codes on the market to compute the decay widths as well as branching ratios at tree level with some leading higher order corrections: FeynHiggs [154] and CPsuperH [155] for both real and complex MSSM; HDCAY [156] for real MSSM. At one- loop level recently the FHOLD package [157] for real MSSM was published. For our purpose of full control and understanding, we have computed all tree-level decay widths of the aforementioned channels in the complex MSSM. The analytic expressions are found in Appendix E. In Fig. 6.1 we show the branching ratios of the charged Higgs boson in the CPX scenario, see in Appendix F.2.2. The total decay widths are displayed in Fig. 6.2.

In the complex MSSM, the CP violating effects related to the complex phases of the soft-breaking parameters manifest considerably in the charged Higgs decays and productions while the ones due to the CKM phase are suppressed. It is worth
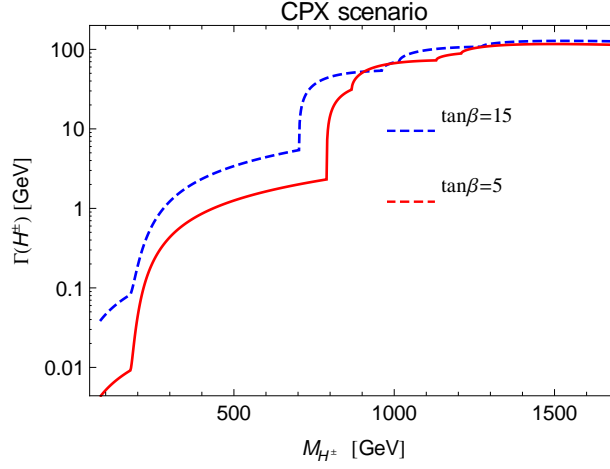
Figure 6.2: The total decay width of charged Higgs as functions of the charged Higgs mass in the CPX scenario.

studying those effects for the future discoveries of the charged Higgs boson to answer the question if there exists new sources of CP violation beyond the well-known CKM phase. The CP violating asymmetries for two important decay modes $H^\pm \to \tau\nu_\tau$ and $H^\pm \to bt$ have been already studied in [158, 159].

Another interesting decay modes of the charged Higgs boson decays $H^- \to W^- h_1$ and $H^+ \to W^+ h_1$, where the asymmetry between the decay rates is a CP-violating observable. A first approximate calculation was done in [24], studying the CP asymmetry as derived from the phases of the trilinear $\tilde{\tau}$ coupling, A_τ, and of M_1, yielding asymmetries of the order 10^{-2}; contributions from the quark/squark sector were not included.

We have extended the calculation of [24] including contributions from all physical phases in the general complex MSSM with minimal flavor violation, in particular from A_t and A_b, which enter through Feynman diagrams with stops and sbottoms involving large Yukawa couplings, further enhanced by the color factor. We show the results from the complete set of one-loop diagrams. The results have been published in [160].

6.2 Decay widths

We can write the decay amplitudes of processes $H^\pm \to W^\pm h_1$ as follows,

$$\mathcal{A}(H^\pm \to W^\pm h_1) = \left(\epsilon_\lambda \cdot p_{H^\pm}\right) \mathcal{M}(H^\pm \to W^\pm h_1) \tag{6.1}$$

with the W polarization vectors ϵ_λ and the $H^\pm$ momentum $p_{H^\pm}$. The decay widths integrated over the 2-particle phase space and summed over the W helicities λ are

obtained in the form

$$\Gamma(H^{\pm} \to W^{\pm} h_1) = R_2 \cdot |M_{H^{\pm} \to W^{\pm} h_1}|^2 \,, \tag{6.2}$$

with

$$R_2 = \frac{\lambda^{3/2}(M_{H^{\pm}}^2, M_W^2, M_{h_1}^2)}{64\pi M_{H^{\pm}}^3 M_W^2}, \; \lambda(x, y, z) = x^2 + y^2 + z^2 - 2xy - 2xz - 2yz \,. \tag{6.3}$$

Following the prescription in Section 5.2, the decay amplitude at higher order can be written in the following way,

$$
\begin{aligned}
\mathcal{M}_{H^{\pm} \to W^{\pm} h_1} = \sqrt{Z_{H^- H^+}} \Big[& \mathbf{Z}_{11} \big(M_{H^{\pm} \to W^{\pm} h}^{\text{tree}} + \delta M_{H^{\pm} \to W^{\pm} h} \big) \\
& + \mathbf{Z}_{12} M_{H^{\pm} \to W^{\pm} H}^{\text{tree}} + \mathbf{Z}_{13} M_{H^{\pm} \to W^{\pm} A}^{\text{tree}} \Big],
\end{aligned}
\tag{6.4}
$$

where the tree-level expressions M^{tree} are given by

$$
\begin{aligned}
M_{H^{\pm} \to W^{\pm} h}^{\text{tree}} &= \frac{e \cos(\beta - \alpha)}{s_W}, \; M_{H^{\pm} \to W^{\pm} H}^{\text{tree}} = -\frac{e \sin(\beta - \alpha)}{s_W}, \\
M_{H^{\pm} \to W^{\pm} A}^{\text{tree}} &= \pm i \frac{e}{s_W}.
\end{aligned}
\tag{6.5}
$$

The charged-Higgs wave function renormalization $\sqrt{Z_{H^- H^+}}$ is defined in Eq. (5.13). The neutral-Higgs wave function renormalization factors $\mathbf{Z}_{kl}$ are given in Eq. (5.10), and

$$\delta M_h \equiv \delta M_{H^{\pm} \to W^{\pm} h} = \delta M_{H^{\pm} \to W^{\pm} h}^{\text{1PI}} + \delta M_{H^{\pm} \to W^{\pm} h}^{G, W mix} \tag{6.6}$$

which summarize the residual 1PI-irreducible contributions to the 3-point vertex function and the mixing of $H^{\pm}$ with $G^{\pm}$ and $W^{\pm}$. The mixing of h with G^0 and Z bosons is not included because the couplings $H^{\pm} W^{\mp} G^0(Z)$ do not exist at tree level. The Feynman diagrams contributing to this term at the one-loop level are shown in figure 6.3. There is no explicit wave function renormalization for the W boson, since the W propagator has been renormalized on-shell yielding residue $= 1$.

For the charged Higgs boson, the factor $Z_{H^- H^+}$ is IR-divergent. We regularise the IR-divergence in the one-loop expanded version with the help of a small photon mass so that we take only the one-loop contribution of the factor $Z_{H^- H^+}$ which is

$$
\begin{aligned}
Z_{H^- H^+} &\simeq 1 - \text{Re} \frac{\partial}{\partial p^2} \hat{\Sigma}_{H^- H^+} \big|_{p^2 = M_{H^{\pm}}^2} \equiv 1 - \delta Z_{H^- H^+}, \\
\sqrt{Z_{H^- H^+}} &\simeq 1 - \frac{1}{2} \delta Z_{H^- H^+}.
\end{aligned}
\tag{6.7}
$$

Substituting the amplitude (6.4) into the expression (6.2), one obtains the decay width, denoted as $\Gamma_{\mathbf{Z}}^{(0+1+2)}$ later in the thesis. Keeping the $\mathbf{Z}$ factors in the squared amplitude is justified since they contain also the leading higher-order terms which
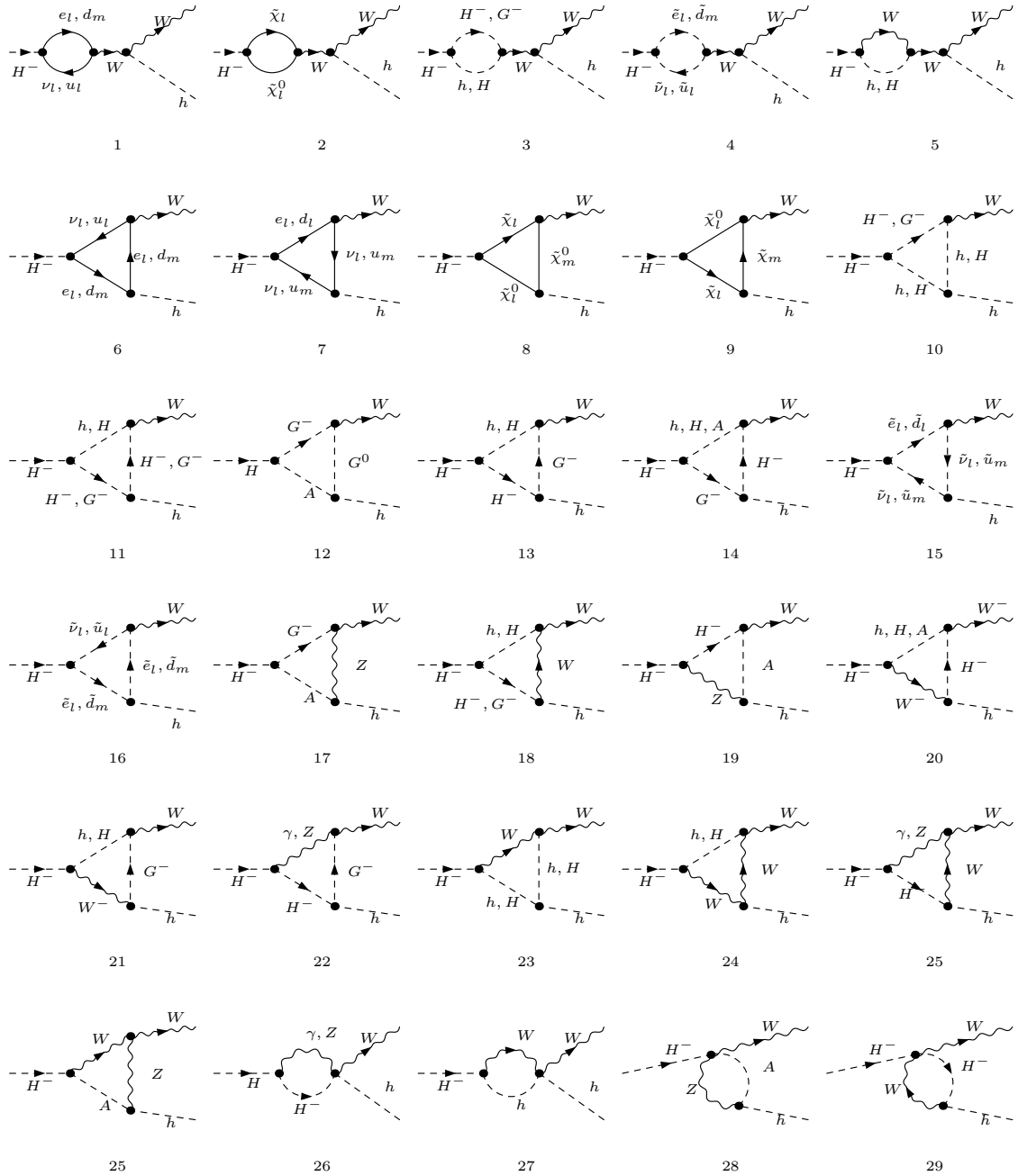
Figure 6.3: One-loop Feynman diagrams contribute to δM_h.

correspond to the effective-potential approximation. In the squared one-loop amplitude, we keep also the term involving δM_h^2. This term can play an important role at large value of M_{H^-}, *i.e.* $M_{H^-} \geq M_{\tilde{t}_1} + M_{\tilde{b}_1}$, where the decay channel into $\tilde{t}_1$ and $\tilde{b}_1$ is open, while it is negligible at lower M_{H^-}. The inclusion of this term while neglecting other two-loop contributions is consistent in perturbation theory, since the tree-level vertex function $M_h^{\text{tree}} \sim \cos(\beta - \alpha) \sim M_Z^2/M_{H^-}^2$ goes to near zero at large M_{H^-}. For the δM_h^2 term, we take only the (s)top/(s)bottom diagrams which are IR finite and give the dominant contributions, as checked in [161].

For comparison with other approximations, we introduce the following notations for decay width:

- The Born appriximation decay width $\Gamma^{(0)}$ is defined by

$$\Gamma^{(0)} = R_2 \cdot \left| M_h^{\text{tree}} \right|^2. \tag{6.8}$$

- The improved Born approximation for the decay width $\Gamma_{\mathbf{Z}}^{(0)}$ with the $\mathbf{Z}$ factors taken into account:

$$\Gamma_{\mathbf{Z}}^{(0)} = R_2 \cdot \left| \sum_i \mathbf{Z}_{1i} M_i^{\text{tree}} \right|^2, \quad i = h, H, A. \tag{6.9}$$

- The one-loop improved decay width $\Gamma_{\mathbf{Z}}^{(0+1)}$ that does not include δM_h^2:

$$
\begin{aligned}
\Gamma_{\mathbf{Z}}^{(0+1)} &= R_2 \cdot \left\{ \left| \sum_i \mathbf{Z}_{1i} M_i^{\text{tree}} \right|^2 \right. \\
&\quad \left. + 2 \sum_i \text{Re} \left[\mathbf{Z}_{11}^* \mathbf{Z}_{1i} M_i^{\text{tree}} (\delta M_h - \frac{1}{2} M_h^{\text{tree}} \delta Z_{H^- H^+})^* \right] \right\}.
\end{aligned}
\tag{6.10}
$$

Real photon emission

The soft singularities in the virtual corrections are canceled by adding the real photon radiation contribution,

$$H^{\pm} \to W^{\pm} + h_1 + \gamma, \tag{6.11}$$

see Fig. 6.4 for the Feynman diagrams. We use the phase space slicing method, then the soft contribution reads

$$
\begin{aligned}
\Gamma^{\text{soft}}(H^{\pm} \to W^{\pm} h_1 \gamma) &= -\frac{\alpha}{2\pi^2} \left(I_{HH} + I_{WW} - I_{HW} - I_{WH} \right) \\
&\quad \times R_2 \cdot \text{Re} \left[\mathbf{Z}_{11} M_h^{\text{tree}} \sum_i \mathbf{Z}_{1i} M_i^{\text{tree}*} \right],
\end{aligned}
\tag{6.12}
$$

where the soft integrals I_{ij} $(i, j = H, W)$ are defined in Eq. (4.68). It should be mentioned that the cancellation of the soft singularities is only ensured if the mass
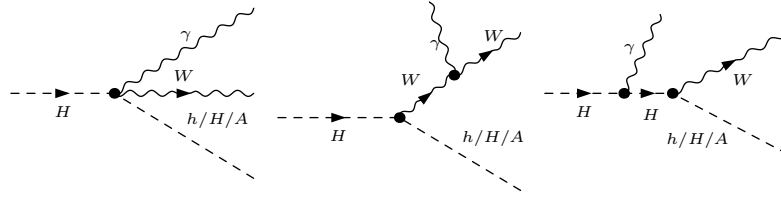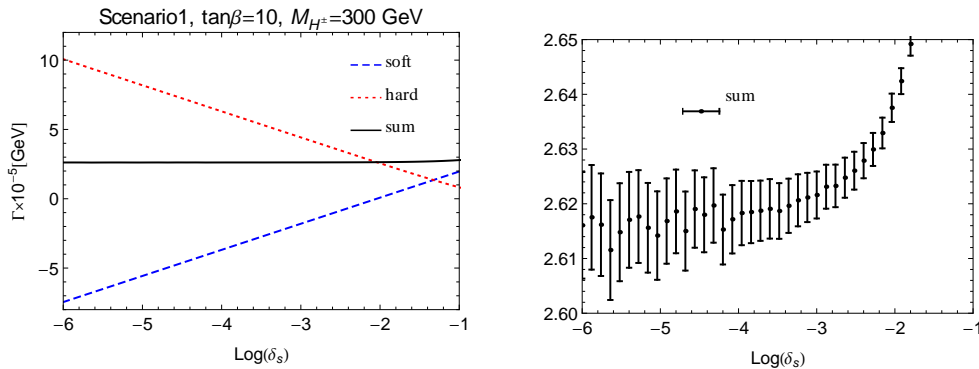
Figure 6.4: Feynman diagrams for $H^- \to W^- + h/H/A + \gamma$.

Figure 6.5: The dependence of the real contribution on the soft cutoff parameter, $\delta_s = \frac{2\Delta E}{M_{H^\pm}}$ for the parameter set defined in Appendix F.2.1. The photon mass regulator λ is set to one so that the terms proportional to $\ln \lambda^2$ vanish.

of h_1 is the tree-level mass. If the loop-corrected mass is used then the tree-level relations are violated. This leads to an incomplete cancellation. We have checked analytically and numerically. For the hard contribution we numerically integrate over the 3-particle phase space with the help of the soft cutoff parameter. In Fig. 6.5, we show the dependence of each contributions on the cutoff. The results are expected as explained in Section 4.3.2. The sum of soft and hard contributions is rather stable around $\delta_s = 10^{-3}$ and the integration error is acceptable. Therefore we chose that as a default value in the following numerical analysis. It should be noted that the results obtained here are computed in the unitary gauge for W boson exchange. For another gauge, one should be careful to include the full set of gauge invariant diagrams and to be consistent with the virtual contributions. Since this is an improved one-loop calculation, finding the full set is not trivial.

6.3   CP asymmetry

The CP violating asymmetry in the charged-Higgs decay into a W-boson and the lightest neutral Higgs, h_1, is defined in terms of the individual partial decay widths
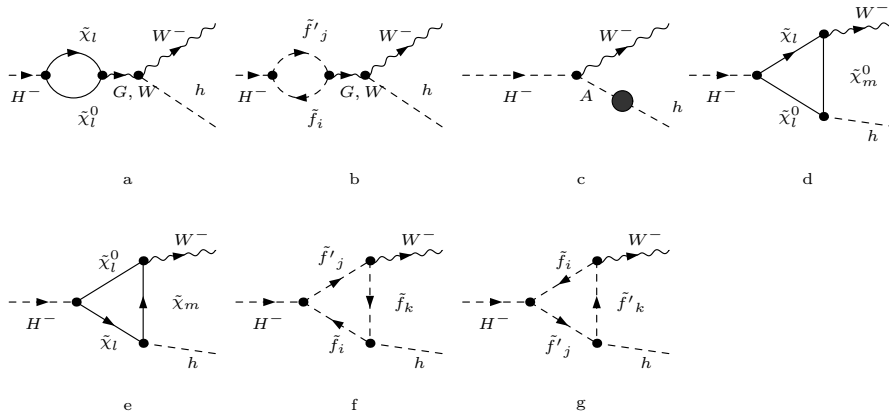
Figure 6.6: Feynman diagrams contain weak phases which contribute to the CP rate asymmetry.

$\Gamma(H^{\pm} \to W^{\pm}h_1)$

$$\delta_{\mathrm{CP}} = \frac{\Gamma(H^- \to W^-h_1) - \Gamma(H^+ \to W^+h_1)}{\Gamma(H^- \to W^-h_1) + \Gamma(H^+ \to W^+h_1)}. \tag{6.13}$$

In practice, there are two ways to compute the CP asymmetry: (i) to compute both decay widths of $H^- \to W^-h_1$ and of the CP-conjugate process $H^+ \to W^+h_1$ and then using the definition (6.13); (ii) to compute separately the CP-violating and the CP-invariant contributions to the decay $M_{H^- \to W^-h_1}$ and then taking their ratio. The CP-violating term comes from the imaginary part of the complex couplings (together with the imaginary part of the loop integrals), while the CP-invariant term is from the real part. Therefore the CP-violating term changes sign, but the CP-invariant term does not when going from $H^- \to W^-h_1$ to $H^+ \to W^+h_1$. Hence, one can identify the Feynman diagrams shown in figure 6.6 as those contributing to the CP-violating part.

We have performed our calculation in the two ways, with perfect agreement. The full result for δ_{CP} is obtained when both the numerator and denominator of the asymmetry (6.13) are computed with the inclusion of higher order terms. This is different with the approximation used in Ref. [24] where the numerator is computed at strict one-loop order and the denominator is tree-level like, and is necessary since in specific case the process is loop dominated, as we will illustrate in the numerical analysis.

6.4 Calculational details

We have used `FeynArts 3.4` [105] to generate the Feynman diagrams. The amplitudes are further evaluated with the help of `FormCalc 6.0` and with the library

`LoopTools 2.4` [96, 162]. All the dependent couplings and masses of internal lines are computed with tree-level relations. The relevant counterterms are presented in Appendix C. The mass of the external neutral Higgs and the renormalization factors $\mathbf{Z}_{ij}$ are calculated by using `FeynHiggs 2.6.5` [132, 65, 131, 66]. In `FeynHiggs 2.6.5` there are serveral obtions which affect our results. Therefore we need to specify them. For renormalization scheme, we chose $\overline{\mathrm{DR}}$ scheme for both Higgs-field renormalization constants and $\tan\beta$ to be consistent with the scheme used in our one-loop calculations. The Higgs self-energies in Eq. (5.5) are computed with full momentum dependence and with the inclusion of various important two-loop contributions ($\alpha_s\alpha_t$, $\alpha_s\alpha_b$, $\alpha_t\alpha_t$, $\alpha_t\alpha_b$) which are so far evaluated at zero momentum. The top mass and bottom mass are chosen to be the pole mass, again to be consistent with our input parameters.

For the CP asymmetry calculation, we have generated two codes as mentioned in previous section. One code is generated by FeynArt, FormCalc and using Looptool while the other one generated by FeynArt further evaluated by our self-made Form code and using the analytic expressions for the imaginary parts of loop integrals.

In our calculation, we encounter normal threshold singularities when $M_{H^\pm}$ approaches the production threshold of two scalar particles, for instance up and down squarks. Let's consider the derivative of the charged Higgs self-energy with the exchange of stops and sbottoms:

$$\frac{d}{dp^2}\left|\ \begin{array}{c} \tilde{t}_i \\ H^- -\!\!-\!\!\prec\ \bigcirc\ \succ\!\!-\!\!- H^- \\ \tilde{b}_j \end{array}\ \right| \quad = \quad |G_{H^-\tilde{t}_i\tilde{b}_j}|^2\frac{d}{dp^2}B_0(p^2, M_{\tilde{t}_i}^2, M_{\tilde{b}_j}^2)$$

where $G_{H^-\tilde{t}_i\tilde{b}_j}$ are the coupling constants and $B_0(p^2, M_{\tilde{t}_i}^2, M_{\tilde{b}_j}^2)$ denotes the scalar two-point function. The derivative of the scalar two-point function reads

$$\frac{d}{dp^2}B_0(p^2, M_{\tilde{t}_i}^2, M_{\tilde{b}_j}^2)\Big|_{p^2=M_{H^\pm}^2} \propto \int_0^1 dx\,\frac{d}{dp^2}\log(p^2x^2 - x(p^2 + M_{\tilde{t}_i}^2 - M_{\tilde{b}_j}^2) + M_{\tilde{t}_i}^2 - i\epsilon)$$

$$\propto \int_0^1 dx\,\frac{x^2 - x}{M_{H^\pm}^2 x^2 - x(M_{H^\pm}^2 + M_{\tilde{t}_i}^2 - M_{\tilde{b}_j}^2) + M_{\tilde{t}_i}^2 - i\epsilon}$$

$$\propto \int_0^1 dx\,\frac{x^2 - x}{M_{H^\pm}^2(x - x_1 - i\epsilon)(x - x_2 + i\epsilon)}, \qquad (6.14)$$

where

$$x_{1/2} = \frac{(M_{H^\pm}^2 + M_{\tilde{t}_i}^2 - M_{\tilde{b}_j}^2) \pm \sqrt{\lambda(M_{H^\pm}^2, M_{\tilde{t}_i}^2, M_{\tilde{b}_j}^2)}}{2M_{H^\pm}^2}. \qquad (6.15)$$

The integral has a pinch singularity (see Section 4.1) if $x_1 = x_2$ and $0 < x_1 < 1$, i.e.

$$\lambda(M_{H^\pm}^2, M_{\tilde{t}_i}^2, M_{\tilde{b}_j}^2) = 0. \qquad (6.16)$$

One of the solutions is

$$M_{H^{\pm}} = M_{\tilde{t}_i} + M_{\tilde{b}_j}, \tag{6.17}$$

if all the masses are real and positive. In fact this singularity is the two-point Landau singularity enhanced by derivative. The singularity part is

$$\left[\frac{d}{dp^2} B(p^2, M_{\tilde{t}_i}^2, M_{\tilde{b}_j}^2)|_{p^2 = M_{H^{\pm}}^2} \right]_{\text{sing}} \propto \frac{1}{x_1 - x_2} \propto \frac{1}{\sqrt{\det(Q)}}, \tag{6.18}$$

where Q is the Landau matrix and $\det(Q) = \lambda(M_{H^{\pm}}^2, M_{\tilde{t}_i}^2, M_{\tilde{b}_j}^2)$, following the convention in Section 4.1. The nature of this singularity is $1/\sqrt{x}$ and divergent. It should be noted that if one mass is zero, the singularity will vanish.

For the diagrams with fermions in the loop, the normal threshold singularity does not appear. Let us explain this. The self-energy in general is given by

$$\Sigma(p^2) \propto \frac{1}{4} \left(|a_L|^2 + |a_R|^2 \right) \left(A_0^2(M_1^2) + A_0^2(M_2^2) \right) \tag{6.19}$$

$$+ \left[M_1 M_2 \text{Re} \left(a_L a_R^* \right) + \frac{1}{4} (M_1^2 + M_2^2 - p^2) \left(|a_L|^2 + |a_R|^2 \right) \right] B_0(p^2, M_1^2, M_2^2),$$

where charged Higgs bosons couple to fermions as $(a_L P_L + a_R P_R)$ and M_1, M_2 are the fermion masses. The derivative of the self-energy with respect to p^2 at $M_{H^{\pm}}$ reads

$$\frac{d}{dp^2} \Sigma(p^2)|_{p^2 = M_{H^{\pm}}^2} \quad \propto \quad \left[M_1 M_2 \text{Re} \left(a_L a_R^* \right) + \frac{1}{4} (M_1^2 + M_2^2 - M_{H^{\pm}}^2) \left(|a_L|^2 + |a_R|^2 \right) \right]$$

$$\times \frac{d}{dp^2} B_0(p^2, M_1^2, M_2^2) \Big|_{p^2 = M_{H^{\pm}}^2}$$

$$- \frac{1}{4} \left(|a_L|^2 + |a_R|^2 \right) B_0(M_{H^{\pm}}^2, M_1^2, M_2^2), \tag{6.20}$$

where the second term is not divergent at the normal threshold. For tree-level couplings of charged Higgs and fermions, a_L and a_R are real and propotional to fermion masses in such way that the factor $\left[M_1 M_2 \text{Re} \left(a_L a_R^* \right) + \frac{1}{4} (M_1^2 + M_2^2 - M_{H^{\pm}}^2) \left(|a_L|^2 + |a_R|^2 \right) \right]$ vanishes.

This normal threshold problem can be overcome by using complex masses for the relevant unstable particles, see [163] and references therein. In our case, the normal threshold of top and bottom squarks is concerned. This singularity appears in the renormalization factor of the charged Higgs boson, $\delta Z_{H^- H^+}$, in particular in the derivative of the two-point functions, which we treat according to the substitutions

$$M_{\tilde{t}_i}^2 \to M_{\tilde{t}_i}^2 - i M_{\tilde{t}_i} \Gamma_{\tilde{t}_i}, \quad M_{\tilde{b}_j}^2 \to M_{\tilde{b}_j}^2 - i M_{\tilde{b}_j} \Gamma_{\tilde{b}_j}, \quad i, j = 1, 2. \tag{6.21}$$

The required decay widths have been computed in lowest order including all significant two-body decays. We do not present the analytic expressions of those decay widths since they are very lengthy.

Table 6.1: Masses of Higgs bosons and SUSY particles (in GeV) for the parameter set (F.2) and $\phi_1 = \phi_\tau = \phi_t = \phi_b = \pi/2$, $M_{H^\pm} = 300$ GeV, $|A_t| = 800$ GeV.

$\tan\beta$	M_{h_1}	$M_{\tilde\nu}$	$M_{\tilde\tau_1}$	$M_{\tilde\tau_2}$	$M_{\tilde\chi_1^\pm}$	$M_{\tilde\chi_2^\pm}$	$M_{\tilde\chi_1^0}$	$M_{\tilde\chi_2^0}$	$M_{\tilde\chi_3^0}$	$M_{\tilde\chi_4^0}$	$M_{\tilde t_1^0}$	$M_{\tilde t_2^0}$	$M_{\tilde b_1^0}$	$M_{\tilde b_2^0}$
5	114.7	190	155	206	138	272	88	142	208	272	373	645	406	508
15	120	189	151	209	146	267	89	148	212	226	373	645	448	515

Various cross checks on our calculations have been performed. Besides numerical and analytical checks of UV- and IR-finiteness, our results were checked against those obtained by a independent calculation [161] for the real MSSM, and very good agreements has been found.

6.5 Numerical studies

In this section we perform a numerical analysis. The SM input parameters are presented Appendix F.1. It should be noted that the masses of top and bottom is understood as the pole masses. For the soft-SUSY breaking parameters we use the modified $m_h^{\max}$ scenario specified in Appendix F.2.1. In addition, we chose μ to be zero as default value in order to be consistent with the experimental data of the electric dipole moments. The phases of trilinear couplings of the first and second generations have marginal effects on the CP rate asymmetry because the masses of the corresponding fermions are small. In the following, those phases are also taken to be zero. The phase of M_3, which enters from two loop order, is set to be zero as default. Since we use the $\overline{\text{DR}}$ scheme for $\tan\beta$ and the Higgs fields, our results depend on the renormalization scale μ_{R}; more details will be given in section 6.5.5. We chose $\mu_{\text{R}} = m_t$, which is the default value in `FeynHiggs`.

The relevant Higgs and SUSY particle masses we show in Table 6.1 for $M_{H^\pm} = 300$ GeV, $|A_t| = 800$ GeV. In the following analysis, we will vary $M_{H^\pm}$, $\tan\beta$, relevant phases and the trilinear couplings $|A_{\tau/t/b}|$ to show their impact on the decay width and the CP asymmetry.

6.5.1 Decay width: full results

We shall investigate the importance of the higher order effects on the $H^- \to W^- h_1$ decay width and show that the Born approximation is in general insufficient. We choose $\phi_1 = \phi_\tau = \phi_t = \phi_b = \pi/2$ for this analysis.

On the top panel of Fig. 6.7, we show the Born, improved Born, improved one-loop and full decay widths as functions of the charged Higgs mass at $\tan\beta = 5$. The Born, improved Born and improved one-loop decay widths are defined in Eq. (6.8), Eq. (6.9) and Eq. (6.11), respectively. The relative corrections for the improved one-loop and full results are shown on the right panels. We define the relative
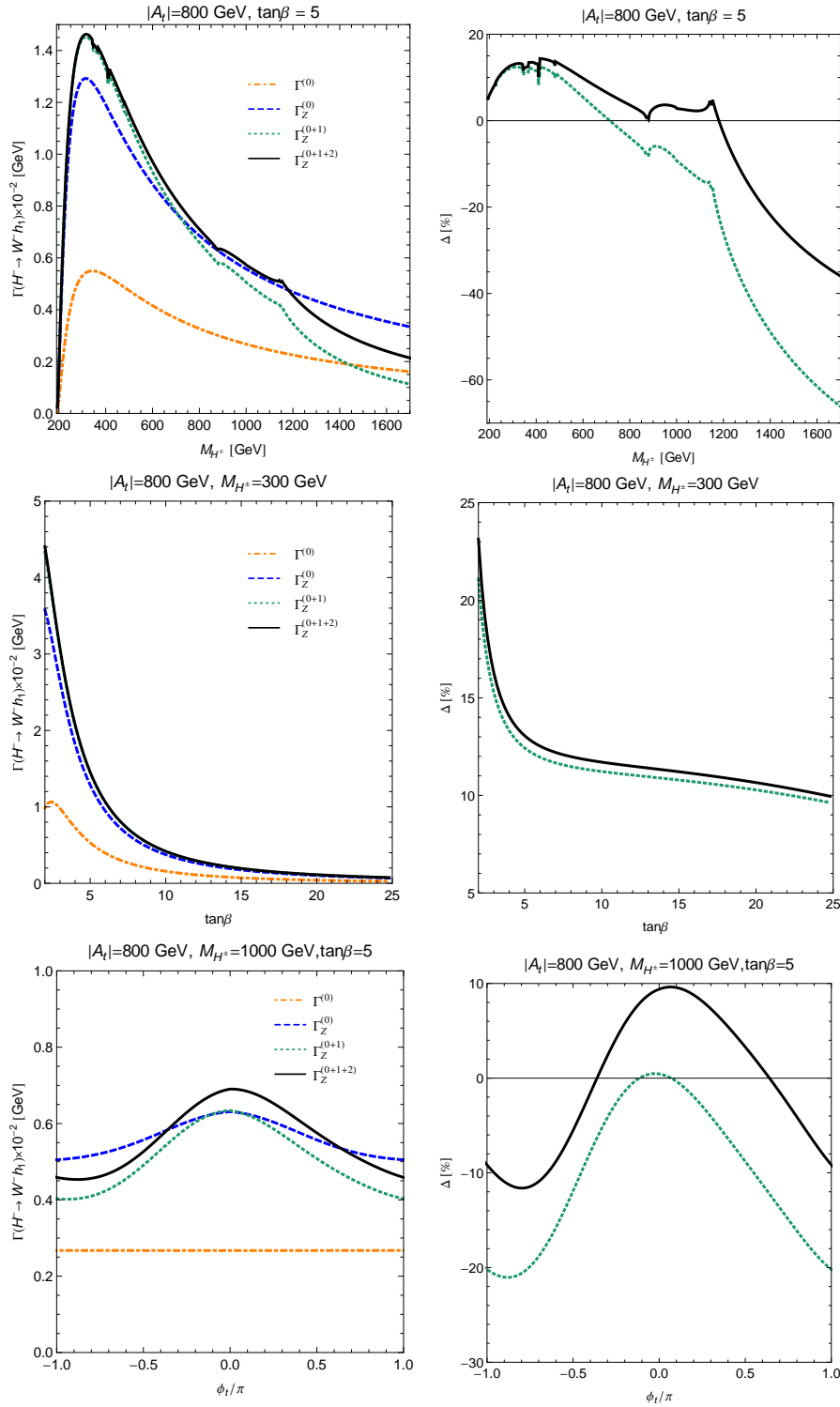
Figure 6.7: The Born, improved Born, improved one-loop and full decay widths corresponding to dot-dashed, dashed, dotted and solid lines are displayed as functions of the charged Higgs boson mass (top panel), $\tan\beta$ (middle panel) and ϕ_t (bottom panel). The right panels show the relative corrections of the improved one-loop and full decay widths compared to the improved Born decay width for $\phi_1 = \phi_\tau = \phi_t = \phi_b = \pi/2$.
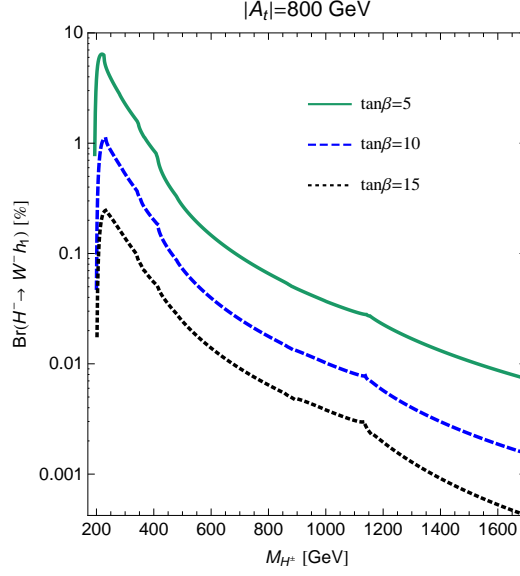
Figure 6.8: The branching ratios of the decay $H^- \to W^- h_1$ as functions of $M_{H^\pm}$ for different values of $\tan \beta$.

correction as $\delta^{(0+1(+2))} = (\Gamma_{\mathbf{Z}}^{(0+1(+2))} - \Gamma_{\mathbf{Z}}^0)/\Gamma_{\mathbf{Z}}^0$. For $M_{H^\pm} = 300\,\text{GeV}$, the one-loop vertex corrections can go up to 12.4% while at $M_{H^\pm} = 1.6\,\text{TeV}$ corrections reduce to -35.4% compared to improved Born result. For low $M_{H^\pm}$, the improved one-loop and the full result are quite close to each other, but around and above the $\tilde{t}_1 \tilde{b}_1$ threshold, the full result is clearly larger. Several normal threshold points as discarded in Section 6.4 can be seen in the plot.

On the middle panel of Fig. 6.7, we display the Born, improved Born and improved one-loop decay widths as function of $\tan \beta$ at $M_{H^\pm} = 300\,\text{GeV}$. It is clear that the decay widths strongly depend on the value of $\tan \beta$. They drop rapidly as $\tan \beta$ increases. Similarly on the bottom panel ϕ_t is varied instead. This shows us how important ϕ_t effects on our full results.

From the Fig. 6.7, we conclude that that the Born result is extremely poor approximation to the full result, thus should not be used.

In Fig. 6.8, we show the branching ratio of the decay $H^- \to h_1 W^-$ for different values of $\tan \beta$, using the full decay width. The other relevant decays of the charged Higgs boson are computed in lowest order as specified in Appendix E. For $\tan \beta = 5$, the branching ratio can reach 6.4% at $M_{H^\pm} \simeq 219\,\text{GeV}$. Around this point, the charged Higgs bosons decay mainly to $t\,b$ and $\tau\,\nu_\tau$. When the mass of charged Higgs boson increases, the channels to charginos and neutralinos, stop and sbottom open. Thus, the branching ratio of $H^- \to h_1 W^-$ drops rapidly, which makes it difficult to access δ_{CP} experimentally. The branching ratio depends also strongly on the value of $\tan \beta$, especially for low values of $\tan \beta$, where the channels $H^\pm \to h_1 W^\pm$ are interesting.
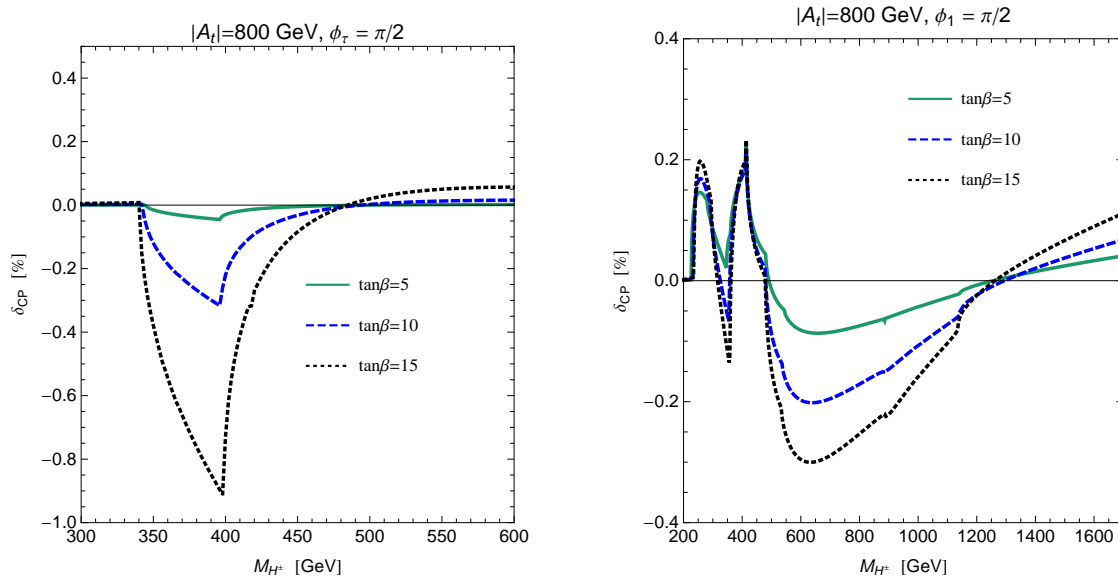
Figure 6.9: δ_{CP} as function of the charged Higgs mass. The left panel is for $\phi_\tau = \pi/2$ while the right panel is for $\phi_1 = \pi/2$. The solid, dashed and dotted lines are for $\tan\beta = 5$, 10 and 15, respectively.

6.5.2 CP asymmetry: ϕ_τ and ϕ_1 dependence

We want to display the impact of individual phases on the CP asymmetry. We therefore keep the phase considered non-zero while all the others are put to zero. The dependence on the phases ϕ_τ and ϕ_1 was studied already in [24][1]. As mentioned before, we improved the calculation by taking important loop contributions into the denominator, hence our numerical results are of two to three times smaller.

For $\phi_\tau = \pi/2$, δ_{CP} as functions of $M_{H^\pm}$ with different values of $\tan\beta$ are shown in the left panel of figure 6.9. The diagrams (b, c, f, g) in figure 6.6 with $\tilde\tau$ and $\tilde\nu_\tau$ loops yield a contribution to the CP violating term. Below the $\tilde\nu_\tau\tilde\tau_1$ threshold at $M_{H^\pm} \simeq 345\,\mathrm{GeV}$, δ_{CP} is negligible, in spite of contributions from beyond-one-loop terms with the **Z** factors. The high peaks correspond to the $\tilde\nu_\tau\tilde\tau_2$ threshold at $M_{H^\pm} \simeq 396\,\mathrm{GeV}$. Increasing $\tan\beta$ leads to a rapid decrease of the denominator, owing to the decreasing tree-level coupling, which is the main reason for the strongly rising δ_{CP}. With $\tan\beta = 5$, the largest value of δ_{CP} is about 0.05%, however with $\tan\beta = 15$, δ_{CP} can go up to 0.91%.

For $\phi_1 = \pi/2$, δ_{CP} is shown in the right panel of figure 6.9. The diagrams (a, c, d, e) in figure 6.6, with neutralino and chargino loops, contribute to the CP

---

[1]For a comparison, we have used the same approximation and the same set of input parameters as in Ref [24] . Our results are in agreement with theirs for the case of $\phi_\tau = -\pi/2$, $\phi_1 = 0$. For the case $\phi_\tau = 0$, $\phi_1 = -\pi/2$, we found a difference resulting from the coupling between neutral Higgs bosons and neutralinos, A_{lk} in eq. (A.3) of Ref. [24] where an extra factor 1/2 is present. Adapting this factor,we get agreement
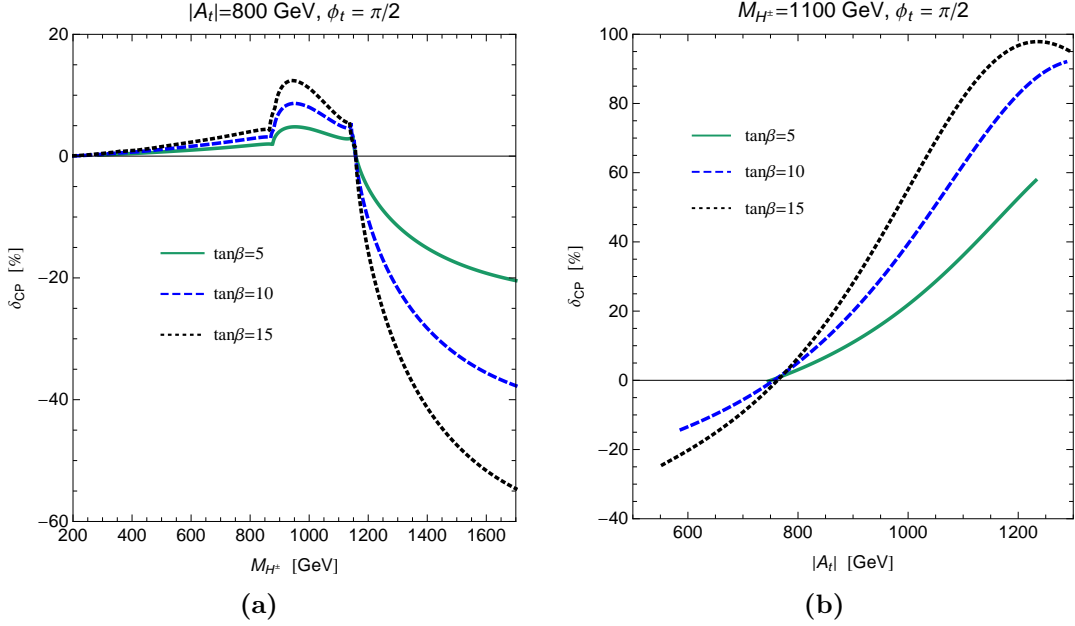
Figure 6.10: The CP asymmetry as functions (a) of the charged Higgs mass, (b) of $|A_t|$. The solid, dashed and dotted lines are for $\tan\beta = 5$, 10 and 15, respectively.

violating term. There are five visible thresholds, $\tilde{\chi}_1^\pm \tilde{\chi}_1^0$ at $M_{H^\pm} \simeq 226$ GeV, $\tilde{\chi}_1^\pm \tilde{\chi}_2^0$ at $M_{H^\pm} \simeq 280$ GeV, $\tilde{\chi}_1^\pm \tilde{\chi}_3^0$ at $M_{H^\pm} \simeq 346$ GeV, $\tilde{\chi}_1^\pm \tilde{\chi}_4^0$ at $M_{H^\pm} \simeq 400$ GeV and $\tilde{\chi}_2^\pm \tilde{\chi}_3^0$ at $M_{H^\pm} \simeq 480$ GeV. $\delta_{\rm CP}$ can reach 0.3% above the $\tilde{\chi}_1^\pm \tilde{\chi}_1^0$ threshold, in general, however, it is rather small.

6.5.3 CP asymmetry: ϕ_t and ϕ_b dependence

Significantly larger values of $\delta_{\rm CP}$ can occur when ϕ_t and ϕ_b are non-zero and the CP violating terms get contributions from diagrams with top and bottom squarks loops (figure 6.6). The left panel of figure 6.10 shows the CP asymmetry as a function of the charged Higgs mass for $\phi_t = \pi/2$. There are two visible thresholds, $\tilde{t}_1 \tilde{b}_1$ at $M_{H^-} \simeq 873$ GeV and $\tilde{t}_2 \tilde{b}_2$ at $M_{H^-} \simeq 1149$ GeV for $\tan\beta = 5$.

The CP asymmetry is sizeable both for $M_{H^\pm}$ below and above the $\tilde{t}_1 \tilde{b}_1$ threshold, especially for larger values of $\tan\beta$. Below the $\tilde{t}_1 \tilde{b}_1$ threshold, the most important term contributing to the CP asymmetry is the interference between diagram (c) in figure 6.6 and the triangles with top and bottom quarks. Close to the threshold, the interference of the diagrams (b, f, g) in figure 6.6 and the tree diagram are dominant. We observe that the individual contribution from the H-W mixing diagrams and the triangles with same particles inside loops can be much larger than the Born-term at the $\tilde{t}_i \tilde{b}_j$ thresholds. However, they carry opposite signs and are almost of the same order of magnitude. The sum of both can be comparable with the Born term and is very sensitive with respect to ϕ_t, $|A_t|$ and $\tan\beta$.
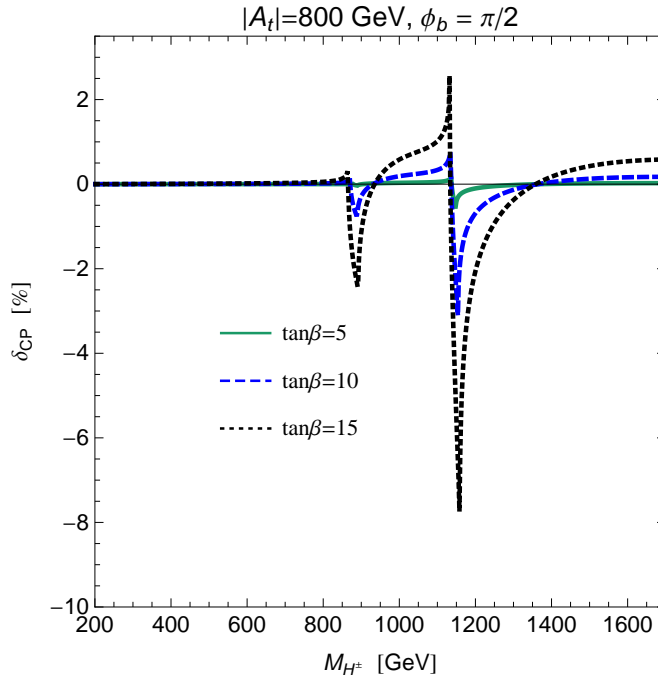
Figure 6.11: The CP asymmetry as function of charged Higgs mass, for $\phi_b = \pi/2$. The solid, dashed and dotted lines are for $\tan \beta = 5$, 10 and 15, respectively.

Above the $\tilde{t}_1 \tilde{b}_1$ threshold, δ_{CP} can become very large. It can rise up to -51.6% at M_{H^-}=1600 GeV, $\tan \beta$=15. This is a common feature of charged Higgs decays, as mentioned in Refs[158, 164]. Moreover, δ_{CP} has a strong dependence on $|A_t|$, as one can see in the right panel of figure 6.10. The $|A_t|$ range is compatible with $M_{h_1} > 114.5$ GeV.

The impact of the phase ϕ_b on δ_{CP} is shown in figure 6.11. It can be sizeable above M_{H^-} around the $\tilde{t}_1 \tilde{b}_1$ threshold, however it is still small compared to the effect of the phase ϕ_t. For $|A_t| = 800$ GeV, the largest value of δ_{CP} obtained for $\tan \beta = 15$ is about 8% close to the $\tilde{t}_2 \tilde{b}_2$ threshold.

The dependence of the CP asymmetry on the phase of A_t is illustrated in figure 6.12a, where we present δ_{CP} as a function of the charged Higgs mass with different values of $\phi_t = \frac{\pi}{2}$, $\frac{\pi}{3}$, $\frac{\pi}{6}$. Figure 6.12b shows the CP asymmetry at $M_{H^-} = 400$ GeV as a function of phase ϕ_t with $\tan \beta = 5$, 10, 15. For $\tan \beta = 15$ the maximum is at 0.92% for $\phi_t = 0.51\pi$. Compared to the contributions from ϕ_1 and ϕ_τ at low values of M_{H^-}, the impact of ϕ_t on δ_{CP} is considerably bigger, although not very strong from the absolute numbers.
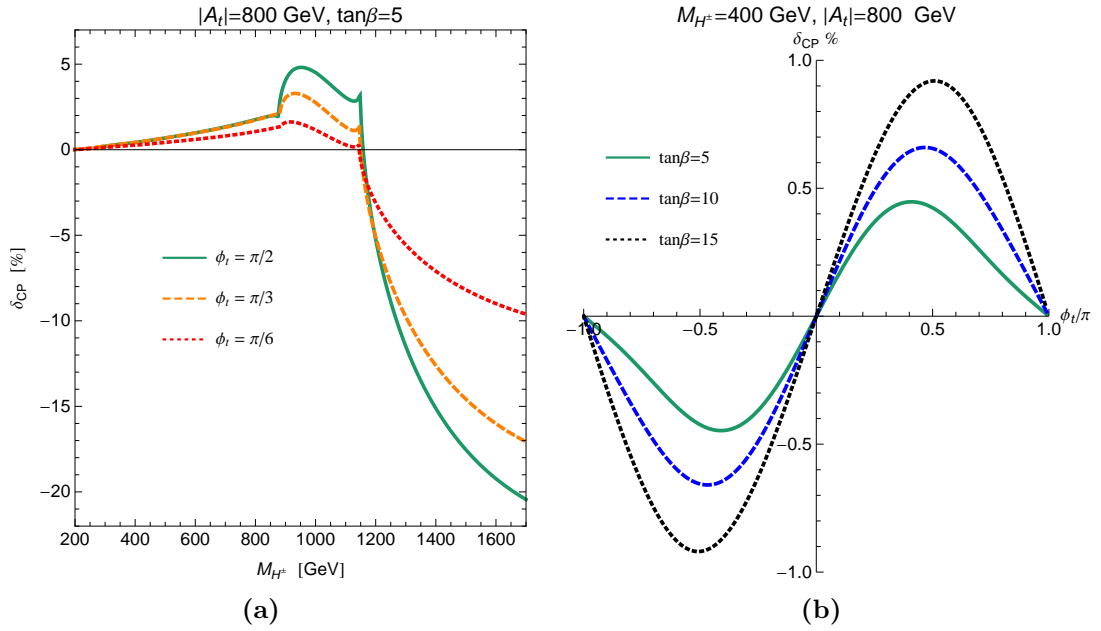
Figure 6.12: The CP asymmetry as function (a) of the charged Higgs mass for different values of $\phi_t = \{\frac{\pi}{2}, \frac{\pi}{3}, \frac{\pi}{6}\}$ (b) of the CP asymmetry as functions the phase ϕ_t for $\tan\beta = 5, 10, 15$.
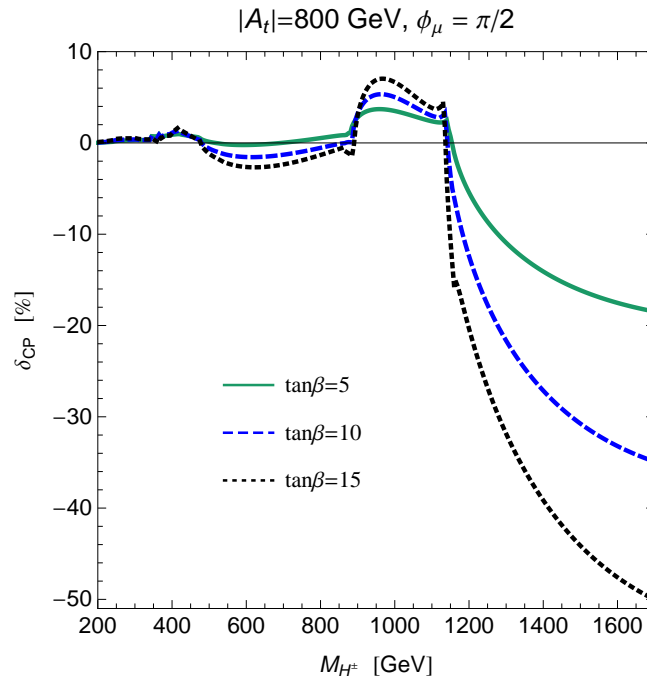

Figure 6.13: The CP asymmetry as functions of charged Higgs mass, for $\phi_\mu = \pi/2$. The solid, dashed and dotted lines are for $\tan\beta = 5, 10$ and 15, respectively.

6.5.4 CP asymmetry: ϕ_μ dependence

The phase of μ is severely constrained by the experimental limits on the electric dipole moments of electron and neutron. This bounds can, however, be circumvented by a specific fine-tuning of the phases of μ and of the non-universal SUSY parameters [165], leaving room also for a large phase ϕ_μ. We thus illustrate the effect of a large ϕ_μ on $\delta_{\rm CP}$ in Figure 6.13, which displays $\delta_{\rm CP}$ as a function of $M_{H^\pm}$ for $\phi_\mu = \pi/2$. The CP violating part receives contributions from all diagrams in figure 6.6. For charged Higgs boson masses below the $\tilde{t}_1 \tilde{b}_1$ threshold, the main contribution to $\delta_{\rm CP}$ comes from the neutralino-chargino loops; above the threshold it is again dominated by the $\tilde{t}_1 \tilde{b}_1$ loops.

6.5.5 Scale dependence

In this section we discuss the dependence of the decay widths and the CP asymmetries on the renormalization scale μ_R. On the left panel of Fig. 6.14 shows decay width versus μ_R at $M_{H^\pm} = 400$ GeV and $\tan\beta = 10$. To understand the dependences, it should be noted that the loop-corrected mass of h_1 varies from 119.1 GeV to 119.6 GeV when μ_R runs from $m_t/2$ to $2m_t$. Therefore the phase-space factor changes slightly. The other reason for the dependences is the $\mathbf{Z}$ factors from the Higgs renormalization. Now we define the uncertainty of the result as $(\Gamma(\mu_R = m_t/2) - \Gamma(\mu_R = 2m_t))/\Gamma(\mu_R = m_t)$. Then for the full decay width, the uncertainty is about 2.7%.

The dependence of $\delta_{\rm CP}$ on μ_R is displayed on the right panel of Fig. 6.14. Unlike the deday width, $\delta_{\rm CP}$ is the ratio of CP violating part and CP conserving part so that the phase-space factor is cancelled out. Therefore the dependence comes mainly from the CP violating contribution in the numerator of (6.13). The strict one-loop contribution to the CP violating part does not depend on μ_R since it arises from the imaginary part of one-loop integrals. We however consider also higher-order terms, like the Higgs-mixing term $\mathbf{Z}_{hA} M_A^{\rm tree} \delta M_h$, which depends on μ_R through the $\mathbf{Z}$ factors. For ϕ_τ and ϕ_1, such terms are negligible and the dependence on μ_R is irrelevant. For ϕ_μ and ϕ_t they are more important, as one can see in the figure. For $M_{H^\pm}$ values above the $\tilde{t}_1 \tilde{b}_1$ threshold, the one-loop contribution is the most important, and then the μ_R dependence is much weaker.

6.5.6 The CPX scenario

A case of particular interest is the CPX scenario (see in Appendix F.2.2) where the SUSY parameters maximize the CP-violating effects due to the large value of the product $\mathrm{Im}\,(\mu A_t)/M_{\rm SUSY}^2$.

In figure 6.15a, we display the CP asymmetry caused by the complex phase of A_t for $\tan\beta = 5, 10, 15$. As one can see, $\delta_{\rm CP}$ is quite large both below and above
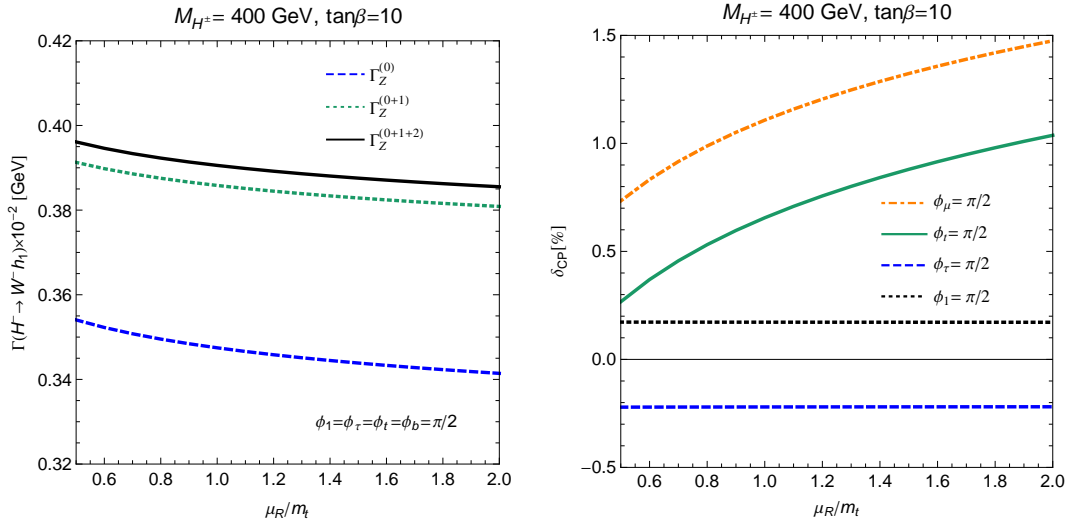
Figure 6.14: The decay widths (left) and CP asymmetry (right) as functions of the renormalization scale. μ_R is varied in the range $[m_t/2, 2m_t]$.

$\tilde{t}_1\tilde{b}_1$ threshold. For $\tan\beta = 5$, δ_{CP} is about -6% at $M_{H^\pm} \simeq 400\,\text{GeV}$ and can reach 100% at $M_{H^\pm} \simeq 1116\,\text{GeV}$. In figure 6.15b, the decay width is shown as function of $M_H^\pm$. Note that above the $\tilde{t}_1\tilde{b}_1$ threshold, the one-loop correction becomes very large, making the improved one-loop width negative, which demonstrates that this kind of approximation is unphysical and shows the importance of not truncating the squared amplitude.
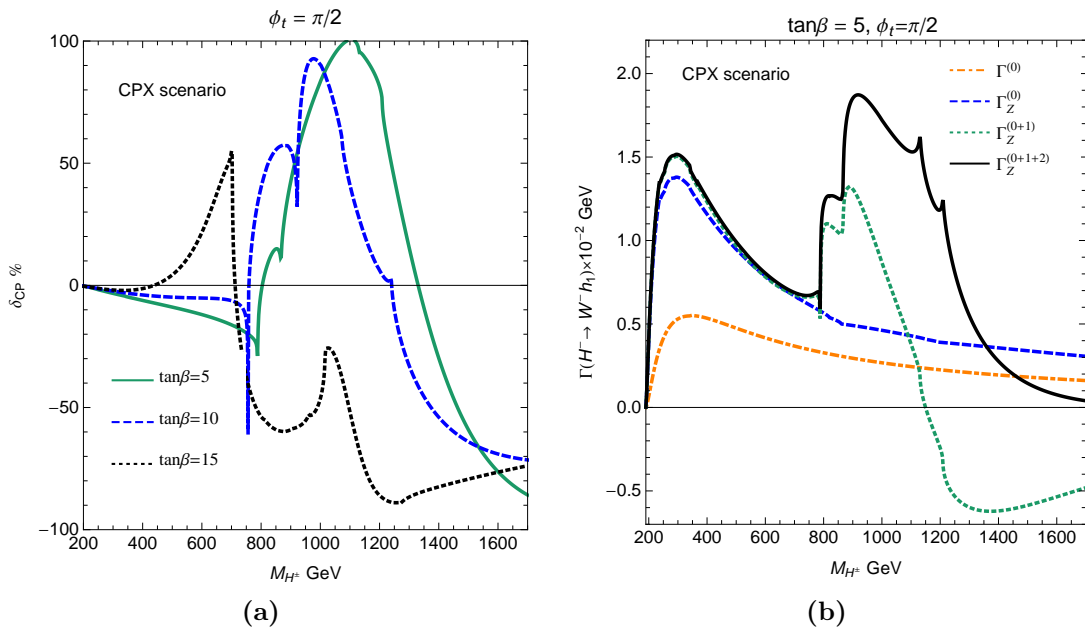
Figure 6.15: (a) $\delta_{\rm CP}$ as function of the charged Higgs mass in the CPX scenario. (b) The Born, improved Born, improved one-loop and full decay widths, corresponding to dot-dashed, dashed, dotted and solid lines, as functions of the charged Higgs mass in the CPX scenario.

Chapter 7

$W^\mp H^\pm$ production and CP asymmetry at the LHC

7.1 Introduction

At the LHC, the charged Higgs bosons can be produced via the following mechanisms:

- $gg, q\bar{q} \to t\bar{t} \to H^+ b\bar{t}$, for $m_t > M_{H^\pm} + m_b$;

- $gb \to tH^-$;

- $gg, q\bar{q} \to H^- t\bar{b}$;

- $b\bar{b}, gg \to W^\pm H^\mp$;

- $gg, q\bar{q} \to H^+ H^-$;

- $q\bar{q}' \to H^- h_i$, $(i = 1, 2, 3)$.

The first channel could be the dominant one if the charged Higgs mass is light enough since the top-pair production cross section is very large at the proton colliders (Tevatron and LHC). If the charged Higgs mass is larger than the top mass, charged Higgs bosons will be produced mainly through the other channels.

The $pp \to W^\pm H^\mp$ is one of the interesting processes. It does not only give a considerable production rate but allows to study CP violating effects. There have been many discussions devoted to the $pp \to W^\pm H^\mp$ processes in the MSSM over the last two decades. These studies assume all the soft supersymmetry-breaking parameters to be real and hence CP violation is absent. The two main partonic processes are $b\bar{b}$ annihilation and the loop-induced gg fusion. The first study [25] computed the tree-level $b\bar{b}$ contribution and the gg process with third-generation quarks in the loops using $m_b = 0$ approximation. This calculation was then extended

for finite m_b, thus allowing the investigation of the process for arbitrary values of $\tan\beta$ [26, 27]. The inclusion of the squark-loop contribution to the gg channel was done in [28, 29]. The next-to-leading order corrections to the $b\bar{b}$ annihilation are more complicated and not complete as yet; the full NLO electroweak corrections are still missing. The Standard Model QCD (SM-QCD) corrections were calculated in [30, 31], the supersymmetric-QCD (SUSY-QCD) corrections in [32, 33], and the Yukawa part of the electroweak corrections in [34]. There are also studies on the experimental possibility of observing $W^{\mp}H^{\pm}$ production at the LHC with subsequent hadronic $H^- \to \bar{t}b$ decay [166] and leptonic $H^- \to \tau^-\bar{\nu}_\tau$ decay [167, 168].

This chapter is devoted to the $W^{\pm}H^{\mp}$ production processes. First, we extend the calculation for $pp \to W^{\pm}H^{\mp}$ to the MSSM with complex parameters. Second, the full NLO EW corrections to the $b\bar{b}$ annihilation channel are calculated and consistently combined with the other contributions to provide the complete NLO corrections to the $pp \to W^{\pm}H^{\mp}$ processes. Third, CP-violating effects arising in the cMSSM are discussed. The important issues related to the neutral Higgs mixing and large radiative corrections to the bottom–Higgs couplings are also systematically addressed. Most of the results presented here have been published in [169].

7.2   The subprocess $b\bar{b} \to W^{\mp}H^{\pm}$
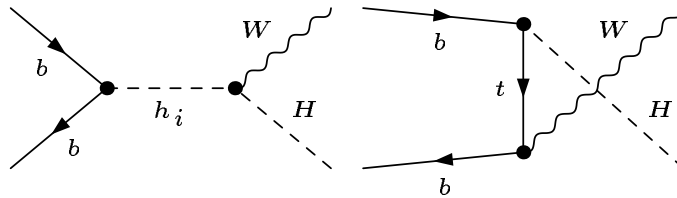
7.2.1   The leading order contribution

Figure 7.1:   Tree-level diagrams for the partonic process $b\bar{b} \to W^{\pm}H^{\mp}$. h_i with $i = 1, 2, 3$ denote the neutral Higgs bosons h, H and A, respectively.

At tree level, there are four Feynman diagrams including three s-channel diagrams with a neutral Higgs exchange and a t-channel diagram, as shown in Fig. 7.1. At very high center-of-mass energy, the t-channel diagram gives dominant contribution.

The hadronic cross section at leading order (LO) is given by

$$\sigma_{LO}^{pp}(S) = \int_0^1 d\tau \frac{d\mathcal{L}_{b\bar{b}}^{pp}}{d\tau} \hat{\sigma}_{LO}^{b\bar{b}}(\hat{s} = \tau S, \alpha^2, \mu_R), \tag{7.1}$$

with the parton luminosity

$$\frac{d\mathcal{L}_{ij}^{pp}}{d\tau} = \frac{1}{1+\delta_{ij}} \int_\tau^1 \frac{dx}{x}[f_i^p(x,\mu_F)f_j^p(\frac{\tau}{x},\mu_F) + f_j^p(x,\mu_F)f_i^p(\frac{\tau}{x},\mu_F)], \tag{7.2}$$

where $f_i^p(x, \mu_F)$ is the PDF of parton i at momentum faction x and factorization scale μ_F and $\hat{\sigma}_{LO}^{b\bar{b}}(\hat{s}, \alpha^2, \mu_R)$ is LO partonic cross section at CM energy $(\sqrt{\hat{s}})$ of the $b\bar{b}$ system and given by

$$\hat{\sigma}_{LO}^{b\bar{b}}(\hat{s}, \alpha^2, \mu_R) = \frac{\lambda^{1/2}(\hat{s}, M_{H^{\pm}}^2, M_W^2)}{32\pi\hat{s}^2} \int_0^1 \mathrm{d}\cos\theta \frac{1}{4}\frac{3}{9} \sum_{\rho,\bar{\rho}=\pm 1, \xi=0,\pm 1} |\mathcal{M}_{\rho,\bar{\rho},\xi}^{LO}|^2. \quad (7.3)$$

The helicity amplitudes,

$$\mathcal{M}_{\rho,\bar{\rho},\xi}^{LO} = \epsilon^{\mu}(\xi, p_w)\bar{v}(\bar{\rho}, p_{\bar{b}})\Gamma_{\mu}u(\rho, p_b), \quad (7.4)$$

are calculated with the tree-level bottom–Higgs couplings in Eq. (5.29) with $m_b = m_b^{\overline{\mathrm{DR}}}(\mu_R)$. $b, \bar{b}$ and W are chracterized by their momemta $p_b, p_{\bar{b}}, p_W$ and their helicities $\rho, \bar{\rho}, \xi$, respectively. θ is an angle between $\vec{p}_W$ and $\vec{p}_b$. It should be noted that other $q\bar{q}$-subprocesses ($q = u, d, c, s$) are neglected due to the smallness of light-quark-Higgs couplings.

One observes that the LO amplitudes contain the bottom–Higgs couplings and the neutral Higgs propagators. These quantities can get large radiative corrections as detailed in Chapter 5. In order to obtain reliable predictions, two important issues related to the bottom–Higgs Yukawa couplings and the neutral Higgs mixing have to be addressed. To quantify these effects, we define two approximations for the tree-level subprocesses $b\bar{b} \rightarrow W^{\mp}H^{\pm}$.

- The improved-Born approximation (IBA): the LO amplitudes are computed with the effective bottom–Higgs couplings in Eq. (5.39) where the large SM-QCD corrections are absorbed into running bottom mass $m_b^{\overline{\mathrm{DR}}}$ and large SUSY corrections are resummed into Δ_b and the resummed neutral Higgs mixing propagators Eq. (5.4) are used.

- The IBA1: the LO amplitudes are computed with the effective bottom–Higgs couplings in Eq. (5.39).
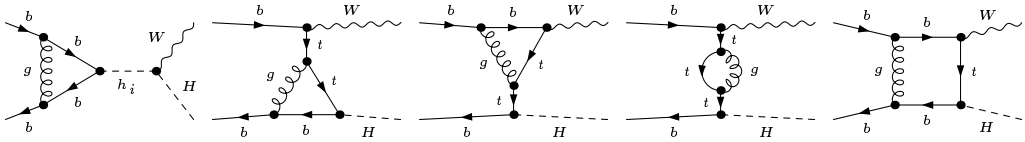
7.2.2 NLO SM-QCD contributions

Figure 7.2: One-loop SMQCD diagrams for the partonic process $b\bar{b} \rightarrow W^{\mp}H^{\pm}$.

The NLO contribution includes the virtual and real gluonic corrections. The calculation suffers UV, soft and collinear divergences. The UV divergences are canceled by the renormalization of the masses and wave functions of top and bottom. The soft divergences are canceled by summing the virtual and real contributions. The leftover initial state collinear divergences are factorized and absorbed into the (anti)bottom PDFs.

The virtual corrections

The virtual corrections, displayed in Fig. 7.2, contain a gluon in the loops. The calculation is done by using the technique of constrained differential renormalization (CDR) [170] which is, at one-loop level, equivalent to regularization by dimensional reduction [94, 96]. We have also checked by explicit calculations that it is also equivalent to dimensional regularization [93] in this case.

Concerning renormalization, the bottom-quark mass appearing in the Yukawa couplings is renormalized by using the $\overline{\text{DR}}$ scheme. It means that the running $m_b^{\overline{\text{DR}}}(\mu_R)$ (see Subsection 5.4.1) is used in the Yukawa couplings and the one-loop counterterm reads

$$\delta m_b^{\overline{\text{DR}}} = -m_b \frac{C_F \alpha_s}{4\pi} 3 C_{UV}, \tag{7.5}$$

where $C_F = 4/3$. The bottom-quark mass related to the initial state (in the kinematics $p_{b,\bar{b}}^2 = m_b^2$ and the spinors) is treated as the pole mass since the correct on-shell (OS) behavior must be assured. Indeed the m_b^{OS} effect here is very small and can be neglected. As mentioned in Subsection 5.4.1, the final results are independent of $\ln(m_b^{\text{OS}})$. We will therefore set $m_b^{\text{OS}} = m_b^{\overline{\text{DR}}}(\mu_R)$ everywhere in this chapter. The finite wave-function normalization factors for the bottom quarks can be taken care of by using the OS scheme for the wave-function renormalization as discussed in Subsection 4.2.3. For the top quark, the pole mass is used throughout this thesis. Accordingly, the mass counterterm is calculated by using the OS scheme (Subsection 4.2.3). Here we list explicit expressions of top mass counterterm and top and bottom wave-function counterterms

$$\delta m_t^{\text{OS}} = -m_t \frac{C_F \alpha_s}{4\pi} \left(3 C_{UV} + 5 - 6 \ln \frac{m_t}{\mu_R} \right), \tag{7.6}$$

$$\delta Z_{q,L}^{\text{OS}} = \delta Z_{q,R}^{\text{OS}} = \frac{C_F \alpha_s}{4\pi} \left(-C_{UV} + 2 \ln \frac{m_q}{\mu_R} - 4 \ln \frac{\lambda^2}{m_q} - 4 \right), \quad q = t, b \tag{7.7}$$

where λ is the gluon mass regulator. Indeed, the results are independent of renormalization scheme for $\delta Z_{t,L/R}$.

The real corrections

The real QCD corrections consist of the processes with external gluons,

$$b + \bar{b} \rightarrow W^- + H^+ + g, \tag{7.8}$$

$$b + g \rightarrow b + H^+ + W^-, \tag{7.9}$$

$$\bar{b} + g \rightarrow \bar{b} + W^- + H^+, \tag{7.10}$$

corresponding to the Feynman diagrams shown in Fig. 7.3. For the gluon-radiation process, soft and collinear divergences occur. The soft singularities cancel against
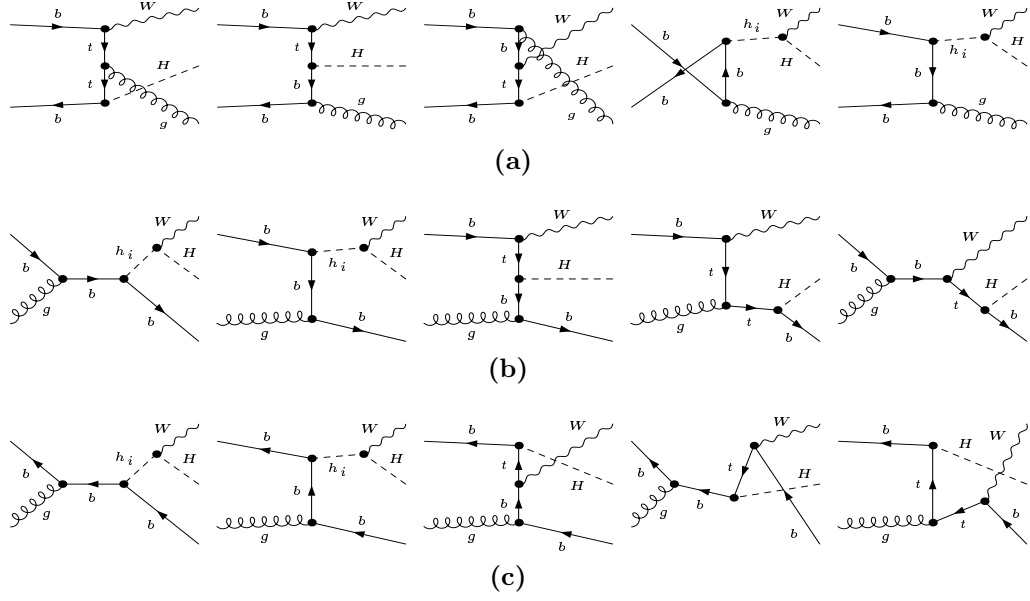
Figure 7.3: Tree-level real QCD radiation diagrams.

those from the virtual corrections, while the collinear singularities are regularized by the bottom-quark mass. The gluon–bottom-induced processes are infrared finite but contain collinear singularities, which are regularized by the bottom-quark mass as well. After adding the virtual and real corrections, the result is collinear divergent and proportional to $\ln(m_b^2/\hat{s})$. These singularities are absorbed into the (anti)bottom PDFs, as discussed in Section 4.3.2.

We apply both the dipole subtraction scheme and the two-cutoff phase space slicing method to extract the singularities from the real corrections as detailed in Subsection 4.3.2. The two techniques give the same results within the integration errors. Fig. 7.4a shows the agreement between the two methods. However, the error of the dipole subtraction scheme is much smaller than the one of the phase space slicing method. Therefore, we use the dipole subtraction scheme for the rest of this chapter.

To summarize, the hadronic cross section of the SM-QCD corrections consist of, for the dipole subtraction method:

$$\Delta_{\text{SMQCD}} \;=\; \int_0^1 d\tau \frac{d\mathcal{L}_{b\bar{b}}^{pp}}{d\tau}\Delta\hat{\sigma}^{b\bar{b}} + \int_0^1 d\tau \frac{d\mathcal{L}_{bg}^{pp}}{d\tau}\Delta\hat{\sigma}^{bg}, \tag{7.11}$$
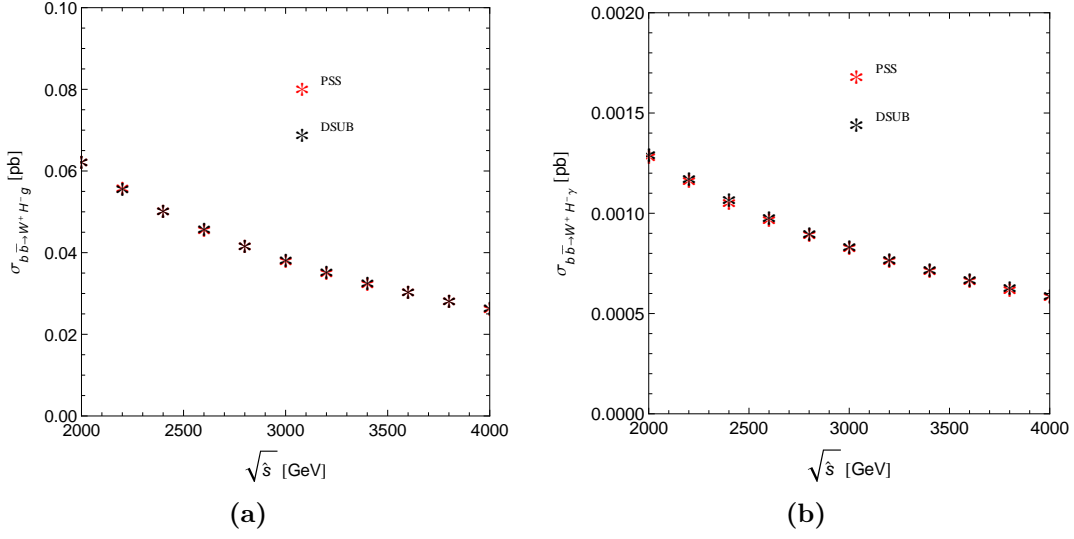
Figure 7.4: Partonic cross sections as functions of CM energy $\sqrt{\hat{s}}$ are shown for a) $b\bar{b} \to W^-H^+g$ and b) $b\bar{b} \to W^-H^+\gamma$. The results are obtained by the phase space slicing method (red stars) and the dipole subtraction method (black stars) in the CPX scenario with $M_{H^{\pm}} = 200$ GeV and $\tan\beta = 10$. Gluon and photon mass regulators are set to be unit.

with

$$
\begin{aligned}
\Delta\hat{\sigma}^{b\bar{b}} =& \hat{\sigma}^{b\bar{b}\to W^-H^+}_{\text{virt,SMQCD}}(\hat{s}, \alpha^2\alpha_s, \mu_R) \\
&+ \frac{C_F\alpha_s}{\pi}G_{b\bar{b}}(\hat{s})\hat{\sigma}^{b\bar{b}\to W^-H^+}_{LO}(\hat{s}, \alpha^2, \mu_R) \\
&+ \frac{C_F\alpha_s}{\pi}\int_0^1 dx \mathcal{G}_{b\bar{b}}(x, \hat{s})\left[\hat{\sigma}^{b\bar{b}\to W^-H^+}_{LO}(x\hat{s}, \alpha^2, \mu_R) - \hat{\sigma}^{b\bar{b}\to W^-H^+}_{LO}(\hat{s}, \alpha^2, \mu_R)\right] \\
&+ \hat{\sigma}^{b\bar{b}\to W^-H^+g}_{LO,\text{finite}}(\hat{s}, \alpha^2\alpha_s, \mu_R),
\end{aligned}
\tag{7.12}
$$

and

$$
\begin{aligned}
\Delta\hat{\sigma}^{bg} =& \frac{C_F\alpha_s}{\pi}\int_0^1 dx \mathcal{H}_{bg}(x, \hat{s})\hat{\sigma}^{b\bar{b}\to W^-H^+}_{LO}(x\hat{s}, \alpha^2, \mu_R) \\
&+ \hat{\sigma}^{bg\to W^-H^+b}_{LO,\text{finite}}(\hat{s}, \alpha^2\alpha_s, \mu_R) \\
&+ \hat{\sigma}^{\bar{b}g\to W^-H^+\bar{b}}_{LO,\text{finite}}(\hat{s}, \alpha^2\alpha_s, \mu_R),
\end{aligned}
\tag{7.13}
$$

where

$$
G_{b\bar{b}}(S) = \ln\frac{m_b^2}{S}\ln\frac{\lambda^2}{S} + \ln\frac{\lambda^2}{S} - \frac{1}{2}\ln^2\frac{m_b^2}{S} + \frac{1}{2}\ln\frac{m_b^2}{S} - \frac{\pi^2}{3} + 2, \tag{7.14}
$$

$$
\mathcal{G}_{b\bar{b}}(x, S) = \frac{1+x^2}{1-x}\left(\ln\frac{S}{m_b^2} - 1\right) + 1 - x + 2\frac{1+x^2}{1-x}\ln(1-x), \tag{7.15}
$$

$$
\mathcal{H}_{bg}(x, S) = [x^2 + (1-x^2)]\ln\frac{S(1-x)^2}{\mu_R^2} + 2x(1-x), \tag{7.16}
$$

the finite contributions of the real gluon and (anti)bottom radiation is defined in Subsection 4.3.2

$$\hat{\sigma}_{LO,\text{finite}}^{2\to3}(\hat{s}, \alpha^2\alpha_s, \mu_R) = \int d\Phi_3(|\mathcal{M}_{LO}^{2\to3}|^2 - |\mathcal{M}_{\text{sub}}|^2), \qquad (7.17)$$

and the parton luminosity $\mathcal{L}_{ij}^{pp}$ are defined in Eq. (7.2). In the above formulae we have combined the PDF counterterm contributions with the convolution piece since they have similar structure. It should be mentioned that we use the effective bottom–Higgs couplings for the SM-QCD corrections. The neutral Higgs mixing resummation is not used for the SM-QCD corrections.

7.2.3 Subtracting the on-shell top-quark contribution

A special feature of the gluon-induced processes in (7.10) is the appearance of on-shell top-quarks decaying into bW (and bH^+ when kinematically allowed), which requires a careful treatment and has been discussed in the previous literature, *e.g.* in [171, 172, 173]. Our approach is similar to the one described in [171, 172], with the difference that we perform the zero top-quark width limit.
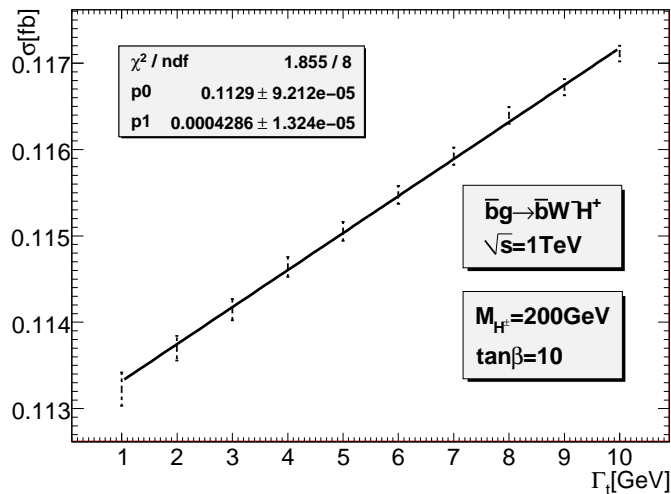

Figure 7.5: Dependence of the partonic cross section $\sigma_{\text{reg}}^{\bar{b}g\to W^-H^+\bar{b}}$ on the width regulator Γ_t.

We demonstrate the procedure in terms of the process $\bar{b}g \to W^-H^+\bar{b}$. The Feynman diagrams (Fig. 7.3c) include a subclass involving the decay $\bar{t} \to \bar{b}W^-$. When the internal $\bar{t}$ can be on-shell, the propagator pole must contain a finite width Γ_t, which is regarded here as a regulator:

$$\frac{i}{q^2 - m_t^2} \longrightarrow \frac{i}{q^2 - m_t^2 + im_t\Gamma_t}. \qquad (7.18)$$

This on-shell contribution is primarily a $\bar{t}H^+$ production and should therefore not be considered a NLO contribution. For the genuine NLO correction, the on-shell

top contribution has to be discarded in a gauge invariant way. Starting from the full set of diagrams, the squared matrix element reads as follows,

$$|M|^2 = |M_{\text{OS}}|^2 + 2\,\text{Re}[M_{\text{OS}}M^*_{\text{non-OS}}] + |M_{\text{non-OS}}|^2, \qquad (7.19)$$

where the subscripts $_{\text{OS}}$ and $_{\text{non-OS}}$ denote the contribution of the on-shell $\bar{t}$ diagrams and the remainder, respectively. The OS part, differential in the bW invariant mass, to be subtracted can be identified as

$$\frac{d\sigma^{\bar{b}g \to W^-H^+\bar{b}}}{dM_{bW}^2}\bigg|_{OS}^{\text{sub}} = \sigma^{\bar{b}g \to H^+\bar{t}}\text{Br}(\bar{t} \to \bar{b}W^-)\frac{m_t\Gamma_t}{\pi[(M_{bW}^2 - m_t^2)^2 + m_t^2\Gamma_t^2]}, \qquad (7.20)$$

where $\text{Br}(\bar{t} \to \bar{b}W^-) = \Gamma^{LO}_{\bar{t}\to\bar{b}W^-}/\Gamma_t$. The ratio on the right-hand side (rhs) of Eq. (7.20) approaches $\delta(M_{bW}^2 - m_t^2)$ when $\Gamma_t \to 0$. The subtracted NLO contributions, regularized with the help of Γ_t, can be written in the following way,

$$\begin{aligned}
\sigma^{\bar{b}g \to W^-H^+\bar{b}}_{\text{reg}}(\Gamma_t) &= \int dM_{bW}^2 \left(\frac{d\sigma^{\bar{b}g \to W^-H^+\bar{b}}_{\text{OS}}}{dM_{bW}^2} - \sigma^{\bar{b}g \to H^+\bar{t}}\frac{m_t\Gamma_t\text{Br}(\bar{t} \to \bar{b}W^-)}{\pi[(M_{bW}^2 - m_t^2)^2 + m_t^2\Gamma_t^2]}\right) \\
&+ \sigma^{\bar{b}g \to W^-H^+\bar{b}}_{\text{inter}} + \sigma^{\bar{b}g \to W^-H^+\bar{b}}_{\text{non-OS}}, \qquad (7.21)
\end{aligned}$$

where the interference and non-OS terms arise from the second and third terms in Eq. (7.19).

There is strong cancellation between the first term in the rhs of Eq. (7.21) and the rest after subtraction of the collinear part, which makes the result of Eq. (7.21) very small, yielding an essentially linear dependence on Γ_t as displayed in Fig. 7.5. We can thus perform the limit $\Gamma_t \to 0$ and obtain a gauge invariant expression by

$$\sigma^{\bar{b}g \to W^-H^+\bar{b}}_{\text{reg}} = \lim_{\Gamma_t \to 0} \sigma^{\bar{b}g \to W^-H^+\bar{b}}_{\text{reg}}(\Gamma_t). \qquad (7.22)$$

Fig. 7.6 shows that the finite gluon-induced contribution obtained in this way at the hadronic level (after proper subtraction of the collinear part) is very small for large values of $M_{H^\pm}$, but it can be of some significance when the charged Higgs boson is light.

The method described above is completely analogous for the process $bg \to W^-H^+b$. For low masses, $M_{H^\pm} < m_t$, the intermediate on-shell top quark can also decay into H^+b. This additional OS contribution can be extracted by using the same extrapolation method. For completeness, we list here the expressions for the decay widths of $t \to bW^+$ and $t \to bH^+$ at lowest order,

$$\Gamma^{LO}_{t\to bW^+} = \frac{\alpha}{16m_t^3M_W^2s_W^2}(m_t^2 - M_W^2)^2(m_t^2 + 2M_W^2), \qquad (7.23)$$

$$\Gamma^{LO}_{t\to bH^+} = \frac{\alpha}{16m_t^3M_W^2s_W^2}(m_t^2 - M_{H^\pm}^2)^2\left[(m_b^{\overline{\text{DR}}}\tan\beta)^2|\Delta_b^3|^2 + \frac{m_t^2}{\tan^2\beta}\right], \qquad (7.24)$$
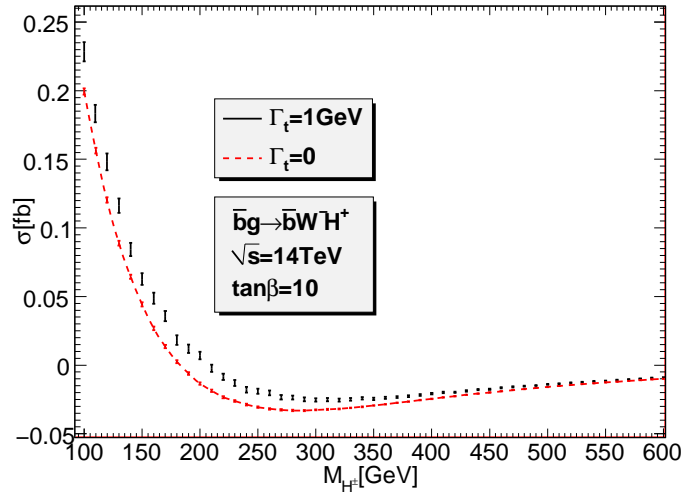
where the b-quark mass has been neglected.

Figure 7.6: The finite hadronic cross section $\sigma_{\mathrm{reg}}^{\bar{b}g \to W^-H^+\bar{b}}$ after subtracting the OS top-quark and the collinear-singularity contributions as a function of $M_{H^{\pm}}$.
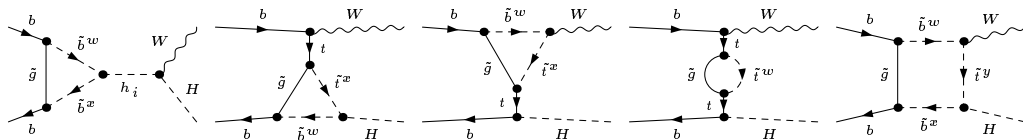

Figure 7.7: One-loop SUSY QCD diagrams for the partonic process $b\bar{b} \to W^{\mp}H^{\pm}$.

7.2.4 NLO SUSY-QCD contributions

The NLO SUSY-QCD contributions consist only of the virtual one-loop corrections, visualized by the Feynman diagrams with gluino loops in Fig. 7.7. The only UV divergent part is the top-quark self energy, which is renormalized in the on-shell scheme. As discussed in Section 5.4.1, large corrections proportional to $\alpha_s M_3^* \mu^* \tan\beta$ have been summed up to all orders in the bottom–Higgs couplings included in the IBA. We therefore have to subtract this part from the explicit one-loop SUSY-QCD corrections to avoid double counting by using the counterterms in Eq. (5.44). We define the remaining one-loop SUSY-QCD corrections as

$$\Delta_{\mathrm{SUSYQCD}} = \int_0^1 d\tau \frac{d\mathcal{L}_{b\bar{b}}^{pp}}{d\tau} \hat{\sigma}_{\mathrm{virt,SUSYQCD}}^{b\bar{b} \to W^-H^+}(\hat{s} = \tau S, \alpha^2 \alpha_s, \mu_R), \qquad (7.25)$$

where the partonic cross section is computed with the effective bottom–Higgs couplings and with the tree-level neutral Higgs propagators.

We have checked the UV finiteness. Our codes have been checked against the results of [33] for the real MSSM. Good agreements have been found.

7.2.5   NLO electroweak contributions

The full NLO EW contributions to the processes $b\bar{b} \to W^{\mp}H^{\pm}$ in the MSSM have not been computed yet. They comprise both virtual and real corrections. Similar to the SM-QCD corrections, the calculation contains UV, soft and collinear divergences. Therefore the similar procedure will be applied here.
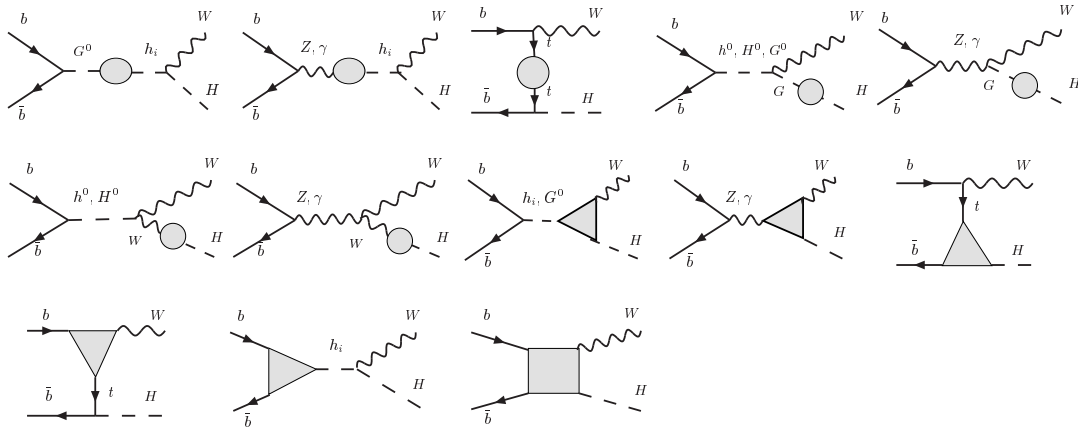
The virtual corrections

Figure 7.8:   One-loop EW contributions for the partonic process $b\bar{b} \to W^{\mp}H^{\pm}$. The shaded regions are the one-particle irreducible vertices.

For the virtual part, Fig. 7.8 illustrates the various classes of one-loop Feynman diagrams. As before, the calculation is performed using the CDR technique. We have also worked out all the necessary counterterms in the cMSSM and implemented them in `FeynArts-3.4`[174, 175]. Explicit expressions for the counterterms can be found in Appendix C.

Concerning renormalization, for the Higgs field wave functions and $\tan\beta$, we use the $\overline{\text{DR}}$ renormalization scheme as specified in Eq. (4.38). Since the charged Higgs is in the external line, we follow the prescription described in Subsection 5.2. The wave function renormalization factor $Z_{H^-H^+}$ should be taken into as explained in Section 6.1. One should aslo include the mixing of $H^{\pm}$ with $G^{\pm}$ and $W^{\pm}$ on the external line of the charged Higgs. The other renormalization constants are determined according to the OS scheme. To make the EW corrections independent of $\ln m_f$ from the light fermions $f \neq t$, we use the fine-structure constant at M_Z, $\alpha = \alpha(M_Z)$ as an input parameter. This means that we have to modify the counterterm as

$$
\begin{aligned}
\delta Z_e^{\alpha(M_Z)} &= \delta Z_e^{\alpha(0)} - \frac{1}{2}\Delta\alpha(M_Z^2), \\
\Delta\alpha(M_Z^2) &= \left.\frac{\partial \Sigma_T^{AA}}{\partial k^2}\right|_{k^2=0} - \frac{\text{Re}\,\Sigma_T^{AA}(M_Z^2)}{M_Z^2},
\end{aligned}
\tag{7.26}
$$

where the photon self-energy includes only the light fermion contribution, to avoid double counting.

The real corrections
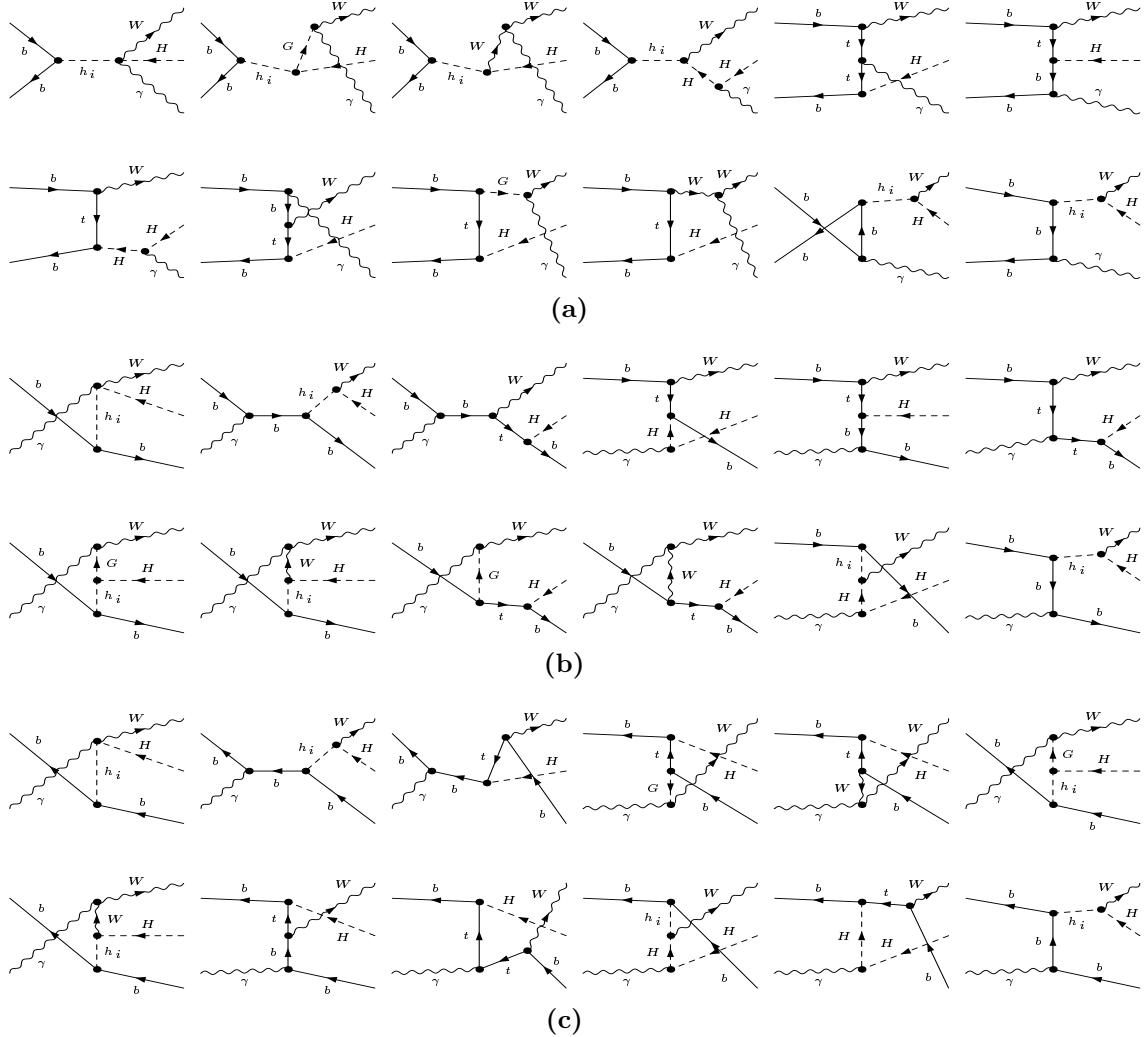

(a)

(b)

(c)

Figure 7.9: Photon-radiation and photon-induced EW diagrams.

The real EW contributions correspond to the processes with external photons,

$$
\begin{aligned}
b + \bar{b} &\to W^- + H^+ + \gamma, \\
b + \gamma &\to b + H^+ + W^-, \\
\bar{b} + \gamma &\to \bar{b} + W^- + H^+,
\end{aligned}
\tag{7.27}
$$

described by the Feynman diagrams of Fig. 7.9. They are calculated in the same way as the real QCD corrections, discussed in Section 7.2.2 and Section 7.2.3. However, the formulae are more complicated than the ones of the QCD case since photon now can be emitted from both initial and final states. It should be mentioned
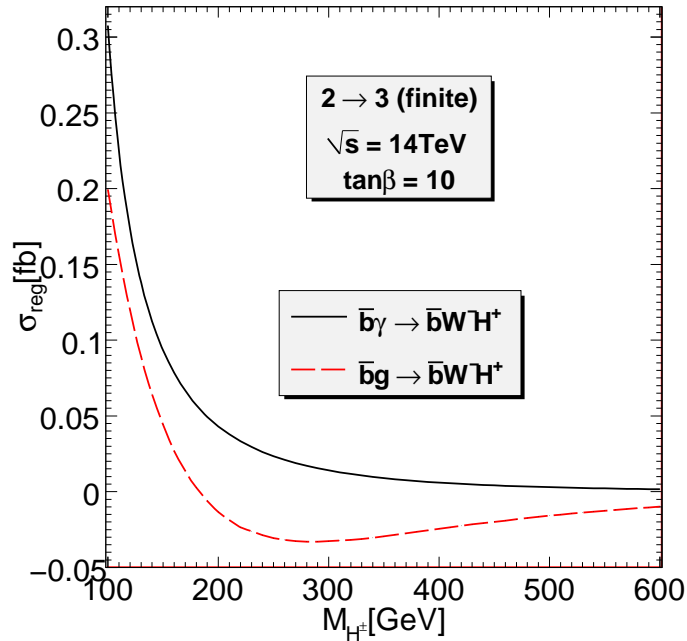
Figure 7.10:   The finite hadronic cross sections $\sigma_{\text{reg}}^{\bar{b}g \to W^- H^+ \bar{b}}$ (dashed line) and $\sigma_{\text{reg}}^{\bar{b}\gamma \to W^- H^+ \bar{b}}$ (solid line) after subtracting the OS top-quark and the collinear-singularity contributions as a function of $M_{H^{\pm}}$.

that we do not use either the effective bottom–Higgs couplings or the Higgs mixing resummation for both virtual and real EW corrections.

Naively, we would expect this photon contribution to be much smaller than the one from the gluon, due to the smallness of the EW coupling α and the photon PDF. This is not always true, however, since the photon couples to the $W^{\pm}$ and $H^{\pm}$ as well. The soft singularities are completely cancelled, as in the case of QCD. The EW splitting $\gamma \to H^+ H^-$ (similarly for $\gamma \to W^+ W^-$), on the other side, can introduce large collinear correction in the limit $M_{H^{\pm}}/Q \to 0$, Q is a typical energy scale. The constraint $M_H^{\pm} > M_W$ prevents those splittings from becoming divergent. We observe, however, that the finite corrections (after subtracting the collinear bottom-photon and the OS top-quark contributions) from the above $\bar{b}\gamma$ process are still larger than the corresponding QCD ones for $M_{H^{\pm}} < 200$GeV, *e.g.* for $M_H = 150$GeV and $\sqrt{s} = 14$TeV by a factor of 2 as illustrated in Fig. 7.10. The photon-induced contribution should thus be included in the NLO calculations for $W^{\pm}/H^{\pm}$ production at high energies. This requires the knowledge of the photon density in the proton, which at present is contained in the set MRST2004qed [130] of PDFs.
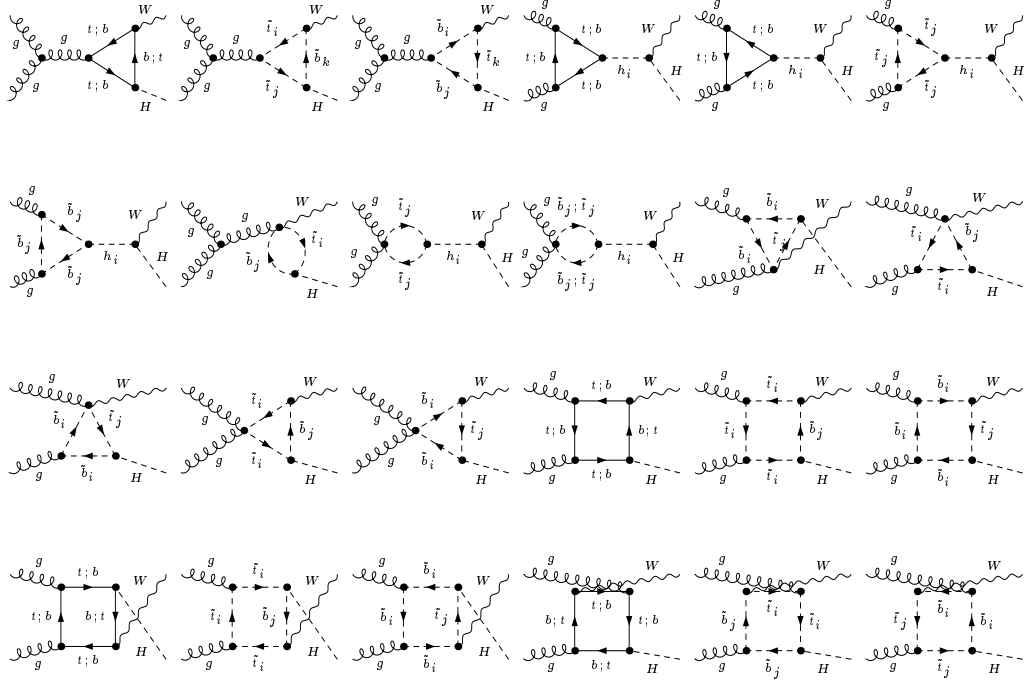
Figure 7.11: One-loop Feynman diagrams for the partonic process $gg \to W^\mp H^\pm$.

7.3 The subprocess $gg \to W^\mp H^\pm$

7.3.1 The leading order cross section

The subprocess $gg \to W^\mp H^\pm$ is loop induced with quark- and squark-loop contributions. Fig. 7.11 summarizes various one-loop Feynman diagrams, which involve three- and four-point vertex functions. No renormalization is needed, the UV divergences cancel among (s)quark loops. The hadronic cross section reads

$$\sigma_{gg}^{pp}(S) = \int_0^1 d\tau \frac{d\mathcal{L}_{gg}^{pp}}{d\tau} \hat{\sigma}^{gg \to W^- H^+}(\hat{s}, \alpha^2 \alpha_s^2), \tag{7.28}$$

where the partonic cross section

$$\hat{\sigma}^{gg \to W^- H^+}(\hat{s}, \alpha^2 \alpha_s^2) = \frac{\lambda^{1/2}(\hat{s}, M_{H^\pm}^2, M_W^2)}{32\pi \hat{s}^2} \int_1^2 d\cos\theta \sum_{\rho,\bar{\rho}=\pm 1,\xi=0,\pm 1} \frac{1}{4} \frac{\text{CF}}{64} |\mathcal{M}_{\rho\bar{\rho}\xi}|^2,$$

$$\text{CF} = \sum_{a,b=1}^{8} \left[\text{Tr}\left(\frac{\lambda_a}{2}\frac{\lambda_b}{2}\right) \right]^2 = 2, \tag{7.29}$$

contains the helicity amplitude

$$\mathcal{M}_{\rho\bar{\rho}\xi}^{gg} = \epsilon^{*\mu}(\xi, p_W)\epsilon^\nu(\rho, p_g)\epsilon^\sigma(\bar{\rho}, p_g)\Gamma_{\mu\nu\sigma}. \tag{7.30}$$

Here $\epsilon^\nu(\rho, p_g), \epsilon^\sigma(\bar{\rho}, p_g)$ denote the polarization vectors of the incoming gluons. This structure of the amplitude will allow us checking for the QCD gauge invariance, see Subsection 7.3.2.

Since the (s)quark couple to a Higgs boson, the one-loop amplitude is proportional to (s)quark-Higgs couplings. The dominant contributions therefore arise from the diagrams with the third-generation (s)quarks. As in [29], the contribution from the first two generations of (s)quarks is neglected in our calculation. Compared to the previous work [29], our calculation is improved by using the effective bottom–Higgs couplings and the resummed neutral Higgs propagators. It turns out that these improvements affect sizably both the cross section and CP-violating asymmetry. We have checked our results against those of [29] for the case of the real MSSM using the tree-level couplings and tree-leve Higgs propagators and found good agreement.

7.3.2   QCD gauge invariance

In our calculation of the matrix elements with gluon or photon in the external lines, we have to deal with polarization vectors. In the squared amplitude method, one can use the completeness relation

$$\sum_{\rho=\pm 1} \epsilon_\mu^{\alpha *}(p,\rho)\epsilon_\nu^\beta(p,\rho) = \delta^{\alpha\beta}\left(-g_{\mu\nu} - \frac{\eta^2 p_\mu p_\nu}{(\eta.p)^2} + \frac{\eta_\mu p_\nu + \eta_\nu p_\mu}{\eta.p}\right), \qquad (7.31)$$

where η is an arbitrary four-vector and satisfies $\eta.\epsilon = 0$ and $\eta.p \neq 0$. The cross-section does not depend on η. In helicity amplitude method, using the two-component Weyl-van-der-Waerden spinors Ref. [176], the two polarization vectors $\epsilon_\pm^\mu$ can be expressed as

$$\epsilon_{+,\dot{A}B} = \frac{\sqrt{2}g_{+,\dot{A}}k_B}{\langle g_+ k\rangle} \qquad \epsilon_{-,\dot{A}B} = \frac{\sqrt{2}k_{\dot{A}}g_{-,B}}{\langle g_- k\rangle}$$

$$\epsilon_{+,\dot{A}B}^* = \frac{\sqrt{2}k_{\dot{A}}g_{+,B}}{\langle g_+ k\rangle} \qquad \epsilon_{-,\dot{A}B}^* = \frac{\sqrt{2}g_{-,\dot{A}}k_B}{\langle g_- k\rangle^*}, \qquad (7.32)$$

where

$$k_A = \sqrt{2k_0}\begin{pmatrix} e^{i\phi}\cos\frac{\theta}{2} \\ \sin\frac{\theta}{2} \end{pmatrix}, \qquad (7.33)$$

the momentum of particle is denoted as $k^\mu = (k_0, |k|\cos\phi\sin\theta, |k|\sin\phi\sin\theta, |k|\cos\theta)$ and $g_\pm$ are arbitrary spinors with $\langle g_\pm k\rangle \neq 0$. The Lorentz-invariant spinor product is defined as

$$\langle gk\rangle = g_A k^B = g_1 k_2 - g_2 k_1. \qquad (7.34)$$

The dotted index relates to the undotted one by complex conjugation,

$$g_{\dot{A}} = g_A^*. \qquad (7.35)$$

We follow the method in [91]. The QCD gauge invariance can be check by varying the two gauge spinor $g_\pm$. We confirm the QCD gauge invariant amplitudes for $gg \to W^{\mp}H^{\pm}$.
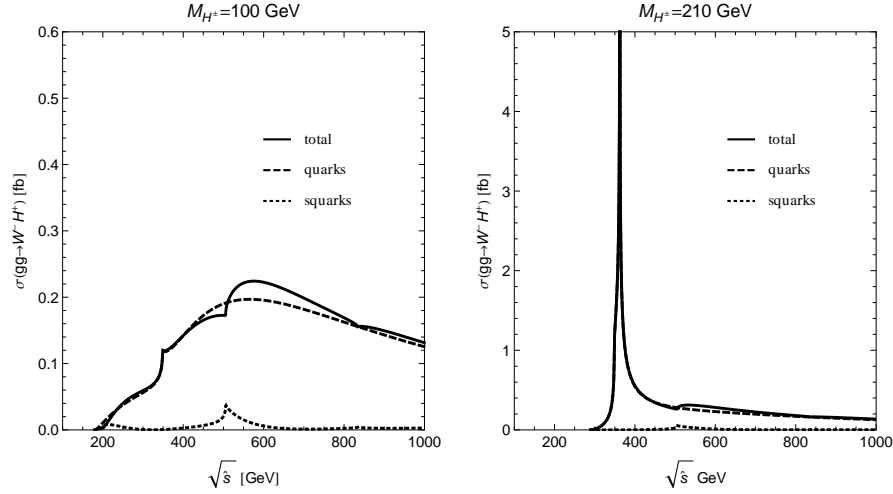
Figure 7.12: Partonic cross section of $gg \to W^-H^+$ using parameter set $M_{\tilde{Q}} = M_{\tilde{U}} = M_{\tilde{D}} = 250\,\text{GeV}, X_b = 0, X_t = -470\,\text{GeV}, \tan\beta = 1.5$ of [29] for $M_{H^{\pm}} = 100\,\text{GeV}$ (left) and $M_{H^{\pm}} = 210\,\text{GeV}$ (right). The dashed lines shows only contribution of quark loop diagrams while the dotted lines are for squark loop ones. The total contributions are presented by the solid lines.

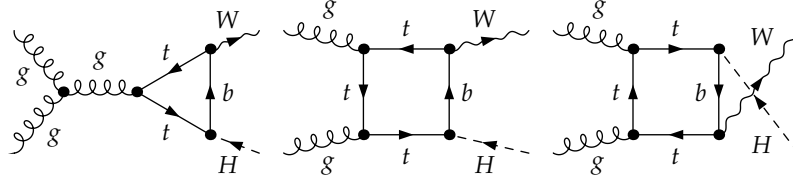### 7.3.3 Three-point Landau singularities

Figure 7.13: Feynman diagrams that can produce three-point Landau singularities.

We notice an interesting feature related to the anomalous thresholds. Figure on the right panel of Fig. 7.12 shows a very sharp peak close to the normal $t\bar{t}$ threshold (similar to Fig. 1b of [29]). Careful observation reveals that the peak position is slightly above $2m_t$ and is obviously more singular than the normal thresholds on the left panel of Fig. 7.12. This is indeed an anomalous threshold corresponding to the three-point Landau singularity of the triangle and box diagrams in Fig. 7.13. the Landau matrix of those triangle and box diagrams reads

$$Q = \begin{pmatrix} 2m_t^2 & m_t^2 + m_b^2 - M_W^2 & 2m_t^2 - \hat{s} \\ m_t^2 + m_b^2 - M_W^2 & 2m_b^2 & m_t^2 + m_b^2 - M_{H^{\pm}}^2 \\ 2m_t^2 - \hat{s} & m_t^2 + m_b^2 - M_{H^{\pm}}^2 & 2m_t^2 \end{pmatrix}. \qquad (7.36)$$

We will use the necessary and sufficient conditions for the appearance of a singularity

in Eq. (4.7). First, the vanishing determination condition gives

$$\hat{s}_{\pm} = \frac{1}{2m_b^2}\big[(M_{H^{\pm}}^2 + M_W^2)(m_t^2 + m_b^2) - (m_b^2 - m_t^2)^2 - M_{H^{\pm}}^2 M_W^2$$
$$\pm \lambda^{1/2}(m_t^2, m_b^2, M_{H_{\pm}}^2)\lambda^{1/2}(m_t^2, m_b^2, M_W^2)\big], \tag{7.37}$$

with $M_{H^{\pm}} \geq m_t + m_b$. Now we can check if those values of $\hat{s}$ satisfy the second condition $x_i \geq 0$, $i = 1, 2, 3$. Since $\det[Q] = 0$, we can chose $x_3 = 1$. The two other solutions are

$$x_1 = -\frac{(m_t^2 - m_b^2)^2 + M_{H^{\pm}}^2 M_W^2 - (m_t^2 + m_b^2)(M_{H^{\pm}}^2 + M_W^2) + 2m_b^2\hat{s}}{\lambda(m_t^2, m_b^2, M_W^2)},$$
$$x_2 = -\frac{\hat{s}(-m_b^2 - m_t^2 + M_W^2) + 2m_t^2(-M_W^2 + M_{H^{\pm}}^2)}{\lambda(m_t^2, m_b^2, M_W^2)}. \tag{7.38}$$

$x_1 > 0$ is satisfied with $\hat{s} = s_-$, but unsatisfied with $\hat{s} = s_+$. We now consider $\hat{s} = s_-$. From condition $x_2 \geq 0$, we get

$$s_- \geq \frac{2m_t^2(M_{H^{\pm}}^2 - M_W^2)}{m_t^2 - M_W^2 + m_b^2}, \tag{7.39}$$

which leads to

$$m_b + m_t \leq M_{H^{\pm}} \leq \sqrt{2(m_t^2 + m_b^2) - M_W^2}, \tag{7.40}$$

and

$$2m_t \leq \sqrt{\hat{s}} \leq \sqrt{\frac{m_t}{m_b}[(m_t + m_b)^2 - M_W^2]}. \tag{7.41}$$

The partonic cross section is divergent at $\hat{s} = \hat{s}_-$ but the result is finite at the hadronic level, *i.e.* after integrating over $\hat{s}$, since this singularity is logarithmic and thus integrable.

Similarly, the three-point Landau singularities can occur in the squark diagrams depicted in Fig. 7.14. The conditions for such singularities are similar to Eq. (7.40) but with the squark masses instead. In Fig. 7.15, we illustrate the three-point singularity of the squark contribution with $M_{H^{\pm}} = 360\,\text{GeV}$.

7.4 NLO hadronic cross section and CP asymmetry

The NLO hadronic cross section

$$\sigma_{NLO}^{pp} = \sigma_{IBA}^{b\bar{b}}(\alpha^2) + \Delta_{\text{SM-QCD}}(\alpha^2\alpha_s) + \Delta_{\text{SUSY-QCD}}(\alpha^2\alpha_s) + \Delta_{EW}(\alpha^3) + \sigma_{gg}(\alpha^2\alpha_s^2) \tag{7.42}$$

contains the various NLO contributions at the parton level, discussed in the previous sections. As mentioned there, the mass singularities of the type $\alpha_s \ln(m_b)$ and
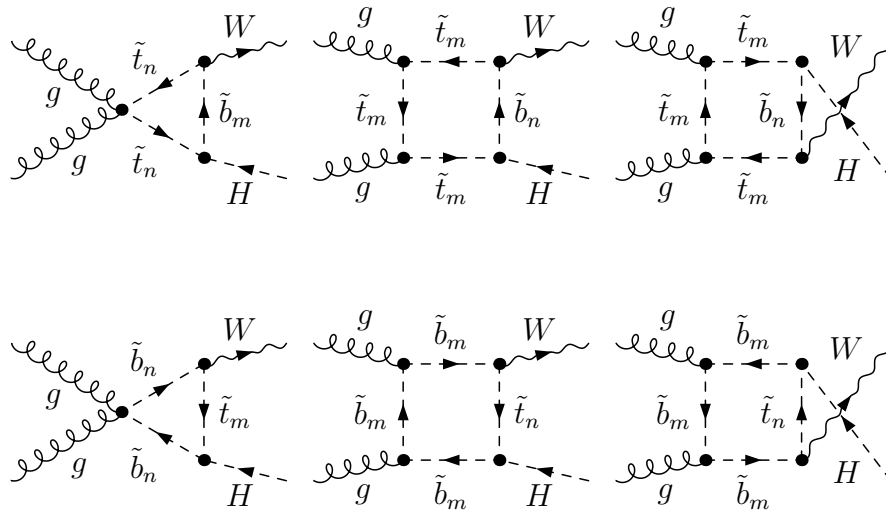
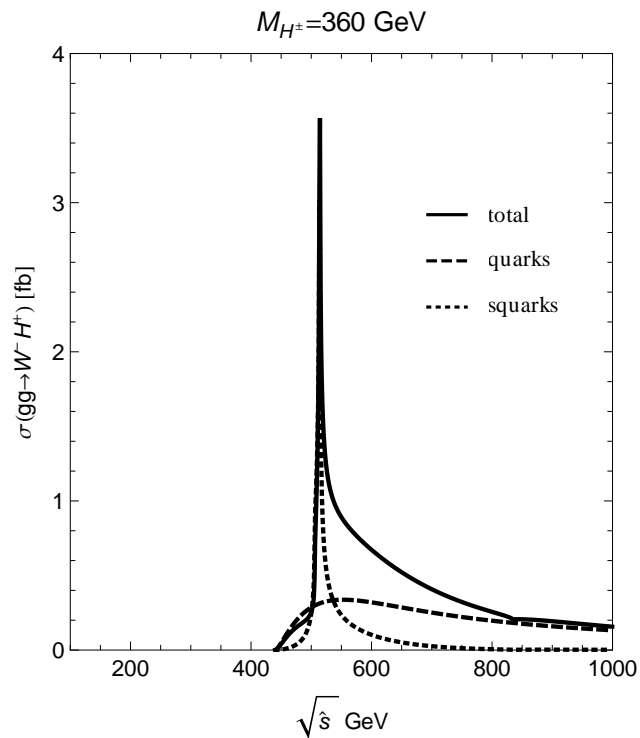Figure 7.14: Several squark box diagrams can produce Landau singularity.

Figure 7.15: Similar to Fig. 7.12 but with $M_{H^\pm} = 360$ GeV instead.

$\alpha \ln(m_b)$ are absorbed in the quark distributions. We use the MRST2004qed set of PDFs [130], which include $\mathcal{O}(\alpha_s)$ QCD and $\mathcal{O}(\alpha)$ photonic corrections. As explained in [129], the consistent use of these PDFs requires the $\overline{\text{MS}}$ factorization scheme for the QCD, but the DIS scheme for the photonic corrections.

Having constructed in this way the hadronic cross sections $\sigma(pp \to W^{\pm}H^{\mp})$, we can define the CP-violating asymmetry at the hadronic level in the following way,

$$\delta_{pp}^{\text{CP}} = \frac{\sigma(pp \to W^-H^+) - \sigma(pp \to W^+H^-)}{\sigma(pp \to W^-H^+) + \sigma(pp \to W^+H^-)}. \tag{7.43}$$

The numerator gets contributions from the NLO-$b\bar{b}$ corrections (the LO is CP conserving) and the loop-induced gg process. However, the latter is much larger than the former due to the dominant gluon PDF. The CP-violating effect is therefore mainly generated by the gg channel. The LO-$b\bar{b}$ contribution adds only to the CP invariant part and therefore reduces the magnitude of the CP asymmetry.

7.5   Numerical studies

In this section we present the numerical results. Here we need to specify our input parameters. In the set of SM parameters presented in Appendix F.1, we use the QCD-$\overline{\text{MS}}$ b-quark mass, $\overline{m}_b(\overline{m}_b)$, as an input parameter while the top-quark mass is understood as the pole mass. For the soft SUSY-breaking parameters, we use the CPX scenario. The complex phases of the trilinear couplings A_t, A_b, A_τ and the gaugino-mass parameters M_i with $i = 1, 2, 3$ are chosen as default according to

$$\phi_t = \phi_b = \phi_\tau = \phi_3 = \phi_1 = \frac{\pi}{2}, \tag{7.44}$$

unless specified otherwise. The phase of μ is chosen to be zero in order to be consistent with the experimental data of the electric dipole moment. We will study the dependence of our results on $\tan\beta$, $M_{H^\pm}$, ϕ_t and ϕ_3 in the numerical analysis. The ϕ_b dependence is not very interesting since it is similar to but much weaker than that of ϕ_t.

The scale of α_s in the SUSY-QCD resummation of the effective bottom–Higgs couplings Eq. (5.41) is set to be $Q = (m_{\tilde{b}_1} + m_{\tilde{b}_2} + m_{\tilde{g}})/3$. If not otherwise specified, we set the renormalization scale equal to the factorization scale, $\mu_R = \mu_F$, in all numerical results. Our default choice for the factorization scale is $\mu_{F0} = M_W + M_{H^\pm}$.

Our study is done for the LHC at 7 TeV and 14 TeV center-of-mass energy. In the numerical analysis, we will focus on the latter since the total cross section is about an order of magnitude larger. Important results will be shown for both energies.
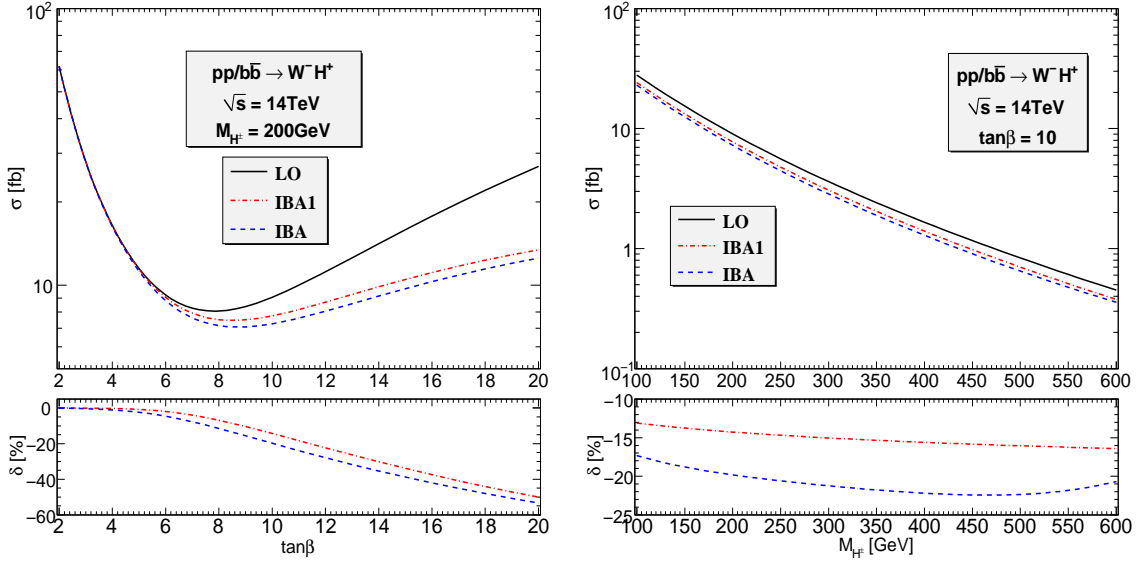
Figure 7.16: The LO cross section with $m_b = m_b^{\overline{\text{DR}}}$ and the two improved Born approximations (IBA) as functions of $\tan\beta$ (left) and $M_{H^\pm}$ (right). σ_{IBA1} includes the Δ_b resummation but not the Higgs mixing resummation, while σ_{IBA} includes both. The lower panels show the corresponding relative corrections with respect to the LO result.

7.5.1 $pp/b\bar{b} \to W^\mp H^\pm$: LO and improved-Born approximations

In this subsection, we study the effect of the bottom–Higgs coupling resummation described in Section 5.4.1 and of the Higgs propagator matrix discussed in Section 5.3.

The results for the approximations IBA and IBA1 defined in section 7.2.1 are illustrated in Fig. 7.16 showing the dependence on $\tan\beta$ in the left panel and on the mass $M_{H^\pm}$ in the right panel. The relative correction δ, with respect to the LO cross section, is defined as $\delta = (\sigma_{\text{IBA}} - \sigma_{\text{LO}})/\sigma_{\text{LO}}$. For small values of $\tan\beta$ the left-chirality contribution proportional to $m_t/\tan\beta$ is dominant while the right-chirality contribution proportional to $m_b \tan\beta$ dominates at large $\tan\beta$. The cross section has a minimum around $\tan\beta = 8$.

The effect of Δ_b resummation is best understood in terms of Fig. 7.16 and Fig. 7.17. The important point is that Δ_b is a complex number and only its real part can interfere with the LO amplitude. Thus, the Δ_b effect is minimum at $\phi_{t,3} = \pm\pi/2$ where the dominant $\Delta m_b^{SQCD,\tilde{H}\tilde{t}}$ are purely imaginary and is largest at $\phi_{t,3} = 0, \pm\pi$. ϕ_t enters via EW corrections and ϕ_3 via the SUSY-QCD contributions. Fig. 7.17 shows that the Δ_b effect can be more than 150%. In Fig. 7.16 where Δ_b is mostly imaginary we see the effect of order $\mathcal{O}(\Delta_b^2)$ which is about -15% at $\tan\beta = 10$. We observe also that the Higgs mixing resummation in the s-channel diagrams has a
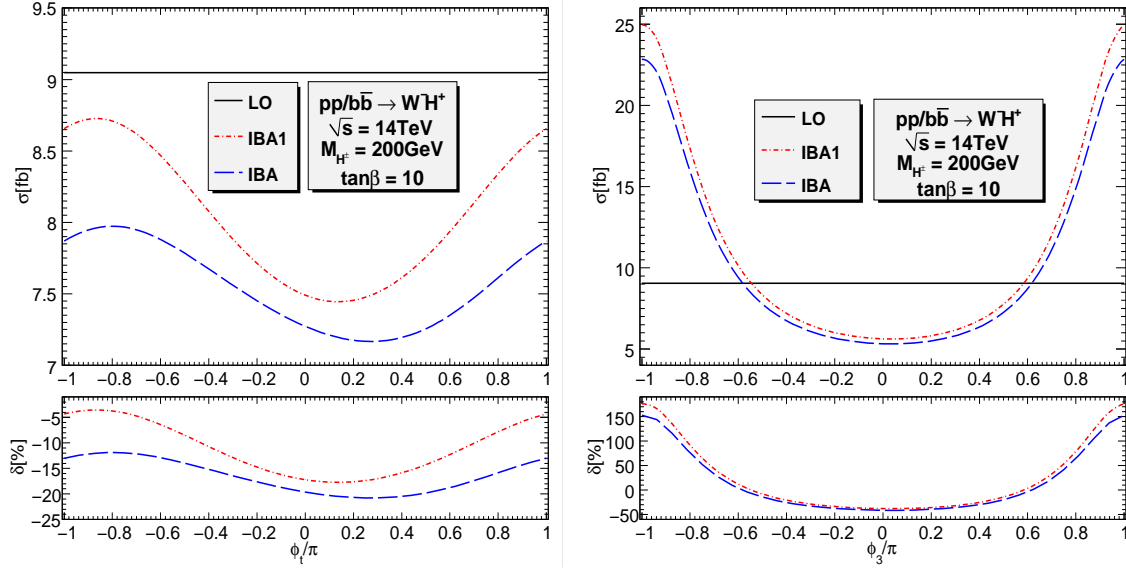
Figure 7.17: Similar to Fig. 7.16, but with ϕ_t (left) and ϕ_3 (right) varied instead.

much smaller impact, less than 10%, as expected.

7.5.2 $pp/b\bar{b} \to W^\mp H^\pm$: full NLO results

In this section, we investigate the effects of the SUSY-QCD, SM-QCD, and EW contributions at NLO. As in the previous section, we present here two sets of plots. In Fig. 7.18 we show the dependence of the total cross sections on $\tan\beta$ and $M_{H^\pm}$ at the default CPX phases, in particular $\phi_t = \phi_3 = \pi/2$. As explained above, the $\mathcal{O}(\Delta_b)$ effect is turned off in this CPX scenario. The SUSY-QCD and EW NLO terms are therefore small at large $\tan\beta$, as shown in Fig. 7.18 (left). The SM-QCD correction is about -20% for small $\tan\beta$ and changes the sign around $\tan\beta = 11$ due to the competition between the $b\bar{b}$ and the g-induced contributions. All the NLO contributions for different values of $\tan\beta$ and $M_{H^\pm}$ can be found in Table 7.1. Fig. 7.19 shows the dependence of the total cross sections on ϕ_t and ϕ_3 for $\tan\beta = 10$ and $M_{H^\pm} = 200\text{GeV}$. The EW corrections depend strongly on ϕ_t, and the SUSY-QCD corrections on ϕ_3. At $\phi_t = \phi_3 = 0, \pm\pi$ the effects are largest. The remaining EW and SUSY-QCD corrections, beyond the $\mathcal{O}(\Delta_b)$ contribution, are still rather large. In particular, there is the following term of the SUSY-QCD correction,

$$
\begin{aligned}
\tilde{\Delta}_t &= \frac{2\alpha_s}{3\pi} M_3^* \mu^* \tan\beta J(m_{\tilde{g}}^2), \\
J(m^2) &= |U_{11}^{\tilde{b}}|^2 |U_{12}^{\tilde{t}}|^2 I(m^2, m_{\tilde{t}_1}^2, m_{\tilde{b}_1}^2) + |U_{21}^{\tilde{b}}|^2 |U_{12}^{\tilde{t}}|^2 I(m^2, m_{\tilde{t}_1}^2, m_{\tilde{b}_2}^2) \\
&\quad + |U_{11}^{\tilde{b}}|^2 |U_{22}^{\tilde{t}}|^2 I(m^2, m_{\tilde{t}_2}^2, m_{\tilde{b}_1}^2) + |U_{21}^{\tilde{b}}|^2 |U_{22}^{\tilde{t}}|^2 I(m^2, m_{\tilde{t}_2}^2, m_{\tilde{b}_2}^2), \quad (7.45)
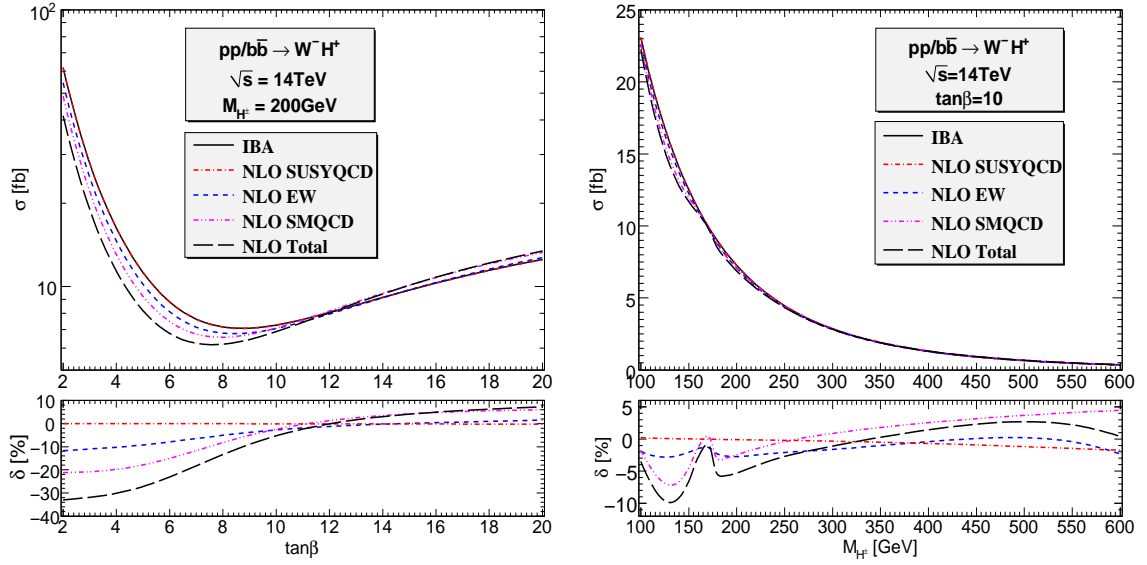\end{aligned}
$$

Figure 7.18: The cross section obtained by using IBA and including various nonuniversal NLO corrections as functions of $\tan\beta$ (left) and $M_{H^\pm}$ (right). The lower panels show the corresponding relative corrections to the IBA result.
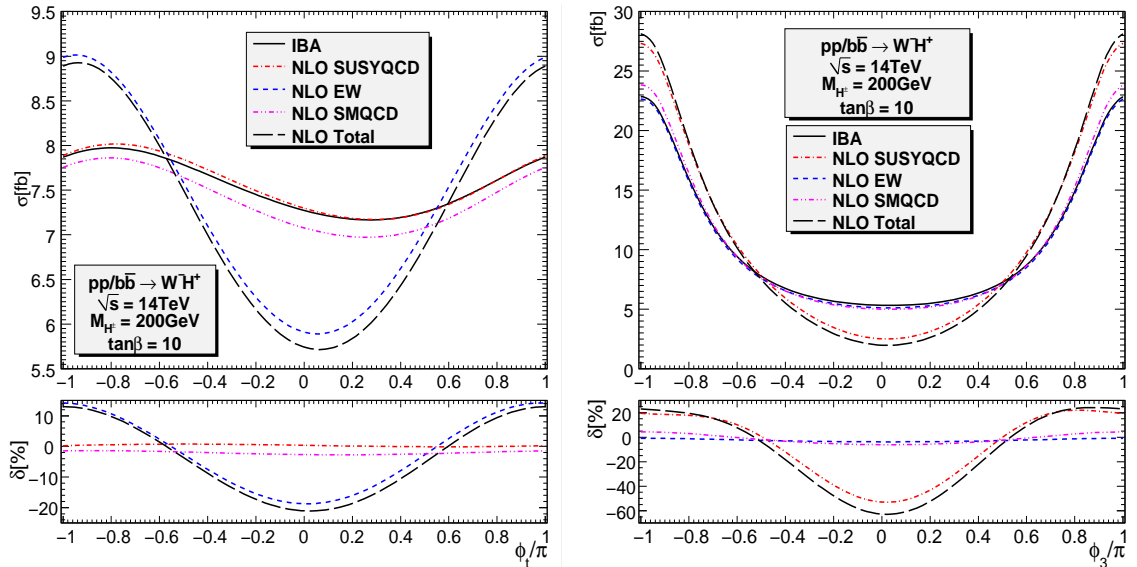

Figure 7.19: Similar to Fig. 7.18, but with ϕ_t (left) and ϕ_3 (right) varied instead.
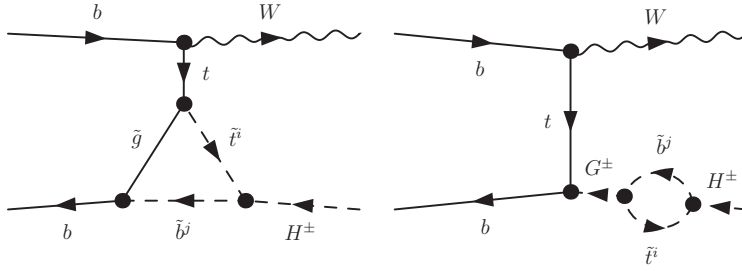
Figure 7.20: Diagrams that can introduce large SUSY-QCD (left) and EW (right) corrections. $G^{\pm}$ are the charged Goldstone bosons.

which can be included in the top-Yukawa part of charged Higgs couplings as follows

$$
\begin{aligned}
\tilde{\lambda}_{b\bar{t}H^+} &= \frac{ie}{\sqrt{2}s_W M_W}\left(\frac{m_t}{\tan\beta}(1-\tilde{\Delta}_t)P_L + m_b^{\overline{\mathrm{DR}}}\tan\beta\Delta_b^{3*}P_R\right), \\
\tilde{\lambda}_{t\bar{b}H^-} &= \frac{ie}{\sqrt{2}s_W M_W}\left(m_b^{\overline{\mathrm{DR}}}\tan\beta\Delta_b^3 P_L + \frac{m_t}{\tan\beta}(1-\tilde{\Delta}_t^*)P_R\right). \quad (7.46)
\end{aligned}
$$

This term originates from the left diagram in Fig. 7.20 and is important for small
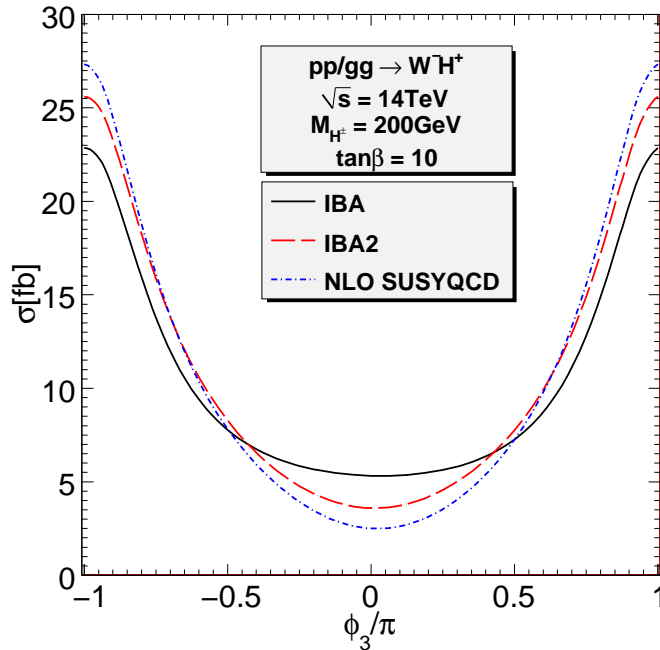
Figure 7.21: In the IBA2, we use the effective bottom–Higgs couplings defined in Eq. (7.46) and the Higgs mixing resummation.

$\tan\beta$. This finding agrees with the discussion in [147] where other subleading corrections are also discussed. If the couplings Eq. (7.46) are used we find that the new-improved LO results move significantly closer to the full NLO results, see in Fig. 7.21. The situation in the left part of Fig. 7.19 is due to the EW corrections. It indicates that there are still large corrections proportional to $A_t\mu\alpha_t/(4\pi)$ which can be associated with the right diagram in Fig. 7.20.

Figure 7.22: The cross section (left) and CP asymmetry (right) as functions of ϕ_t.

The SM-QCD corrections (and EW corrections to a lesser extend) have a striking structure for small masses $M_{H^\pm} < m_t$ (Fig. 7.18, right part). This is due to the finite contribution of the process $bg \to W^- H^+ b$. When $M_{H^\pm} < m_t$ the intermediate top quark can be on-shell and can decay to $H^+ b$. As discussed in Section 7.2.3, this OS contribution has to be properly subtracted. The structure indicates that the OS top-quark effect 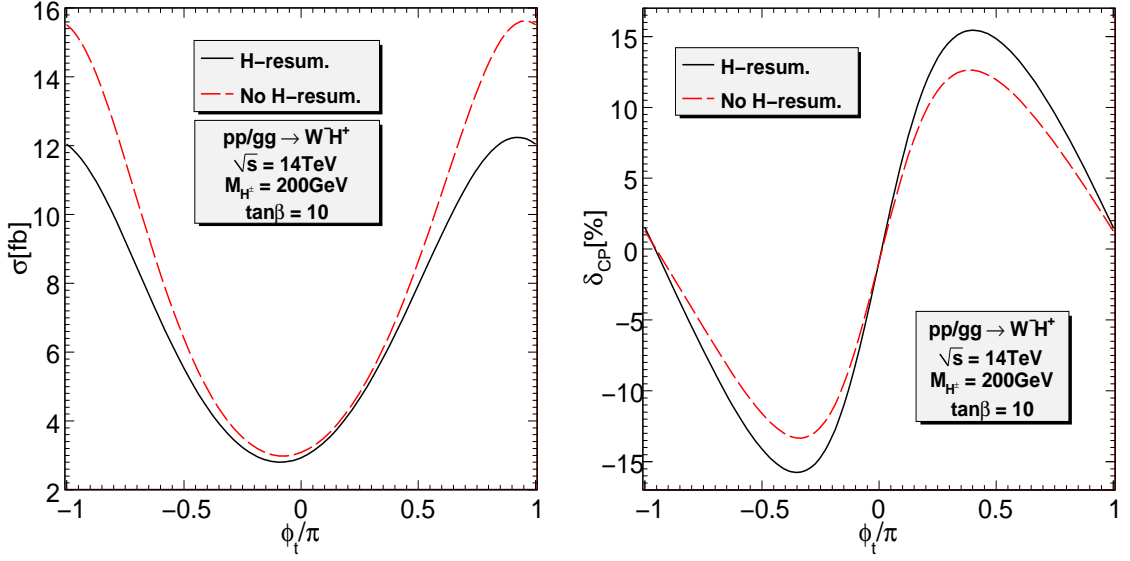cannot be completely removed and this quantum effect on the $W^- H^+$ production rate is an interesting feature, which was not discussed in previous studies [30, 31].

7.5.3 $pp/gg \to W^\mp H^\pm$: neutral Higgs-propagator effects

Even though the gg-fusion subprocess is loop induced, its contribution can be of the same order as the tree-level $b\bar{b} \to W^\mp H^\pm$ contribution. Neutral Higgs bosons are exchanged in the s-channel and can be described by using effective bottom–Higgs couplings and the full Higgs-propagator matrix. The impact of the latter on the total cross section and CP asymmetry is large as can be seen from Fig. 7.22. The cross section can be reduced by 20% at $\phi_t = \pm\pi$, while the CP asymmetry increases about 25% at $\phi_t = \pm\pi/2$. We observe also that the gg contribution is very sensitive to ϕ_t.

7.5.4 $pp \to W^\mp H^\pm$: total results at $7\,\text{TeV}$ and $14\,\text{TeV}$

The total production cross section for the $W^- H^+$ final state at the LHC is shown in Fig. 7.23 and Fig. 7.24, as well as in Table 7.1. The cross section increases by an

Table 7.1: The total cross section in fb for $pp/bb \to W^- H^+$ including the IBA and various nonuniversal NLO corrections and for $pp/gg \to W^- H^+$ at $\sqrt{s} = 14\,\text{TeV}$. The charged Higgs-boson masses are given in GeV.

| $\tan\beta$	$M_{H^\pm}$	σ_{IBA}	Δ_{EW}	Δ_{SMQCD}	Δ_{SUSYQCD}	σ_{gg}	all
5	200	11.241(1)	-1.0383(3)	-2.012(3)	-0.00821(1)	13.194(1)	21.377(3)
10	200	7.2568(9)	-0.1989(5)	-0.178(1)	-0.00721(2)	7.9428(5)	14.815(2)
20	200	12.546(2)	0.1881(6)	0.752(3)	-0.03570(6)	7.9968(6)	21.447(4)
10	150	12.497(1)	-0.2574(5)	-0.561(2)	0.00191(4)	8.7064(5)	20.387(3)
10	400	1.2907(2)	-0.00530(7)	0.0328(2)	-0.008954(7)	4.4386(3)	5.7477(4)
10	600	0.35740(5)	-0.00832(2)	0.01594(5)	-0.006263(4)	2.7481(1)	3.1069(2)

order of magnitude when the center-of-mass energy goes from $7\,\text{TeV}$ to $14\,\text{TeV}$. The gg contribution is largest for small $\tan\beta$ and large $M_{H^\pm}$ while the $b\bar{b}$ dominates when $\tan\beta > 12$ and, approximately, $M_{H^\pm} < 200\,\text{GeV}$. In the right panel of Fig. 7.23, one can see a little bump on the gg contribution around $M_{H^\pm} = 200$ GeV, attributed to the three-point Landau singularities discussed in Section 7.3. The total cross section depends strongly on the phases ϕ_t and ϕ_3 as can be seen from Fig. 7.24. The gg contribution is almost independent of ϕ_3 since the gluino does not appear at the one-loop level (the contribution through Δ_b resummation is of higher-order effect).

The CP violating asymmetry is shown in Fig. 7.25 as a function of $\tan\beta$ and $M_{H^\pm}$, and in Fig. 7.26 versus ϕ_t and ϕ_3. The uncertainty bands obtained by varying the renormalization and factorization scales (we set $\mu_R = \mu_F$ for simplicity) in the range $\mu_{F0}/2 < \mu_F < 2\mu_{F0}$ are shown only in Fig. 7.25 since the uncertainty depends strongly on $\tan\beta$ and in particular on $M_{H^\pm}$, but not on the phases. A more detailed account of the scale uncertainty of our results is given in the next section. As discussed at the end of Section 7.4, the CP violating effect is dominantly generated by the gluon-gluon fusion channel. The $b\bar{b}$ channel contributes significantly to the symmetric cross section and thus to the denominator of the CP asymmetry. It is therefore easy to understand why δ_{CP} is small for large $\tan\beta$ and small $M_{H^\pm}$, as seen in Fig. 7.25. The dependence on ϕ_3 is explained by the same reasons: the numerator is independent of ϕ_3 while the denominator including $\sigma_{b\bar{b}}$ has a minimum at $\phi_3 = 0$. The CP asymmetry is therefore maximum around $\phi_3 = 0$.

7.5.5 Scale dependence

In this section we discuss the scale dependence of the total cross sections and CP asymmetries. Since the calculation of the loop-induced subprocess $gg \to W^\mp H^\pm$ includes only the leading order contribution (with improvements on the bottom–Higgs couplings and neutral Higgs-mixing propagators), there is no cancellation of the renormalization/factorization-scale dependence in this channel. We therefore concentrate on the scale dependence of the $b\bar{b} \to W^\mp H^\pm$ cross section calculated at
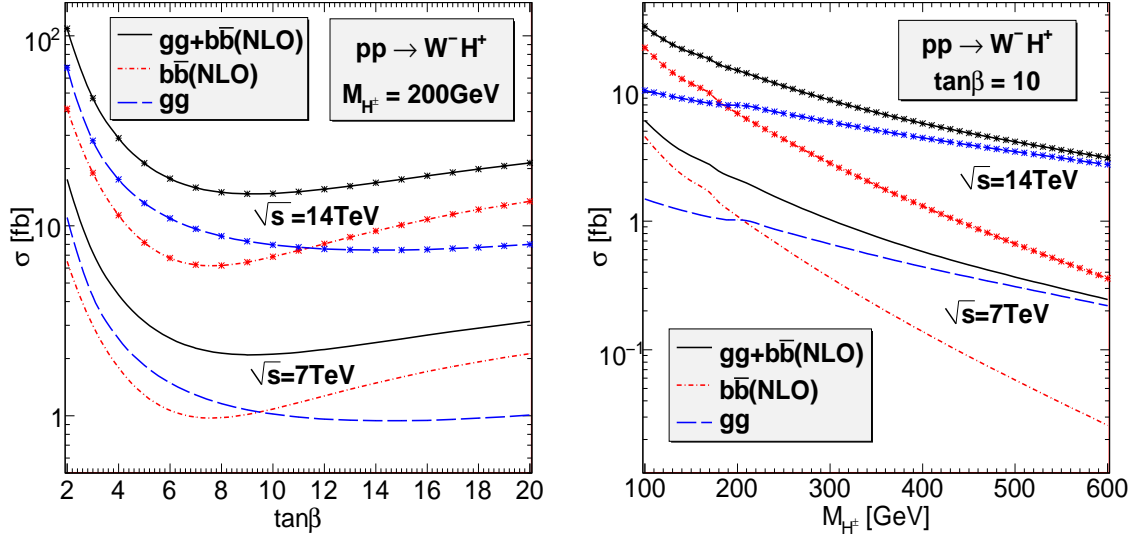
Figure 7.23: The cross section as a function of $\tan\beta$ (left) and $M_{H^\pm}$ (right).
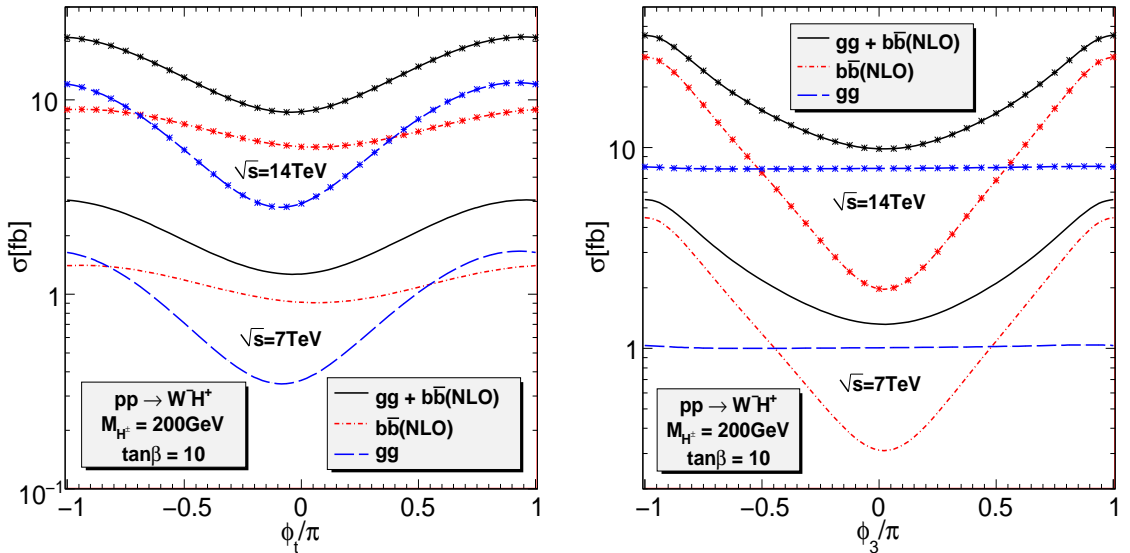
Figure 7.24: The cross section as a function of ϕ_t (left) and ϕ_3 (right).
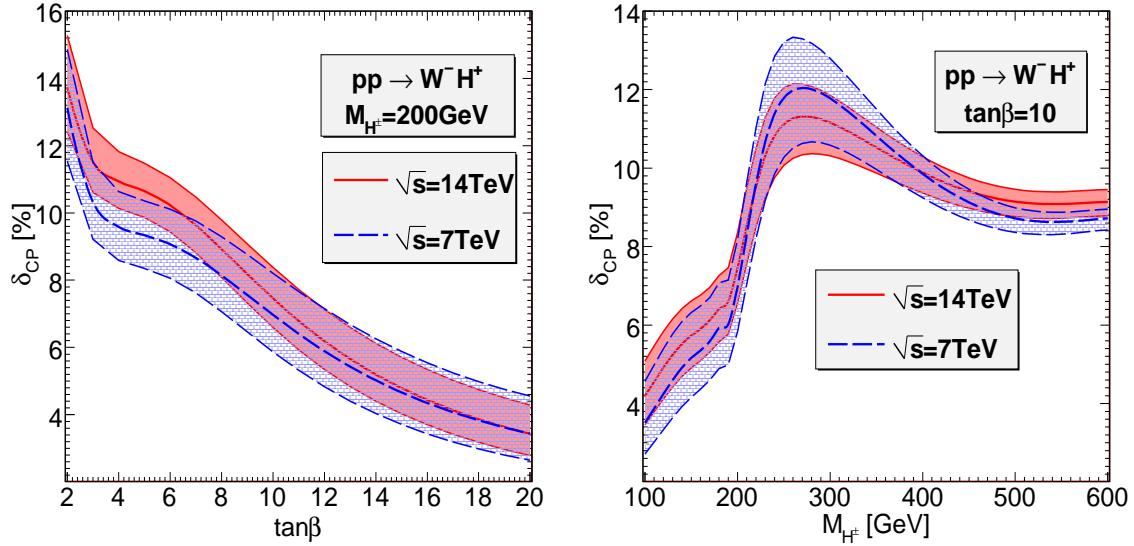
Figure 7.25: CP asymmetry as a function of $\tan\beta$ (left) and $M_{H^{\pm}}$ (right). Within the band, the scale $\mu_R = \mu_F$ is varied in the range $\mu_{F0}/2 < \mu_F < 2\mu_{F0}$.
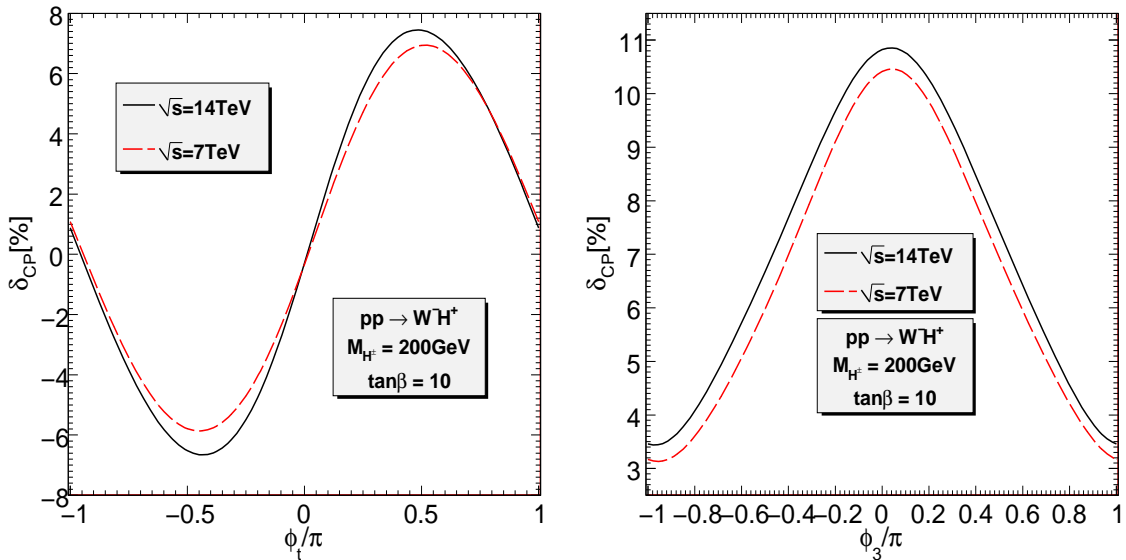

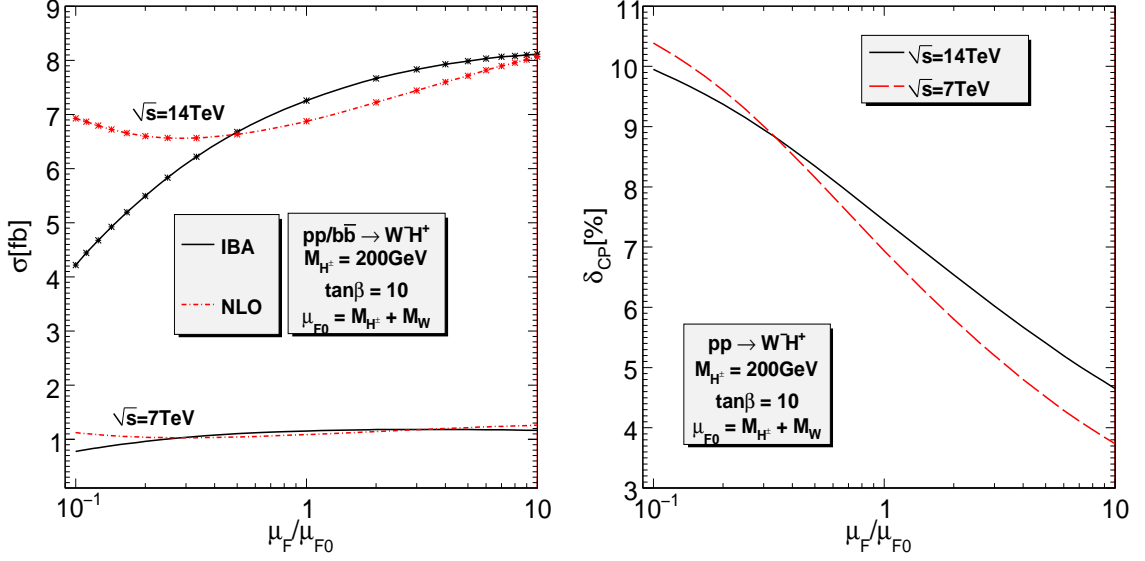Figure 7.26: CP asymmetry as a function of ϕ_t (left) and ϕ_3 (right).

Figure 7.27: The cross section (left) and CP asymmetry (right) as functions of the renormalization and factorization scales ($\mu_R = \mu_F$).

Table 7.2: Cross sections in fb for $pp/b\bar{b} \to W^- H^+$ and $pp/gg \to W^- H^+$ at different values of the factorization(renormalization) scale. The CP asymmetries in percentage are also shown.

	$\sqrt{s} = 7\,\mathrm{TeV}$				$\sqrt{s} = 14\,\mathrm{TeV}$			
$\mu_R = \mu_F$	σ_{IBA}	$\sigma_{\mathrm{NLO}}^{bb}$	σ^{gg}	δ_{CP}	σ_{IBA}	$\sigma_{\mathrm{NLO}}^{bb}$	σ^{gg}	δ_{CP}
$\mu_{F0}/2$	1.1028(2)	1.0434(3)	1.42088(9)	8.207(8)	6.6774(8)	6.633(2)	10.4606(6)	8.380(7)
μ_{F0}	1.1544(1)	1.0870(2)	1.02168(6)	6.967(8)	7.2568(9)	6.873(1)	7.9428(5)	7.457(8)
$2\mu_{F0}$	1.1790(1)	1.1445(2)	0.7631(5)	5.868(7)	7.6648(9)	7.224(1)	6.2204(4)	6.591(8)

NLO, see Fig. 7.27 (left). We set $\mu_R = \mu_F$ for simplicity. The remaining uncertainty of the NLO scale dependence is approximately 9% (9%) when μ_F is varied between $\mu_{F0}/2$ and $2\mu_{F0}$, compared to approximately 14% (7%) for the IBA, at 14 TeV (7 TeV) center-of-mass energy. The uncertainty is defined as $\delta = [|\sigma(\mu_{F0}/2) - \sigma(\mu_{F0})| + |\sigma(2\mu_{F0}) - \sigma(\mu_{F0})|]/\sigma(\mu_{F0})$. The IBA scale dependence looks quite small because we have set both renormalization and factorization scales equal, leading to an "accidental" cancellation. The IBA cross section increases as μ_F increases while it decreases as μ_R increases. We recall that μ_F enters via the bottom-distribution functions and μ_R appears in the running b-quark mass. That accidental cancellation depends strongly on the value of $\tan \beta$. We have verified, by studying separately the renormalization and factorization scale dependence, that including NLO corrections does reduce significantly each scale dependence.

Concerning the CP asymmetries, the scale dependence is shown in Fig. 7.27 (right). We again set here $\mu_R = \mu_F$. If μ_F is varied between $\mu_{F0}/2$ and $2\mu_{F0}$, the uncertainty is approximately 24% (34%) for 14 TeV (7 TeV) center-of-mass en-

ergy. This uncertainty is so large because the dominant contribution to the CP asymmetries (the subprocess $gg \to W^{\mp}H^{\pm}$) is calculated only at LO.

In Table 7.2 we show the values of the cross sections for the two subprocesses as well as the CP asymmetries. The scale-dependence uncertainty of the $gg \to W^{\mp}H^{\pm}$ process is indeed very large. It is mainly due to the running strong coupling $\alpha_s(\mu_R)$ which depends logarithmically on the renormalization scale.

Chapter 8

Electroweak corrections to $gg \rightarrow H^-t\bar{b}$ at the LHC

8.1 Introduction

In this chapter we investigate charged Higgs boson production in association with a bottom quark and a top quark at the LHC. The dominant mechanism is $gg \rightarrow H^\mp tb$. The cross section for $gg \rightarrow H^\mp tb$ contains large logarithms, $\sim \ln \mu_F / m_b$, where μ_F is of the order of the charged Higgs mass. They arise from the splitting of a gluon into a collinear $b\bar{b}$ pair. These large logarithms can be factorized and resummed to all orders in perturbation theory. In doing so one introduces the (anti)bottom-quark densities and defines a five-flavour scheme. For an inclusive observable, this channel should be consistently combined with the channel $gb \rightarrow tH^-$.

In our calculation, we assume the bottom quark to be tagged and hence consider exclusive observables. The large logarithms are avoided by applying the following cuts

$$p_{T,b} > 20 \, \text{GeV}, \quad |\eta_b| < 2.5, \tag{8.1}$$

where $p_{T,b}$ is the transverse momentum and η_b is then pseudo rapidity of the bottom quark. The cross section after cuts is still considerable. This makes it a potential channel for the searches of charged Higgs bosons.

This channel has been studied at the LHC (for a review see [62]). The study in [177] showed a possibility of observing the charged Higgs boson via this channel with four b-tags at the LHC. The conclusion was based on the comparison of the signal arising from $gg \rightarrow H^-t\bar{b}$ and the main background from $gg \rightarrow t\bar{t}b\bar{b}$ provided that a good b-tagging efficiency $\sim 50\%$ is achieved. The QCD corrections to the exclusive $pp \rightarrow H^-t\bar{b}$ were calculated in [35]. Recently, Ref. [36] has studied the QCD corrections to inclusive and exclusive $pp \rightarrow H^-t\bar{b}$ [1]. They have done the first

---

[1]For the inclusive cross sections, the NLO QCD corrections are in the range $[-2, 7]\%$ compared to the LO cross sections, which were computed with LO PDFs and the effective bottom–Higgs

comparison of the $H^\pm$ production with heavy quarks in the four-flavor and five-flavor schemes.

In our study, the EW corrections to the $gg \to H^- t\bar{b}$ process are calculated in the complex MSSM. In the real MSSM, the corrections are equal for both $gg \to H^- t\bar{b}$ and $gg \to H^+ \bar{t}b$. However, in the cMSSM they can be different. The differences give rise to a CP violating asymmetry. This is the subject of our future studies. Similar to the process $pp \to W^\mp H^\pm$, the EW corrections may have a large impact on the total cross section. The NLO EW contributions are rather involved. On the technical side, this calculation is challenging since it contains a large number of one-loop diagrams involving two-, three-, four- and five-point loop integrals. The results presented in this chapter will be published in [178].

8.2   The leading order cross section

At tree level, the gg contributions of order $\mathcal{O}(\alpha_s^2 \alpha)$ are dominant. Other contributions of the same order arising from quark-antiquark annihilations are much smaller, since they involve only the s channel diagrams which are suppressed at high energy. The quark-antiquark annihilations give also $\mathcal{O}(\alpha^3)$ contributions coming from tree-level EW Feynman diagrams. A striking feature of the $\mathcal{O}(\alpha^3)$ contributions is that they have a charged Higgs resonance,*i.e.* when $M_{H^\pm}$ is larger than the sum of top and bottom masses, the charged Higgs bosons can be on-shell and decay into top and bottom quarks. It requires a consistent treatment in order to obtain the gauge invariant results. This problem becomes more difficult at NLO and is not discussed in this thesis.

The three classes of subprocesses contributing are

$$g + g \to H^- + t + \bar{b}, \tag{8.2}$$
$$q + \bar{q} \to H^- + t + \bar{b}, \tag{8.3}$$
$$b + \bar{b} \to H^- + t + \bar{b}, \tag{8.4}$$

where q denotes the light quarks, $q = u, c, d, s$. The first two channels have been calculated in [179, 180, 177, 35, 36]. The corresponding Feynman diagrams of those subprocesses are shown in Fig. 8.1.

There exists contributions of order $\mathcal{O}(\alpha_s \alpha^2)$ arising from the $g\gamma$ induced process,

$$g + \gamma \to H^- + t + \bar{b}, , \tag{8.5}$$

whose Feynman diagrams are depicted in Fig. 8.2.

couplings, for $M_{H^\pm}$ from 200 to 500 GeV in the SPS 1b benchmark scenario characterized by large $\tan\beta$ $(= 30)$. For the exclusive ones with $p_{T,b} > 20$ GeV, the NLO QCD corrections are negative and larger than -20% in the same charged Higgs mass range. Ref. [36] claimed that their results disagree with the ones in [35]. The exclusive cross sections of the former are two to three times larger than that of the later.

(a)

(b)

(c)
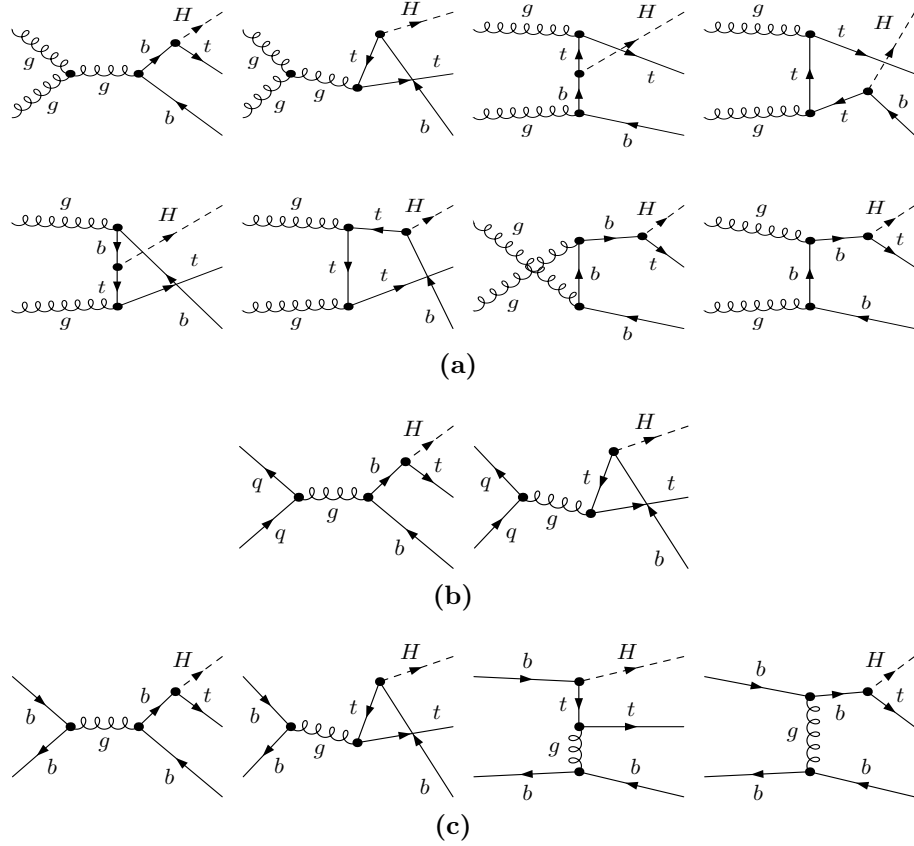
Figure 8.1: The QCD tree-level diagrams: (a) for $gg \to H^- t\bar{b}$ subprocess, (b) for $q\bar{q} \to H^- t\bar{b}$ subprocesses ($q = u, c, d, s$) and (c) for $b\bar{b} \to H^- t\bar{b}$ subprocess.

The hadronic LO cross section is given by convolution of the partonic cross sections with the corresponding parton luminosity, see Eq. (7.2),

$$
\sigma_{\mathrm{LO}}^{pp} = \sum_{ij=gg,q\bar{q},b\bar{b}} \int_0^1 \mathrm{d}\tau \frac{d\mathcal{L}_{ij}^{pp}}{d\tau} \hat{\sigma}_{\mathrm{LO}}^{ij \to H^- t\bar{b}}(\hat{s}, \alpha_s^2 \alpha, \mu_R)
$$
$$
+ \int_0^1 \mathrm{d}\tau \frac{d\mathcal{L}_{g\gamma}^{pp}}{d\tau} \hat{\sigma}_{\mathrm{LO}}^{g\gamma \to H^- t\bar{b}}(\hat{s}, \alpha_s \alpha^2, \mu_R), \tag{8.6}
$$

where s and $\hat{s} = \tau s$ are the squared CM energies of the hadronic and partonic processes, respectively.

The LO amplitudes involve the Yukawa couplings of the charged Higgs bosons to the top and bottom quarks which can be modified to include the large universal SM-QCD, SUSY-QCD and SUSY-EW corrections as discussed in Section 5.4. To quantify the Δm_b effect we define the improved Born approximation (IBA) where the effective bottom–Higgs couplings in Eq. (5.39) are used. The LO cross section is computed with the tree-level bottom–Higgs couplings in Eq. (5.29) with $m_b = m_b^{\overline{\mathrm{DR}}}(\mu_R)$.

Figure 8.2: The tree-level diagrams for $g\gamma \to H^- t\bar{b}$ subprocess. For the diagrams marked with the star, the diagrams with an exchange of the incoming gluon and photon also contribute.
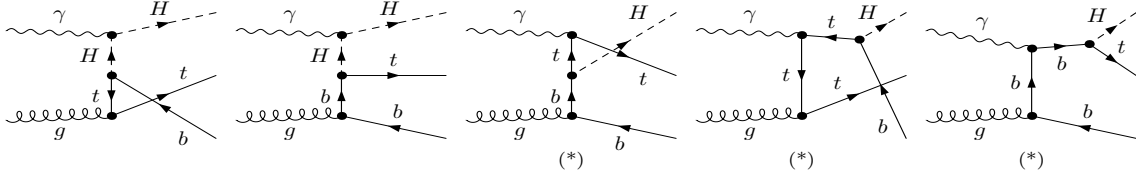
8.3 The NLO electroweak contributions to $gg \to H^- t\bar{b}$

In this section we discuss the NLO EW corrections to the $gg \to H^- t\bar{b}$ subprocess. These corrections are of order $\mathcal{O}(\alpha_s^2 \alpha^2)$. Other contributions of the same order arising from the remaining subprocesses in Eq. (8.3), Eq. (8.4) and Eq. (8.5) are much smaller and will not be discussed here.

The NLO EW contributions are composed of a virtual part and a real part. The virtual part contains UV divergences, soft and collinear singularities. In order to cancel the UV divergence, a renormalization scheme is needed. We follow the renormalization procedure described in Subsection 7.2.5 for the process $pp \to W^\mp H^\pm$.

The virtual part comprises contributions of bottom- and top-quark self-energies, of $H^- t\bar{b}$ and $gq\bar{q}$ vertices, of box and pentagon diagrams. The generic classes of self-energy and vertex diagrams which include the corresponding counterterms are shown in Fig. 8.3. The box and pentagon diagrams which give UV-finite contributions are depicted in Fig. 8.4 and Fig. 8.5, respectively.

The real EW corrections arise from the photonic bremsstrahlung process,

$$g + g \to H^- + t + \bar{b} + \gamma, \tag{8.7}$$

whose diagrams are shown in Fig. 8.6. This contribution is divergent in both soft region ($p_\gamma^0 \to 0$) and quasi-collinear region ($p_b p_\gamma \to \mathcal{O}(m_b^2)$). Mass regularization is used to separate the divergent terms. In particular, the photon mass (λ_γ) is used for the soft singularities while the bottom mass is used for the collinear singularities. The soft singularities cancel against the one in the virtual contribution. If no cut is applied on the bottom quark, the quasi-collinear singularities cancel also in the sum of the virtual and the real contributions. However we required the bottom quark to be tagged, the quasi-collinear singularities cancel incompletely. We do not need to worry about the leftover quasi-collinear singularities since in this case bottom quark is considered to be massive.

Similar to the $pp \to W^\mp H^\pm$ calculation, the real corrections are computed by using both the dipole subtraction method and phase-space slicing method. The results are in good agreement as illustrated in Fig. 8.7. Although this statement is not new, it provides a good check on our computational codes. In the numerical
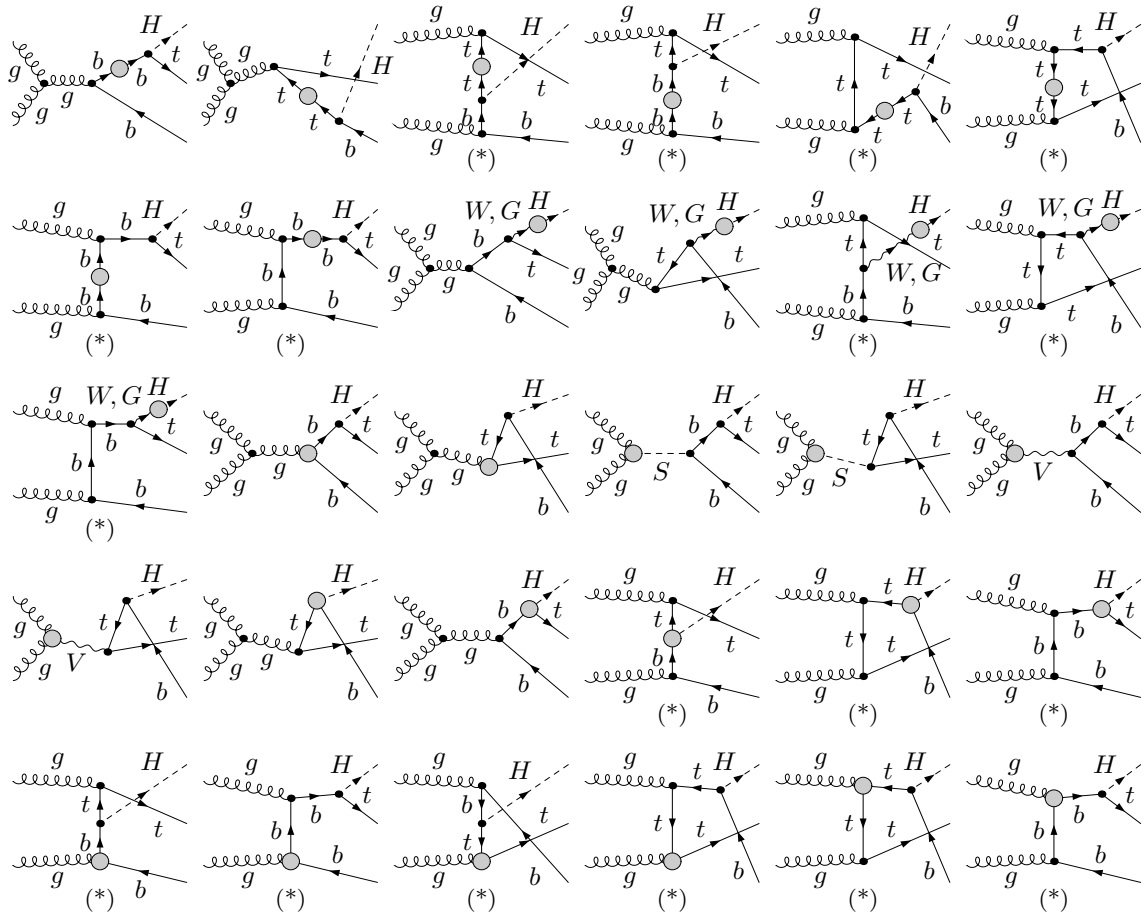
Figure 8.3: The one-loop self-energy and vertex diagrams for the electroweak virtual corrections to the $gg \to H^- t\bar{b}$ subprocess. The shaded regions are the one-particle irreducible vertices. For the diagrams marked with the star, the diagrams with an exchange of the two incoming gluons also contribute. $S = h, H, A$ and $V = \gamma, Z$.
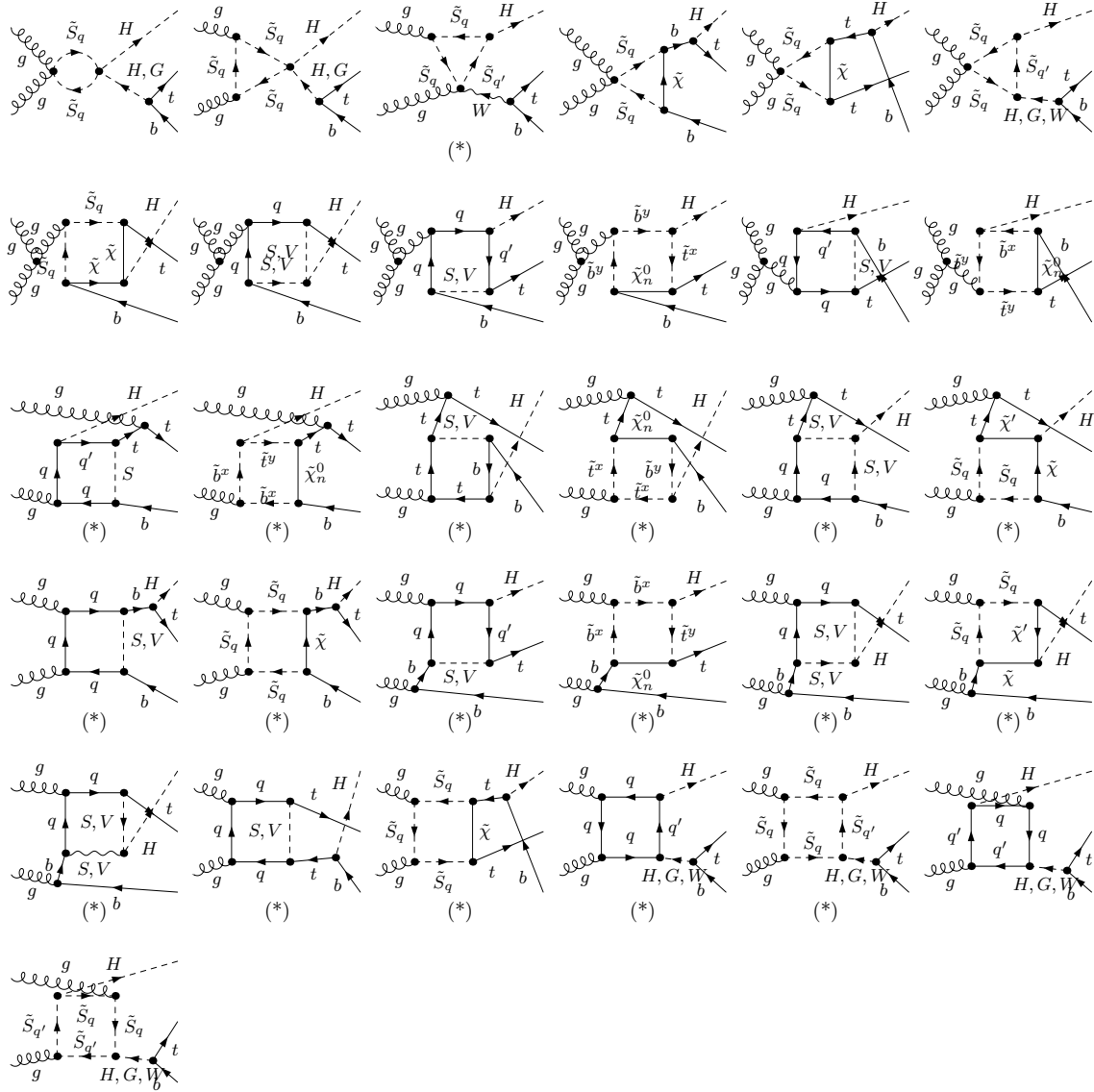
Figure 8.4: Diagrams with irreducible four-point vertices for the electroweak virtual corrections to $gg \to H^- t\bar{b}$ subprocess. S denotes $h, H, A, G^0, H^\pm, G^\pm$, $\tilde{S}_q$ denotes top and bottom squarks and V denotes electroweak gauge boson γ, Z, W.
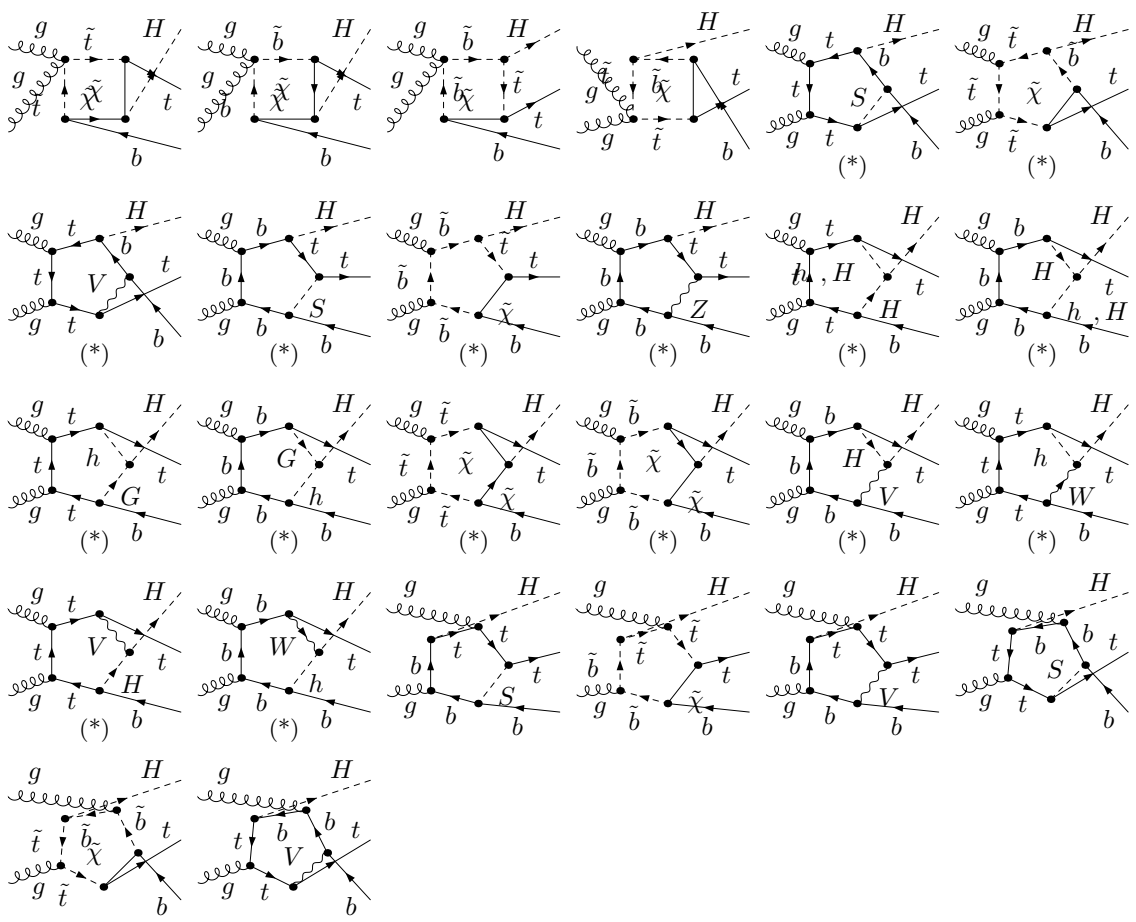
Figure 8.5: Diagrams with irreducible five-point vertices for the electroweak virtual corrections to $gg \to H^- t\bar{b}$ subprocess. $S = h, H, A, G^0$ and $V = \gamma, Z$.
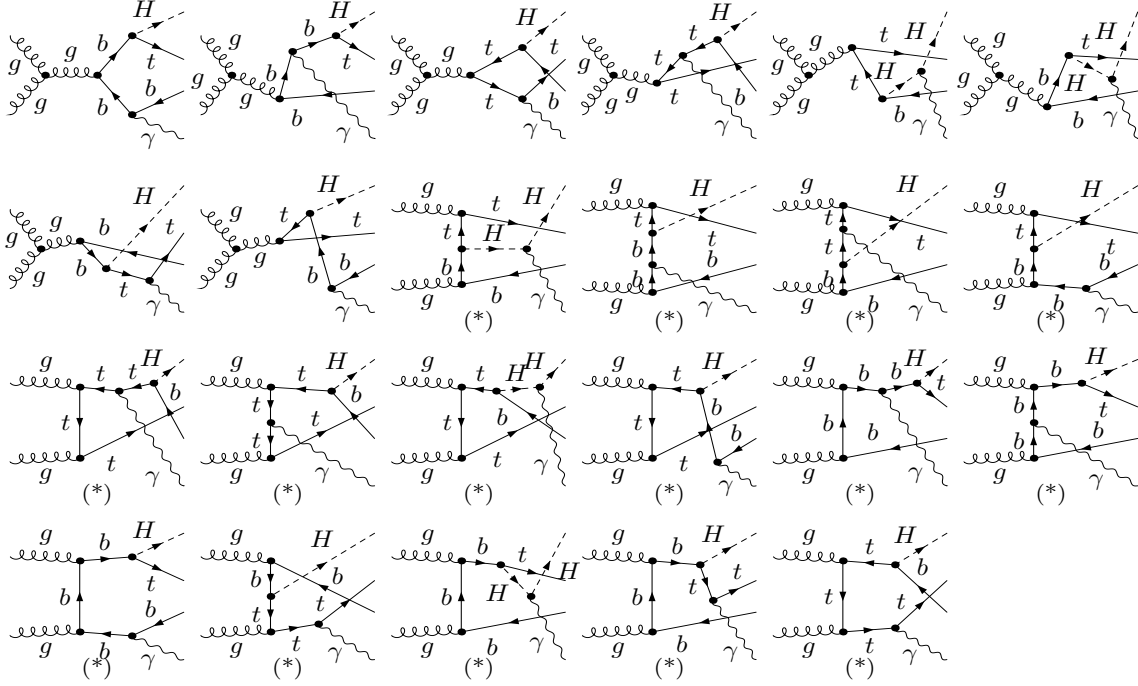
Figure 8.6: Diagrams for real photon emission.

study, we will present the results of the dipole subtraction method because the integration errors are smaller.

We conclude this section by summarizing the structure of the full NLO EW hadronic cross section,

$$\sigma_{\text{NLO,EW}}^{pp} = \sigma_{\text{IBA}}^{pp} + \Delta_{EW}^{pp/gg}, \tag{8.8}$$

where

$$\Delta_{EW}^{pp/gg} = \int_0^1 d\tau \frac{d\mathcal{L}_{gg}^{pp}}{d\tau} \left[\hat{\sigma}_{\text{NLO,virt}}^{gg \to H^- t\bar{b}}(\hat{s}, \alpha_s^2 \alpha^2, \mu_R) + \hat{\sigma}_{\text{NLO,real}}^{gg \to H^- t\bar{b}\gamma}(\hat{s}, \alpha_s^2 \alpha^2, \mu_R) \right]. \tag{8.9}$$

8.4 Numerical studies

Similar to the process $pp \to W^\mp H^\pm$, we present the numerical results in this section for the CPX scenario. The renormalization scale and the factorization scale are chosen as $\mu_R = \mu_F = (m_t + M_{H^\pm})/3$. We use also the MRST2004qed set of PDFs [130]. For the other input parameters we refer to Section 7.5.

Our study is done for the LHC at $7\,\text{TeV}$ and $14\,\text{TeV}$ center-of-mass energy. As for the case of $pp \to W^\mp H^\pm$ we find similar effects for both energies. We therefore focus on the case of $14\,\text{GeV}$ since the cross section is about an order of magnitude larger. Important results will be shown for both energies.
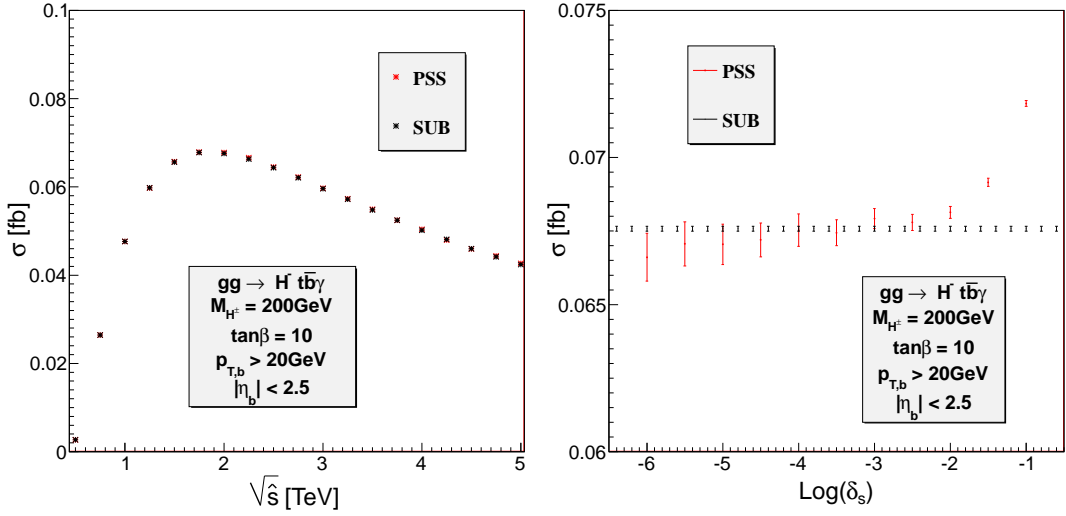
Figure 8.7: Partonic cross sections as functions of CM energy $\sqrt{\hat{s}}$ in the left panel and of cutoff parameter δ_s in the right panel are presented for the $gg \rightarrow H^- t\bar{b}\gamma$ process. The results are obtained by using the phase space slicing method (red stars) and the dipole subtraction method (black stars) in the CPX scenario with $M_{H^\pm} = 200$ GeV and $\tan\beta = 10$. The photon mass regulator is set to be unit so that all terms proportional to $\ln\lambda_\gamma$ vanish.

8.4.1 Checks on the results

The amplitudes are generated by using `FeynArts-3.6` [105] and further simplified with the support of `FormCalc-6.1` [96]. The loop integrals contain five-point tensor integrals up to rank three, four-point tensor integrals up to rank three. The pentagon integrals are reduced to the box integrals by using the reduction method in [181]. The two-, three- and four-point tensor integrals are further reduced into the scalar integrals by using Passarino-Veltman reduction method [85]. The loop integrals are evaluated with two independent libraries, `LoopTools/FF` [182, 162] and `LoopInts` [183]. The latter uses the method of [184] and has an option to use quadruple precision when numerical instabilities are detected. A good agreement has been found. The phase-space integration is done by using the Monte Carlo integrator `BASES` [185] and `VEGAS` [186].

Both the virtual and real contributions have been computed by two independent codes. We have obtained full agreement. Moreover in the sum, both UV and IR finiteness are verified. Using the method of the QCD gauge invariant check described in Subsection 7.3.2, we have confirmed that the $gg \rightarrow H^- t\bar{b}$ amplitudes are gauge invariant at LO, IBA and NLO.

Figure 8.8: The LO and IBA cross sections for $pp \to H^- t\bar{b}$ as functions of $\tan\beta$ in the left panel and of ϕ_t in the right panel. The lower parts of the figures show the relative corrections.

8.4.2   Hadronic cross sections

We first study the effects of Δm_b resummation. In Fig. 8.8, we show the LO and IBA cross sections defined in Section 8.2 as functions of $\tan\beta$ in the left panel and of ϕ_t in the right panel. We define the relative corrections as $\delta = (\sigma_{\text{IBA}} - \sigma_{\text{LO}})/\sigma_{\text{LO}}$. As expected, the dependences on $\tan\beta$ and ϕ_t are determined by the $H^- t\bar{b}$ coupling in a similar way to the $b\bar{b} \to W^\mp H^\pm$ process described in Subsection 7.5.1.

Table 8.1 shows the separated IBA contributions of the three subprocesses and the NLO EW corrections to $gg \to H^- t\bar{b}$ at $\sqrt{s} = 14$ TeV for different values of $M_{H^\pm}$ and $\tan\beta$. Similar results are presented in Table 8.2 but for $\sqrt{s} = 7$ TeV. We see that the contributions of the gg fusion are dominant. They contribute more than 90% (83%) of the total IBA for $\sqrt{s} = 14$ TeV ($\sqrt{s} = 7$ TeV). The contribution of the $b\bar{b}$ is less than 1%. The contribution of the $g\gamma$ is a bit larger than that of the $b\bar{b}$. The NLO EW contributions are comparable to the $q\bar{q}$ contributions but with the opposite sign.

In Fig. 8.9 we show the dependence of the IBA and NLO EW cross sections on $\tan\beta$, $M_{H^\pm}$ and ϕ_t at $\sqrt{s} = 14$ TeV. The lower parts of the figures show the relative corrections which are defined as $\delta = (\sigma_{\text{NLO}} - \sigma_{\text{IBA}})/\sigma_{\text{IBA}}$. After subtracting the Δm_b corrections, the magnitude of the remaining EW contributions are still large. The relative corrections increase with $\tan\beta$ and $M_{H^\pm}$ for the default value $\phi_t = \pi/2$. Similar to the $b\bar{b} \to W^\mp H^\pm$, the NLO EW corrections depend strongly on ϕ_t. The cross section can be reduced by 25% at $\phi_t = 0$. Similar behavior of the relative corrections for $\sqrt{s} = 7$ TeV can be seen in Fig. 8.10.

Table 8.1: The total cross section in fb for $pp \to H^- t\bar{b}$ including the IBA of the four subprocesses and EW NLO corrections to $gg \to H^- t\bar{b}$ at $\sqrt{s} = 14\,\text{TeV}$. The charged Higgs-boson masses are given in GeV. The numbers in brackets show the integration uncertainty in the last digit if they are significant.

$\tan\beta$	$M_{H^\pm}$	$\sigma_{\text{IBA}}^{pp/gg}$	$\sigma_{\text{IBA}}^{pp/q\bar{q}}$	$\sigma_{\text{IBA}}^{pp/bb}$	$\sigma_{\text{IBA}}^{pp/g\gamma}$	$\Delta_{\text{EW}}^{pp/gg}$	all
5	200	38.833(7)	3.5810	0.3192	0.5587	-1.54(1)	41.75(2)
10	200	25.447(5)	2.3719	0.21044	0.3671	-2.64(1)	25.75(1)
20	200	43.992(8)	3.9727	0.3573	0.6297	-10.19(4)	38.76(4)
10	300	10.740(2)	0.45682	0.07538	0.13852	-1.19(2)	10.22(2)
10	400	5.207(1)	0.14292	0.03105	0.06405	-0.618(6)	4.827(6)
10	600	1.4829(3)	0.024444	0.006866	0.018339	-0.198(1)	1.334(1)

Table 8.2: Similar to Table 8.1 but for $\sqrt{s} = 7\,\text{TeV}$.

$\tan\beta$	$M_{H^\pm}$	$\sigma_{\text{IBA}}^{pp/gg}$	$\sigma_{\text{IBA}}^{pp/q\bar{q}}$	$\sigma_{\text{IBA}}^{pp/bb}$	$\sigma_{\text{IBA}}^{pp/g\gamma}$	$\Delta_{\text{EW}}^{pp/gg}$	all
5	200	5.3652(9)	0.9885	0.03113	0.10578	-0.206(3)	6.284(3)
10	200	3.5138(6)	0.6551	0.020530	0.06948	-0.354(2)	3.905(2)
20	200	6.085(1)	1.0953	0.03483	0.11925	-1.369(6)	5.965(6)
10	300	1.2570(2)	0.09739	0.005772	0.22350	-0.141(4)	1.241(4)
10	400	0.5164(1)	0.024191	0.0019014	0.008903	-0.0597(8)	0.4917(9)
10	600	0.10583(2)	0.0026766	0.0002700	0.0019113	-0.01379(6)	0.09681(7)

8.4.3 Differential distributions

In this section we consider the differential distributions for IBA and NLO EW corrections with respect to three kinematical variables: transverse momentum, rapidity and invariant mass. The results are obtained with $M_{H^\pm} = 200\,\text{GeV}$, $\tan\beta = 10$ and $\sqrt{s} = 14\,\text{TeV}$.

The transverse momentum and pseudo rapidity distributions of the charged Higgs boson are shown in Fig. 8.11. The EW corrections do not change the shapes of those distributions but reduce the number of the produced charged Higgs bosons. The magnitude of the relative corrections increase with $p_T(H^-)$ and has a maximum (about 10%) at the central pseudo rapidity.

In Fig. 8.12 we depict the distributions of the top quark. The behavior of the p_T-distributions is similar to the one of the charged Higgs boson. For the pseudo rapidity distribution, the relative corrections are rather flat (about -10%) in the region $|\eta_t| < 3$.

The distributions of the bottom quark depicted in Fig. 8.13 are quite different from the ones of the heavy particles. At the very low and the very high p_T, the magnitude of the relative corrections are larger than the ones at the moderate p_T. For the pseudo distribution, the EW corrections reduced more the produced bottom
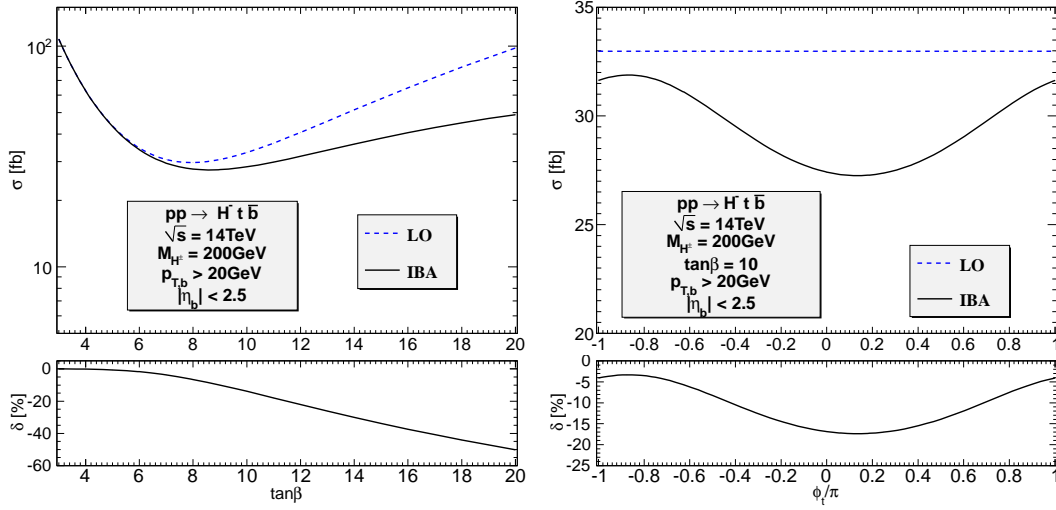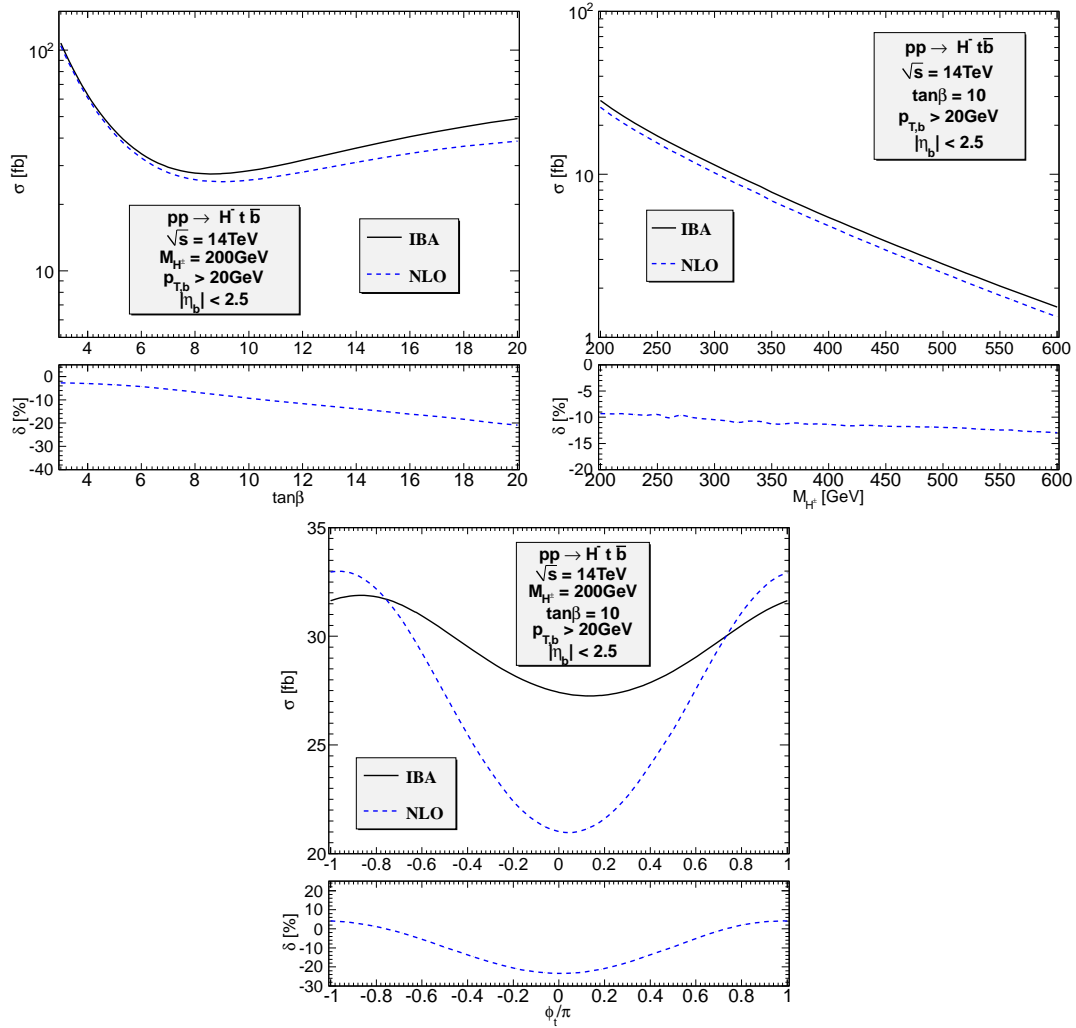
Figure 8.9: The IBA and NLO EW cross sections for $pp \to H^- t\bar{b}$ as functions of $\tan\beta$ in the left panel, of $M_{H^\pm}$ in the right panel and of ϕ_t in the lower panel for $\sqrt{s} = 14\,\text{TeV}$.

quarks at the two edges than at the centre.

Fig. 8.14 shows the invariant mass and p_T distributions of the $t\bar{b}$ system. The magnitude of the relative corrections increase with both invariant mass and p_T.
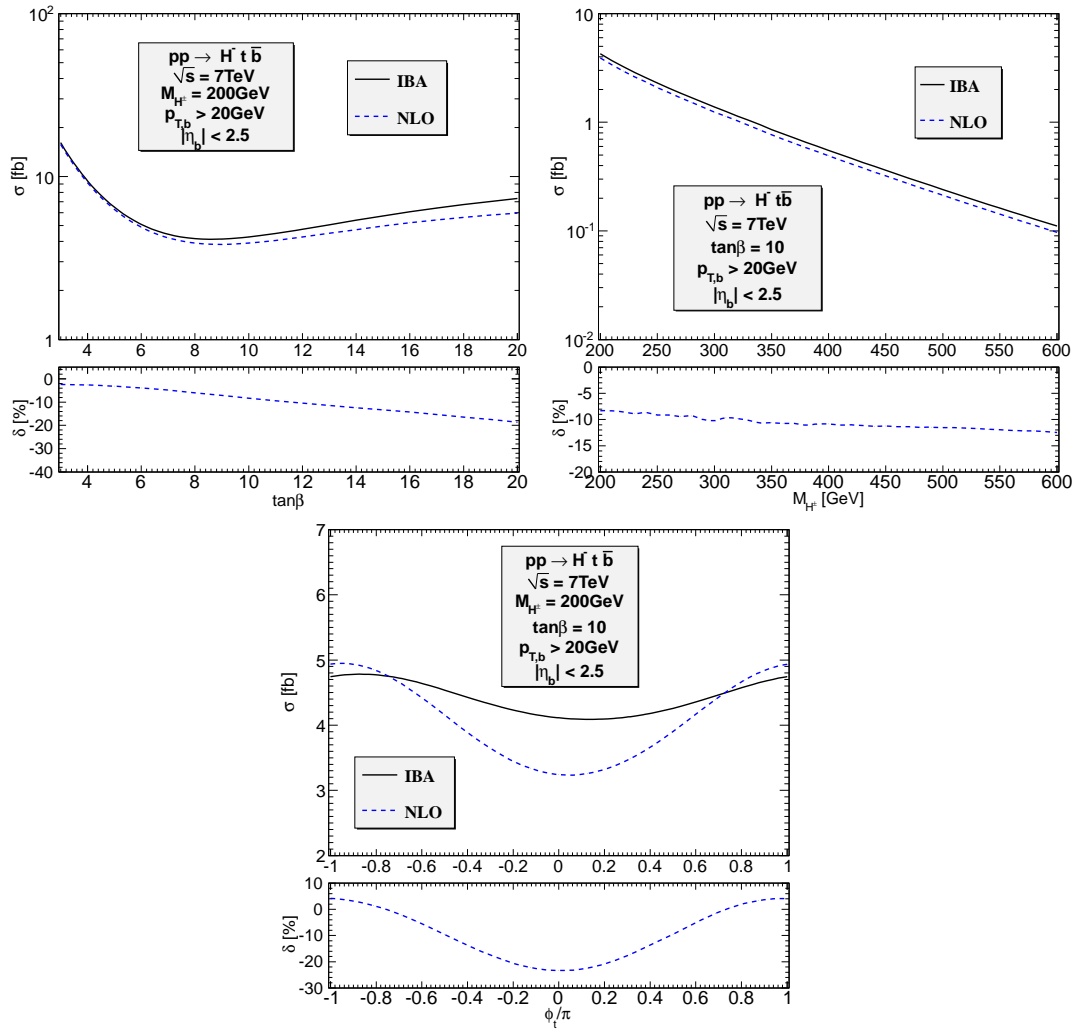
Figure 8.10: Similar to Fig. 8.9 but for $\sqrt{s} = 7\,\mathrm{TeV}$.
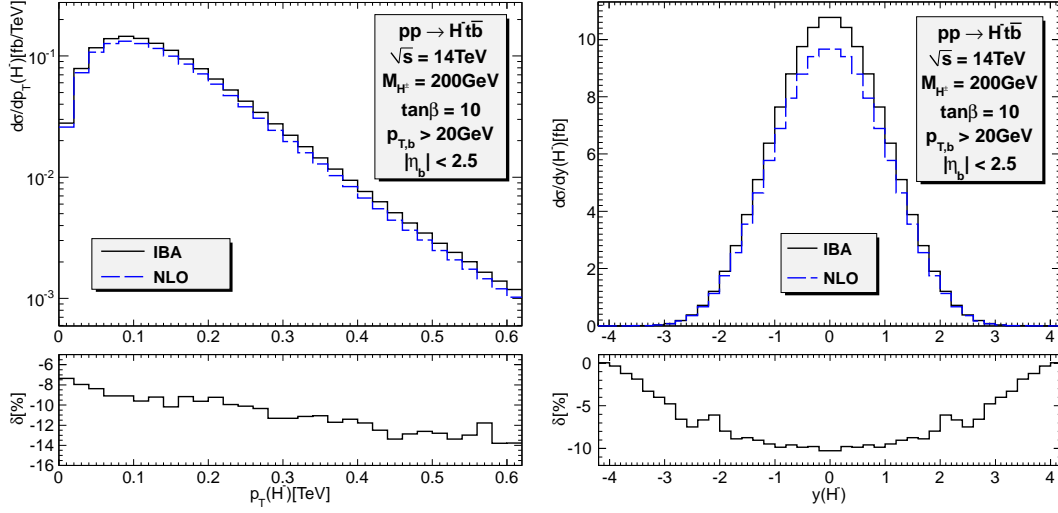
Figure 8.11: The IBA and NLO EW transverse momentum (left) and pseudo (right) distributions of the charged Higgs bosons. The lower panels show the relative corrections.
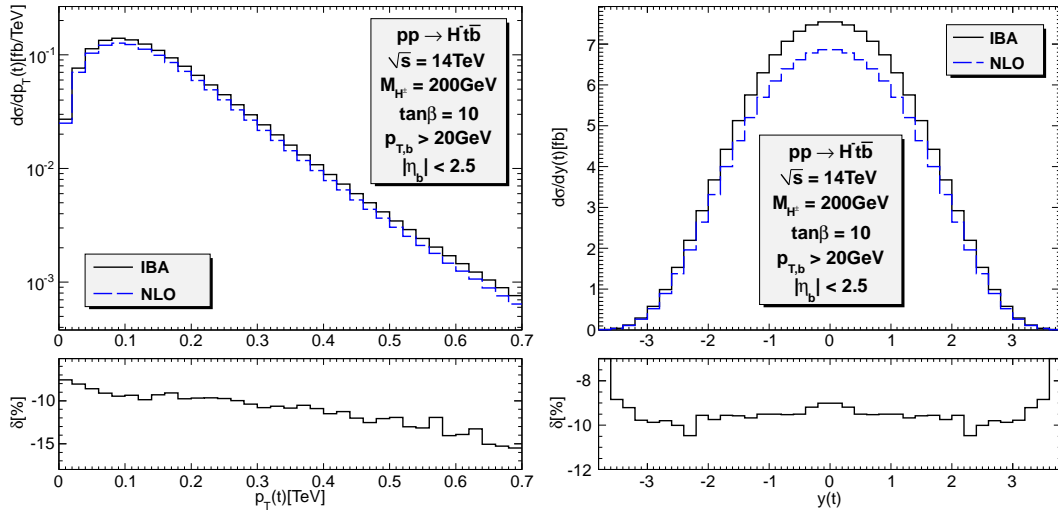
Figure 8.12: Similar to Fig. 8.11 but for the top quark p_T and pseudo rapidity distributions
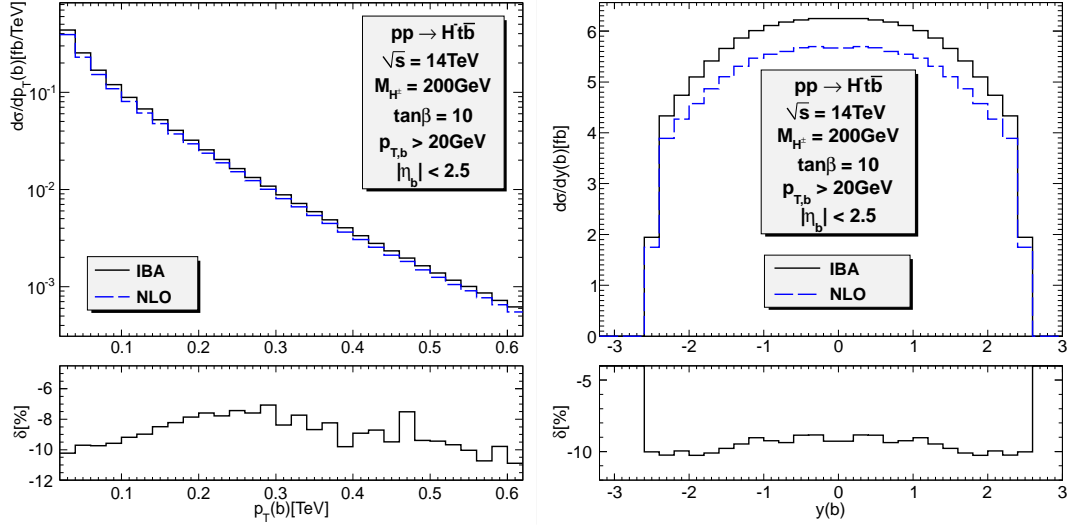
Figure 8.13: Similar to Fig. 8.11 but for the bottom quark p_T and pseudo rapidity distributions.
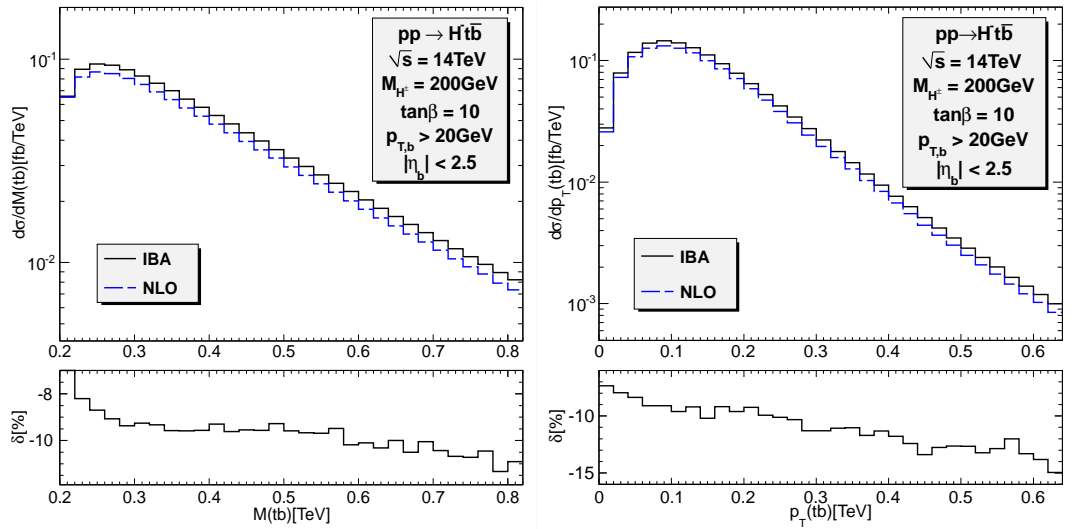
Figure 8.14: Invariant mass (left) and transverse momentum (right) distributions of the $t\bar{b}$ system.

Chapter 9

Conclusions

In this thesis, we have considered charged Higgs boson decay and production processes at the LHC in the context of the complex MSSM. Those processes play an important role for the searches of charged Higgs bosons. The decay widths and production rates were computed at one-loop level where many techniques are involved. In the first part of the thesis a review of the SM and the MSSM was presented and one-loop computational techniques were discussed. In the second part, we presented the detailed calculations for various processes and discussed numerical results.

We first computed the one-loop corrections to the decay modes $H^\pm \to W^\pm h_1$. It is one of the important modes for the low charged Higgs mass besides the decays into the third generations of fermions. We have presented the decay width and the branching ratio of the decay $H^- \to h_1 W^-$ and confirmed the importance of the higher order contributions and strong dependence on complex phases. The higher order contributions can increase the branching ratio of this decay mode significantly and thus make it be an important mode for the searches of charged Higgs bosons. The relative correction can change sign when the complex phase of the top trilinear coupling, ϕ_t, varies from $-\pi$ to π. The partial decay width turns out to be significant in particular for small values of $\tan\beta$ and low masses of the charged Higgs boson. With increasing mass it becomes rather small.

Furthermore, we have calculated the CP violating asymmetry, $\delta_{\rm CP}$, from the decays $H^\pm \to W^\pm h_1$ originating from non-vanishing complex phases of the soft SUSY breaking parameters and of the Higgsino mixing parameter, μ. All the phases that can give sizable contributions to $\delta_{\rm CP}$ are taken into account and discussed. The impact of the phases of the τ and bottom trilinear couplings and of the gaugino mass, M_1, on CP rate asymmetry is of some significance only above the normal thresholds. ϕ_t and ϕ_μ can yield large contributions to the CP asymmetry both below and above the normal thresholds and can induce large $\delta_{\rm CP}$ at large $M_{H^\pm}$. $\delta_{\rm CP}$ depends strongly on $M_{H^\pm}$, $|A_t|$ and $\tan\beta$.

The dependence of the partial decay width and δ_{CP} on the renormalization scale is also studied. We observed a small dependence for the former. However, the CP

asymmetry induced by ϕ_t and ϕ_μ shows a large scale dependence resulting from the wave function renormalization factor of the neutral Higgs boson, h_1.

Second, we have studied the production of charged Higgs bosons in association with a W boson at the LHC. The next-to-leading order (NLO) electroweak (EW), SM-QCD and SUSY-QCD contributions to the $b\bar{b}$ annihilation are calculated together with the loop-induced gg fusion. Moreover, the CP violating asymmetry, dominantly generated by the gg fusion, has been investigated. The leading order (LO) cross sections contain the bottom–Higgs couplings which receive large SM-QCD and SUSY-QCD and SUSY-EW corrections. In order to obtain reliable predictions, these large universal corrections are absorbed into the bottom–Higgs couplings. The SM-QCD corrections proportional to $\alpha_s \ln m_b$ are absorbed by using the running bottom-quark mass. The SUSY corrections proportional to $\tan\beta$ and parameterized via Δm_b are resummed to all orders of perturbation theory. We have shown that after subtracting the Δm_b effects the remaining NLO SUSY corrections are still sizable. Another care relating to the neutral Higgs mixing propagator was addressed. In the complex MSSM, the h, H and A neutral Higgs bosons in general mix and form three mass eigenstates ($h_{1,2,3}$) with both CP-even and odd properties. We have resummed these mixing effects in the propagators and shown that they have a large impact on the production rates and CP asymmetry.

Numerical results have been presented for the CPX scenario. It is shown that the production rate and the CP asymmetry depend strongly on $\tan\beta$, $M_{H^\pm}$ and the phases ϕ_t and of the gaugino mass M_3. Large production rates prefer small $\tan\beta$, small $M_{H^\pm}$ and the phases ϕ_t, ϕ_3 about $\pm\pi$. Large CP asymmetries occur at small $\tan\beta$, for $M_{H^\pm}$ of about $250\,\mathrm{GeV}$, and $\phi_t \approx \pm\pi/2$ and $\phi_3 = 0$.

We have also studied the dependence of the results on the renormalization and factorization scales. For the $b\bar{b}$ subprocess, the NLO corrections reduce significantly the scale dependence while the gg fusion suffers from large scale uncertainty mainly due to the running $\alpha_s(\mu_R)$. This makes the final results, in particular the CP asymmetry, depend significantly on the scales. A two-loop calculation would be needed to reduce this uncertainty to the level of a few percents.

Third, we have studied the NLO EW corrections to H^- production via $gg \to H^- t\bar{b}$ where the bottom quark is considered to be tagged with transverse momentum and pseudo rapidity cuts applied on the bottom quark. Although we have subtracted the large $\tan\beta$ enhanced corrections, the remaining NLO EW contributions are still sizable, as in the case of $pp \to W^\pm H^\mp$.

We have shown the dependence of the NLO EW corrections on $\tan\beta$, $M_{H^\pm}$ and ϕ_t. Especially, the dependence on ϕ_t is rather strong. The correction can go from positive to negative values if ϕ_t is varied between $-\pi$ and π.

We have also studied the differential distributions of the final state particles at $\phi_t = \pi/2$. We have shown that the NLO EW corrections do not change the shape of those distributions and are negative.

In summary, the higher order effects are important for the charged Higgs boson productions and decays, in particular for the complex SUSY parameters. The complex phase effects enter cross sections and decay widths via one-loop contributions and induce a considerable CP violating asymmetry. For the searches of charged Higgs bosons at the LHC, those corrections should be taken into account when doing analysis. For experimental purpose, a consistent combination of the decay modes and production processes should be done and implemented in a Monte Carlo generator. This is a subject of our future studies.

Appendix A

Notations and conventions

A.1 Metric conventions and Dirac matrices

We use the following conventions through this thesis, if not otherwise specified. The covariant and contravariant four-vector position and momentum of a particle are

$$x_\mu = (t, \vec{x}), \qquad\qquad p_\mu = (E, \vec{p}),$$
$$x^\mu = (t, -\vec{x}), \qquad\qquad p^\mu = (E, -\vec{p}). \qquad (A.1)$$

The indices can be lowered and raised by using the spacetime metric tensor

$$x_\mu = \eta_{\mu\nu} x^\nu, \qquad x^\mu = \eta^{\mu\nu} x_\nu, \qquad (A.2)$$

with

$$\eta_{\mu\nu} = \eta^{\mu\nu} = \mathrm{diag}(1, -1, -1, -1). \qquad (A.3)$$

The covariant and contravariant derivatives are

$$\partial_\mu \equiv \frac{\partial}{\partial x^\mu} = (\frac{\partial}{\partial t}, \vec{\nabla}), \quad \partial^\mu \equiv \frac{\partial}{\partial x_\mu} = (\frac{\partial}{\partial t}, -\vec{\nabla}). \qquad (A.4)$$

The Dirac matrices γ_μ are defined so that they satisfy the anticommutation relations

$$\{\gamma_\mu, \gamma_\nu\} \equiv \gamma_\mu \gamma_\nu + \gamma_\mu \gamma_\mu = 2\eta_{\mu\nu}. \qquad (A.5)$$

In four dimensional space, the chirality matrix is

$$\gamma^5 = i\gamma^0\gamma^1\gamma^2\gamma^3 \equiv -\frac{i}{4!}\epsilon^{\mu\nu\rho\sigma}\gamma_\mu\gamma_\nu\gamma_\rho\gamma_\sigma, \qquad (A.6)$$

where the Levi-Civita tensor is totally antisymmetric and $\epsilon^{0123} = -\epsilon_{0123} = +1$. The left- and right-handed projection operators are

$$P_L = \frac{1 - \gamma^5}{2}, \qquad P_R = \frac{1 + \gamma^5}{2}. \qquad (A.7)$$

There are several representations of the Dirac matrices. Here we use the Weyl or chiral basis in which the 4×4 matrices are given in 2×2 blocks,

$$\gamma_\mu = \begin{pmatrix} 0 & \sigma_\mu \\ \bar{\sigma}_\mu & 0 \end{pmatrix}, \qquad \gamma^5 = \begin{pmatrix} -1 & 0 \\ 0 & 1 \end{pmatrix}, \tag{A.8}$$

where

$$\sigma_\mu = (\sigma_0, \sigma_1, \sigma_2, \sigma_3), \quad \bar{\sigma}_\mu = (\sigma_0, -\sigma_1, -\sigma_2, -\sigma_3). \tag{A.9}$$

σ_0 is unit matrix and σ_i (i=1,2,3) are the three Pauli matrices

$$\sigma_0 = \begin{pmatrix} 1 & 0 \\ 0 & 1 \end{pmatrix}, \quad \sigma_1 = \begin{pmatrix} 0 & 1 \\ 1 & 0 \end{pmatrix}, \quad \sigma_2 = \begin{pmatrix} 0 & -i \\ i & 0 \end{pmatrix}, \quad \sigma_3 = \begin{pmatrix} 1 & 0 \\ 0 & -1 \end{pmatrix}. \tag{A.10}$$

The followings are some useful identities of Dirac matrices in d dimensional space:

$$\gamma^\mu \gamma_\mu = d, \tag{A.11}$$
$$\gamma^\mu \gamma^\nu \gamma_\mu = (2-d)\gamma^\nu, \tag{A.12}$$
$$\gamma^\mu \gamma^\nu \gamma^\sigma \gamma_\mu = d\eta^{\nu\sigma}, \tag{A.13}$$
$$\gamma^\mu \gamma^\nu \gamma^\rho \gamma^\sigma \gamma_\mu = (2-d)\gamma^\sigma \gamma^\rho \gamma^\nu, \tag{A.14}$$
$$\text{Tr}\,(\gamma^\mu) = 0, \tag{A.15}$$
$$\text{Tr}\,(\gamma^\mu \gamma^\nu) = d\eta^{\mu\nu}, \tag{A.16}$$
$$\text{Tr}\,(\gamma^\mu \gamma^\nu \gamma^\rho \gamma^\sigma) = d\left(\eta^{\mu\nu}\eta^{\rho\sigma} - \eta^{\mu\rho}\eta^{\nu\sigma} + \eta^{\mu\sigma}\eta^{\nu\rho}\right), \tag{A.17}$$
$$\text{Tr}\,(\gamma^5) = \text{Tr}\,(\gamma^\mu \gamma^5) = \text{Tr}\,(\gamma^\mu \gamma^\nu \gamma^5) = 0, \tag{A.18}$$
$$\text{Tr}\,(\gamma^\mu \gamma^\nu \gamma^\rho \gamma^\sigma \gamma^5) = -4i\epsilon^{\mu\nu\rho\sigma}. \tag{A.19}$$
$$\tag{A.20}$$

A.2   Representations of Lorentz group: Weyl, Dirac and Majorana spinors

The Lorentz group is composed of the boosts in three directions and the rotations about three axes. Three boost generators K_i and three rotation generators J_i (i=1, 2, 3) obey the following commutation relations,

$$\begin{aligned} [K_i, K_j] &= -i\epsilon_{ijk} J_k, \\ [J_i, K_j] &= i\epsilon_{ijk} K_k, \\ [J_i, J_j] &= i\epsilon_{ijk} J_k. \end{aligned} \tag{A.21}$$

We define the generators

$$A_i = \frac{1}{2}(J_i + iK_i), \qquad B_i = \frac{1}{2}(J_i - iK_i), \tag{A.22}$$

which sastify

$$\begin{aligned}
[A_i, A_j] &= i\epsilon_{ijk}A_k, \\
[A_i, B_j] &= 0, \\
[B_i, B_j] &= i\epsilon_{ijk}B_k.
\end{aligned} \tag{A.23}$$

Those six generators generate two separate groups of $SU(2)$ Lie algebra. Therefore, a representation of the Lorentz group can be labeled by two half-integer indices (j, j').

Weyl spinors are complex two component objects belong to irreducible representations $(1/2, 0)$ and $(0, 1/2)$ of the Lorentz group. The left-handed spinor ξ is the $(0, 1/2)$ representation while the right-handed χ is the $(1/2, 0)$ representation. They transform under the Lorentz group as

$$\begin{aligned}
\xi &\rightarrow \exp\left(\frac{i\omega_i\sigma_i + \theta_i\sigma_i}{2}\right)\xi \equiv M\xi, \\
\chi &\rightarrow \exp\left(\frac{i\omega_i\sigma_i - \theta_i\sigma_i}{2}\right)\chi \equiv N\chi.
\end{aligned} \tag{A.24}$$

Two irreducible representations are inequivalent. The two matrices are related by

$$M = \epsilon N^* \epsilon^{-1}, \qquad \epsilon = i\sigma_2 \equiv \begin{pmatrix} 0 & 1 \\ -1 & 0 \end{pmatrix}. \tag{A.25}$$

Using a property of Pauli matrices

$$\sigma_2 \sigma_i^* \sigma_2 = -\sigma_i, \tag{A.26}$$

one can easily show that $\sigma_2 \xi^*$ transforms like χ and vice versa. To indicate two different Weyl spinors, one can introduce undotted and dotted indices for the left- and right-handed spinors, respectively. Those indices are lowered and raised by using the ϵ tensor

$$\xi_\alpha = \epsilon_{\alpha\beta}\xi^\beta, \qquad\qquad \xi^\alpha = \epsilon^{\alpha\beta}\xi_\beta, \tag{A.27}$$

$$\chi_{\dot\alpha} = \epsilon_{\dot\alpha\dot\beta}\chi^{\dot\beta}, \qquad\qquad \chi^{\dot\alpha} = \epsilon^{\dot\alpha\dot\beta}\chi_{\dot\beta}, \tag{A.28}$$

where the antisymmetric tensor takes the convention $\epsilon_{12} = \epsilon^{12} = \epsilon_{\dot1\dot2} = \epsilon^{\dot1\dot2} = +1$. It can be proved that the following quantities are invariant under Lorentz transformation

$$\xi\eta \equiv \xi_\alpha\eta^\alpha = \xi_\alpha\epsilon^{\alpha\beta}\eta_\beta, \quad \chi\zeta \equiv \chi^{\dot\alpha}\zeta_{\dot\alpha} = \chi_{\dot\alpha}\epsilon^{\dot\alpha\dot\beta}\zeta_{\dot\beta}. \tag{A.29}$$

Dirac spinor is composed of two types of Weyl spinor,

$$\psi = \begin{pmatrix} \xi_\alpha \\ \chi^{\dot\alpha} \end{pmatrix}, \tag{A.30}$$

hence it contains four complex components. In other words, it is a $(1/2, 0) \oplus (0, 1/2)$ representation which transform under Lorentz group as

$$\psi \rightarrow \begin{pmatrix} \exp\left(\frac{i\omega_i\sigma_i + \theta_i\sigma_i}{2}\right) & 0 \\ 0 & \exp\left(\frac{i\omega_i\sigma_i - \theta_i\sigma_i}{2}\right) \end{pmatrix} \psi. \tag{A.31}$$

The adjoint spinor of ψ is defined as

$$\bar{\psi} = \psi^\dagger \gamma^0. \tag{A.32}$$

From Dirac spinors, one can construct the following quantities with specific property under Lorentz transformations,

$$\begin{aligned} \bar{\psi}\psi &: \text{scalar,} \\ \bar{\psi}\gamma^5\psi &: \text{pseudo scalar,} \\ \bar{\psi}\gamma^\mu\psi &: \text{vertor,} \\ \bar{\psi}\gamma^\mu\gamma^5\psi &: \text{axial vertor,} \\ \bar{\psi}(\gamma^\mu\gamma^\nu - \gamma^\nu\gamma^\mu)\psi &: \text{antisymmetric tensor.} \end{aligned} \tag{A.33}$$

Majorana spinor is defined as

$$\psi \equiv \begin{pmatrix} \xi_\alpha \\ \bar{\xi}^{\dot{\alpha}} \end{pmatrix} = \begin{pmatrix} \xi \\ i\sigma_2\xi^* \end{pmatrix}. \tag{A.34}$$

Majorana spinors are used to represent neutral fermions while Dirac spinors are for charged fermions.

A.3   Grassmann numbers

Grassmann numbers are numbers that satisfy the anticommutation relation,

$$\{\theta_i, \theta_j\} = 0. \tag{A.35}$$

In superspace one needs two Weyl spinors θ_α and $\bar{\theta}^{\dot{\alpha}}$ ($\alpha, \dot{\alpha} = 1, 2$) which their components are Grassmann numbers. Owing to the fermionic property of Grassmann numbers, a function of θ has a finite Taylor series,

$$\Phi(x, \theta) = \phi(x) + \theta\psi(x) + \theta^2 F(x), \tag{A.36}$$

where $\theta^2 = \epsilon^{\alpha\beta}\theta_\alpha\theta_\beta$.

Derivatives of Grassmann variables are defined by

$$\partial_\alpha\theta^\beta \equiv \frac{\partial}{\partial\theta^\alpha} = +\delta_\alpha^\beta, \quad \partial^\alpha\theta_\beta \equiv \frac{\partial}{\partial\theta_\alpha} = -\delta_\beta^\alpha. \tag{A.37}$$

The integrals over Grassmann variables satisfy the following properties.

- Linearity

$$\int d\theta (af(\theta) + bg(\theta)) = a \int d\theta f(\theta) + b \int d\theta g(\theta), \qquad \text{(A.38)}$$

where a, b are ordinary numbers.

- Integration by parts

$$\int \frac{\partial}{\partial \theta} f(\theta) d\theta = 0. \qquad \text{(A.39)}$$

- Shift invariance

$$\int d\theta f(\theta + \eta) = \int d\theta f(\theta). \qquad \text{(A.40)}$$

From the above properties, one can write down some specific rules:

$$\int d\theta = 0, \qquad \text{(A.41)}$$

$$\int d\theta \ \theta = 1, \qquad \text{(A.42)}$$

$$d\theta \ \theta = -\theta \ d\theta, \qquad \text{(A.43)}$$

$$\int d\theta = \frac{\partial}{\partial \theta}, \qquad \text{(A.44)}$$

$$\delta(\theta) = \theta, \quad \delta(\theta) \text{ is Dirac delta function.} \qquad \text{(A.45)}$$

The followings are some useful formulae for the two-component Grassmann variable θ:

$$\partial_\alpha \theta^2 = 2\theta_\alpha, \qquad\qquad (\partial\partial)\theta^2 = -4, \qquad \text{(A.46)}$$

$$\int d\theta d\theta \ \theta^2 = -4. \qquad \text{(A.47)}$$

Appendix B

Dipole subtraction functions

In this appendix we present explicitly the functions needed for the dipole subtraction method which are applied for the processes $pp \to W^\pm H^\mp$, $pp \to H^- t\bar{b}$. The mass of initial state quarks are considered as regulators. For detailed derivation and momentum mapping we refer to [126]. We have four different cases.

- Initial-state emitter (a) and initial-initial state spectator (b): the auxiliary function is defined as

$$g_{ab}^{\text{sub}}(p_a, p_b, q) = \frac{1}{(p_a q) x_{ab}} \left(\frac{2}{1 - x_{ab}} - 1 - x_{ab} \right),$$

(B.1)

where $x_{ab} = (p_a p_b - p_a k - p_b k)/(p_a p_b)$. The distribution function is given by

$$\mathcal{G}_{ab}(x) = P_{ff}(x) \left[\ln \left(\frac{s}{m_a^2} \right) - 1 \right] + 1 - x,$$

(B.2)

and the endpoint function reads

$$G_{ab}(s) = \ln \frac{m_a^2}{s} \ln \frac{\lambda^2}{s} + \ln \frac{\lambda^2}{s} - \frac{1}{2} \ln^2 \frac{m_a^2}{s} + \frac{1}{2} \ln \frac{m_a^2}{s} - \frac{\pi^2}{3} + 2.$$

(B.3)

- Initial-state emitter (a) and final-state spectator (i) and vice versa: the auxiliary functions are defined by

$$g_{ai}^{\text{sub}}(p_a, p_i, q) = \frac{1}{(p_a q) x_{ia}} \left[\frac{2}{2 - x_{ia} - z_{ia}} - 1 - x_{ia} \right],$$

(B.4)

$$g_{ia}^{\text{sub}}(p_i, p_a, q) = \frac{1}{(p_i q) x_{ia}} \left[\frac{2}{2 - x_{ia} - z_{ia}} - 1 - z_{ia} - \frac{m_i^2}{p_i q} \right],$$

(B.5)

where

$$x_{ia} = \frac{p_a p_i + p_a q - p_i q}{p_a p_i + p_a q}, \quad z_{ia} = \frac{p_a p_i}{p_a p_i + p_a q}.$$

(B.6)

The distribution functions are given by

$$
\mathcal{G}_{ia}(x) = \frac{1}{1-x}\left\{ 2\ln\frac{2-x-z_1(x)}{1-x}\right.
\tag{B.7}
$$

$$
\left. +\frac{1}{2}[z_1(x)-1]\left[3+z_1(x)-\frac{4m_i^2 x}{(P_{ia}^2-m_i^2)(1-x)}\right]\right\},
$$

$$
\mathcal{G}_{ai}(x) = P_{ff}(x)\left\{ \ln\frac{m_i^2-P_{ia}^2}{m_a^2 x}+\ln[1-z_1(x)]-1\right\}
$$

$$
-\frac{2}{1-x}\ln[2-x-z_1(x)]+(1+x)[\ln(1-x)+1], \tag{B.8}
$$

where

$$
z_1(x)=\frac{m_i^2 x}{m_i^2-P_{ia}^2(1-x)}, P_{ia}=p_i-p_a-q. \tag{B.9}
$$

The endpoint functions reads

$$
G_{ia} = \ln\frac{m_i^2}{\lambda^2}\ln\left(2-\frac{P_{ia}^2}{m_i^2}\right)+2\ln\frac{\lambda m_i}{m_i^2-P_{ia}^2}-2\mathrm{Li}_2\frac{P_{ia}^2}{P_{ia}^2-2m_i^2} \tag{B.10}
$$

$$
+\frac{1}{2}\ln^2\left(2-\frac{P_{ia}^2}{m_i^2}\right)+\frac{(P_{ia}^2-m_i^2)^2}{2P_{ia}^4}\ln\left(1-\frac{P_{ia}^2}{m_i^2}\right)-\frac{\pi^2}{6}+\frac{3}{2}+\frac{m_i^2}{2P_{ia}^2},
$$

$$
G_{ia} = \ln\frac{\lambda^2}{m_a^2}\ln\frac{m_a^2(2m_i^2-P_{ia}^2)}{(m_i^2-P_{ia}^2)^2}+\ln\frac{\lambda^2}{m_a^2}+2\mathrm{Li}_2\frac{P_{ia}^2}{2m_i^2-P_{ia}^2}
$$

$$
-2\mathrm{Li}_2\frac{m_i^2}{2m_i^2-P_{ia}^2}+2\ln\frac{m_a^2 m_i^2}{(m_i^2-P_{ia}^2)(2m_i^2-P_{ia}^2)}\ln\frac{2m_i^2-P_{ia}^2}{m_i^2-P_{ia}^2}
$$

$$
+\frac{1}{2}\ln^2\frac{m_a^2}{2m_i^2-P_{ia}^2}+\frac{3}{2}\ln\frac{m_a^2}{m_i^2-P_{ia}^2}+\frac{m_i^2(m_i^2-4P_{ia}^2)}{2P_{ia}^4}\ln\left(1-\frac{P_{ia}^2}{m_i^2}\right)
$$

$$
+\frac{\pi^2}{3}-1+\frac{m_i^2}{2P_{ia}^2}. \tag{B.11}
$$

• Final-state emitter (i) and final-state spectator (j): the auxiliary function reads

$$
g_{ij}^{\mathrm{sub}} = \frac{1}{p_i q R_{ij}(y_{ij})}\left[\frac{2}{1-z_{ij}(1-y_{ij})}-1-z_{ij}-\frac{m_i^2}{p_i q}\right], \tag{B.12}
$$

where

$$
y_{ij}=\frac{p_i q}{p_i p_j+p_i q+p_j q}, \qquad z_{ij}=\frac{p_i p_j}{p_i p_j+p_j p_k},
$$

$$
P_{ij}=p_i+p_j+q, \qquad \bar{P}_{ij}^2=P_{ij}^2-m_i^2-m_j^2,
$$

$$
\lambda_{ij}=\lambda(P_{ij}^2,m_i^2,m_j^2), \qquad R_{ij}(y)=\frac{\sqrt{(2m_j^2+\bar{P}_{ij}^2-\bar{P}_{ij}^2 y)^2-4P_{ij}^2 m_j^2}}{\sqrt{\lambda_{ij}}} \tag{B.13}
$$

and

$$
\lambda(x,y,z)=x^2+y^2+z^2-xy-yz-xz. \tag{B.14}
$$

The endpoint function is given by

$$
\begin{aligned}
G_{ij} &= \ln\left(\frac{\lambda^2 a_3^2}{m_i^2}\right) - 2\ln(1 - a_3^2) + \frac{a_3^2}{2} + \frac{3}{2} + \frac{\bar{P}_{ij}^2}{\sqrt{\lambda_{ij}}}\left[\lambda a_1 \ln \frac{\lambda^2 m_j^2}{\lambda_{ij} a_2}\right. \\
&\quad \left. + 2\mathrm{Li}_2(a_1) + 4\mathrm{Li}_2\left(-\sqrt{\frac{a_2}{a_1}}\right) - 4\mathrm{Li}_2(-\sqrt{a_1 a_2}) + \frac{1}{2}\ln^2 a_1 - \frac{\pi^2}{3}\right].
\end{aligned}
$$

(B.15)

Appendix C

Counterterms and renormalization constants

In this section, we list the Feynman rules and counterterms for vertices and propagators which appear in our calculation. They can be expressed in terms of coupling and field renormalization constants (RC) which relate the bare and renormalized quantities. The RCs are defined as in Ref. [101] for the SM-like fields and as in Ref. [23] for the Higgs sector. The following one-loop Feynman rules use the standard convention and notation of `FeynArts` [175]. In the vertices all momenta are considered as incoming. We introduce the shorthand notation $s_\alpha = \sin\alpha$, $c_\alpha = \cos\alpha$, $t_\alpha = \tan\alpha$, $s_\beta = \sin\beta$, $c_\beta = \cos\beta$, $t_\beta = \tan\beta$.

Fermion-Fermion-Scalar:

$$\begin{array}{c} F_1 \\ \\ F_2 \end{array} \!\!\!\!\!\!\!\!\!\! \times\!\!-\!-\!-\!-\!-\!\cdot \ \ = ie(C^- P_L + C^+ P_R)$$

$$\bar{b}bh^0 : \quad \begin{cases} C^- = \frac{s_\alpha\, m_b}{2c_\beta M_W s_W}\Big(1 + \delta Z_e + \frac{\delta m_b}{m_b} + s_\beta^2 \delta\tan\beta - \frac{\delta M_W^2}{2M_W^2} \\ \qquad\qquad - \frac{\delta s_W}{s_W} + \frac{1}{2}\delta Z_{hh} - \frac{1}{2t_\alpha}\delta Z_{Hh} + \frac{1}{2}\delta Z_{b,L} + \frac{1}{2}\delta Z_{b,R}^*\Big) \\ C^+ = \frac{s_\alpha\, m_b}{2c_\beta M_W s_W}\Big(1 + \delta Z_e + \frac{\delta m_b}{m_b} + s_\beta^2 \delta\tan\beta - \frac{\delta M_W^2}{2M_W^2} \\ \qquad\qquad - \frac{\delta s_W}{s_W} + \frac{1}{2}\delta Z_{hh} - \frac{1}{2t_\alpha}\delta Z_{Hh} + \frac{1}{2}\delta Z_{b,L}^* + \frac{1}{2}\delta Z_{b,R}\Big) \end{cases}$$

$$\bar{b}bH^0 : \quad \begin{cases} C^- = -\frac{c_\alpha\, m_b}{2c_\beta M_W s_W}\Big(1 + \delta Z_e + \frac{\delta m_b}{m_b} + s_\beta^2 \delta\tan\beta - \frac{\delta M_W^2}{2M_W^2} \\ \qquad\qquad - \frac{\delta s_W}{s_W} + \frac{1}{2}\delta Z_{HH} - \frac{1}{2}t_\alpha\delta Z_{hH} + \frac{1}{2}\delta Z_{b,L} + \frac{1}{2}\delta Z_{b,R}^*\Big) \\ C^+ = -\frac{c_\alpha\, m_b}{2c_\beta M_W s_W}\Big(1 + \delta Z_e + \frac{\delta m_b}{m_b} + s_\beta^2 \delta\tan\beta - \frac{\delta M_W^2}{2M_W^2} \\ \qquad\qquad - \frac{\delta s_W}{s_W} + \frac{1}{2}\delta Z_{HH} - \frac{1}{2}t_\alpha\delta Z_{hH} + \frac{1}{2}\delta Z_{b,L}^* + \frac{1}{2}\delta Z_{b,R}\Big) \end{cases}$$

$$\bar{b}bA^0 : \begin{cases} C^- = -i\frac{t_\beta\, m_b}{2M_W s_W}\left(1 + \delta Z_e + \frac{\delta m_b}{m_b} + s_\beta^2\delta\tan\beta - \frac{\delta M_W^2}{2M_W^2}\right. \\ \qquad\qquad \left. - \frac{\delta s_W}{s_W} + \frac{1}{2}\delta Z_{AA} - \frac{1}{2t_\beta}\delta Z_{G^0A} + \frac{1}{2}\delta Z_{b,L} + \frac{1}{2}\delta Z_{b,R}^*\right) \\ C^+ = i\frac{t_\beta\, m_b}{2M_W s_W}\left(1 + \delta Z_e + \frac{\delta m_b}{m_b} + s_\beta^2\delta\tan\beta - \frac{\delta M_W^2}{2M_W^2} - \frac{\delta s_W}{s_W}\right. \\ \qquad\qquad \left. + \frac{1}{2}\delta Z_{AA} - \frac{1}{2t_\beta}\delta Z_{G^0A} + \frac{1}{2}\delta Z_{b,L}^* + \frac{1}{2}\delta Z_{b,R}\right) \end{cases}$$

$$\bar{d}_j u_i H^- : \begin{cases} C^- = \frac{s_\beta}{\sqrt{2}c_\beta s_W M_W}\left\{V_{ij}^*\delta m_d + V_{ij}^*m_d(1 + \delta Z_e - \frac{\delta s_W}{s_W} + s_\beta^2\delta\tan\beta\right. \\ \qquad\qquad - \frac{\delta M_W^2}{2M_W^2} + \frac{1}{2}\delta Z_{H^-H^+} - \frac{1}{2}\delta Z_{G^-H^+}/t_\beta) \\ \qquad\qquad \left. + \frac{m_d}{2}\left[2\delta V_{ij}^* + \sum_k(V_{ik}^*\delta Z_{kj,R}^{d*} + V_{kj}^*\delta Z_{ki,L}^u)\right]\right\} \\ C^+ = \frac{c_\beta}{\sqrt{2}s_\beta s_W M_W}\left\{V_{ij}^*\delta m_u + V_{ij}^*m_u(1 + \delta Z_e - \frac{\delta s_W}{s_W} - c_\beta^2\delta\tan\beta\right. \\ \qquad\qquad - \frac{\delta M_W^2}{2M_W^2} + \frac{1}{2}\delta Z_{H^-H^+} + \frac{1}{2}\delta Z_{G^-H^+}t_\beta) \\ \qquad\qquad \left. + \frac{m_u}{2}\left[2\delta V_{ij}^* + \sum_k(V_{ik}^*\delta Z_{kj,L}^{d*} + V_{kj}^*\delta Z_{ki,R}^u)\right]\right\} \end{cases}$$

$$\bar{u}_i d_j H^+ : \begin{cases} C^- = \frac{c_\beta}{\sqrt{2}s_\beta s_W M_W}\left\{V_{ij}\delta m_u + V_{ij}m_u(1 + \delta Z_e - \frac{\delta s_W}{s_W} - c_\beta^2\delta\tan\beta\right. \\ \qquad\qquad - \frac{\delta M_W^2}{2M_W^2} + \frac{1}{2}\delta Z_{H^-H^+} + \frac{1}{2}\delta Z_{G^-H^+}t_\beta) \\ \qquad\qquad \left. + \frac{m_u}{2}\left[2\delta V_{ij} + \sum_k(V_{ik}\delta Z_{kj,L}^d + V_{kj}\delta Z_{ki,R}^{u*})\right]\right\} \\ C^+ = \frac{s_\beta}{\sqrt{2}c_\beta s_W M_W}\left\{V_{ij}\delta m_d + V_{ij}m_d(1 + \delta Z_e - \frac{\delta s_W}{s_W} + s_\beta^2\delta\tan\beta\right. \\ \qquad\qquad - \frac{\delta M_W^2}{2M_W^2} + \frac{1}{2}\delta Z_{H^-H^+} - \frac{1}{2}\delta Z_{G^-H^+}/t_\beta) \\ \qquad\qquad \left. + \frac{m_d}{2}\left[2\delta V_{ij} + \sum_k(V_{ik}\delta Z_{kj,R}^d + V_{kj}\delta Z_{ki,L}^{u*})\right]\right\} \end{cases}$$

$$\text{(C.1)}$$
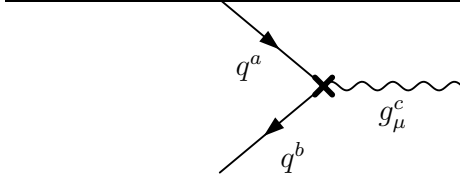
Fermion-Fermion-Vector:

$$= ie\gamma_\mu C^- P_L$$

$$\bar{d}_j u_i W^- : \qquad C^- = -\frac{1}{\sqrt{2}s_W}\left[V_{ij}^*(1 + \delta Z_e - \frac{\delta s_W}{s_W} + \frac{1}{2}\delta Z_W) + \delta V_{ij}^*\right.$$
$$\left. + \frac{1}{2}\sum_k(V_{kj}^*\delta Z_{ki,L}^u + V_{ik}^*\delta Z_{kj,L}^{d*})\right] \qquad \text{(C.2)}$$

$$\bar{u}_i d_j W^+ : \qquad C^- = -\frac{1}{\sqrt{2}s_W}\left[V_{ij}(1 + \delta Z_e - \frac{\delta s_W}{s_W} + \frac{1}{2}\delta Z_W) + \delta V_{ij}\right.$$
$$\left. + \frac{1}{2}\sum_k(V_{kj}\delta Z_{ki,L}^{u*} + V_{ik}\delta Z_{kj,L}^d)\right],$$
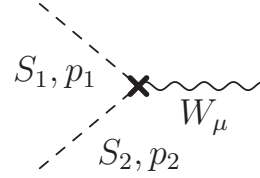
Quark-Quark-gluon:

$$= -ig_s T^c_{ab} \gamma_\mu (C^- P_L + C^+ P_R)$$

$$q\bar{q}g: \qquad C^- = 1 + \delta g_s + \delta Z_g + \delta Z_{q,L},$$
$$C^+ = 1 + +\delta g_s + \delta Z_g + \delta Z_{q,R}.$$

Scalar-Scalar-Vector:

$$= ieC(p_1 - p_2)^\mu$$

$$hH^-W^+: \qquad C = -\frac{\cos(\beta-\alpha)}{2s_W}\Big[1 + \delta Z_e - \frac{\delta s_W}{s_W} + \frac{1}{2}\delta Z_{WW} + \frac{1}{2}\delta Z_{hh}$$
$$+ \frac{1}{2}\delta Z_{H^+H^-} - \frac{\sin(\beta-\alpha)}{2\cos(\beta-\alpha)}\big(\delta Z_{Hh} - \delta Z_{G^-H^+}\big)\Big]$$

$$hH^+W^-: \qquad C = \frac{\cos(\beta-\alpha)}{2s_W}\Big[1 + \delta Z_e - \frac{\delta s_W}{s_W} + \frac{1}{2}\delta Z_{WW} + \frac{1}{2}\delta Z_{hh}$$
$$+ \frac{1}{2}\delta Z_{H^+H^-} - \frac{\sin(\beta-\alpha)}{2\cos(\beta-\alpha)}\big(\delta Z_{Hh} - \delta Z_{G^-H^+}\big)\Big]$$
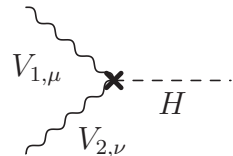
$$HH^-W^+: \qquad C = \frac{\sin(\beta-\alpha)}{2s_W}\Big[1 + \delta Z_e - \frac{\delta s_W}{s_W} + \frac{1}{2}\delta Z_{WW} + \frac{1}{2}\delta Z_{HH}$$
$$+ \frac{1}{2}\delta Z_{H^+H^-} - \frac{\cos(\beta-\alpha)}{2\sin(\beta-\alpha)}\big(\delta Z_{hH} + \delta Z_{G^-H^+}\big)\Big]$$

$$HH^+W^-: \qquad C = -\frac{\sin(\beta-\alpha)}{2s_W}\Big[1 + \delta Z_e - \frac{\delta s_W}{s_W} + \frac{1}{2}\delta Z_{WW} + \frac{1}{2}\delta Z_{HH}$$
$$+ \frac{1}{2}\delta Z_{H^+H^-} - \frac{\cos(\beta-\alpha)}{2\sin(\beta-\alpha)}\big(\delta Z_{hH} + \delta Z_{G^-H^+}\big)\Big]$$

$$AH^\pm W^\mp: \qquad C = -\frac{i}{2s_W}\Big[1 + \delta Z_e - \frac{\delta s_W}{s_W} + \frac{1}{2}\delta Z_{WW} + \frac{1}{2}\delta Z_{AA} + \frac{1}{2}\delta Z_{H^+H^-}\Big]$$

$$G^0 H^\pm W^\mp: \qquad C = -\frac{i}{4s_W}\big(\delta Z_{AG} + \delta Z_{G^-H^+}\big)$$

Vector-Vector-Scalar:

$$= ieg_{\mu\nu}C$$

The vertices $VW^{\mp}H^{\pm}$ with $V = \gamma, Z$ do not appear at tree level. The counterterms are generated at one-loop level, however.

$$\gamma W^{\pm}H^{\mp} : \qquad C = \frac{M_W}{2}(\delta Z_{G^-H^+} + \sin 2\beta \delta \tan \beta),$$

$$ZW^{\pm}H^{\mp} : \qquad C = -\frac{M_W s_W}{2c_W}(\delta Z_{G^-H^+} + \sin 2\beta \delta \tan \beta).$$

One needs also counterterms for the renormalized propagators. The complete set of counterterms for the scalar-scalar case can be found in Ref. [23]. We list here extra pieces needed in our calculation.

Scalar-Vector:

$$\overset{\text{------}\times\!\!\sim\!\sim\!\sim}{A^0,\, p \qquad Z_\mu} \quad = -\tfrac{M_Z}{2}(\delta Z_{AG} + \sin 2\beta \delta \tan \beta)p_\mu$$

$$\overset{\text{------}\times\!\!\sim\!\sim\!\sim}{H^-,\, p \qquad W^+_\mu} \quad = -\tfrac{iM_W}{2}(\delta Z_{G^-H^+} + \sin 2\beta \delta \tan \beta)p_\mu$$

Appendix D

Explicit calculation of Δm_b

In this Appendix we calculate the one-loop contributions to Δm_b given in Eq. (5.41). They consist of SUSY-QCD and SUSY-EW contributions. For the internal squarks we use the mass eigenstates. For the internal neutralinos and charginos we use gauginos masses and Higgsino mixing parameter. All the external momenta are set to zero. These contributions are UV and infrared finite so we can work in 4 dimensional space.

The SUSY QCD contributions

$$-i\delta\tilde{\lambda}_b^{\text{SQCD}}\bar{b}P_Lb\langle H_2^0\rangle = \frac{4}{3}\bar{b}(ig_s\sqrt{2}\sqrt{\frac{M_3^*}{m_{\tilde{g}}}}U_{\tilde{b}}^*(j,2)P_L)(im_{\tilde{g}})(-ig_s\sqrt{2}\sqrt{\frac{M_3^*}{m_{\tilde{g}}}}U_{\tilde{b}}(i,1)P_L)$$

$$\times(-ih_{ij}^{\tilde{b}})b\int\frac{d^4q}{(2\pi)^4}\frac{i}{q^2-M_{\tilde{b}_i}^2}\frac{i}{q^2-M_{\tilde{b}_j}^2}\frac{1}{q^2-m_{\tilde{g}}^2} \quad \text{(D.1)}$$

$$= -\frac{4}{3}\frac{2ig_s^2}{16\pi^2}M_3^*h_{ij}^{\tilde{b}}U_{\tilde{b}}^*(j,2)U_{\tilde{b}}(i,1)C_0(M_{\tilde{b}_i}^2,M_{\tilde{b}_j}^2,m_{\tilde{g}}^2)\bar{b}P_Lb$$

where

$$m_bX_b\tilde{b}_R^*\tilde{b}_L + m_bX_b^*\tilde{b}_L^*\tilde{b}_R = h_{ij}^{\tilde{b}}\tilde{b}_j^*\tilde{b}_i,$$

$$\tilde{b}_R^* = U_{\tilde{b}}(i,2)\tilde{b}_i^*, \quad \tilde{b}_L = U_{\tilde{b}}^*(i,1)\tilde{b}_i, \quad \text{(D.2)}$$

then

$$h_{ij}^{\tilde{b}} = m_bX_bU_{\tilde{b}}(j,2)U_{\tilde{b}}^*(i,1) + m_bX_b^*U_{\tilde{b}}(j,1)U_{\tilde{b}}^*(i,2). \quad \text{(D.3)}$$

Substituting (D.3) into (D.2), one gets

$$
\delta\tilde{\lambda}_b^{\text{SQCD}}\frac{v_2}{\sqrt{2}} = \frac{2}{3}\frac{\alpha_s}{\pi}M_3^*m_b(X_bU_{\tilde{b}}(j,2)U_{\tilde{b}}^*(i,1) + X_b^*U_{\tilde{b}}(j,1)U_{\tilde{b}}^*(i,2))
$$
$$
\times U_{\tilde{b}}^*(j,2)U_{\tilde{b}}(i,1)C_0(M_{\tilde{b}_i}^2, M_{\tilde{b}_j}^2, m_{\tilde{g}}^2).
$$

(D.4)

Using the following relations

$$
U_{\tilde{b}}(1,1) = U_{\tilde{b}}(2,2) = c_{\tilde{b}}, \quad U_{\tilde{b}}(1,2) = -U_{\tilde{b}}^*(2,1) = s_{\tilde{b}},
$$

(D.5)

then we have

$$
\delta\tilde{\lambda}_b^{\text{SQCD}}\frac{v_2}{\sqrt{2}} = \frac{2}{3}\frac{\alpha_s}{\pi}M_3^*m_b(X_bs_{\tilde{b}}c_{\tilde{b}} + X_b^*c_{\tilde{b}}s_{\tilde{b}}^*)s_{\tilde{b}}^*c_{\tilde{b}}C_0(M_{\tilde{b}_1}^2, M_{\tilde{b}_1}^2, m_{\tilde{g}}^2)
$$
$$
+ \frac{2}{3}\frac{\alpha_s}{\pi}M_3^*m_b(-X_bc_{\tilde{b}}s_{\tilde{b}} - X_b^*s_{\tilde{b}}^*c_{\tilde{b}})c_{\tilde{b}}(-s_{\tilde{b}}^*)C_0(M_{\tilde{b}_2}^2, M_{\tilde{b}_2}^2, m_{\tilde{g}}^2)
$$
$$
+ \frac{2}{3}\frac{\alpha_s}{\pi}M_3^*m_b\left[(-X_bs_{\tilde{b}}^2 + X_b^*c_{\tilde{b}}^2)s_{\tilde{b}}^*(-s_{\tilde{b}}^*) + (X_bc_{\tilde{b}}^2 - X_b^*s_{\tilde{b}}^*s_{\tilde{b}}^*)(c_{\tilde{b}}c_{\tilde{b}})\right]
$$
$$
\times C_0(M_{\tilde{b}_1}^2, M_{\tilde{b}_2}^2, m_{\tilde{g}}^2)
$$
$$
= \frac{2}{3}\frac{\alpha_s}{\pi}M_3^*m_b(X_bs_{\tilde{b}}c_{\tilde{b}} + X_b^*c_{\tilde{b}}s_{\tilde{b}}^*)s_{\tilde{b}}^*c_{\tilde{b}}
$$
$$
\times\left[C_0(M_{\tilde{b}_1}^2, M_{\tilde{b}_1}^2, M_{\tilde{g}}^2) + C_0(M_{\tilde{b}_2}^2, M_{\tilde{b}_2}^2, m_{\tilde{g}}^2)\right]
$$
$$
+ \frac{2}{3}\frac{\alpha_s}{\pi}M_3^*m_b\left[-(-X_bs_{\tilde{b}}^2 + X_b^*c_{\tilde{b}}^2)(s_{\tilde{b}}^*)^2 + (X_bc_{\tilde{b}}^2 - X_b^*s_{\tilde{b}}^*s_{\tilde{b}}^*)c_{\tilde{b}}^2\right]
$$
$$
\times C_0(M_{\tilde{b}_1}^2, M_{\tilde{b}_2}^2, m_{\tilde{g}}^2).
$$

(D.6)

Using the tree-level relations

$$
c_{\tilde{b}} = \cos\theta_{\tilde{b}}, \quad s_{\tilde{b}} = e^{-i\varphi_{X_b}}\sin\theta_{\tilde{b}}
$$
$$
\varphi_{X_b} = \arg X_b^*
$$
$$
c_{\tilde{b}}s_{\tilde{b}} = \frac{m_bX_b^*}{M_{\tilde{b}_1}^2 - M_{\tilde{b}_2}^2},
$$

(D.7)

then we get

$$
\delta\tilde{\lambda}_b^{\text{SQCD}}\frac{v_2}{\sqrt{2}} = \frac{1}{3}\frac{\alpha_s}{\pi}M_3^*m_bX_b\sin^2 2\theta_{\tilde{b}}\left[C_0(M_{\tilde{b}_1}^2, M_{\tilde{b}_1}^2, M_{\tilde{g}}^2) + C_0(M_{\tilde{b}_2}^2, M_{\tilde{b}_2}^2, m_{\tilde{g}}^2)\right]
$$
$$
+ \frac{2}{3}\frac{\alpha_s}{\pi}M_3^*m_bX_b\cos^2 2\theta_{\tilde{b}}C_0(M_{\tilde{b}_1}^2, M_{\tilde{b}_2}^2, m_{\tilde{g}}^2)
$$
$$
= \frac{1}{3}\frac{\alpha_s}{\pi}M_3^*m_bX_b\sin^2 2\theta_{\tilde{b}}\left[C_0(M_{\tilde{b}_1}^2, M_{\tilde{b}_1}^2, m_{\tilde{g}}^2)\right.
$$
$$
\left. + C_0(M_{\tilde{b}_2}^2, M_{\tilde{b}_2}^2, m_{\tilde{g}}^2) - 2C_0(M_{\tilde{b}_1}^2, M_{\tilde{b}_2}^2, m_{\tilde{g}}^2)\right]
$$
$$
+ \frac{2}{3}\frac{\alpha_s}{\pi}M_3^*m_bX_bC_0(M_{\tilde{b}_1}^2, M_{\tilde{b}_2}^2, m_{\tilde{g}}^2)
$$
$$
= \frac{4}{3}\frac{\alpha_s}{\pi}M_3^*m_b^3X_b|X_b|^2\frac{1}{i\pi^2}\int d^4q\frac{1}{(q^2 - m_{\tilde{g}}^2)(q^2 - M_{\tilde{b}_1}^2)^2(q^2 - M_{\tilde{b}_2}^2)^2}
$$
$$
+ \frac{2}{3}\frac{\alpha_s}{\pi}M_3^*m_bX_bC_0(M_{\tilde{b}_1}^2, M_{\tilde{b}_2}^2, m_{\tilde{g}}^2).
$$

(D.8)

The first term is much smaller than the second term, hence we neglect it. The second term we keep only term proportional to $\tan\beta$, thus

$$\delta\tilde{\lambda}_b^{\text{SQCD}}\frac{v_2}{\sqrt{2}} = -\frac{2\alpha_s}{3\pi}m_b\mu^*M_3^*t_\beta C_0(M_{\tilde{b}_1}^2, M_{\tilde{b}_2}^2, m_{\tilde{g}}^2). \tag{D.9}$$

The Higgsino contributions

$$= \qquad -i\delta\lambda_b^{\tilde{H}\tilde{t}}\bar{b}P_Lb < H_{22}^{0*} >$$

$$-i\delta\tilde{\lambda}_b^{\tilde{H}\tilde{t}}\bar{b}P_Lb\langle H_2^0\rangle = \bar{b}\left(i\lambda_bU_{\tilde{t}}^*(j,1)\sqrt{\frac{\mu^*}{|\mu|}}P_L\right)(i|\mu|)\left(i\lambda_tU_{\tilde{t}}(i,2)\sqrt{\frac{\mu^*}{|\mu|}}P_L\right)$$

$$\times(-ih_{ij}^{\tilde{t}})b\int\frac{d^4q}{(2\pi)^4}\frac{i}{q^2-M_{\tilde{t}_i}^2}\frac{i}{q^2-M_{\tilde{t}_j}^2}\frac{1}{q^2-|\mu|^2}, \tag{D.10}$$

where

$$h_{ij}^{\tilde{t}} = m_tX_tU_{\tilde{t}}(j,2)U_{\tilde{t}}^*(i,1) + m_tX_t^*U_{\tilde{t}}(j,1)U_{\tilde{t}}^*(i,2). \tag{D.11}$$

One can simplify as

$$\delta\tilde{\lambda}_b^{\tilde{H}\tilde{t}}v_2 = \frac{1}{16\pi^2}m_b\lambda_t^2\mu^*t_\beta U_{\tilde{t}}(i,2)U_{\tilde{t}}^*(j,1)(X_tU_{\tilde{t}}(j,2)U_{\tilde{t}}^*(i,1)$$

$$+ X_t^*U_{\tilde{t}}(j,1)U_{\tilde{t}}^*(i,2))C_0(M_{\tilde{t}_i}^2, M_{\tilde{t}_j}^2, |\mu|^2). \tag{D.12}$$

Expressing it in terms of $s_{\tilde{t}}$ and $c_{\tilde{t}}$, one gets

$$\delta\tilde{\lambda}_b^{\tilde{H}\tilde{t}}v_2 = -\frac{\alpha_t}{4\pi}m_b\mu^*t_\beta c_{\tilde{t}}s_{\tilde{t}}(X_tc_{\tilde{t}}s_{\tilde{t}} + X_t^*c_{\tilde{t}}^*s_{\tilde{t}}^*)\big[C_0(M_{\tilde{t}_1}^2, M_{\tilde{t}_1}^2, |\mu|^2)$$

$$+ C_0(M_{\tilde{t}_2}^2, M_{\tilde{t}_2}^2, |\mu|^2)\big]$$

$$- \frac{\alpha_t}{4\pi}m_b\mu^*t_\beta\big[-s_{\tilde{t}}^2(X_tc_{\tilde{t}}^2 - X_t^*s_{\tilde{t}}^*s_{\tilde{t}}^*) + c_{\tilde{t}}^2(-X_ts_{\tilde{t}}^2 + X_t^*c_{\tilde{t}}^2)\big]$$

$$\times C_0(M_{\tilde{t}_1}^2, M_{\tilde{t}_2}^2, |\mu|^2)$$

$$= -\frac{\alpha_t}{8\pi}m_b\mu^*t_\beta X_t^*\sin^2 2\theta_{\tilde{t}}\big[C_0(M_{\tilde{t}_1}^2, M_{\tilde{t}_1}^2, |\mu|^2) + C_0(M_{\tilde{t}_2}^2, M_{\tilde{t}_2}^2, |\mu|^2)\big]$$

$$- \frac{\alpha_t}{4\pi}m_b\mu^*t_\beta X_t^*\cos^2 2\theta_{\tilde{t}}C_0(M_{\tilde{t}_1}^2, M_{\tilde{t}_2}^2, |\mu|^2)$$

$$= -\frac{\alpha_t}{8\pi}m_b\mu^*t_\beta X_t^*\sin^2 2\theta_{\tilde{t}}\big[C_0(M_{\tilde{t}_1}^2, M_{\tilde{t}_1}^2, |\mu|^2) + C_0(M_{\tilde{t}_2}^2, M_{\tilde{t}_2}^2, |\mu|^2)$$

$$- 2C_0(M_{\tilde{t}_1}^2, M_{\tilde{t}_2}^2, |\mu|^2)\big] - \frac{\alpha_t}{4\pi}m_b\mu^*t_\beta X_t^*C_0(M_{\tilde{t}_1}^2, M_{\tilde{t}_2}^2, |\mu|^2)$$

$$= -\frac{\alpha_t}{2\pi}m_b\mu^*t_\beta X_t^*m_t^2|X_t|^2\frac{1}{i\pi^2}\int d^4q\frac{1}{(q^2-M_{\tilde{g}}^2)(q^2-M_{\tilde{t}_1}^2)^2(q^2-M_{\tilde{t}_2}^2)^2}$$

$$- \frac{\alpha_t}{4\pi}m_b\mu^*t_\beta X_t^*C_0(M_{\tilde{t}_1}^2, M_{\tilde{t}_2}^2, |\mu|^2). \tag{D.13}$$

Keep only the leading term, one gets

$$\delta\tilde{\lambda}_b^{\tilde{H}\tilde{t}}v_2 = -\frac{\alpha_t}{4\pi}m_b\mu^*t_\beta A_t^*C_0(M_{\tilde{t}_1}^2, M_{\tilde{t}_2}^2, |\mu|^2). \tag{D.14}$$

The wino contributions

$$-i\delta\tilde{\lambda}_b^{\tilde{W}}\bar{b}P_Lb\langle H_2^0\rangle = \bar{b}\left(\frac{iem_bU_{\tilde{t}}^*(i,1)}{\sqrt{2}c_\beta s_W M_W}P_L\right)(i\mu^*)(-i\sqrt{2}s_\beta M_W)(iM_2^*)$$

$$\times\left(\frac{-ie}{s_W}U_{\tilde{t}}(i,1)P_L\right)\int\frac{d^4q}{(2\pi)^4}\frac{i}{q^2-M_{\tilde{t}_i}^2}\frac{1}{q^2-|\mu|^2}\frac{1}{q^2-|M_2|^2}$$

$$+\bar{b}\left(\frac{-iem_b}{\sqrt{2}c_\beta s_W M_W}U_{\tilde{b}}^*(i,1)P_L\right)(i\mu^*)(-iM_Zc_Ws_\beta)(iM_2^*)$$

$$\times\left(\frac{ie}{\sqrt{2}s_W}U_{\tilde{b}}(i,1)P_L\right)\int\frac{d^4q}{(2\pi)^4}\frac{i}{q^2-M_{\tilde{b}_i}^2}\frac{1}{q^2-|\mu|^2}\frac{1}{q^2-|M_2|^2}$$

$$= -i\frac{g^2}{16\pi^2}m_b\mu^*M_2^*t_\beta|U_{\tilde{t}}(i,1)|^2\bar{b}P_LbC_0(M_{\tilde{t}_i}^2, |M_2|^2, |\mu|^2)$$

$$-i\frac{g^2}{32\pi^2}m_b\mu^*M_2^*t_\beta|U_{\tilde{b}}(i,1)|^2\bar{b}P_LbC_0(M_{\tilde{b}_i}^2, |M_2|^2, |\mu|^2). \tag{D.15}$$

Simplify the above expression, one gets

$$\begin{aligned}\delta\tilde{\lambda}_b^{\tilde{W}}v_2 &= \frac{\alpha}{8\pi s_W^2}m_b\mu^*M_2^*t_\beta\big[2|U_{\tilde{t}}(i,1)|^2C_0(M_{\tilde{t}_i}^2, |M_2|^2, |\mu|^2)\\&\quad+|U_{\tilde{b}}(i,1)|^2C_0(M_{\tilde{b}_i}^2, |M_2|^2, |\mu|^2)\big].\end{aligned} \tag{D.16}$$

The bino contributions

$$-i\delta\tilde{\lambda}_b^{\tilde{B}}\bar{b}P_Lb\langle H_2^0\rangle = \frac{-1}{16\pi^2}\bar{b}\left(\frac{-2ie}{3\sqrt{2}c_W}U_{\tilde{b}}^*(i,2)P_L\right)(iM_1^*)(-iM_Zs_Ws_\beta)(i\mu^*)$$

$$\times\left(\frac{-iem_b}{\sqrt{2}c_\beta M_Ws_W}U_{\tilde{b}}(i,2)P_L\right)C_0(M_{\tilde{b}_i}^2,|M_1|^2,|\mu|^2)$$

$$+\frac{-1}{16\pi^2}\bar{b}\left(\frac{-iem_b}{\sqrt{2}c_\beta M_Ws_W}U_{\tilde{b}}(i,1)P_L\right)(i\mu^*)(-iM_Zs_Ws_\beta)$$

$$\times(iM_1^*)\left(\frac{-ie}{3\sqrt{2}c_W}U_{\tilde{b}}(i,1)P_L\right)C_0(M_{\tilde{b}_i}^2,|M_1|^2,|\mu|^2)$$

$$+\frac{-i}{16\pi^2}\bar{b}\left(\frac{-ie2}{3\sqrt{2}c_W}U_{\tilde{b}}^*(j,2)P_L\right)(iM_1^*)(-im_b)$$

$$\times\left(X_bU_{\tilde{b}}(j,2)U_{\tilde{b}}^*(i,1)+X_b^*U_{\tilde{b}}(j,1)U_{\tilde{b}}^*(i,2)\right)$$

$$\times\left(\frac{-ie}{3\sqrt{2}c_W}U_{\tilde{b}}(i,1)P_L\right)C_0(M_{\tilde{b}_i}^2,M_{\tilde{b}_j}^2,|M_1|^2). \tag{D.17}$$

Simplifying the above expression, one gets

$$\delta\tilde{\lambda}_b^{\tilde{B}}h_bv_2 = \frac{\alpha}{24\pi c_W^2}\mu^*M_1^*t_\beta\left(2|U_{\tilde{b}}(i,2)|^2+|U_{\tilde{b}}(i,1)|^2\right)C_0(M_{\tilde{b}_i}^2,|M_1|^2,|\mu|^2)$$

$$-\frac{\alpha}{36\pi c_W^2}m_bM_1^*X_bC_0(M_{\tilde{b}_1}^2,M_{\tilde{b}_2}^2,|M_1|^2)-2\frac{\alpha}{36\pi c_W^2}m_b^3M_1^*X_b|X_b|^2$$

$$\times\frac{1}{i\pi^2}\int d^4q\frac{1}{(q^2-M_{\tilde{g}}^2)(q^2-M_{\tilde{b}_1}^2)^2(q^2-M_{\tilde{b}_2}^2)^2}. \tag{D.18}$$

Keeping only the leading terms, then the bino contributions read

$$\delta\tilde{\lambda}_b^{\tilde{B}}v_2 = \frac{\alpha}{72\pi c_W^2}m_b\mu^*M_1^*t_\beta\left[3\left(2|U_{\tilde{b}}(i,2)|^2+|U_{\tilde{b}}(i,1)|^2\right)C_0(M_{\tilde{b}_i}^2,|M_1|^2,|\mu|^2)\right.$$

$$\left.+2C_0(M_{\tilde{b}_1}^2,M_{\tilde{b}_2}^2,|M_1|^2)\right]. \tag{D.19}$$

Using the relation of three-point scalar function with zero-external momentum and the auxiliary function,

$$C_0(a,b,c) = -I(a,b,c),\quad(a\neq b\neq c), \tag{D.20}$$

and

$$\delta\tilde{\lambda}_bv_2 = m_b\Delta m_bt_\beta, \tag{D.21}$$

one can get the expressions in Eq. (5.41).

Appendix E

Two-body decay widths of charged Higgs bosons

In this section we present the decay widths at tree level for all possible channels listed in Section 6.1. We use $g = 1, 2, 3$ for generation index, $i, j = 1, 2$ for sfermion index, $c = 1, 2$ for chargino index and $n = 1, 2, 3, 4$ for neutralino index.

$$
\Gamma_{H^- \to \bar{u}_{g1} d_{g2}} = \frac{6\alpha\lambda^{1/2}(M_{H^\pm}^2, m_{u_{g1}}^2, m_{d_{g2}}^2)}{16 M_W^2 s_W^2 M_{H^\pm}^3} |V_{\mathrm{CKM}, g1g2}|^2 \left[\frac{m_{u_{g1}}^2}{t_\beta^2} \left(M_{H^\pm}^2 - m_{u_{g1}}^2 \right) \right.
$$
$$
\left. - m_{u_{g1}}^2 m_{d_{g2}}^2 \left(4 + \frac{1}{t_\beta^2} + t_\beta^2 \right) + m_{d_{g2}}^2 t_\beta^2 \left(M_{H^\pm}^2 - m_{d_{g2}}^2 \right) \right], \tag{E.1}
$$

$$
\Gamma_{H^- \to e_g \bar{\nu}_g} = \frac{2\alpha\lambda^{1/2}(M_{H^\pm}^2, m_{e_i}^2, 0)}{16 M_W^2 s_W^2 M_{H^\pm}^3} t_\beta^2 m_{e_g}^2 \left(M_{H^\pm}^2 - m_{e_g}^2 \right), \tag{E.2}
$$

$$
\Gamma_{H^- \to \tilde{u}_{g1,i} \tilde{d}_{g2,j}} = \frac{6\alpha\lambda^{1/2}(M_{H^\pm}^2, m_{\tilde{u}_{g1,i}}^2, m_{\tilde{d}_{g2,j}}^2)}{16 M_W^2 s_W^2 M_{H^\pm}^3} |V_{\mathrm{CKM}, g1g2}|^2 |\mathcal{A}_{ij}^{g1g2}|^2, \tag{E.3}
$$

$$
\Gamma_{H^- \to \tilde{e}_{g,i} \tilde{\nu}_g} = \frac{2\alpha\lambda^{1/2}(M_{H^\pm}^2, m_{\tilde{e}_{g,i}}^2, m_{\tilde{n}u_g}^2)}{16 M_W^2 s_W^2 M_{H^\pm}^3} |\mathcal{B}_i^g|^2, \tag{E.4}
$$

$$
\Gamma_{H^- \to \tilde{\chi}_{c1}^- \tilde{\chi}_{n1}^0} = \frac{4\alpha\lambda^{1/2}(M_{H^\pm}^2, m_{\tilde{\chi}_{c1}^-}^2, m_{\tilde{\chi}_{n1}^0}^2)}{16 s_W^2 M_{H^\pm}^3} \left[-2 m_{\tilde{\chi}_{c1}^-} m_{\tilde{\chi}_{n1}^0} \left(\mathcal{W}_L^{n1c1} \mathcal{W}_R^{n1c1*} + \mathrm{h.c} \right) \right.
$$
$$
\left. + \left(M_{H^\pm}^2 - m_{\tilde{\chi}_{c1}^-}^2 - m_{\tilde{\chi}_{n1}^0}^2 \right) \left(|\mathcal{W}_L^{n1c1}|^2 + |\mathcal{W}_R^{n1c1}|^2 \right) \right],
$$

$$
\Gamma_{H^- \to W^- h} = \frac{\alpha\lambda^{3/2}(M_{H^\pm}^2, M_W^2, M_h^2)}{16 M_W^2 s_W^2 M_{H^\pm}^3} \cos(\beta - \alpha), \tag{E.5}
$$

$$
\Gamma_{H^- \to W^- H} = \frac{\alpha\lambda^{3/2}(M_{H^\pm}^2, M_W^2, M_H^2)}{16 M_W^2 s_W^2 M_{H^\pm}^3} \sin(\beta - \alpha), \tag{E.6}
$$

$$
\Gamma_{H^- \to W^- A} = \frac{\alpha\lambda^{3/2}(M_{H^\pm}^2, M_W^2, M_A^2)}{16 M_W^2 s_W^2 M_{H^\pm}^3}, \tag{E.7}
$$

where

$$\lambda(x,y,x) = x^2 + y^2 + z^2 - 2xy - 2yz - 2xz, \tag{E.8}$$

$$\begin{aligned}
\mathcal{A}_{ij}^{g1g2} =& U_{\tilde{u}_{g1}}^*(i,1)\big[\big(-2s_\beta M_W^2 + m_{u_{g1}}^2 + m_{d_{g2}}^2 t_\beta^2\big)U_{\tilde{d}_{g2}}(j,1) \\
&+ t_\beta m_{d_{g2}}\big(\mu^* + t_\beta A_{d_{g2}}\big)U_{\tilde{d}_{g2}}(j,2)\big] + m_{u_{g1}}U_{\tilde{u}_{g1}}^*(i,2) \\
&\times \big[m_{d_{g2}}U_{\tilde{d}_{g2}}(j,2)(1+t_\beta^2) + U_{\tilde{d}_{g2}}(j,1)(A_{u_{g1}}^* + \mu t_\beta)\big],
\end{aligned} \tag{E.9}$$

$$\mathcal{B}_i^g = m_{e_g}U_{\tilde{e}_g}(i,2)(\mu^* + A_{e_g}t_\beta) - U_{\tilde{e}_g}(i,1)(M_W^2 s_{2\beta} - m_{e_g}t_\beta^2), \tag{E.10}$$

$$\begin{aligned}
\mathcal{W}_L^{n1c1} =& s_\beta\bigg[\frac{1}{\sqrt{2}}\left(\mathbf{U_n}^*(n1,2) + t_W\mathbf{U_n}^*(n1,3)\right)\mathbf{U_c}^*(c1,2) \\
&+ \mathbf{U_n}^*(n1,3)\mathbf{U_c}^*(c1,1)\bigg],
\end{aligned} \tag{E.11}$$

$$\begin{aligned}
\mathcal{W}_R^{n1c1} =& -c_\beta\bigg[\frac{1}{\sqrt{2}}\left(\mathbf{U_n}(n1,2) + t_W\mathbf{U_n}(n1,1)\right)\mathbf{V_c}(c1,1) \\
&+ \mathbf{U_n}(n1,4)\mathbf{V_c}(c1,1)\bigg],
\end{aligned} \tag{E.12}$$

and for the other notations we refer to Subsection 3.5.3.

Appendix F

Input parameters

F.1 The SM parameters

The SM input parameters are taken from [187].

$$
\begin{aligned}
&\alpha^{-1}(0) = 137.0359895, \quad \alpha(M_Z) = 1/128.926, \quad \alpha_s(M_Z) = 0.1197, \\
&M_Z = 91.1876\,\text{GeV}, \qquad M_W = 80.398\,\text{GeV} \qquad m_e = 0.51099891\,\text{MeV}, \\
&m_\mu = 105.658367\,\text{MeV}, \qquad m_\tau = 1.777\,\text{GeV}, \qquad m_u = 66\,\text{MeV}, \\
&m_c = 1.2\,\text{GeV}, \qquad m_t = 173.1\,\text{GeV}, \qquad m_d = 66\,\text{MeV}, \\
&m_s = 150\,\text{MeV}, \qquad \overline{m}_b(\overline{m}_b) = 4.2\,\text{GeV}, \qquad m_b^{\text{OS}} = 4.3\,\text{GeV}. \qquad \text{(F.1)}
\end{aligned}
$$

For the mass of the light quarks, they are chosen to be consistent with the experimental data of hadronic contribution to the photonic vacuum polarization [188]. The top mass is taken from the recent measurements [189]. $\overline{m}_b(\overline{m}_b)$ is the QCD-$\overline{\text{MS}}$ b-quark mass, while the top-quark mass is understood as the pole mass.

F.2 The soft SUSY-breaking parameters

F.2.1 The modified m_h^{max} scenario

The soft parameters are

$$
\begin{aligned}
&\mu = 200\,\text{GeV}, \, M_2 = 200\,\text{GeV}, \, M_3 = 0.8\,M_{\text{SUSY}}, \, |A_\tau| = |A_t| = |A_b| = 800\,\text{GeV}, \\
&M_{\tilde{Q}} = M_{\tilde{D}} = M_{\tilde{U}} = M_{\text{SUSY}} = 500\,\text{GeV}, \, M_{\tilde{L}} = 200\,\text{GeV}, \, M_{\tilde{E}} = 150\,\text{GeV}. \qquad \text{(F.2)}
\end{aligned}
$$

The values of μ and M_3 are chosen as in the m_h^{max} scenario to maximize the lightest neutral Higgs mass [190]. M_1 and M_2 are connected via the GUT relation $|M_1| = 5/3 \tan^2 \theta_W |M_2|$.

F.2.2   The CPX senario:

The CPX scenario is chosen to maximize the CP-violating effects due to the large value of the product $\mathrm{Im}\,(\mu A_t)/M_{\mathrm{SUSY}}^2$ [191]. According to [192], we use the following set of (on-shell) parameters

$$
\begin{aligned}
&\mu = 2000\,\mathrm{GeV},\, M_{\mathrm{SUSY}} = 500\,\mathrm{GeV},\, |A_f| = 900\,\mathrm{GeV},\\
&M_3 = 1000\,\mathrm{GeV},\, M_2 = 200\,\mathrm{GeV},\, M_1 = 5/3\tan^2\theta_W M_2.
\end{aligned}
\tag{F.3}
$$

Bibliography

[1] S. L. Glashow. Partial symmetries of weak interactions. *Nucl. Phys.*, 22:579, 1961.

[2] S. Weinberg. A model of leptons. *Phys. Rev. Lett.*, 19:1264, 1967.

[3] A. Salam. *Elementary particle physics ed N Svartholm (Stockholm: Almqvist and Wiksells)*, 1968.

[4] M. Gell-Mann. A schematic model of baryons and mesons. *Phys. Lett.*, 8:214, 1964.

[5] H. Fritzsch, M. Gell-Mann, and H. Leutwyler. Advantages of the color octet gluon picture. *Phys. Lett.*, B47:365, 1973.

[6] D. J. Gross and F. Wilczek. Utraviolet behavior of non-Abelian gauge theories. *Phys. Rev. Lett.*, 30:1343, 1973.

[7] H. D. Politzer. Reliable perturbative results for strong interactions? *Phys. Rev. Lett.*, 30:1346, 1973.

[8] P. W. Higgs. Broken symmetries, massless particles and gauge fields. *Phys. Lett.*, 12:132, 1964.

[9] P. W. Higgs. Spontaneous symmetry breakdown without massless bosons. *Phys. Rev.*, 145:1156, 1966.

[10] F. Englert and R. Brout. Broken symmetry and the mass of gauge vector mesons. *Phys. Rev. Lett.*, 13:321, 1964.

[11] G. S. Guralnik, C. R. Hagen, and T. W. B. Kibble. Global conservation laws and massless particles. *Phys. Rev. Lett.*, 13:585, 1964.

[12] T. W. B. Kibble. Symmetry breaking in non-Abelian gauge theories. *Phys. Rev.*, 155:1554, 1967.

[13] H. P. Nilles. Supersymmetry, supergravity and particle physics. *Phys. Rept.*, 110:1, 1984.

[14] H. E. Haber and G. L. Kane. The search for supersymmetry: probing physics beyond the Standard Model. *Phys. Rept.*, 117:75, 1985.

[15] R. Barbieri. Looking beyond the Standard Model: The supersymmetric option. *Riv.Nuovo Cim.*, 11N4:1, 1988.

[16] L. Girardello and Marcus T. Grisaru. Soft breaking of supersymmetry. *Nucl. Phys.*, B194:65, 1982.

[17] E. Witten. Dynamical breaking of supersymmetry. *Nucl. Phys.*, B188:513, 1981.

[18] R. K. Kaul. Gauge hierarchy in a supersymmetric model. *Phys. Lett.*, B109:19, 1982.

[19] M. Kobayashi and T. Maskawa. CP Violation in the renormalizable theory of weak interaction. *Prog. Theor. Phys.*, 49:652, 1973.

[20] T. Ibrahim and P. Nath. CP violation from standard model to strings. *Rev. Mod. Phys.*, 80:577, 2008, arXiv:0705.2008.

[21] ATLAS collaboration. ATLAS detector and physics performance: Technical Design Report. CERN-LHCC-99-014/015.

[22] G. L. Bayatian et al. CMS technical design report, volume II: Physics performance. *J. Phys.*, G34:995, 2007.

[23] M. Frank et al. The Higgs boson masses and mixings of the complex MSSM in the Feynman-diagrammatic approach. *JHEP*, 02:047, 2007, hep-ph/0611326.

[24] E. Christova, E. Ginina, and M. Stoilov. Supersymmetry through CP violation in $H^{\pm} \to W^{\pm} h_0$. *JHEP*, 11:027, 2003, hep-ph/0307319.

[25] D. A. Dicus, J. L. Hewett, C. Kao, and T. G. Rizzo. $W^{\mp} H^{\pm}$ production at hadron colliders. *Phys. Rev.*, D40:787, 1989.

[26] A. A. Barrientos Bendezu and B. A. Kniehl. $W^{\mp} H^{\pm}$ associated production at the Large Hadron Collider. *Phys. Rev.*, D59:015009, 1999, hep-ph/9807480.

[27] A. A. Barrientos Bendezu and B. A. Kniehl. Quark-loop amplitudes for $W^{\mp} H^{\pm}$ associated hadroproduction. *Phys. Rev.*, D61:097701, 2000, hep-ph/9909502.

[28] A. A. Barrientos Bendezu and B. A. Kniehl. Squark loop correction to $W^{\mp} H^{\pm}$ associated hadroproduction. *Phys. Rev.*, D63:015009, 2001, hep-ph/0007336.

[29] O. Brein, W. Hollik, and S. Kanemura. The MSSM prediction for $W^{\mp} H^{\pm}$ production by gluon fusion. *Phys. Rev.*, D63:095001, 2001, hep-ph/0008308.

[30] W. Hollik and Shou-hua Zhu. $\mathcal{O}(\alpha_s)$ corrections to $b\bar{b} \to W^{\mp} H^{\pm}$ at the CERN Large Hadron Collider. *Phys. Rev.*, D65:075015, 2002, hep-ph/0109103.

[31] Jun Gao, Chong Sheng Li, and Zhao Li. Next-to-leading order QCD effects in associated charged Higgs and W boson production in the MSSM at the CERN Large Hadron Collider. *Phys. Rev.*, D77:014032, 2008, arXiv:0710.0826.

[32] Jun Zhao, Chong Sheng Li, and Qiang Li. SUSY-QCD corrections to $W^{\mp}H^{\pm}$ associated production at the CERN Large Hadron Collider. *Phys. Rev.*, D72:114008, 2005, hep-ph/0509369.

[33] M. Rauch. Quantum effects in Higgs-boson production processes at hadron colliders. 2008, arXiv:0804.2428.

[34] Ya-Sheng Yang, Chong-Sheng Li, Li-Gang Jin, and Shou Hua Zhu. Supersymmetric electroweak corrections to $W^{\mp}H^{\pm}$ associated production at the CERN Large Hadron Collider. *Phys. Rev.*, D62:095012, 2000, hep-ph/0004248.

[35] Wu Peng et al. NLO supersymmetric QCD corrections to the $t\bar{b}H^{-}$ associated production at hadron colliders. *Phys. Rev.*, D73:015012, 2006, hep-ph/0601069. [Erratum-ibid.D80:059901,2009].

[36] S. Dittmaier, M. Kramer, M. Spira, and M. Walser. Charged-Higgs-boson production at the LHC: NLO supersymmetric QCD corrections. 2009, arXiv:0906.2648.

[37] K. Nakamura et al. Review of particle physics. *J. Phys.*, G37:075021, 2010.

[38] J. Alcaraz et al. A Combination of preliminary electroweak measurements and constraints on the standard model. 2006, hep-ex/0612034.

[39] Y. Nambu. Quasi-particles and gauge invariance in the theory of superconductivity. *Phys. Rev.*, 117:648, 1960.

[40] Y. Nambu. Axial vector current conservation in weak interactions. *Phys. Rev. Lett.*, 4:380, 1960.

[41] Z. Maki, M. Nakagawa, and S. Sakata. Remarks on the unified model of elementary particles. *Prog. Theor. Phys.*, 28:870, 1962.

[42] S. L. Glashow, J. Iliopoulos, and L. Maiani. Weak interactions with lepton-hadron symmetry. *Phys. Rev.*, D2:1285, 1970.

[43] T. D. Lee. A theory of spontaneous T violation. *Phys. Rev.*, D8:1226, 1973.

[44] H. E. Haber, G. L. Kane, and T. Sterling. The fermion mass scale and possible effects of Higgs bosons on experimental observables. *Nucl. Phys.*, B161:493, 1979.

[45] J. F. Donoghue and L. F. Li. Properties of charged Higgs bosons. *Phys. Rev.*, D19:945, 1979.

[46] T. P. Cheng and M. Sher. Mass-matrix ansatz and flavor nonconservation in models with multiple higgs doublets. *Phys. Rev. D*, 35(11):3484, Jun 1987.

[47] G. Senjanovic. Course on grand unification. pages 137–179, 2006.

[48] P. V. Dong, H. N. Long, D. T. Nhung, and D. V. Soa. SU(3)C x SU(3)L x U(1)X model with two Higgs triplets. *Phys. Rev.*, D73:035004, 2006, hep-ph/0601046.

[49] A. Strumia and F. Vissani. Neutrino masses and mixings and . . .. 2006, hep-ph/0606054.

[50] G. Bertone, D. Hooper, and J. Silk. Particle dark matter: Evidence, candidates and constraints. *Phys. Rept.*, 405:279, 2005, hep-ph/0404175.

[51] A. D. Sakharov. Violation of CP invariance, C asymmetry, and baryon asymmetry of the universe. *Pisma Zh. Eksp. Teor. Fiz.*, 5:32, 1967. [JETP Lett.5:24-27,1967].

[52] F. Jegerlehner and A. Nyffeler. The muon g-2. *Phys.Rept.*, 477:1, 2009, arXiv:0902.3360.

[53] T. Teubner, K. Hagiwara, R. Liao, A.D. Martin, and D. Nomura. Update of $(g - 2)$ of the muon and $\Delta\alpha$. *AIP Conf.Proc.*, 1343:340, 2011.

[54] S. R. Coleman and J. Mandula. All possible symmetries of the S matrix. *Phys. Rev.*, 159:1251, 1967.

[55] Y. A. Golfand and E. P. Likhtman. Extension of the algebra of Poincaré group generators and violation of p invariance. *JETP Lett.*, 13:323, 1971.

[56] D. V. Volkov and V. P. Akulov. Is the neutrino a Goldstone particle? *Phys. Lett.*, B46:109, 1973.

[57] J. Wess and B. Zumino. A Lagrangian model invariant under supergauge transformations. *Phys. Lett.*, B49:52, 1974.

[58] J. Wess and B. Zumino. Supergauge transformations in four-dimensions. *Nucl. Phys.*, B70:39, 1974.

[59] D. Z. Freedman, P. van Nieuwenhuizen, and S. Ferrara. Progress toward a theory of supergravity. *Phys. Rev.*, D13:3214, 1976.

[60] S. Deser and B. Zumino. Consistent supergravity. *Phys. Lett.*, B62:335, 1976.

[61] R. Haag, J. T. Lopuszanski, and M. Sohnius. All possible generators of supersymmetries of the S matrix. *Nucl. Phys.*, B88:257, 1975.

[62] A. Djouadi. The anatomy of electroweak symmetry breaking. II. The Higgs bosons in the minimal supersymmetric model. *Phys. Rept.*, 459:1, 2008, hep-ph/0503173.

[63] K. Lane. Two lectures on technicolor. 2002, hep-ph/0202255.

[64] S. P. Martin. A supersymmetry primer. 1997, hep-ph/9709356.

[65] S. Heinemeyer, W. Hollik, and G. Weiglein. The masses of the neutral CP-even Higgs bosons in the MSSM: Accurate analysis at the two loop level. *Eur. Phys. J.*, C9:343, 1999, hep-ph/9812472.

[66] G. Degrassi, S. Heinemeyer, W. Hollik, P. Slavich, and G. Weiglein. Towards high-precision predictions for the MSSM Higgs sector. *Eur. Phys. J.*, C28:133, 2003, hep-ph/0212020.

[67] S. Marchetti, S. Mertens, U. Nierste, and D. Stockinger. $\tan\beta$-enhanced supersymmetric corrections to the anomalous magnetic moment of the muon. *Phys.Rev.*, D79:013010, 2009, arXiv:0808.1530.

[68] G. 't Hooft. Symmetry breaking through Bell-Jackiw anomalies. *Phys. Rev. Lett.*, 37:8, 1976.

[69] L. D. Faddeev and V. N. Popov. Feynman diagrams for the Yang-Mills field. *Phys. Lett.*, B25:29, 1967.

[70] H. K. Dreiner. An introduction to explicit R-parity violation. 1997, hep-ph/9707435.

[71] S. N. Ahmed et al. Constraints on nucleon decay via 'invisible' modes from the Sudbury Neutrino Observatory. *Phys. Rev. Lett.*, 92:102004, 2004, hep-ex/0310030.

[72] A. Y. Smirnov and F. Vissani. Upper bound on all products of R-parity violating couplings λ' and λ'' from proton decay. *Phys. Lett.*, B380:317, 1996, hep-ph/9601387.

[73] LEP Higgs Working Group for Higgs boson searches. Search for charged Higgs bosons: Preliminary combined results using LEP data collected at energies up to 209 GeV. 2001, hep-ex/0107031.

[74] S. Schael et al. Search for neutral MSSM Higgs bosons at LEP. *Eur. Phys. J.*, C47:547, 2006, hep-ex/0602042.

[75] B. Abbott et al. Search for charged Higgs bosons in decays of top quark pairs. *Phys. Rev. Lett.*, 82:4975, 1999, hep-ex/9902028.

[76] V. M. Abazov et al. Direct search for charged Higgs bosons in decays of top quarks. *Phys. Rev. Lett.*, 88:151803, 2002, hep-ex/0102039.

[77] A. Abulencia et al. Search for charged Higgs bosons from top quark decays in $p\bar{p}$ collisions at $\sqrt{s} = 1.96\,\text{TeV}$. *Phys. Rev. Lett.*, 96:042003, 2006, hep-ex/0510065.

[78] V. M. Abazov et al. Combination of $t\bar{t}$ cross section measurements and constraints on the mass of the top quark and its decays into charged Higgs bosons. *Phys. Rev.*, D80:071102, 2009, arXiv:0903.5525.

[79] V.M. Abazov et al. Search for charged Higgs bosons in top quark decays. *Phys.Lett.*, B682:278, 2009, arXiv:0908.1811.

[80] V. M. Abazov et al. Search for charged higgs bosons decaying into top and bottom quarks in $p\bar{p}$ collisions. *Phys. Rev. Lett.*, 102(19):191802, May 2009.

[81] CMS collaboration. Search for charged Higgs boson in the etau and mutau dilepton channels of top quark pair decays. CMS Physics Analysis Summaries: CMS-PAS-HIG-11-002, July 2011.

[82] CMS collaboration. $h^+ \to \bar{\tau}\nu_\tau$ in top quark decays. CMS Physics Analysis Summaries: CMS-PAS-HIG-11-008, July 2011.

[83] ATLAS collaboration. Search for charged higgs bosons in the τ+jets final state in $t\bar{t}$ decays with 1.03 fb^{-1} of pp collision data recorded at $\sqrt{s} = 7$ TeV with the ATLAS experiment. ATLAS note number: ATLAS-CONF-2011-138, Sep 2011.

[84] U. Haisch. $\bar{B} \to X_s\gamma$: Standard Model and beyond. 2008, arXiv:0805.2141.

[85] G. Passarino and M.J.G. Veltman. One-loop corrections for e^+e^- annihilation into $\mu^+\mu^-$ in the Weinberg model. *Nucl.Phys.*, B160:151, 1979.

[86] L. D. Landau. On analytic properties of vertex parts in quantum field theory. *Nucl. Phys.*, 13:181, 1959.

[87] S. Coleman and R. E. Norton. Singularities in the physical region. *Nuovo Cim.*, 38:438, 1965.

[88] R.J Eden, P.V. Landshoff, D.I Olive, and J.C Polkinghorne. The analytic S-matrix. *Cambridge University Press*, 1966.

[89] C. Itzykson and J. B. Zuber. Quantum field theory. New York, Usa: Mcgraw-hill (1980) 705 P.(International Series In Pure and Applied Physics).

[90] A. Denner. Reduction of multiparticle one-loop integrals and amplitudes lectures at the Third Graduate School in Physics at Colliders, Torino, 2008.

[91] D. N. Le. One-loop Yukawa corrections to the process $pp \to b\bar{b}H$ in the Standard Model at the LHC: Landau singularities. PhD thesis, Université de Savoie. 2008, arXiv:0810.4078.

[92] W. Pauli and F. Villars. On the invariant regularization in relativistic quantum theory. *Rev. Mod. Phys.*, 21:434, 1949.

[93] G. 't Hooft and M. J. G. Veltman. Regularization and renormalization of gauge fields. *Nucl. Phys.*, B44:189, 1972.

[94] W. Siegel. Supersymmetric dimensional regularization via dimensional reduction. *Phys. Lett.*, B84:193, 1979.

[95] D. Z. Freedman, K. Johnson, and J. I. Latorre. Differential regularization and renormalization: A new method of calculation in quantum field theory. *Nucl. Phys.*, B371:353, 1992.

[96] T. Hahn and M. Perez-Victoria. Automatized one-loop calculations in four and D dimensions. *Comput. Phys. Commun.*, 118:153, 1999, hep-ph/9807565.

[97] W. Siegel. Inconsistency of supersymmetric dimensional regularization. *Phys. Lett.*, B94:37, 1980.

[98] D. Stockinger. Regularization by dimensional reduction: consistency, quantum action principle, and supersymmetry. *JHEP*, 0503:076, 2005, hep-ph/0503129.

[99] K. I. Aoki, Z. Hioki, M. Konuma, R. Kawabe, and T. Muta. Electroweak theory. Framework of On-Shell renormalization and study of higher order effects. *Prog. Theor. Phys. Suppl.*, 73:1, 1982.

[100] M. Bohm, H. Spiesberger, and W. Hollik. On the one-loop renormalization of the electroweak Standard Model and its application to leptonic processes. *Fortsch. Phys.*, 34:687, 1986.

[101] A. Denner. Techniques for calculation of electroweak radiative corrections at the one loop level and results for W physics at LEP-2000. *Fortschr. Phys.*, 41:307, 1993, arXiv:0709.1075.

[102] G. 't Hooft. Dimensional regularization and the renormalization group. *Nucl. Phys.*, B61:455, 1973.

[103] W. A. Bardeen, A. J. Buras, D. W. Duke, and T. Muta. Deep inelastic scattering beyond the leading order in asymptotically free gauge theories. *Phys. Rev.*, D18:3998, 1978.

[104] A. J. Buras. Asymptotic freedom in deep inelastic processes in the leading order and beyond. *Rev. Mod. Phys.*, 52:199, 1980.

[105] J. Kublbeck, M. Bohm, and A. Denner. FeynArts: computer algebraic generation of Feynman graphs. *Comput. Phys. Commun.*, 60:165, 1990.

[106] P. H. Chankowski, S. Pokorski, and J. Rosiek. Complete on-shell renormalization scheme for the minimal supersymmetric Higgs sector. *Nucl. Phys.*, B423:437, 1994, hep-ph/9303309.

[107] A. Dabelstein. The one-loop renormalization of the MSSM Higgs sector and its application to the neutral scalar Higgs masses. *Z. Phys.*, C67:495, 1995, hep-ph/9409375.

[108] S. Heinemeyer, W. Hollik, and G. Weiglein. Electroweak precision observables in the minimal supersymmetric standard model. *Phys. Rept.*, 425:265, 2006, hep-ph/0412214.

[109] A. Freitas and D. Stockinger. Gauge dependence and renormalization of $\tan\beta$ in the MSSM. *Phys. Rev.*, D66:095014, 2002, hep-ph/0205281.

[110] Lang-Hui Wan, Wen-Gan Ma, Ren-You Zhang, and Yi Jiang. Electroweak corrections to the charged Higgs boson decay into chargino and neutralino. *Phys. Rev.*, D64:115004, 2001, hep-ph/0107089.

[111] M. Frank, S. Heinemeyer, W. Hollik, and G. Weiglein. FeynHiggs1.2: Hybrid MS-bar / on-shell renormalization for the CP-even Higgs boson sector in the MSSM. 2002, hep-ph/0202166.

[112] A. Freitas, W. Hollik, W. Walter, and G. Weiglein. Electroweak two-loop corrections to the M(W) - M(Z) mass correlation in the standard model. *Nucl. Phys.*, B632:189, 2002, hep-ph/0202131.

[113] N. Baro, F. Boudjema, and A. Semenov. Automatised full one-loop renormalisation of the MSSM I: The Higgs sector, the issue of $\tan\beta$ and gauge invariance. *Phys. Rev.*, D78:115003, 2008, arXiv:0807.4668.

[114] K. E. Williams. PhD thesis, Durham University (2008).

[115] T. Kinoshita. Mass singularities of Feynman amplitudes. *J. Math. Phys.*, 3:650, 1962.

[116] T. D. Lee and M. Nauenberg. Degenerate systems and mass singularities. *Phys. Rev.*, 133:1549, 1964.

[117] S. Dittmaier. Separation of soft and collinear singularities from one-loop N-point integrals. *Nucl. Phys.*, B675:447, 2003, hep-ph/0308246.

[118] K. Fabricius, I. Schmitt, G. Kramer, and G. Schierholz. Higher order perturbative QCD calculation of jet cross- sections in e^+e^- annihilation. *Zeit. Phys.*, C11:315, 1981.

[119] G. Kramer and B. Lampe. Jet cross-sections in e^+e^- annihilation. *Fortschr. Phys.*, 37:161, 1989.

[120] H. Baer, J. Ohnemus, and J. F. Owens. A next-to-leading logarithm calculation of jet photoproduction. *Phys. Rev.*, D40:2844, 1989.

[121] B. W. Harris and J. F. Owens. The two cutoff phase space slicing method. *Phys. Rev.*, D65:094032, 2002, hep-ph/0102128.

[122] R. K. Ellis, D. A. Ross, and A. E. Terrano. The perturbative calculation of jet structure in e^+e^- annihilation. *Nucl. Phys.*, B178:421, 1981.

[123] M. L. Mangano, P. Nason, and G. Ridolfi. Heavy quark correlations in hadron collisions at next-to-leading order. *Nucl. Phys.*, B373:295, 1992.

[124] S. Frixione, Z. Kunszt, and A. Signer. Three jet cross-sections to next-to-leading order. *Nucl. Phys.*, B467:399, 1996, hep-ph/9512328.

[125] S. Catani and M. H. Seymour. A general algorithm for calculating jet cross sections in NLO QCD. *Nucl. Phys.*, B485:291, 1997, hep-ph/9605323.

[126] S. Dittmaier. A general approach to photon radiation off fermions. *Nucl. Phys.*, B565:69, 2000, hep-ph/9904440.

[127] G. 't Hooft and M. J. G. Veltman. Scalar one-loop integrals. *Nucl. Phys.*, B153:365, 1979.

[128] U. Baur, S. Keller, and D. Wackeroth. Electroweak radiative corrections to W boson production in hadronic collisions. *Phys. Rev.*, D59:013002, 1999, hep-ph/9807417.

[129] K. P. O. Diener, S. Dittmaier, and W. Hollik. Electroweak higher-order effects and theoretical uncertainties in deep-inelastic neutrino scattering. *Phys. Rev.*, D72:093002, 2005, hep-ph/0509084.

[130] A. D. Martin, R. G. Roberts, W. J. Stirling, and R. S. Thorne. Parton distributions incorporating QED contributions. *Eur. Phys. J.*, C39:155, 2005, hep-ph/0411040.

[131] S. Heinemeyer, W. Hollik, and G. Weiglein. FeynHiggs: a program for the calculation of the masses of the neutral CP-even Higgs bosons in the MSSM. *Comput. Phys. Commun.*, 124:76, 2000, hep-ph/9812320.

[132] T. Hahn, S. Heinemeyer, W. Hollik, H. Rzehak, and G. Weiglein. FeynHiggs: A program for the calculation of MSSM Higgs-boson observables - Version 2.6.5. *Comput. Phys. Commun.*, 180:1426, 2009.

[133] S. Heinemeyer, W. Hollik, H. Rzehak, and G. Weiglein. The Higgs sector of the complex MSSM at two-loop order: QCD contributions. *Phys. Lett.*, B652:300, 2007, arXiv:0705.0746.

[134] J. S. Lee et al. CPsuperH: A computational tool for Higgs phenomenology in the minimal supersymmetric standard model with explicit CP violation. *Comput. Phys. Commun.*, 156:283, 2004, hep-ph/0307377.

[135] J. A. Casas, J. R. Espinosa, M. Quiros, and A. Riotto. The lightest Higgs boson mass in the minimal supersymmetric standard model. *Nucl. Phys.*, B436:3, 1995, hep-ph/9407389.

[136] M. S. Carena, J. R. Espinosa, M. Quiros, and C. E. M. Wagner. Analytical expressions for radiatively corrected Higgs masses and couplings in the MSSM. *Phys. Lett.*, B355:209, 1995, hep-ph/9504316.

[137] M. S. Carena, M. Quiros, and C. E. M. Wagner. Effective potential methods and the Higgs mass spectrum in the MSSM. *Nucl. Phys.*, B461:407, 1996, hep-ph/9508343.

[138] M. S. Carena et al. Reconciling the two-loop diagrammatic and effective field theory computations of the mass of the lightest CP-even Higgs boson in the MSSM. *Nucl. Phys.*, B580:29, 2000, hep-ph/0001002.

[139] A. Dabelstein. Fermionic decays of neutral MSSM Higgs bosons at the one loop level. *Nucl.Phys.*, B456:25, 1995, hep-ph/9503443.

[140] E. Braaten and J. P. Leveille. Higgs boson decay and the running mass. *Phys. Rev.*, D22:715, 1980.

[141] M. S. Carena, D. Garcia, U. Nierste, and Carlos E. M. Wagner. Effective Lagrangian for the $\bar{t}bH^+$ interaction in the MSSM and charged Higgs phenomenology. *Nucl. Phys.*, B577:88, 2000, hep-ph/9912516.

[142] L. V. Avdeev and M. Yu. Kalmykov. Pole masses of quarks in dimensional reduction. *Nucl. Phys.*, B502:419, 1997, hep-ph/9701308.

[143] S. Bethke. The 2009 wolrd average of $\alpha_s(M_Z)$. *Eur. Phys. J.*, C64:689, 2009, arXiv:0908.1135.

[144] S. Heinemeyer, W. Hollik, H. Rzehak, and G. Weiglein. High-precision predictions for the MSSM Higgs sector at $\mathcal{O}(\alpha_b\alpha_s)$. *Eur. Phys. J.*, C39:465, 2005, hep-ph/0411114.

[145] L. Hofer, U. Nierste, and D. Scherer. Resummation of tan-beta-enhanced supersymmetric loop corrections beyond the decoupling limit. *JHEP*, 10:081, 2009, arXiv:0907.5408.

[146] M. S. Carena, J. R. Ellis, A. Pilaftsis, and C. E. M. Wagner. Renormalization-group-improved effective potential for the MSSM Higgs sector with explicit CP violation. *Nucl. Phys.*, B586:92, 2000, hep-ph/0003180.

[147] M. S. Carena, J. R. Ellis, S. Mrenna, A. Pilaftsis, and C. E. M. Wagner. Collider probes of the MSSM Higgs sector with explicit CP violation. *Nucl. Phys.*, B659:145, 2003, hep-ph/0211467.

[148] J. Guasch, P. Hafliger, and M. Spira. MSSM Higgs decays to bottom quark pairs revisited. *Phys. Rev.*, D68:115001, 2003, hep-ph/0305101.

[149] S. Dittmaier, M Kramer, A. Muck, and T. Schluter. MSSM Higgs-boson production in bottom-quark fusion: Electroweak radiative corrections. *JHEP*, 03:114, 2007, hep-ph/0611353.

[150] A. Djouadi and P. Gambino. QCD corrections to Higgs boson selfenergies and fermionic decay widths. *Phys. Rev.*, D51:218, 1995, hep-ph/9406431.

[151] H. Eberl, K. Hidaka, S. Kraml, W. Majerotto, and Y. Yamada. Improved SUSY QCD corrections to Higgs boson decays into quarks and squarks. *Phys. Rev.*, D62:055006, 2000, hep-ph/9912463.

[152] A. Bartl et al. QCD corrections to the decay $H^+ \to t\bar{b}$ in the Minimal Supersymmetric Standard Model. *Phys. Lett.*, B378:167, 1996, hep-ph/9511385.

[153] A. Arhrib, A. Djouadi, W. Hollik, and C. Junger. SUSY Higgs boson decays into scalar quarks: QCD corrections. *Phys. Rev.*, D57:5860, 1998, hep-ph/9702426.

[154] http://www.feynhiggs.de/.

[155] http://www.hep.man.ac.uk/u/jslee/CPsuperH.html.

[156] http://people.web.psi.ch/spira/hdecay/.

[157] http://www.hephy.at/tools.

[158] E. Christova, H. Eberl, W. Majerotto, and S. Kraml. CP violation in charged Higgs decays in the MSSM with complex parameters. *Nucl. Phys.*, B639:263, 2002, hep-ph/0205227.

[159] E. Christova, H. Eberl, W. Majerotto, and S. Kraml. CP violation in charged Higgs boson decays into tau and neutrino. *JHEP*, 12:021, 2002, hep-ph/0211063.

[160] W. Hollik and D. T. Nhung. CP violating asymmetry in $H^{\pm} \to W^{\pm}h_1$ decays. *JHEP*, 01:060, 2011, arXiv:1008.2659.

[161] S. Bejar, W. Hollik, and D. Lopez-Val. The Wh_1 decay mode of the charged Higgs boson: a complete 1-loop analysis, to appear.

[162] G. J. van Oldenborgh and J. A. M. Vermaseren. New algorithms for one-loop integrals. *Z. Phys.*, C46:425, 1990.

[163] B. A. Kniehl, C. P. Palisoc, and A. Sirlin. Higgs boson production and decay close to thresholds. *Nucl. Phys.*, B591:296, 2000, hep-ph/0007002.

[164] A. Arhrib, R. Benbrik, and M. Chabab. $H^{\pm} \to W^{\pm}Z$ and $H^{\pm} \to W^{\pm}\gamma$ in the MSSM. *Acta Phys. Polon. Supp.*, 1:417, 2008, arXiv:0710.3555.

[165] T. Ibrahim and P. Nath. The neutron and the electron electric dipole moment in N = 1 supergravity unification. *Phys. Rev.*, D57:478, 1998, hep-ph/9708456.

[166] S. Moretti and K. Odagiri. The phenomenology of $W^{\mp}H^{\pm}$ production at the Large Hadron Collider. *Phys. Rev.*, D59:055008, 1999, hep-ph/9809244.

[167] D. Eriksson, S. Hesselbach, and J. Rathsman. Associated charged Higgs and W boson production in the MSSM at the CERN Large Hadron Collider. *Eur. Phys. J.*, C53:267, 2008, hep-ph/0612198.

[168] M. Hashemi. Possibility of observing MSSM charged Higgs in association with a W boson at LHC. 2010, arXiv:1008.3785.

[169] Dao Thi Nhung, W. Hollik, and Le Duc Ninh. $W^{\mp}H^{\pm}$ production and CP asymmetry at the LHC. *Phys. Rev.*, D83:075003, 2011, arXiv:1011.4820.

[170] F. del Aguila, A. Culatti, R. Munoz Tapia, and M. Perez-Victoria. Techniques for one-loop calculations in constrained differential renormalization. *Nucl. Phys.*, B537:561, 1999, hep-ph/9806451.

[171] W. Beenakker, R. Hopker, M. Spira, and P. M. Zerwas. Squark and gluino production at hadron colliders. *Nucl. Phys.*, B492:51, 1997, hep-ph/9610490.

[172] T. M. P. Tait. The tW^- mode of single top production. *Phys. Rev.*, D61:034001, 2000, hep-ph/9909352.

[173] S. Frixione, E. Laenen, P. Motylinski, B. R. Webber, and C. D. White. Single-top hadroproduction in association with a W boson. *JHEP*, 07:029, 2008, arXiv:0805.3067.

[174] T. Hahn. Generating Feynman diagrams and amplitudes with FeynArts 3. *Comput. Phys. Commun.*, 140:418, 2001, hep-ph/0012260.

[175] T. Hahn and C. Schappacher. The implementation of the minimal supersymmetric standard model in FeynArts and FormCalc. *Comput. Phys. Commun.*, 143:54, 2002, hep-ph/0105349.

[176] S. Dittmaier. Weyl-van-der-Waerden formalism for helicity amplitudes of massive particles. *Phys. Rev.*, D59:016007, 1999, hep-ph/9805445.

[177] D.J. Miller, S. Moretti, D.P. Roy, and W. J. Stirling. Detecting heavy charged Higgs bosons at the CERN LHC with four b quark tags. *Phys.Rev.*, D61:055011, 2000, hep-ph/9906230.

[178] Dao Thi Nhung, W. Hollik, and Le Duc Ninh. Electroweak corrections to $gg \rightarrow H^- t\bar{b}$ at the LHC to appear.

[179] J. L. Diaz-Cruz and O. A. Sampayo. Contribution of gluon fusion to the production of charged Higgs at hadron colliders. *Phys. Rev.*, D50:6820–6823, 1994.

[180] F. Borzumati, J. L. Kneur, and N. Polonsky. Higgs-strahlung and R-parity violating slepton-strahlung at hadron colliders. *Phys. Rev.*, D60:115011, 1999, hep-ph/9905443.

[181] A. Denner and S. Dittmaier. Reduction of one-loop tensor 5-point integrals. *Nucl. Phys.*, B658:175, 2003, hep-ph/0212259.

[182] T. Hahn and M. Rauch. News from FormCalc and LoopTools. *Nucl. Phys. Proc. Suppl.*, 157:236, 2006, hep-ph/0601248.

[183] A private code of Le Duc Ninh.

[184] Dao Thi Nhung and Le Duc Ninh. D0C : A code to calculate scalar one-loop four-point integrals with complex masses. *Comput. Phys. Commun.*, 180:2258, 2009, arXiv:0902.0325.

[185] S. Kawabata. A new version of the multidimensional integration and event generation package BASES/SPRING. *Comp. Phys. Commun.*, 88:309, 1995.

[186] G. P. Lepage. A new algorithm for adaptive multidimensional integration. *J. Comput. Phys.*, 27:192, 1978.

[187] C. Amsler et al. Review of particle physics. *Phys. Lett.*, B667:1, 2008.

[188] F. Jegerlehner. The Effective fine structure constant at TESLA energies. 2001, hep-ph/0105283.

[189] The Tevatron Electroweak Working Group for the CDF and D0 Collaboration. Combination of CDF and D0 results on the mass of the top quark. 2009, arXiv:0903.2503.

[190] M. S. Carena, S. Heinemeyer, C. E. M. Wagner, and G. Weiglein. Suggestions for improved benchmark scenarios for Higgs boson searches at LEP2. 1999, hep-ph/9912223.

[191] M. S. Carena, J. R. Ellis, A. Pilaftsis, and C. E. M. Wagner. CP-violating MSSM Higgs bosons in the light of LEP 2. *Phys. Lett.*, B495:155, 2000, hep-ph/0009212.

[192] K. E. Williams and G. Weiglein. Precise predictions for $h_a \to h_b h_c$ decays in the complex MSSM. *Phys. Lett.*, B660:217, 2008, arXiv:0710.5320.